

Geomorphology Field Guide

Tectonic Geomorphology of Western Oregon:
Monmouth-Cape Arago-Sunset Bay-Roseburg Transect

Steve Taylor, Ph.D.
Earth and Physical Sciences Dept.
Western Oregon University
Monmouth, OR 97361

Table of Contents

Adams (1984), Active Deformation of the Oregon Coast	1-7
McInelly and Kelsey (1990), Tectonic Deformation Cape Arago	8-22
Komar (1992), Ocean Processes and Hazards	23-26
Mitchell et al (1994) Vertical Deformation	27-31
Kelsey et al (1994) Coast Range Topography and Deformation	32-36
Kelsey et al (1996) Quaternary Plate Deformation in Oregon	37-42
Dariento and Peterson (1990), Tectonic Subsidence and Buried Marshes	43-49
Hart (1997), Buried Forests of Oregon	50-54
Armentrout (198X), Geologic Field Guide to Cape Arago-Coos Bay	55-64C

Class Notes and Exercises

Fluvial Notes	65-82
Paleoflood Hydrology, Fluvial Process	83-104
Soils and Mass Wasting	105-118
Surficial Mapping Methodology	119-122
Field Maps / Site Resources	
Geologic Map of Cape Arago / Garden Valley Areas	123
Cape Arago-Sunset Bay Maps	124-127
Garden Valley Maps	128-130A
Soil Survey Cape Arago / Coos County	131-157
Geomorphic Mapping Exercise (Sunset Bay)	158-163
Oregon Coast Tectonic Geomorphology Exercise	164-176
Conversion Charts	177-182

Bretz Club Field Guide - Sunset Bay Area 2012 p.183-198

Wallick et al., 2011, Umpqua River Channel Change & Transport p. 199-215

ACTIVE DEFORMATION OF THE PACIFIC
NORTHWEST CONTINENTAL MARGIN

John Adams

Earth Physics Branch, Energy, Mines and
Resources, Ottawa, Canada K1A 0Y3

Abstract. Tilted and uplifted marine terraces in southern Oregon show progressive landward tilting of the coastal ranges at about $5 - 16 \times 10^{-8}$ rad. yr^{-1} for the last 0.25 m.y. Tide gauges in Washington and British Columbia, and ten resurveyed leveling lines running inland from the coast, indicate contemporary landward (down-to-the-east) tilt rates of about $1-12 \times 10^{-8}$ rad. yr^{-1} averaged over periods of from 10 to 50 years. The leveling lines traverse, and the terraces cut across, dipping Cenozoic strata: Pleistocene (dips to 3°), Miocene (dips to 30°) and Eocene (dips to 60°). Southern Oregon from Cape Blanco to the Siletz River shows geodetic or terrace tilting in the same direction as the underlying stratal dips. Hence present-day deformation continues past deformation of the coastal ranges and is most likely related to active subduction of the Juan de Fuca plate. The steep stratal dips, lack of major active faults and historic earthquakes, and presence of very young bedding-plane faults suggest that much of the onshore deformation and shortening within the overlying North American plate is taken up by folding rather than thrust faulting. Present shortening rates across

north-trending folds near the coast are between 0.02 and 1.9×10^{-7} yr^{-1} . The rate of shortening decreases rapidly eastwards from the Juan de Fuca - North American plate boundary. A total of about 25 mm yr^{-1} of permanent shortening could be occurring within the North American plate; most of it in the westernmost 40 km. The landward tilt and shortening rates are similar to those above many other subduction zones that have experienced great thrust earthquakes. While a high strain rate measured near Seattle, Washington, has been interpreted as elastic strain accumulation before a thrust earthquake, the low level of historic seismicity and the similarity of short- and long-term deformation rates suggest alternatively that the subduction beneath Washington is aseismic. The issue has considerable implications for seismic hazard evaluation in the Pacific Northwest and could be resolved by a search for the effects (or lack of effects) of prehistoric great earthquakes.

INTRODUCTION

The Pacific coast of Oregon and Washington lies close to the boundary between the North American and Juan de Fuca plates. South of Vancouver Island marine magnetic anomalies indicate present convergence at 35 mm yr^{-1} between the two plates [Riddihough and Hyndman, 1976; Riddihough, 1977]. The calc-alkaline vol-

Copyright 1984
by the American Geophysical Union.

Paper number 4T0560.
0278-7407/84/004T-0560\$10.00

canic rocks of the Cascade Range, the morphology of the sea floor and the deformation of young offshore sediments, all suggest subduction of the Juan de Fuca plate beneath the North American plate, but present-day underthrusting is unproven.

The case for active subduction has been well presented by Riddiough and Hyndman [1976], who explained the absence of a deep, well-defined Benioff Zone in terms of the low plate-convergence rate and the young age (and hence hot and more plastic nature) of the underthrust sea floor. Recently, Ando and Balazs [1979] showed a simple landward tilt for the Olympic Peninsula of northwest Washington from both repeated geodetic level surveys and tide gauge records. They compared the simple tilt with the well-documented and complex pattern of pre-, co-, and post-seismic movements observed in Japan, and interpreted the Washington data to indicate contemporary, though aseismic, subduction.

An earlier paper [Reilinger and Adams, 1982], closely related to the present one, analyzed leveling and tide gauge data for Oregon and Washington, showed that there was a well-defined landward tilting of the 600-km-long coastal ranges at about 3×10^{-8} rad. yr^{-1} and noted that the tilting agreed with studies in progress on the deformation rate of marine terraces in Oregon (now published in the present paper). Although the agreement between long- and short-term deformation rates suggests that the subduction is occurring by aseismic creep as hypothesized by Ando and Balazs, recent measurements of horizontal deformation on northwest Washington, interpreted as elastic strain accumulation by Savage et al. [1981], seem to be incompatible with aseismic subduction. Further contemporary deformation studies seemed needed before the correct alternative--aseismic subduction, or subduction with large, infrequent thrust earthquakes--might be determined.

In this paper I describe coastal terraces in Oregon and Washington and quantify their deformation. By analysis of east-west geodetic leveling lines and tide gauge records I show that contemporary deformation rates are similar to the rates for the last 0.25 m.y. and by extrapolation of terrace tilts to the dip on the underlying strata that the pattern of deformation in the coastal ranges of the Pacific Northwest has remained substantially the same over the last half

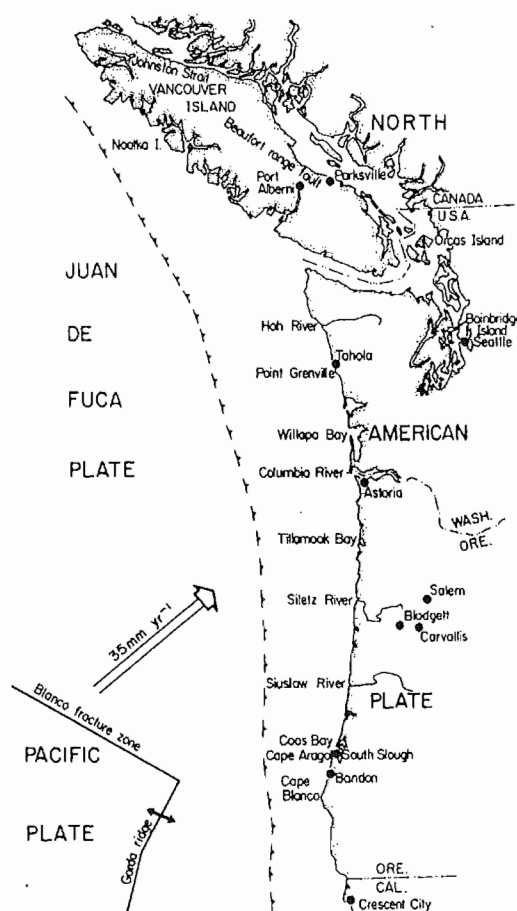


Fig. 1. Map of Pacific Northwest coast showing localities mentioned in the text, inferred trench position (broken barbed line), and compression vector representing motion of the Juan de Fuca plate relative to North America [Riddiough, 1977].

million years. Both the rates and the persistence of deformation patterns argue that subduction continues beneath Oregon and Washington despite the lack of shallow thrust earthquakes.

GEOMORPHIC EVIDENCE FOR LANDWARD TILT OF THE COASTAL RANGES

Marine Terraces in Oregon and Washington

Along much of the Oregon coast (Figure 1) there are emerged wave-cut surfaces and terraces that demonstrate coastal uplift. The highest and most spectacular terraces are to the south between Cape Arago and Cape Blanco, and have

TABLE 1. Uplift and Tilt of Marine Terraces Near Coos Bay, Oregon

Terrace	Assigned Age, yr	Elevation, ^a m	Eustatic Correction, m	Uplift ^a Rate, mm yr ⁻¹	Tilt, rad.	Average Tilt Rate, 10 ⁻⁸ rad. yr ⁻¹
A Cape Arago						
Metcalf	230,000	150	0	0.65	0.019	8
Seven Devils	124,000	85	-6	0.64	0.006	5
Pioneer	103,000	55	+15	0.68	0.005	5
Whisky Run	83,000	21	+13	0.41	0.004	5
B Trig 691						
Metcalf	230,000	230	0	1.0	0.037	16
Seven Devils	124,000	123	-6	0.94	0.017	14
Pioneer	103,000	44	+15	0.57	0.0098	10

^aRelative to sea level at longitude 124.376 degrees west.

of sea level rise approximates that of the land uplift, as is well explained by Bloom [1980]. In regions of slow uplift the youngest emerged feature is the Holocene (~6000 yr) bench, the next, the bench or benches that correspond to high sea levels about 100,000 yr (at 82,000, 103,000, and 124,000 yr ago), and above that a bench 230,000 yr old. In regions of more rapid uplift there may be additional benches cut during periods 28,000, 42,000 and 60,000 yr ago when sea level was relatively high but still lower than the present [Bloom et al., 1974].

Radiocarbon dating of wood and shells from the Whisky Run and Pioneer terraces near Bandon gives ages between 36,000 and 45,000 yr [Janda, 1972, p. 63], but are probably minimum ages. A more definite age for the Whisky Run terrace at Bandon is a Th/U date of $72,200 \pm 5300$ yr on solitary corals [Kennedy et al., 1982]; G.L. Kennedy (personal communication, 1982) infers the terrace to represent the 82,000-yr sea level maximum. This plausible age of 82,000 yr for the Whisky Run and consideration of the known sea level history leads to the following ages for the terraces near Cape Arago: Whisky Run, 82,000; Pioneer, 103,000; Seven Devils, 124,000; and Metcalf 230,000 years. When these ages are applied to the tilted terraces near Cape Arago, they indicate approximately constant tilt and uplift rates for the last 230,000 years (Table 1), a geologically reasonable result given the tectonic environment.

At Cape Blanco, C14 and Th/U dating

of shells on the main wave-cut surface (widely considered to correlate with the Pioneer, e.g., Beaulieu and Hughes [1976]), gave ages of 35,000 yr, but in view of carbonate-closure problems supply only a minimum age [Richards and Thurber, 1966]. More recently, Wehmiller et al. [1977] have determined an amino acid racemization date of $50,000 \pm 20,000$ yr for shells from the same place, considered the terrace to represent either the 42,000 or 60,000 yr sea level maxima of Bloom et al. [1974], and hence calculated an uplift rate of either 2.75 or 1.5 mm yr⁻¹. If the dates for both the Whisky Run and main Cape Blanco terrace are correct, the Blanco terrace cannot correlate with the Pioneer as widely thought, but must instead represent a post-Whisky Run terrace.

Above the main terrace at Cape Blanco, there are three named terraces: the Silver Butte (about 60 m elevation), the Indian Creek (170 m), and the Poverty Ridge (270 m) [Janda, 1972; Beaulieu and Hughes, 1976]. It is not possible to assign terrace ages unambiguously, but the elevations and Janda's [1972] correlation of the Indian Creek and Seven Devils terraces are more consistent with a 60,000 yr age for the main Blanco terrace rather than 42,000 yr.

The present uncertainty in the absolute ages of the terraces at Cape Arago and at Cape Blanco does not detract from the evidence they provide for progressive tilting and uplift. At worst, the adopted ages could be wrong by a factor of 2 (e.g.,

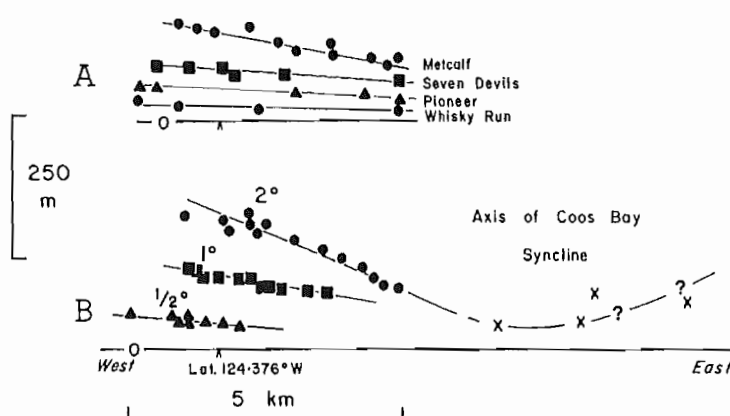


Fig. 3. East-west cross section of terrace elevations north (A) and south (B) of Cape Arago showing the landward tilt of the terraces and demonstrating the progressive nature of the deformation. Elevations are of the terrace surface and not the wave-cut platform and are taken from Griggs [1944, plate 42]. Note that individual terraces cannot be distinguished on the east side of South Slough, but the highest remnants appear to rise above sea level on the east flank of the Coos Bay Syncline.

the youngest plausible age for the Whiskey Run terrace is 42,000 yr) and so the derived rates, even if in error by this factor, still represent rapid deformation.

Landward Tilting of Marine Terraces, Coastal Oregon

Because the Oregon coast is nearly parallel to the subduction trench, there are only a few places where irregularities allow marine terraces to demonstrate tilting normal to the trench.

Wave-cut surfaces that form today in California have an initial seaward slope of 0.3° – 1.0° [Bradley and Griggs, 1976], and it is therefore likely that the newly emerged wave-cut surfaces in Oregon had similar seaward slopes. Hence their present landward tilt represents not only tilting from the horizontal but also back-tilting of the initial seaward slope. For an initial seaward slope of 0.3° , surfaces of 42,000, 60,000, 100,000 and 230,000 years would need to be tilted landward at 12 , 8 , 5 , and 2×10^{-8} rad. yr^{-1} , respectively, to be horizontal, and any present tilt in the landward direction increases the total tilt rate. Therefore tilt rates calculated assuming a horizontal surface may be low by a factor of 2 or more, the error being greatest for the youngest terraces. The seaward slope correction applies only to surfaces cut

across wide platforms parallel to the tilt direction and is not applicable at Cape Arago because those platforms were cut perpendicular to the tilt direction. At Cape Blanco, however, the main terrace is 6 km wide, probably 60,000 years old, and cut parallel to the tilt direction, so that although it has a landward tilt of 0.10° (see map of Cape Blanco in the work of Beaulieu and Hughes [1976]), and also Janda [1972, p. 48], the total amount of landward tilting, including removal of an initial seaward tilt, could be as much as 0.4° , corresponding to a mean tilt rate of 11×10^{-8} rad. yr^{-1} .

The terraces near Cape Arago have a distinct landward (down-to-the-east) dip [Baldwin, 1966]. For example, Janda [1972, p. 28] gives the elevation of the Whiskey Run wave-cut surface at Cape Arago as 29 m, but as less than 5 m at Charleston, 5.5 km to the east. Ideally, the elevation of the wave-cut surface for every terrace should be plotted against distance normal to the trench, but, in general, only the elevations of the terrace cover beds are known. The terrace cover beds lie on the wave-cut surface and may be 15–20 m thick; to determine tilt of the terraces from elevation of the cover beds, it is necessary to assume that their thickness is constant. When terrace elevations (taken from Griggs [1945, plate 42]) are plotted as two east-west pro-

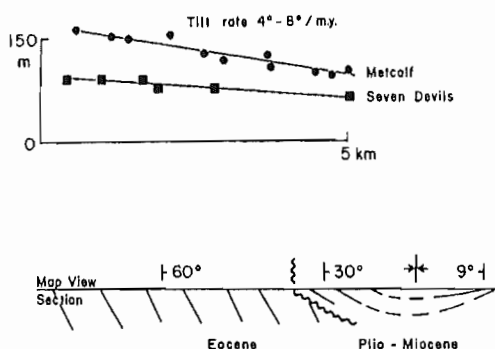


Fig. 4. Relationship between tilted marine terraces (top) and underlying geologic structure (bottom), Coos Bay Syncline, Oregon. The terraces are tilted down toward the axis of the syncline.

files, one north (A) and one south (B) of Cape Arago, they show simple eastward tilt with the amount of tilt being greatest for the oldest and highest surface (Figure 3). The simple pattern for each surface suggests that in each case a single surface has been identified (Table 1).

For the oldest surface, the maximum dip is about 2° on profile B. From an assigned age of 230,000 years, the average landward tilt rate is 16×10^{-8} rad. yr $^{-1}$ (9° per million years). Profile A gives 8×10^{-8} rad. yr $^{-1}$, and both profiles indicate progressive tilting of surfaces of successive age. Two further profiles (not shown) to the south give rates of 6 and 7×10^{-8} rad. yr $^{-1}$ from the tilt of the Metcalf terrace. A few kilometers to the south of all four profiles a geodetic tilt rate of $(12 \pm 7) \times 10^{-8}$ rad. yr $^{-1}$ between Bandon and Coquille (see below) suggests that tilting in the region has continued at substantially its present rate for 230,000 years.

The easterly tilting of the Cape Arago terraces is related to the tightening of the underlying north trending syncline (Figure 4). Volume constraints require bedding-plane slip during the tightening of folds, the fault throws being opposite in sense to the tilt trend (Figure 5). Hence the apparently smooth landward tilt of the terraces shown in Figure 3 may in fact be interrupted by successive faults.

Youthful Faulting in the Coastal Ranges

Faults with throws of less than 10 m would not show on the 50-foot contour interval map [Griggs, 1945, plate 42] used

to construct Figure 3, but are observed in the coastal section east of Cape Arago where there has been an extensive study of the structure and stratigraphy of the Coos Bay Coalfield. Fault displacements probably occur at many places on terraces throughout coastal Oregon and Washington but have been inadequately studied.

At Mussel Reef (Yokam Point), near Cape Arago, a reverse bedding-plane fault which dips east at 70° displaces the Whisky Run terrace surface by 5 m, west side down [Baldwin, 1966, p. 199]. Across Sunset Bay, the Whisky Run Terrace is 6 m lower to the east than the west and may well be offset by a concealed fault [Beaulieu and Hughes, 1975, p. 43]. A further fault has displaced the wave-cut platform by a meter and formed a ridge on the sand [Allen and Baldwin, 1944, p. 40].

At the Seven Devils Mine, on the Seven Devils terrace and 8 km southeast of Cape Arago, a southeast-striking fault in the terrace cover beds displaces the bedrock by more than 3 m, with the northeast side being upthrown [Griggs, 1945]. Along the Whisky Run terrace north of Bandon there are several offsets in the Eocene bedrock, and faulting of the terrace is illustrated by Murphy et al. [1979]. The illustrated fault is one of several faults within the cover beds of the Whisky Run terrace. It strikes $N42^\circ W$, dips $30^\circ W$ and has 0.3 m of thrust displacement (P.J. Murphy, Stone and Webster Corp., written communication, 1981).

Further south at Cape Blanco, Dott [1971, p. 52, 56] notes "youthful

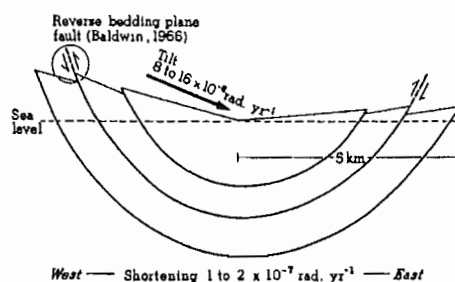


Fig. 5. Schematic cross section across the Coos Bay Syncline showing slip on reverse bedding-plane faults as a consequence of compression across the syncline. Tilt on the flanks is superimposed on a lesser landward tilt (see Figure 9) and produces greater uplift on the western (Cape Arago) flank than on the eastern flank.

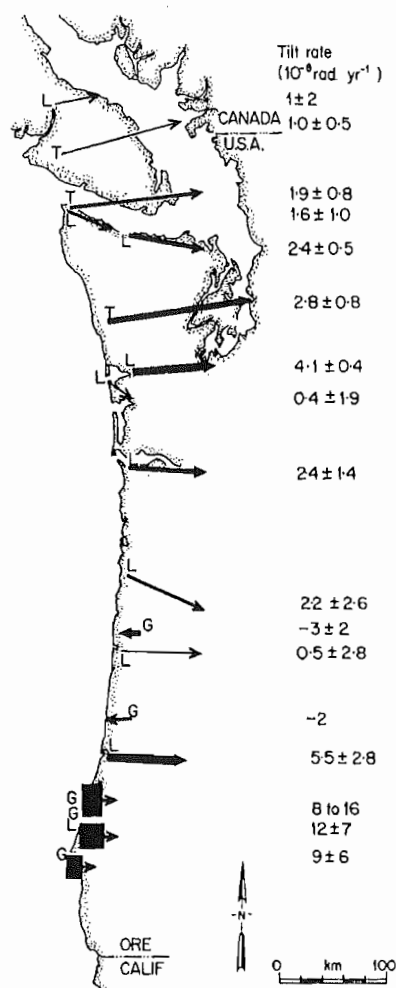


Fig. 10. Summary of tilt rates and directions derived from geodetic, tide gauge, and terrace deformation data. Arrow lengths represent spatial extent of data, arrow widths represent magnitude of tilt rate. Negative rates represent seaward tilting. Letters beside arrows represent nature of evidence for rate: G, geomorphic, L, leveling, T, tide gauge. Note the consistent direction and similar magnitude of tilting in the coast ranges. The exceptions are the short coastal profiles in the south, which are controlled by local structure.

most cases fortuitous and need not represent the true tilt direction, they are uniformly down to the east, and overall suggest an easterly or east-northeasterly tilt. Further, although the rates are determined for periods as short as 10 yr and as long as 230,000 yr, there are no

serious differences in magnitude among them. The rates are most rapid in the south where they are determined for the flanks of individual folds, but where they span the entire width of the coast range the rates are consistently about 3×10^{-8} rad. yr^{-1} south of Vancouver Island, and on rather scant evidence perhaps half that rate to the north. The general agreement between the rates and their consistency with stratal dips and geologic structure suggest that deformation has continued in the coastal ranges at the contemporary rate for about the last half million years; the rates are similar to those observed near other active subduction zones that are associated with earthquakes.

ONSHORE LANDWARD TILTING AND ITS RELATION TO SUBDUCTION ELSEWHERE

Landward tilting of the coastal ranges is a distinctive component of onshore deformation in the Pacific Northwest, and similar tilting occurs adjacent to subduction zones elsewhere. Away-from-trench tilting is usually easily documented for island arcs, as the islands have shorelines that are normal to the trench. Thus tilting has been established for the Ryukyu Islands [Ota and Yoshikawa, 1978], and for the New Hebrides [Taylor et al., 1980]; rate about 10×10^{-8} rad. yr^{-1} .

Landward tilting of coastal ranges is commonly more difficult to quantify as the coasts themselves are parallel to the trench, and measurements must be made at fortuitous places where peninsulas or reentrants occur. Thus in Costa Rica, landward tilting across the Nicoya Peninsula is indicated by drowned shorelines to the east and elevated terraces to the west [Alt et al., 1980] and by bioerosion morphology on coastal platforms [Fischer, 1980]. In Chile, marine terraces on the Arauco Peninsula and adjacent islands are tilted 1° - 3° down the east (landward) at inferred rates of 5 to 60×10^{-8} rad. yr^{-1} [Kaizuka et al., 1973, Table 3]. The landward tilt rate from the terraces is very nearly the same as the rate of 10 - 40×10^{-8} rad. yr^{-1} deduced from the uplift pattern caused by historic earthquakes and their probable frequency.

The North Island of New Zealand is being obliquely underthrust by the Pacific plate at 50 mm yr^{-1} [Cole and Lewis, 1981] and the complexity of deformation decreases along the east coast

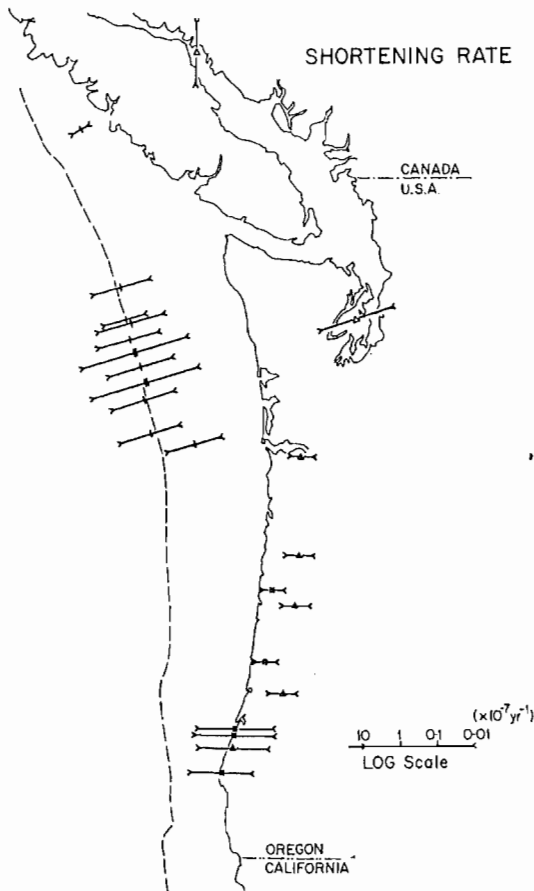


Fig. 11. Summary of contemporary shortening rates and directions derived from trilateration (open triangles), leveling (filled triangles), terrace tilting (squares), stratal folding (single bars), folding and faulting (double bars) as discussed in the text. In order to plot the large range of rates, arrow lengths are proportional to the logarithm of the rate.

The straight line on Figure 12 represents an exponential decay of shortening rate away from the plate boundary. Obviously, the exact decay relationship is poorly defined, but the one on the figure is equivalent to total shortening across the margin of 25 mm yr^{-1} , 80% of which occurs in the most westerly 40 km. The total shortening rate could be a sizeable fraction of the plate convergence rate. For the slope, shelf, and the immediate coast, the young geologic structures indicate contemporary shortening in a direction approximately parallel to the

Juan de Fuca-North American plate compression vector.

SHORTENING AND STRESS DIRECTIONS IN THE PACIFIC NORTHWEST

For the central part of the Pacific Northwest continental margin, the analysis of magnetic anomalies indicates relative convergence between the Juan de Fuca and North American plates of 35 mm yr^{-1} along $N50^\circ E$, or 32 mm yr^{-1} normal to the continental margin [Riddiough, 1977]. The convergence rate has decreased sharply in the last 4.5 m.y. Two fragments of the Juan de Fuca plate appear to be moving independently of the main plate. North of the Nootka Fault Zone, the Explorer plate is moving $N6^\circ E$ at 19 mm yr^{-1} relative to North America and 14 mm yr^{-1} normal to the Vancouver Island continental margin [Riddiough, 1977]. South of $42^\circ N$ the Gorda plate is moving north, parallel to

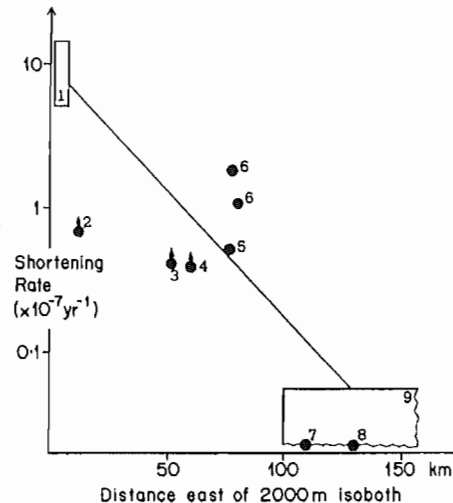


Fig. 12. Composite profile of shortening rate eastwards from the Juan de Fuca-North American plate boundary (represented by the 2000 m isobath). Note logarithmic scale. Straight line (with equation $y = 10^{-6} \exp(-0.04 x)$) represents suggested rapid decay of shortening rate eastwards. Data are 1, folding and thrusting of marginal folds [Barnard, 1978]. 2, folding of marginal folds [Carson et al., 1974]. 3, folded unconformity on shelf. 4, tilted terrace at Cape Blanco. 5, leveling near Bandon. 6, tilted terraces at Cape Arago. 7, terrace on Siuslaw River. 8, terrace on Siletz River. 9, range of values for leveling across coast ranges.

7

Late Quaternary Tectonic Deformation in the Cape Arago-Bandon Region of Coastal Oregon as Deduced From Wave-Cut Platforms

GALAN W. MCINNELLY¹ AND HARVEY M. KELSEY

Department of Geology, Western Washington University, Bellingham

The Cape Arago region of south central Oregon sits on the upper plate of the Cascadia subduction zone about 80 km east of the base of the continental slope. The style of late Pleistocene deformation along the Cascadia forearc near Cape Arago is well expressed by the altitudinal variation of a set of five uplifted wave-cut platforms. These platforms record open folding, with a half wavelength of about 6-7 km, as well as late Quaternary offset on flexural-slip reverse faults that parallel bedding in the underlying bedrock. The folds have produced both landward and seaward tilts to the uplifted wave-cut platforms. Because the folds cut obliquely across the coastline, the magnitude of coastal uplift is variable. In the case of the lowest, 80 ka wave-cut platform, this variable uplift has resulted in coastal deformation ranging from subsidence to a maximum uplift rate of 0.8 m/kyr. Quantitative analysis of the mechanism of flexural slip folding for the South Slough syncline near Cape Arago indicates that the late Quaternary strain rate has decreased in the last 200 kyr. Evidence of past great subduction-style earthquakes, such as regional uplift and regional landward tilting of wave-cut platforms, or regional submergence of coastlands, is lacking in the Cape Arago region. Instead, the deformational style is controlled by folding. Though localized folding is dominant, the occurrence of great subduction-style earthquakes is not precluded because localized folding could occur concurrently with regional coseismic deformation.

INTRODUCTION

Late Pleistocene marine terraces, formed by wave abrasion during interglacial and interstadial eustatic high stands of sea, are preserved in several localities along the Cascadia forearc [Griggs, 1945; Adams, 1984; West and McCrumb, 1988; R. J. Janda, Field guide to Pleistocene sediments and landforms and soil development in the Cape Arago-Cape Blanco area of Coos and Curry Counties, southern coastal Oregon, Friends of the Pleistocene, hereinafter referred to as unpublished guidebook, 1970]. Such platforms represent spatial and temporal reference surfaces from which the style, rates, and mechanisms of supracrustal tectonic deformation may be deduced [Lajoie, 1986].

One of the best areas within the Cascadia forearc for analysis of tectonic deformation of marine terraces is the Cape Arago region of southwestern Oregon (Figure 1). At Cape Arago a flight of five marine terraces, four of which are extensively preserved, have been uplifted and deformed [Griggs, 1945; Baldwin, 1945, 1966; Lund, 1973; Ehlen, 1967; Beaulieu and Hughes, 1975; Armentrout, 1980; Adams, 1984; R. J. Janda, unpublished guidebook, 1970]. Cape Arago is 52 km north of Cape Blanco in the southern portion of the Cascadia subduction zone and lies within 80 km east of the Cascadia trench (Figure 1, inset). The three youngest terraces at Cape Arago are the Whisky Run, Pioneer, and Seven Devils terraces, respectively [Griggs, 1945]. The fourth terrace is the Metcalf terrace [Adams, 1984]. The fifth and oldest terrace is herein informally designated as the Arago Peak terrace.

The marine terraces are cut into sediments that range in age from Eocene to Pliocene [Baldwin, 1966; Armentrout, 1980]. Most of the rocks are part of an Eocene and Oligocene

overlap assemblage in the Oregon coast ranges and consist of arkosic sandstones, siltstones, and mudstones. Sediments of the "Miocene beds" and the Pliocene Empire Formation [Armentrout, 1980] overlie the Eocene and Oligocene bedrock on the margins of Coos Bay near Charleston.

The northern portion of the study area (Figure 1) is underlain by the north plunging South Slough syncline. The syncline is an asymmetric fold, steeper on the west limb, with an axis that coincides with South Slough [Baldwin, 1966] (Figures 1 and 2). Initiation of folding began at least by pre-Miocene time based on the angular discordance between Oligocene and Miocene sediments [Armentrout, 1980; Baldwin, 1966].

On the basis of marine terrace tilting and geodetic leveling surveys, Adams [1984] reported shortening rates of as much as 25 mm/yr within the westernmost continental margin in the vicinity of Cape Arago. Adams [1984] suggested that the eastward (landward) tilt of the terraces at Cape Arago is, in large part, due to progressive tightening of the underlying South Slough syncline. On the basis of volumetric considerations of a growing fold, Adams predicted interruptions of the smooth eastward tilt of the Cape Arago terraces by successive bedding-plane flexural-slip faults. One such bedding-plane fault displaces the Whisky Run terrace platform at Yoakam Point [Baldwin, 1966; Adams, 1984] (Figure 2).

The purpose of our paper is to document late Pleistocene and Holocene deformation along the Cascadia subduction zone in the Cape Arago to Bandon portion of the Oregon coast (Figure 1). We analysed deformation by mapping the distribution, structure, and altitudinal variation of uplifted wave-cut platforms. In light of the uncertainty surrounding the response of the Cascadia forearc to subduction [Heaton and Kanamori, 1984; Atwater, 1987; Spence, 1989] the distinction between a deformation event restricted to a few folds near Cape Arago and a more regional deformation event that includes local folds is significant. Therefore a second purpose of our paper is to comment on the role of local folds in subduction tectonics, using the late Quaternary

¹Now at Geo Engineers, Bellevue, Washington.

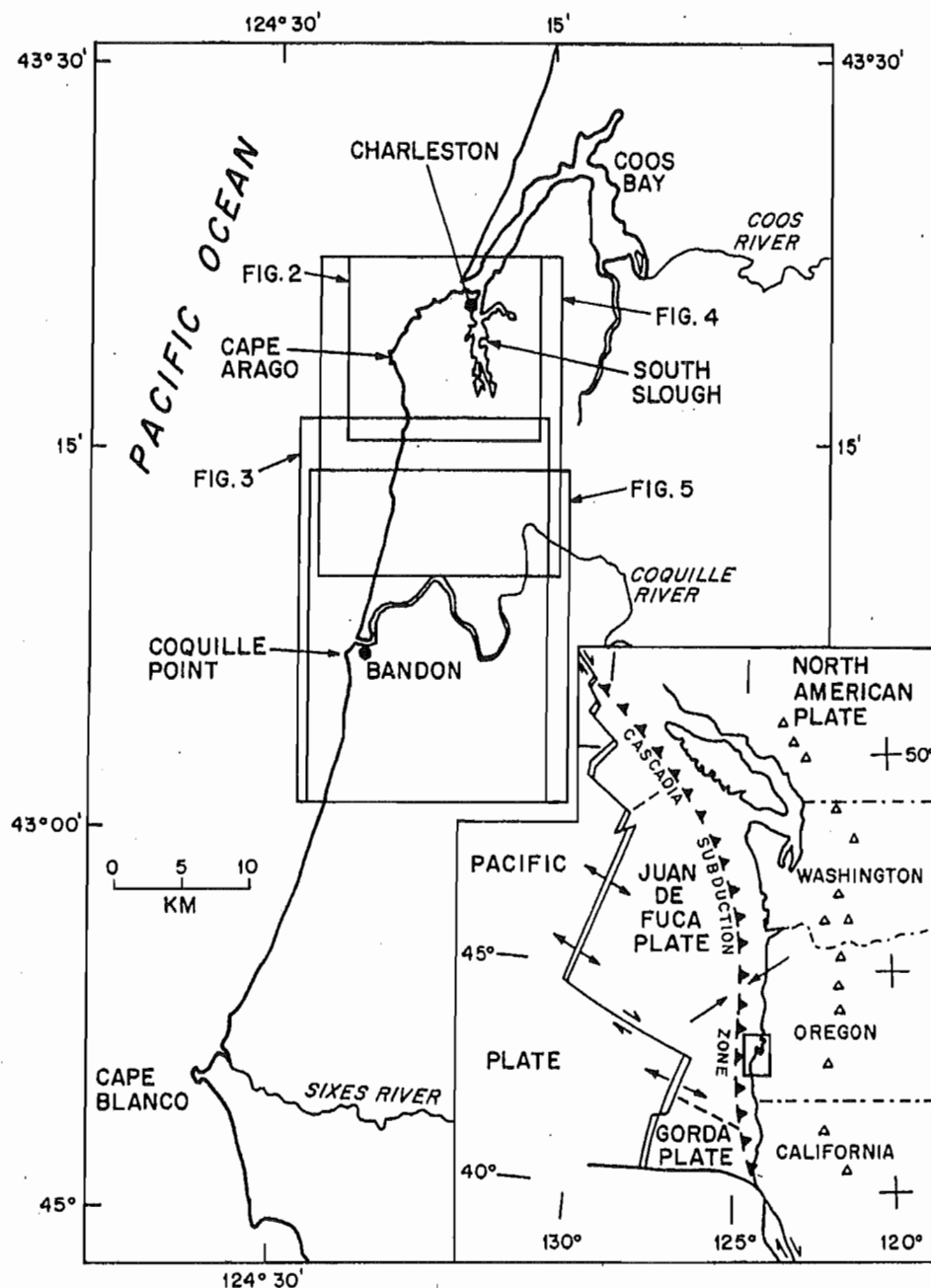


Fig. 1. Location map of the study area (boxes locate Figures 2-5) within the context of the regional tectonic setting of the Pacific Northwest and the Cascadia subduction zone (inset). Triangles are volcanoes of the Cascade Range.

folds in the Cape Arago-Bandon region as a basis of discussion.

DISTRIBUTION OF MARINE TERRACES

We differentiated marine terraces on the basis of elevation and degree of erosional dissection. Marine terrace distribution in all cases except for the area immediately east of South Slough closely follows terrace distribution as originally mapped by Griggs [1945]. For these terraces, platform elevations were obtained by altimeter survey (error of ± 2 m) or well log data (error of ± 6 m). All altimeter surveys were closed on either a U.S. Geological Survey bench mark or point of known altitude. We obtained platform altitudes along the coast exclusively by altimeter survey. Quantitative

analysis of uplift history and strain rate (see below) used only elevation data obtained by the more accurate altimeter method.

East of South Slough, marine terraces were previously undifferentiated. In this area we mapped terrace distribution exclusively by aerial photograph interpretation. With the exception of coastal exposures we obtained relatively limited and poorer quality platform altitude data in this area.

The four younger terraces (Whisky Run, Pioneer, Seven Devils, and Metcalf) are regionally extensive and extend from Coos Bay to about 12 km south of Bandon (Figures 2 and 3). Highly dissected remnants of the fifth and oldest terrace (Arago Peak terrace) are found only at higher elevations on the Cape Arago headlands (Figure 2). The terrace

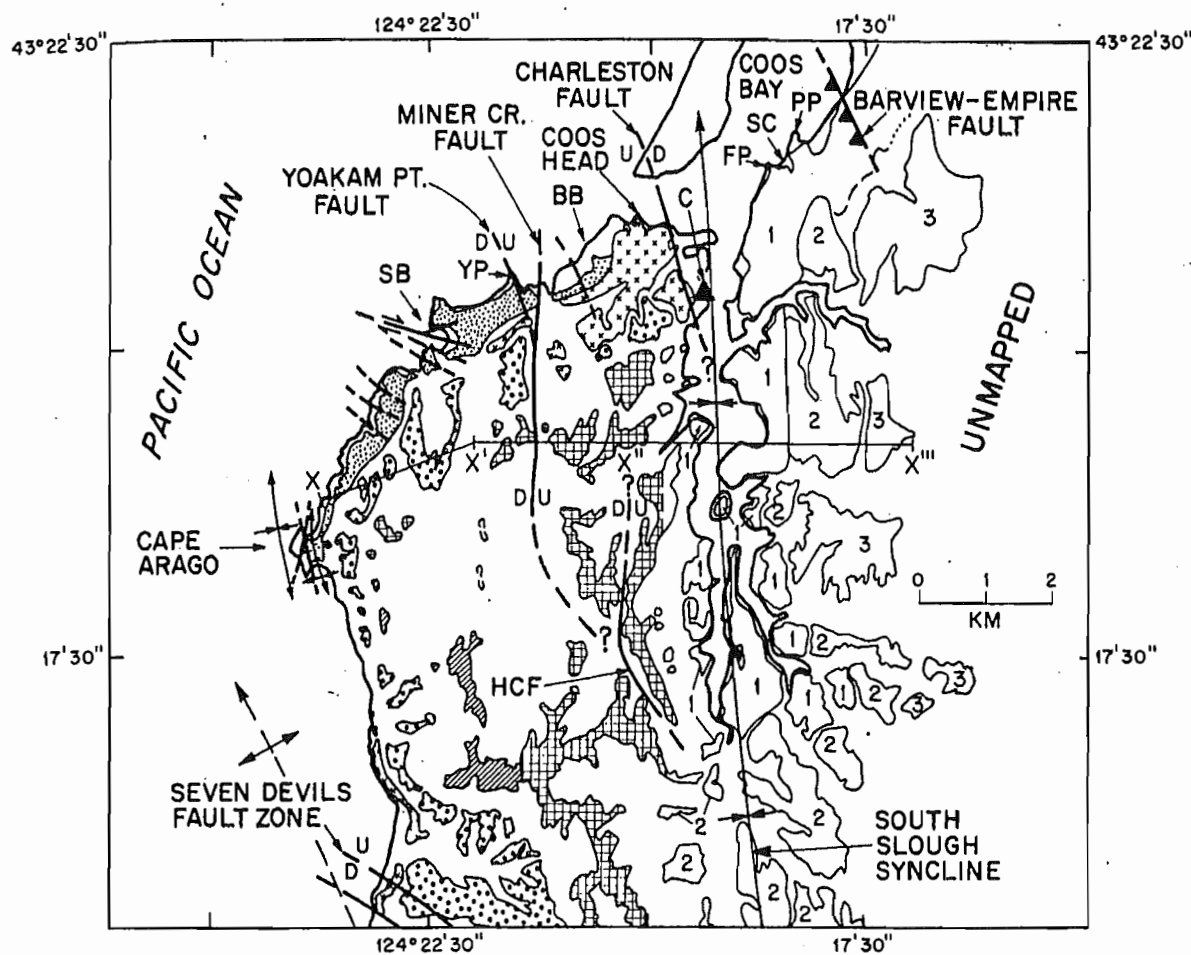


Fig. 2. Map showing distribution of late Pleistocene marine terrace sediments for the five uplifted surfaces in northern portion of study area. Map units for cover sediments on Quaternary wave-cut platforms: solid circles, Whisky Run; crosses, Pioneer; open circles, Seven Devils; checked pattern, Metcalf; diagonal shading, Arago Peak. Map units for cover sediments on Quaternary wave-cut platforms east of South Slough: 1, lowest surface; 2, middle surface; 3, upper surface. SB, Sunset Bay; YP, Yoakam Point; BB, Bastendorff Beach; CH, Coos Head; C, Charleston; FP, Fossil Point; SC, Stinky Cove; PP, Pigeon Point; HCF, Hayward Creek fault. Onshore structural data in part from Baldwin [1966], Ehlen [1967], R. J. Janda (unpublished guidebook, 1970), and Armentrout [1980]. Offshore data from Newton *et al.* [1980] and Clarke *et al.* [1985].

surfaces are moderately to well dissected in the northern portion of the study area (Figure 2). In contrast, in the southern portion of the study area the lower three terraces form a relatively undissected, broad coastal plain at lower elevations (Figure 3).

The Whisky Run and Pioneer terraces are younger and therefore, in general, better preserved than the Seven Devils and Metcalf terraces (Figures 2 and 3). Between Cape Arago and Charleston the Whisky Run terrace forms a prominent, nearly continuous surface.

We recognize three distinct surfaces to the east and northeast of South Slough (Figure 2). Individual surfaces are less apparent because relatively low uplift rates east of the South Slough syncline have minimized spacial separation of Pleistocene wave-cut platforms [Adams, 1984]. There is presently no basis, other than altitude, for correlation of these surfaces with surfaces across South Slough to the west.

We follow previous workers and tentatively correlate the lowest surface east of South Slough with Whisky Run terrace [Baldwin, 1966; R. J. Janda, unpublished guidebook,

1970]. However, the presence of the Charleston fault (Figure 2) raises the possibility that the platform underlying this lowest surface may be correlative with the Pioneer platform. Alternatively, the platform may have been cut in Pioneer or Seven Devils time and reoccupied by the Whisky Run eustatic sea level high stand. We retain the Whisky Run terrace designation for the lowest surface but acknowledge that the surface may be older than Whisky Run.

Marine cover sediments of the Metcalf, Seven Devils, Pioneer, and Whisky Run terraces vary in thickness from about 2.5 to 20 m (Table 1). Sediments on terraces in the Cape Arago area are generally no thicker than about 6 m, although the sediments of the Pioneer terrace are about 15 m thick near Coos Head (Figure 2). South of the Cape Arago headland, sediment thicknesses for the three lower terraces increase to about 20 m. The variation in sediment thickness on the modern wave-cut platforms in the Cape Arago area is consistent with the variation in sediment thickness on late Pleistocene wave-cut platforms, as described by Peterson *et al.* [1987]. The present coastline to the northeast of the Cape Arago headland is generally stripped of sand, while beaches

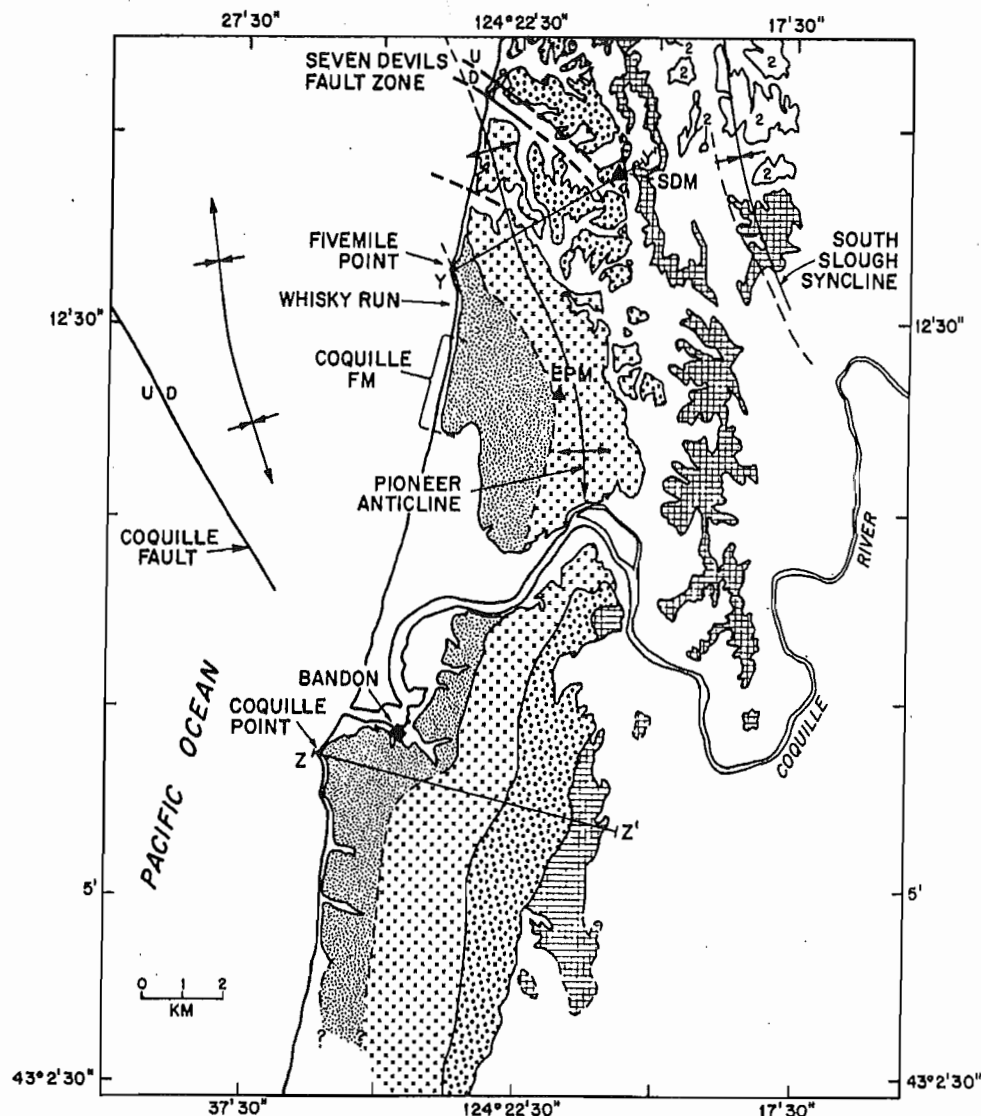


Fig. 3. Map showing distribution of late Pleistocene marine terrace sediments for the four extensively preserved surfaces in southern portion of study area. For explanation of map units, see caption for Figure 2. Triangles locate placer mines: SDM, Seven Devils Mine; EPM, Eagle-Pioneer Mine. Offshore data from Newton *et al.* [1980] and Clarke *et al.* [1985].

to the south of the headland have relatively thick accumulations of sand; cover sediments on the uplifted terraces show the same pattern.

DEFORMATION OF WAVE-CUT PLATFORMS

Overview

Differential uplift of wave-cut platforms along the coast reflects late Quaternary folding and faulting of the underlying bedrock. Platforms west of South Slough rise to the southwest from Coos Head to maximum elevations in the vicinity of Cape Arago, where the oldest platform is uplifted to 212 m (Figures 2 and 4). The platforms also descend gradually to the south from Cape Arago and reach elevation minimums 12–15 km south of Bandon (Figures 4 and 5). The Whisky Run platform descends from a high point at Cape Arago (35 m) to sea level just north of the Coquille River (Figures 4 and 5). South of the Coquille River, the Whisky Run platform is

again emergent and again descends to sea level near the southern boundary of the study area (Figure 5).

East of South Slough, terrace cover sediments have been uplifted to about 90 m [Griggs, 1945]. The terrace surfaces slope toward South Slough (Figure 6).

Deformation Associated With South Slough Syncline

Evidence for late Quaternary growth of the South Slough syncline comes from the more steeply dipping and better exposed west limb. On the west limb, wave-cut platforms are back tilted from initial seaward dips of about 1° (seaward dip estimate from Bradley and Griggs [1976]). The back tilted platforms dip toward the axis of the syncline [Griggs, 1945; Adams, 1984; R. J. Janda, unpublished guidebook, 1970]. On the basis of platform elevation data (Figure 4) the Metcalf platform dips about N60°E (downdip) with a slope of 1.0° between Cape Arago and Charleston. The relative north versus east component of tilt for the Seven Devils, Pioneer,

11

TABLE 1. Characteristics of Marine Terraces: Cape Arago Region

Terrace	Radiometric Age, ka	Preservation and Occurrence	Platform Elevation Range, m	Backedge Elevation Range, m	Terrace Sediment Thickness, m	Faults Cutting Terrace Platforms
Whisky Run	80 ^a	well preserved, regionally extensive	0-35	0-31	3-20	Miner Creek Yoakam Point Bastendorf Beach Barview-Empire Sunset Bay Coquille (?)
Pioneer	...	well preserved, regionally extensive	5-60	15-60	4-20	Miner Creek Charleston Yoakam Point (?) Sunset Bay (?)
Seven Devils	...	well preserved, regionally extensive, moderately dissected	43-104	50-91	3-18	Miner Creek Seven Devils
Metcalf	...	moderately well preserved, regionally extensive, highly dissected	87-167	169-?	3-16	Miner Creek Hayward Creek
Arago Peak	...	poorly preserved, extremely limited, highly dissected	212	?	17 (?)	?

^aMuhs *et al.* [this issue] and Kennedy *et al.* [1982].

and Whisky Run terraces cannot be resolved from the spatial distribution of altitude data. However, these data are consistent with a N60°E tilt direction (Figure 4). Altitude differences between Cape Arago and the Coos Head-Charleston area for the Metcalf, Seven Devils, Pioneer, and Whisky Run platforms are 82, 47, 36, and 16 m, respectively. The increasing altitudinal difference documents the progressive tilting of the west limb of the syncline in the late Pleistocene.

On the west limb of the syncline, bedding-plane, flexural-slip faults parallel to the bedding planes of the underlying folded strata offset the wave-cut platforms up to the east (Figures 6 and 7). The structural blocks defined by these faults are rotated down to the east and movement on these faults accommodates strain during tightening of the syncline [Adams, 1984; McInnelly *et al.*, 1989]. Three bedding-plane faults cut the Whisky Run platform east of Sunset Bay (Figures 4 and 7). Vertical displacements of the Whisky Run platform on the Yoakam Point [Baldwin, 1966], Miner Creek, and Bastendorf Beach faults are 4, 5, and 4 m, respectively. Flexural-slip faults also cut the Metcalf and/or Seven Devils platforms (Figures 2, 4, and 6) (Table 1). Minimum vertical displacements of the Metcalf wave-cut platform are 25 and 6 m for the Miner Creek (Figure 6) and Hayward Creek faults, respectively. A possible third bedding-plane fault may offset the Seven Devils platform by as much as 12 m (Figure 6, segment X-X').

The Charleston fault (Figure 4) displaces the Pioneer platform by 19 m in a down-to-the-east sense of displacement. Compared to other faults west of South Slough, the Charleston fault has an opposite offset sense, cuts across bedding planes of the Tertiary bedrock and is steeply dipping to subvertical. The main fault plane is not exposed, but mesoscale faults directly adjacent to the main fault are steeply dipping, conjugate normal faults. On the basis of a mapped trend of N15°W, the Charleston fault may be the onshore extension of one of a group of north-northwest trending, up-to-the-west faults that deform seafloor sediments northwest of Coos Bay [Clarke *et al.*, 1985].

The Charleston fault appears to be a more regionally significant fault than the neighboring flexural-slip faults. The fault separates steeply dipping (40°-70°) beds on the west limb of the South Slough syncline from gently dipping (12°-30°) beds on the east limb. In addition, the fault has displaced the Whisky Run wave-cut platform such that if this platform is projected eastward across the Charleston fault to the axis of the South Slough syncline, the platform is approximately 20 m above sea level. In the absence of offset and tilt due to the Charleston fault the Whisky Run platform would probably project below the level of South Slough. The 19 m offset on the Charleston fault may be therefore younger than the Whisky Run platform.

Holocene Deformation on the Shores of Outer Coos Bay

The eastern shoreline of outer Coos Bay (Figure 2) provides evidence for Holocene growth of the South Slough syncline. Along this shore the Whisky Run platform undulates above and below sea level at least twice. At one locality, platform submergence is associated with offset on the low angle Barview-Empire fault (Figures 2 and 4).

The Barview-Empire fault is inferred to be a thrust fault on the basis of mesoscale thrust faults exposed in the overlying terrace cover sediments above the fault trace. Slip indicators for the mesoscale faults show dip-slip motion. The inferred thrust fault is coplanar with bedding (N25°W, 28°SW) of the underlying Miocene beds and we infer that the Barview-Empire fault is a flexural-slip fault similar to bedding-plane faults west of South Slough.

A group of five drowned Sitka spruce stumps occur within the intertidal zone on the downthrown side of the Barview-Empire fault. The stumps are 0.6-1.5 m below the rooting level of adjacent living Sitka spruce trees. The stumps occur only in proximity to the fault and therefore appear to be related to displacement on the fault. Samples from two of the drowned stumps yield ages of 220 ± 50 ¹⁴C years B.P. (Beta

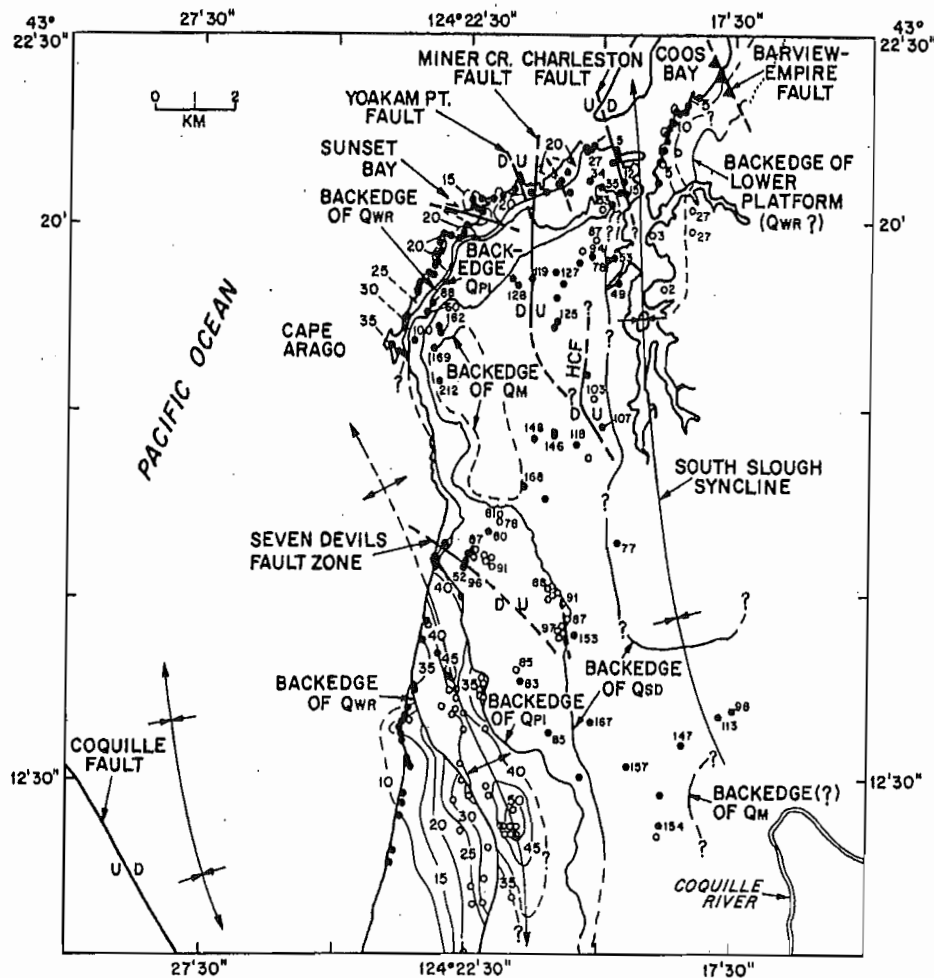


Fig. 4. Wave-cut platform elevation and contour map showing postemergence platform deformation, northern portion of study area. Contour interval is 5 m. Note the northeast dip of all wave-cut platforms on the west limb of the South Slough syncline between Cape Arago and outer Coos Bay. Late Pleistocene to Holocene(?) folding and faulting has warped the wave-cut platforms in the southern portion of the figure. Solid circles are altimeter survey locations, open circles represent platform altitudes calculated from water well logs or minerals exploration boreholes. Labeled backedges on the figure refer to the position of the shoreline angle for the following marine terraces: Qwr, Whisky Run; Qpi, Pioneer; Qsd, Seven Devils; Qm, Metcalf; HCF, Hayward Creek fault. Offshore data from Newton *et al.* [1980] and Clarke *et al.* [1985].

analytic sample Beta-23276) and modern (A. R. Nelson, personal communication; 1988; University of Pittsburgh sample Pitt-185). On the basis of the age of the stumps, we infer late Holocene activity on the Barview-Empire fault. The Whisky Run wave-cut platform is also submerged at Pigeon Point (PP, Figure 2), 1 km southwest of the Barview-Empire fault, and this abrupt change in elevation may be fault controlled as well.

Pioneer Anticline and Coquille Fault

To the southwest and south of the South Slough Syncline, platform warping is controlled mainly by the Pioneer anticline. The northwest trending Pioneer anticline is delineated by the structure contours of the Pioneer wave-cut surface (Figure 4). The half wavelength of the Pioneer anticline is about 6–7 km. The east limb of the Pioneer anticline is cut by high-angle reverse faults of the Seven Devils fault zone (Figure 8). The N50°W strike of the Seven Devils fault zone matches the strike of the underlying Eocene siltstone. Both the reverse sense of slip and the coplanarity of the fault zone

and bedding (Figure 8) lead us to suggest the Seven Devils fault is a bedding-plane flexural-slip fault as well. The Seven Devils fault zone extends to the Seven Devils Mine area (SDM, Figure 3) where Griggs [1945] documents a northwest striking fault which cuts Seven Devils terrace sediments. The fault last moved prior to cutting of the Pioneer terrace, which is not deformed by the fault zone.

Between Fivemile Point and the mouth of the Coquille River the southwest dip of the Whisky Run platform is related to folding of the Pioneer anticline. An abrupt gain in elevation at Coquille Point (Figure 5), however, is accompanied by a distinctive change in platform tilt from southwest to west. This abrupt elevation gain and change in tilt may correspond to an onshore extension of the informally designated Coquille fault (Figure 5). Offshore, the Coquille fault trends N30°W and displaces Pleistocene sediments in a down-to-the-northeast sense [Clarke *et al.*, 1985]. The extrapolated southeast extension of the fault intersects the coast at the mouth of the Coquille River (Figure 5). The wave-cut platforms south of the Coquille River generally dip

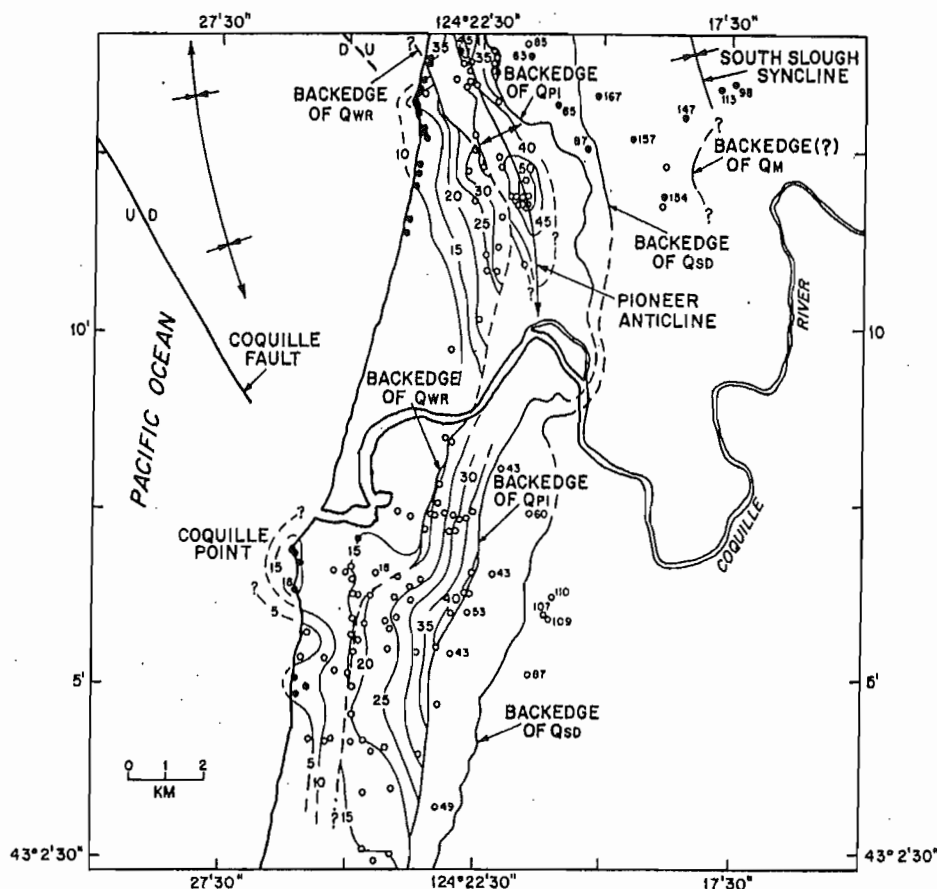


Fig. 5. Wave-cut platform elevation and contour map showing postemergence platform deformation, southern portion of study area. Also shown are offshore structures in this area. Contour interval is 5 m. Note that the Whisky Run platform descends below sea level north of the Coquille River and rises abruptly to 18 m south of the Coquille River. Platforms south of the Coquille River dip seaward in contrast to the back tilted platforms in the vicinity of Cape Arago. Terrace platform elevations gradually descend south of the Coquille River and dip below sea level south of the study area. Symbols and abbreviations are the same as for Figure 4. Offshore data from Newton *et al.* [1980] and Clark *et al.* [1985].

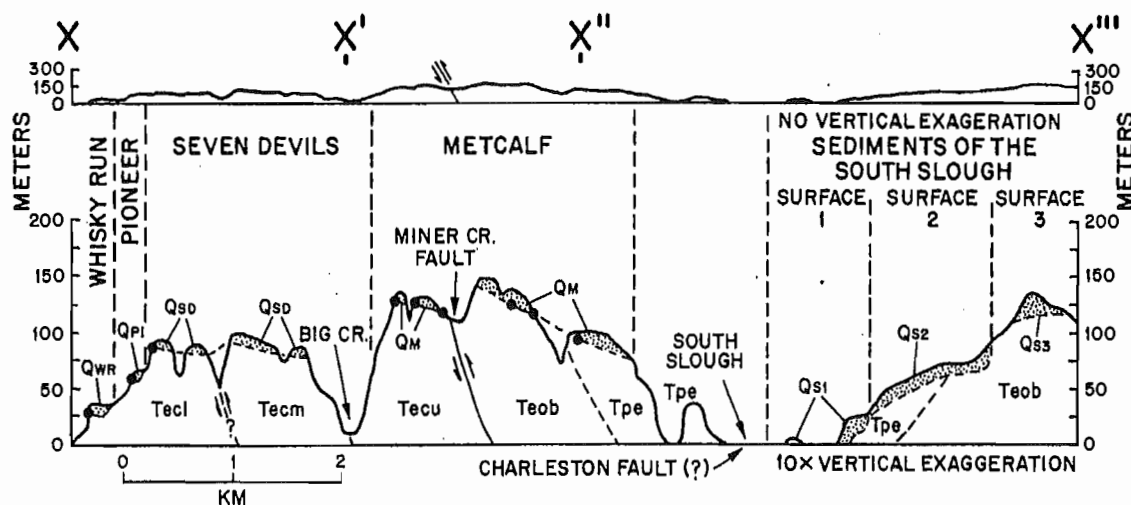


Fig. 6. Northeast to east trending cross section (view to north) showing tilting and faulting of wave-cut platforms near Cape Arago. Differential back tilt of the wave-cut platforms occurs due to offset on flexural-slip faults such as the Miner Creek fault. Surfaces 1, 2, and 3, east of South Slough, slope west toward the syncline axis. Bedrock stratigraphy: Tpe, Pliocene Empire Formation; Totp, Oligocene Tunnel Point Formation; Teob, Eocene-Oligocene Bastendorff Formation; Tecu, Eocene Coaledo Formation, upper member; Tecm, Eocene Coaledo Formation, middle member; Tecl, Eocene Coaledo Formation, lower member; Tees, Eocene Elkton Siltstone Formation. See Figure 2 for location of cross section X to X'''.

14

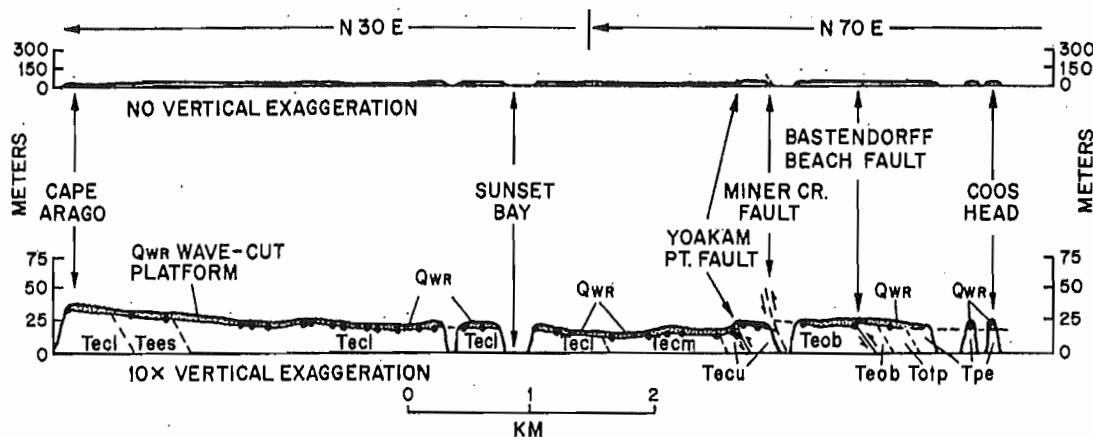


Fig. 7. Post-80 ka deformation of the Whisky Run wave-cut platform is illustrated in this coastwise transect from Cape Arago to Coos Head (view to northwest and north-northwest). Solid circles are altimeter survey locations. Data are projected onto a line that trends N30°E from Cape Arago to Sunset Bay, then N70°E to Coos Head. The gradual descent of the Whisky Run Wave-cut platform from Cape Arago to Coos Head is interrupted repeatedly by flexural-slip faults at Yoakam Point, Miner Creek, and Bastendorff Beach. Geologic units are same as previous figure.

west, except the Whisky Run platform at Coquille Point where it is slightly back tilted (Figures 5 and 9).

TERRACE AGES

We obtained a revised, numerical age estimate for the Whisky Run terrace and a correlation age estimate for the Pioneer terrace. Age assignments for the older terraces are speculative.

To obtain a numerical age estimate for the Whisky Run terrace, we collected fossils for U series, amino acid, and oxygen isotope analyses. Solitary corals (*Balanophyllia ele-*

gans) and bivalve mollusks (*Saxidomus giganteus* and *Mya truncata*) were collected at Coquille Point (U.S. Geological Survey (USGS) locality M2798; Los Angeles County Museum of Natural History (LACMNH) locality 2636), and bivalve mollusks were collected at Cape Blanco (USGS locality M1450 and M1452; LACMNH locality 2641). Analyses of the fossils from both localities are reported by *Muhs et al.* [this issue].

U series analyses of the fossil coral yields an age of 83 ± 5 ka for the Whisky Run terrace at Coquille Point [*Muhs et al.*, this issue]. *Kennedy et al.* [1982] reported a U

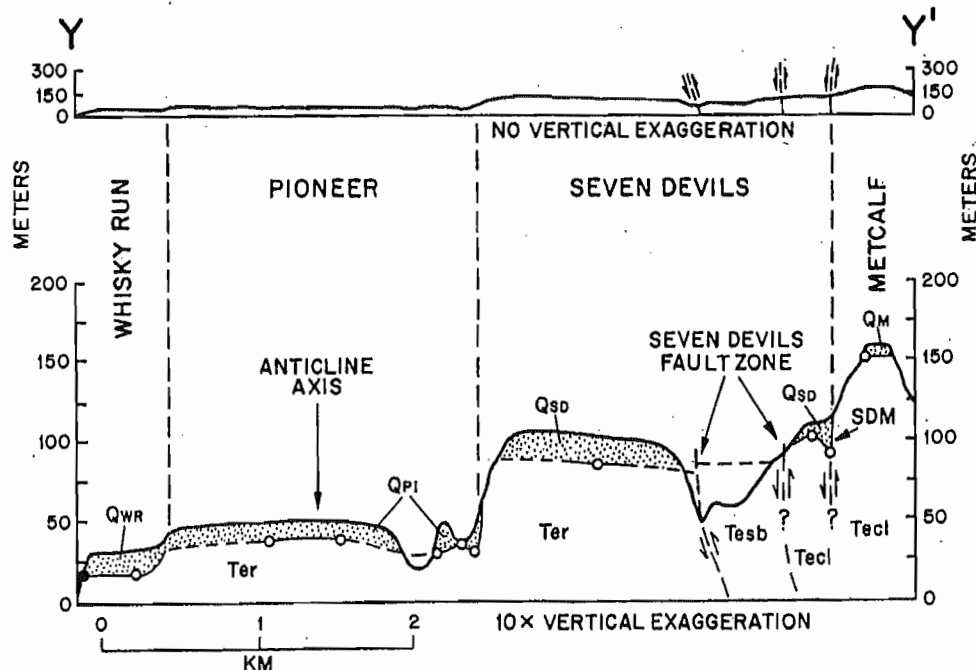


Fig. 8. Cross section Y-Y' (view to northwest) showing anticlinal warping of the Pioneer wave-cut platform. The section is located in the transition zone between wave-cut platforms with eastward tilts (northern portion of study area) and platforms with westward tilts (southern portion of study area). Bedrock stratigraphy: Ter, Eocene Roseburg Formation; Tesb, Eocene Sacchi Beach Beds; Tecu, Eocene Coaledo Formation, lower member. SDM is the Seven Devils placer mine. Displacement of the Seven Devils platform in the Seven Devils fault zone is accommodated either within the siltstone of the Sacchi Beach Beds or along the formation contacts. See Figure 3 for location of cross section.

15

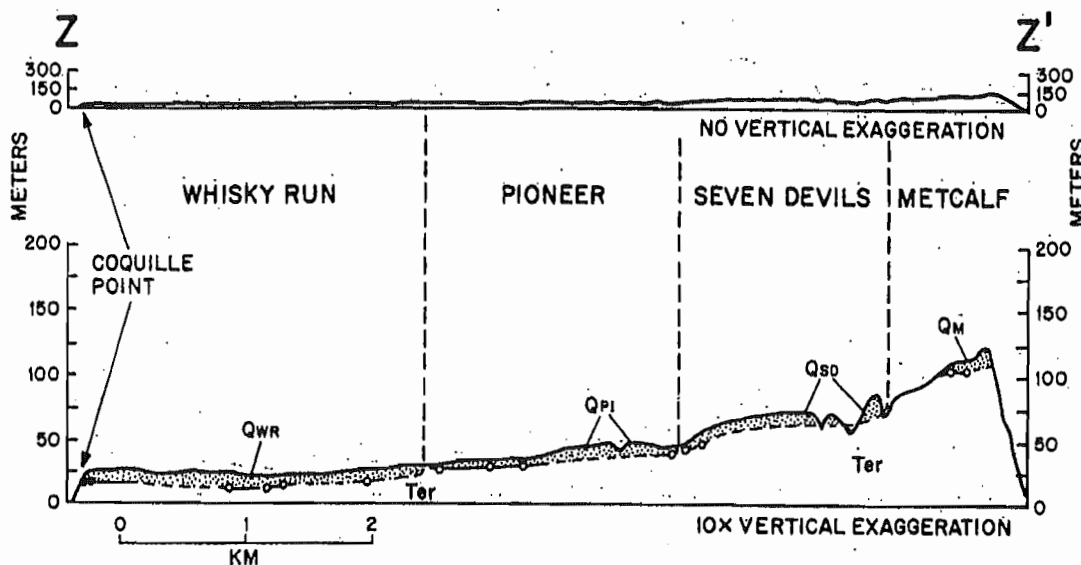


Fig. 9. Cross section Z-Z' (view to north) showing only slightly deformed wave-cut platforms in southern portion of study area. Solid circles are altimeter survey locations; open circles represent altitudes derived from water well logs. Terrace platforms dip seaward, and younger platforms show successively less relief at backedges. A slight downwarping of the Whisky Run platform can be seen east of Coquille Point. See Figure 3 for cross-section location.

series age of approximately 72 ka determined on fossil coral from the same locality but noted isotopic discordance in their fossil corals. *Muhs et al.* [this issue] correlate the Whisky Run wave-cut platform at Coquille Point with the circa 80 ka eustatic high stand of sea level (deep-sea isotope stage 5a) of *Mesolella et al.* [1969] and *Shackleton and Opdyke* [1973]. Amino acid and oxygen isotope data from bivalve shells collected at Cape Blanco suggest that the two lowest terraces at Cape Blanco, the newly designated Cape Blanco terrace [*Muhs et al.*, this issue; *Kelsey*, 1990] and the Pioneer terrace [*Janda*, 1969, also unpublished guidebook, 1970], are probably correlative with the 80 and 105 ka sea level high stands, respectively [*Muhs et al.*, this issue]. Platform elevation data, determined from water well logs, show physical continuity between the 105 ka Pioneer wave-cut platform at Cape Blanco and the Pioneer wave-cut platform at Coquille Point. Therefore the Pioneer platform at Coquille Point was probably formed during the circa 105 ka sea level high stand.

A minimum feasible age for the Seven Devils wave-cut platform is 125 ka, which is the age of the interglacial high stand of sea level that directly preceeded the 105 ka high stand. It is possible that the 125 ka terrace was totally removed in the Cape Arago area due to coastal retreat, in which case the Seven Devils terrace is older than 125 ka. We feel our 125 ka age assignment is feasible because the 125 ka sea level was 6 m above present sea level [*Ku et al.*, 1974; *Harmon et al.*, 1983] and platforms attributed to this high stand are present worldwide on both tectonically stable and uplifted coastlines (see review by *Muhs et al.* [this issue]).

The Metcalf terrace must have been cut during a relatively high stand of the sea sometime in the late Pleistocene prior to 125 ka. A minimum age of platform cutting for the Metcalf is about 200 ka (oxygen isotope stage 7 of *Shackleton and Opdyke* [1973]). On the tectonically stable platform of Bermuda, sea level was at 2-m elevation at about 200 ka [*Harmon et al.*, 1983]; and data from Barbados [*Bender et al.*, 1979] and from the tectonically stable New Providence

Islands of the Bahamas [*Muhs and Bush*, 1987; D. R. Muhs, personal communication, 1989] also lead to the conclusion that sea level was a few meters above present at about 200 ka. We recognize, however, that the age of the Metcalf platform could be significantly older than 200 ka.

RATES OF DEFORMATION

Uplift Rates

Maximum rates of uplift for wave-cut platforms at Cape Arago range from 0.5 to 0.8 m/kyr (Table 2). Calculation of maximum uplift rate depends on the age of the platform, the elevation of paleo-sea level (with respect to present sea level) at the time of platform formation, and the present elevation of the platform. In order to calculate alternative uplift rates we employed two different Pleistocene paleo-sea level curves, one for New Guinea [*Bloom et al.*, 1974; *Chappell and Shackleton*, 1986] and one based on data for Japan [*Machida*, 1975] and California and Baja California [*Muhs et al.*, 1988] (Table 2). For platforms that are not landward tilted the shoreline angle (the base of the paleo-sea cliff) is the point of maximum uplift. The shoreline angle is assumed to have been cut during a eustatic sea level high stand and thus represents the paleo-sea level at the time of platform formation. At Cape Arago the wave-cut platforms are tilted landward and the point of maximum uplift for these platforms is seaward of the paleoshoreline angle. Therefore the point of maximum uplift had an initial elevation that was lower than the elevation of paleo-sea level during the time of platform formation. The degree to which the initial elevation is lower than the paleoshoreline angle is dependent on the initial, nontectonic, seaward slope of the wave-cut platform. Modern and ancient wave-cut platforms cut on sandstones similar to the bedrock at Cape Arago have seaward slopes of 20–40 m/km for a 300–600 m wide segment near the backedges and a 7–17 m/km slope farther offshore [*Bradley and Griggs*, 1976]. These seaward slopes are used as a

TABLE 2. Marine Wave-Cut Platforms at Cape Arago: Ages, Uplift Rates, Tilt Rates, and Horizontal Strain Rates

Wave-Cut Platform	Estimated Age, ka	Maximum Elevation, ^a m	Shore-Normal Distance From Shoreline Angle, km	Original Gradient of Platform, m/km	Original Depth of Platform, m	Paleo-Sea Level, m	Sea Level Model ^c	Maximum Uplift Rate, m/kyr	Elevation of Shoreline Angle, m	Uplift Rate at Shoreline angle, m/kyr	Maximum Observed Tilt, ° rad	Tilt Rate rad/yr	Horizontal Strain Rate, yr ⁻¹
Whisky Run	80	35	0.2	20	4	-19 ± 5	NG	0.73 ± 0.07	31	0.63 ± 0.07	2.3 × 10 ⁻³	2.9 × 10 ⁻⁸	0.44 × 10 ⁻⁷
	80	35	0.2	40	8	-19 ± 5	NG	0.78 ± 0.07	31	0.63 ± 0.07			
	80	35	0.2	20	4	-5 ± 2	CA-JP	0.55 ± 0.03	31	0.45 ± 0.03			
	80	35	0.2	40	8	-5 ± 2	CA-JP	0.60 ± 0.03	31	0.45 ± 0.03			
Pioneer	105	68 ^g	0	NA	0	-9 ± 3	NG	0.73 ± 0.03	68	0.73 ± 0.03	5.7 × 10 ⁻³	5.4 × 10 ⁻⁸	0.83 × 10 ⁻⁷
	105	68 ^g	0	NA	0	-2	CA-JP	0.67	68	0.67			
Seven Devils ^h	125	100	0.2	20	4	+6	both	0.78?	98 ^g	0.74?	8.1 × 10 ⁻³ ?	6.5 × 10 ⁻⁸ ?	1.0 × 10 ⁻⁷ ?
	125	100	0.2	40	8	+6	both	0.82?	98 ^g	0.74?			
Metcalf ^h	200?	169	0	NA	0	B+2		0.84?	169	0.84?	17 × 10 ⁻³ ?	8.5 × 10 ⁻⁸	1.3 × 10 ⁻⁷ ?

^aFor Whisky Run and Seven Devils platforms, the maximum elevation near Cape Arago is 200 m seaward (westward) of the paleoshoreline angle. For Pioneer and Metcalf platforms the maximum elevation near Cape Arago is at the paleoshoreline angle. All platforms are landward tilted at Cape Arago.

^bRelative to present sea level.

^cNG, New Guinea model [Chappell and Shackleton, 1986]; CA-JP, California-Japan model [Machida, 1975; Muhs *et al.*, 1988]; B, Bermuda data for 200 ka high stand [Harmon *et al.*, 1983].

^dUncertainties for Whisky Run and Seven Devils wave-cut platforms: (1) paleo-sea level, (2) paleo-water depth during the 80 and 105 ka sea level high stands for the present point of maximum elevation.

^eFor all terrace platforms, tilt is measured from the vicinity of Cape Arago N60°E to the vicinity of South Slough. Tilts measured parallel to the N60°E down-dip direction.

^fSee assumptions for derivation of strain rate in text.

^gElevation is extrapolated from known distance measured in down-tilt direction and using average platform tilt.

^hThe estimated ages of the Seven Devils and Metcalf platforms are minimum ages and not constrained by isotopic data. Therefore all calculated rates based on these ages are maximum rates and are queried because of the large uncertainties.

correction for determining maximum uplift rates on landward tilted platforms (Table 2). For the Whisky Run and Seven Devils wave-cut platforms at Cape Arago, uncertainties in maximum uplift rates are therefore a combination of paleo-sea level uncertainties and the uncertainty as to the paleobathymetry during the 80 and 125 ka sea level high stands at the present points of maximum elevation. Maximum platform elevations on these two terraces are about 200 m westward of the respective terrace shoreline angles, so the correction for landward tilting involves an additional 4–8 m of uplift (Table 2). The maximum elevation of the Pioneer and Metcalf platforms at Cape Arago is at the shoreline angle because these platforms are not extensively preserved at the cape. Therefore no landward tilt correction is necessary for these latter two platforms (Table 2). For the lowest four platforms at Cape Arago we also tabulated uplift rates at the shoreline angle (Table 2) so that we could compare uplift rates among wave-cut platforms. In general, uplift rates increase slightly, within error limits, with increasing age of the terrace (Table 2). However, if the Seven Devils and Metcalf platforms are older than the suggested minimum ages, then there is no consistent trend in uplift rate with increasing age.

Tilt Rates

At Cape Arago the degree of landward tilt increases with increasing age of the wave-cut platform (Table 2). The increasing tilts reflect progressive tilting of platforms on the west limb of the South Slough syncline and also presumably reflects tightening of the syncline throughout late Pleistocene time.

During steady growth of a sinusoidal fold, tilt rates of bedding on the fold limbs decrease as the amount of horizontal shortening increases [Adams, 1984]. If a horizontal surface such as a wave-cut platform is cut across bedding on the limb of such a fold, the wave-cut platform will be tilted at the same rate as the underlying beds. Therefore, as folding progresses, greater amounts of horizontal shortening are required to produce the same degree of tilting for successively younger wave-cut platforms. Constant or decreasing shortening rates will be manifest as a progressive decrease in tilt rates for younger wave-cut platforms. Because tilt rates systematically change with constant shortening rates, horizontal strain rates are more meaningful in terms of analyses of deformation of the fold.

Horizontal Strain Rates

The maximum principal strain direction (direction of maximum contraction) for the South Slough syncline is parallel to the assumed N60°E tilt direction for the tilted wave-cut platforms. The magnitude of the maximum principal strain is

$$\epsilon_z = (L - D)(L^{-1}) \quad (1)$$

where L is the original horizontal length and D is the horizontal length after shortening (Figure 10). The strain rate ϵ'_z is the strain divided by the amount of time over which the strain occurred:

$$\epsilon'_z = (L - D)(L^{-1})(T^{-1}) \quad (2)$$

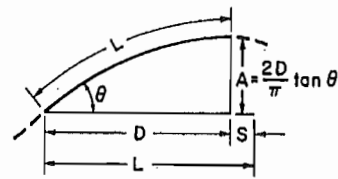


Fig. 10. Geometric relationships for a sinusoidal fold: original length along bedding (L), the horizontal extent across bedding after shortening (D), the amount of horizontal shortening (S), and the maximum flank dip (θ) at the point of inflection of the sinusoidal fold (modified from Rockwell *et al.* [1988]).

In order to calculate horizontal strain rate over time across the South Slough syncline the folded strata of the syncline are assumed to approximate sine curves [Currie *et al.*, 1962], and the syncline is modeled as a flexural-slip, sinusoidal fold using mathematical techniques outlined by Currie *et al.* [1962], Adams [1984], and Rockwell *et al.* [1988]. It is also assumed that original length along bedding is retained during folding, which necessitates that flexural slip must occur along bedding planes. The assumption of a flexural-slip fold mechanism is reasonable because of the occurrence of several flexural-slip faults in the Cape Arago region.

After folding the length L along a geologic stratum (originally a horizontal length) cannot be measured directly and must be calculated from the variable D [Rockwell *et al.*, 1988]:

$$L = (2D/\pi)(E(\theta)/\cos(\theta)) \quad (3)$$

where L is the length along a sine curve or geologic stratum (the original horizontal length) and D is the present horizontal length after shortening measured from the fold axis to the nearest point of inflection. D is therefore one-quarter of a complete sine curve and represents one-quarter of the wavelength of the fold. Theta (θ) is the maximum flank dip of the geologic stratum in the fold (slope of the sine curve), measured at the point of inflection on the fold limb (Figure 10), and $E(\theta)$ is the complete elliptic integral of the second kind (used to approximate the length along a sine curve and described by Weast [1979]). Theta (θ) was measured in the field, and D was measured from a published geologic map [Newton *et al.*, 1980].

To calculate the strain rate, the horizontal shortening rate must be calculated. The horizontal shortening rate is the rate at which the horizontal length D changes with time:

$$\frac{dD}{dt} = \frac{d}{dt} \left[\left(\frac{L\pi}{2} \right) \left(\frac{\cos(\theta)}{E(\theta)} \right) \right] \quad (4)$$

$$\frac{dD}{dt} = \frac{L\pi}{2} \left[\frac{E(\theta) \left(-\sin(\theta) \frac{d\theta}{dt} \right)}{[E(\theta)]^2} \right] - \left[\frac{\cos(\theta) E'(\theta)}{[E(\theta)]^2} \right] \quad (5)$$

$$\frac{dD}{dt} = \frac{L\pi \cos(\theta)}{2 E(\theta)} \left\{ \left[\frac{-E(\theta) \left(\tan(\theta) \frac{d\theta}{dt} \right)}{E(\theta)} \right] - \left[\frac{E'(\theta)}{E(\theta)} \right] \right\} \quad (6)$$

18

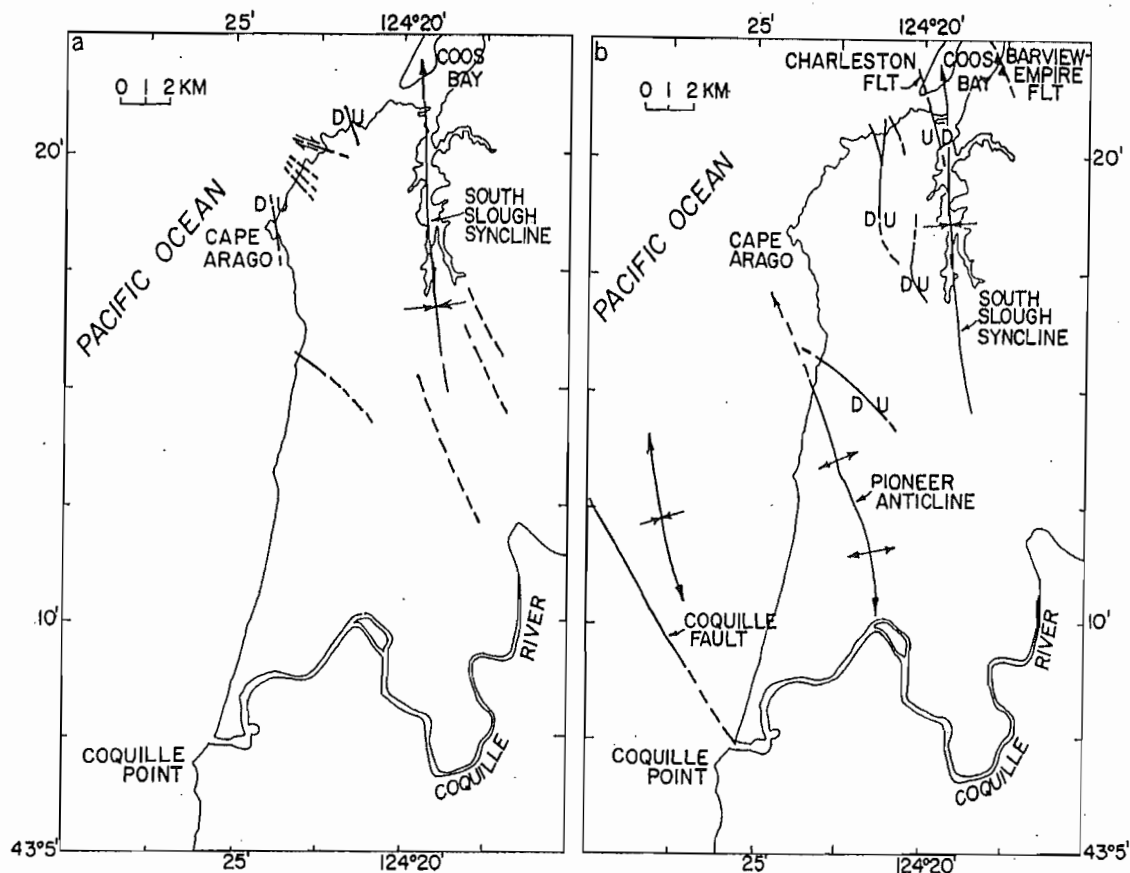


Fig. 11. (a) Tectonic map showing all folds and faults previously mapped in the Eocene to Pliocene bedrock [after Baldwin, 1966; Ehlen, 1967; Newton *et al.*, 1980]. (b) Tectonic map showing folds and faults expressed in late Quaternary wave-cut platforms in the Cape Arago area.

$$\frac{dD}{dt} = -\frac{L\pi \cos(\theta)}{2 E(\theta)} \left\{ \left[\frac{E'(\theta)}{E(\theta)} \right] + \left[\tan(\theta) \frac{d\theta}{dt} \right] \right\} \quad (7)$$

where $E'(\theta)$ is the rate of change of the complete elliptic integral of the second kind for a given change in θ .

Finally, the horizontal strain rate (ϵ'_x , units = yr^{-1}) is calculated by dividing the horizontal shortening rate by the original bedding length L :

$$\epsilon'_x = (dD/dt)(L^{-1}) \quad (8)$$

Application of the above technique to the South Slough syncline requires some relaxation of the assumptions for the model. It is uncertain if the point of inflection actually occurs where maximum flank dip was measured. Thus the measured horizontal distance D may not represent a full one-quarter of the fold wavelength. In addition, the South Slough syncline is not strictly sinusoidal because of the asymmetry of the fold. However, the west limb of the syncline roughly approximates one-quarter of a sine wave.

Recognizing the above uncertainties, evaluation of the deformation of the west limb of the South Slough syncline provides a first-order approximation of late Pleistocene crustal strain rates in the vicinity of Cape Arago. The late Pleistocene strain rates decrease with time (Table 2). In calculating the strain rates we use speculative ages for the Seven Devils and Metcalf platforms. The speculative ages are minimum possible ages, and all alternative ages would yield lower strain rates. Therefore for the two oldest plat-

forms in Table 2, strain rates may not decrease with time. A decrease in strain rate over time would reflect a slowing in the rate of east-west horizontal shortening on the west limb of the South Slough syncline during progressive tightening of the fold. As the total amount of horizontal shortening during folding grows large, horizontal shortening may begin to occur by other mechanisms [Currie *et al.*, 1962]. Therefore the apparent decreasing horizontal strain rates for the west limb of the South Slough syncline may indicate that a component of crustal shortening in the vicinity of Cape Arago is being accommodated elsewhere.

DISCUSSION

Folding: Dominant Style of Deformation

Late Pleistocene deformation of wave-cut platforms in the Cape Arago-Bandon region is dominated by open folds and related flexural-slip, bedding-plane faults. The open folds have half wavelengths of about 6–7 km and subaerially exposed axial lengths of 15–20 km. A comparison of folds and faults that have been previously mapped in the Tertiary bedrock [Ehlen, 1967; Newton *et al.*, 1980] with those that are expressed in the deformed wave-cut platforms (Figure 11) shows that most of the flexural-slip faults are only apparent from offset of late Pleistocene platforms. Furthermore, though the South Slough syncline deforms Eocene strata, the Pioneer anticline is a new fold that has developed in Quaternary sediments but is not apparent in older rocks

(Figure 11). Folding in this region along the Cascadia subduction zone therefore appears to be a persistent style of deformation at least since the late Oligocene, but growth on individual folds can be transitory. Flexural-slip faults are difficult to detect in the Tertiary sediments because they are parallel to bedding planes. The South Slough syncline and the Pioneer anticline are an on-land expression of the landward edge of a fold belt that deforms Cenozoic and Quaternary sediments on the continental shelf of the Cascadia margin [Kulm and Fowler, 1974; Clarke *et al.*, 1985; Peterson *et al.*, 1986].

The folds produce a wide variation in coastal uplift rates where the coastline cuts obliquely across structural trend (Figures 4, 5, and 11). This fold-induced variability in net uplift makes questionable assertions that coastal uplift rate is an indicator of the type of convergent margin [Uyeda and Kanamori, 1979] or the degree of plate interaction [Yonekura, 1983]. To the contrary, local structures can result in a wide range of late Pleistocene coastal uplift rates at any one subduction zone or subduction zone type [Muhs *et al.*, this issue].

While the association of flexural-slip, bedding-plane faults with the open folds is most evident, the folds may also be associated with other faults at depth. The flexural-slip, bedding-plane faults may be seismogenic, but they are not major seismic hazards [Yeats *et al.*, 1981], and such faults are probably not the primary source of seismicity in the Cape Arago-Bandon region. Rather, tightening of the South Slough syncline, subsidence of the axial region, and offset on associated flexural-slip faults may be triggered by reverse faulting on deeper structures.

Though results of our study do not elucidate how the folds grow, from several lines of circumstantial evidence we suggest that these folds may develop during earthquakes. First, in contractional setting similar to the Cape Arago area, earthquakes of magnitude 6.0–7.5 have occurred on blind thrust faults that lie beneath active folds [King and Vita-Finzi, 1981; Stein and King, 1984]. The folds apparently grow episodically during earthquakes generated by movements on these blind faults. Second, several instances of abrupt submergence in the late Holocene are documented in South Slough along the axis of the syncline. Both Nelson [1987, 1988] and Peterson and Darienzo [1989] observed seven to eight instances of abrupt submergence since 4–5 ka in the salt marsh stratigraphy of the slough. At other localities in southwestern Oregon including Coos Bay and the Coquille River estuary (Figure 1), Nelson [1987, 1988] and Peterson and Darienzo [1989] find no evidence of repeated instances of abrupt submergence. Nelson [1988] hypothesized that the local distribution of submerged peat layers in South Slough may record repeated localized Holocene coseismic contraction of the syncline.

We infer that flexural-slip faulting on the wave-cut platforms may occur simultaneously with the postulated coseismic subsidence along the South Slough syncline axis. The best evidence for coseismic flexural-slip faulting is the drowned Sitka spruce stumps in the intertidal zone on the downdropped block of the Barview-Empire fault (Figure 2). The submergence that killed these trees was either a rapid aseismic deformation or, more likely, a coseismic deformation that occurred contemporaneously with abrupt submergence along the syncline axis only 8 km to the southwest. The most recent episode of abrupt submergence of salt

marsh in South Slough, about 200–500 years ago [Nelson, 1988], could have been contemporaneous with the drowning of the Sitka spruce trees on the Barview-Empire fault.

Several observations with regards to the South Slough syncline are open to more than one interpretation. First, the decrease in strain rate on the west limb between 105 ka and the present (Table 2) may reflect a migration of contractional strain to neighboring structures or may reflect that the principal contraction direction is no longer east-west but rather north-south, which is the present direction of regional principal contraction as deduced from historical seismicity [Spence, 1989]. A change to a more northerly direction of principle contraction would result in progressively less contraction of structures with north trending fold axes, such as the South Slough syncline. Second, the role of the Charleston fault is problematic. The fault has the greatest amount of offset (20 m) of all the faults that disrupt the Whisky Run platform. Even though the fault strikes parallel to the syncline axis, the fault does not appear to be a flexural-slip fault because it is steeply dipping and cuts across bedding of the moderately inclined Tertiary strata. One plausible interpretation is that the inferred post-Whisky Run offset on the Charleston fault and the decrease in strain rate on the west limb of the syncline in the last 100 kyr may both be related to changing stress orientations in the Cape Arago region in the late Quaternary.

Regional Vertical Deformation Versus Localized Folding

The Cascadia subduction zone has not experienced historic great earthquakes [Heaton and Kanamori, 1984]. Yet the Cascadia subduction zone has several physical characteristics in common with subduction zones in Alaska, southwest Japan, Chile, and Columbia that have experienced great ($M_w > 8$) subduction-style earthquakes in historic time [Heaton and Kanamori, 1984; Heaton and Hartzell, 1987; Spence, 1989]. In the light of the prevalence of open folding in the forearc of the Cascadia subduction zone in the Cape Arago-Bandon region, as well as in the Cape Blanco region 55 km to the south [Kelsey, 1990], how common are folds along the other subduction zones that have produced great earthquakes?

The most obvious strain that is observed in historic, great subduction-style earthquakes is regional tilting, regional submergence, and regional uplift. For instance, during the 1960 earthquake in Chile and the 1964 earthquake in Alaska, large regions of the forearc (100,000–200,000 km²) underwent coseismic uplift and adjacent regions equally as large (80,000–190,000 km²) underwent coseismic subsidence [Plafker, 1969, 1972]. In southwest Japan, Ota [1986] describes a region of coastal uplift on Muroto Peninsula that developed in response to the 1946 earthquake in the Nankai Trough. The vertical deformation during the earthquake was accompanied by notable landward tilting of a 50-km-wide segment of the coast. Similar landward tilting accompanied coseismic uplift that was associated with the 1964 Alaska and 1960 Chile earthquakes [Plafker, 1972]. Although mapping of the deformation in Chile and Alaska was limited by accessible exposure, the coseismic vertical movements do not appear to have been dominated by development of local structures such as supracrustal folds or faults.

From historic data therefore it is evident that regional

vertical deformation of areas greater than 10^5 km^2 is associated with subduction-style great earthquakes. However, localized folding occurred during at least one of the above great earthquakes and may be more prevalent than recognized. Superimposed on the regional uplift during the 1964 Alaska earthquake was the growth of a localized anticlinal fold that pierces above sea level to form Middleton Island [Plafker, 1969], an island whose 30-km length is similar to the subaerially exposed axial length of folds at Cape Arago [Plafker, 1969]. The island consists of five uplifted wave-cut platforms of mid to late Holocene age. These five platforms record periodic abrupt emergence of this island, and a sixth uplifted platform was generated in 1964 when the island was again coseismically uplifted, this time by 3.3 m [Plafker, 1969]. The Middleton Island anticline therefore grew coseismically during the same 1964 event that elsewhere in the Alaskan forearc resulted in more regional vertical uplift or subsidence. It is likely that local growth of folds during the 1964 Alaska earthquake was more common than was documented because most folding probably occurred below sea level. From the Alaskan deformation data we reason that localized folds of the scale observed near Cape Arago can be generated by great earthquakes that deform a much larger region of the forearc.

SUMMARY

Late Quaternary strain in the Cape Arago region appears to be accommodated mostly by contraction on local folds with half wavelengths of 6–7 km and axial lengths of greater than 20 km. These folds produce both landward and seaward tilts to the wave-cut platforms rather than a uniform landward tilt to platforms such as is observed on the convergent margin in southwest Japan. The observed strain in south coastal Oregon therefore lacks in a simple sense the evidence for regional vertical uplift and subsidence associated with historic, large-magnitude subduction-related earthquakes elsewhere [Plafker, 1972].

Localized folding can occur during great earthquakes, as exemplified by the 1964 coseismic growth of the Middleton Island (Alaska) anticline, even though the historic record indicates that the most notable strain pattern during great earthquakes is regional vertical movement. Therefore, though the late Quaternary folds at Cape Arago need not develop during great subduction-related earthquakes, the folds do not preclude the possibility of great earthquakes whose deformation would include the Cape Arago portion of the Cascadia subduction zone.

Acknowledgments. Field work was supported by U.S. Geological Survey Earthquake Hazards Reduction Program, contract 14-08-0001-G1387. A. R. Nelson provided funding for a ^{14}C age determination. Discussion with D. R. Muhs improved the manuscript. We thank D. C. Engebretson, D. Merritts, D. R. Muhs, A. R. Nelson, J. L. Talbot, and R. S. Yeats for reviews.

REFERENCES

- Adams, J., Active deformation of the Pacific Northwest continental margin, *Tectonics*, **3**, 449–472, 1984.
- Armentrout, J. M., Field trip road log for the Cenozoic stratigraphy of Coos Bay and Cape Blanco, southwestern Oregon, *Geologic Field Trips in Western Oregon and Southwestern Washington*, edited by K. Oles, J. Johnson, A. Niem, and W. Niem, *Bull. Oreg. Dep. Geol. Miner. Ind.*, **101**, 177–180, 1980.
- Atwater, B. F., Evidence for great Holocene earthquakes along the outer coast of Washington State, *Science*, **236**, 942–944, 1987.
- Baldwin, E. M., Some revisions of the late Cenozoic stratigraphy of the southern Oregon coast, *J. Geol.*, **52**, 35–46, 1945.
- Baldwin, E. M., Some revisions of the geology of Coos Bay area, Oregon, *Ore. Bin*, **28**, 189–204, 1966.
- Beaulieu, J. D., and P. W. Hughes, Environmental geology of western Coos and Douglas counties, Oregon, *Bull. Oreg. Dep. Geol. Miner. Ind.*, **87**, 148 pp., 1975.
- Bender, M. L., R. G. Fairbanks, F. W. Taylor, R. K. Matthews, J. G. Goddard, and W. S. Broecker, Uranium-series dating of the Pleistocene reef tracts of Barbados, West Indies, *Geol. Soc. Am. Bull., Part 1*, **90**, 577–594, 1979.
- Bloom, A. L., W. S. Broecker, J. M. A. Chappell, R. K. Matthews, and K. J. Mesolella, Quaternary sea level fluctuations on a tectonic coast: New $^{230}\text{Th}/^{234}\text{U}$ dates from the Huon Peninsula, New Guinea, *Quat. Res. N. Y.*, **4**, 185–205, 1974.
- Bradley, W. C., and G. B. Griggs, Form, genesis, and deformation of central California wave-cut platforms, *Geol. Soc. Am. Bull.*, **87**, 433–449, 1976.
- Chappell, J., and N. J. Shackleton, Oxygen isotopes and sea level, *Nature*, **324**, 137–140, 1986.
- Clarke, S. H., M. E. Field, and C. A. Hirozawa, Reconnaissance geology and geologic hazards of the offshore Coos Bay basin, Oregon, *U.S. Geol. Surv. Bull.*, **1645**, 41 pp., 1985.
- Currie, J. B., H. W. Patnode, and R. P. Trump, Development of folds in sedimentary strata, *Geol. Soc. Am. Bull.*, **73**, 655–674, 1962.
- Ehlen, J., Geology of state parks near Cape Arago, Coos County, Oregon, *Ore. Bin*, **29**, 63–83, 1967.
- Griggs, A. B., Chromite-bearing sands of the southern part of the coast of Oregon, *U.S. Geol. Surv. Bull.*, **945-E**, 113–150, 1945.
- Harmon, R. S., R. M. Mitterer, N. Kriausakul, L. S. Land, H. P. Schwarcz, P. Garrett, G. J. Larson, H. L. Vacher, and M. Rowe, U-series and amino-acid racemization geochronology of Bermuda—Implications for eustatic sea-level fluctuation over the past 250,000 years, *Palaeogeogr. Palaeoclimatol. Palaeoecol.*, **44**, 41–70, 1983.
- Heaton, T. H., and S. H. Hartzell, Earthquake hazards on the Cascadia subduction zone, *Science*, **236**, 162–168, 1987.
- Heaton, T. H., and H. Kanamori, Seismic potential associated with subduction in the northwestern United States, *Bull. Seismol. Soc. Am.*, **74**, 933–941, 1984.
- Janda, R. J., Age and correlation of marine terraces near Cape Blanco, Oregon, *Geol. Soc. Am. Abst. Programs*, **3**, 29–30, 1969.
- Kelsey, H. M., Late Quaternary deformation of marine terraces on the Cascadia subduction zone near Cape Blanco, Oregon, *Tectonics*, in press, 1990.
- Kennedy, G. L., K. R. Lajoie, and J. F. Wehmiller, Aminostratigraphy and faunal correlations of late Quaternary marine terraces, Pacific coast, USA, *Nature*, **299**, 545–547, 1982.
- King, G. C. P., and C. Vita-Finzi, Active folding in the Algerian earthquake of 10 October 1980, *Nature*, **292**, 22–26, 1981.
- Ku, T.-L., M. A. Kimmel, W. H. Easton, and T. J. O'Neil, Eustatic sea level 120,000 years ago on Oahu, Hawaii, *Science*, **183**, 959–962, 1974.
- Kulm, L. D., and G. A. Fowler, Oregon continental margin structure and stratigraphy: A test of the imbricate thrust model, in *The Geology of Continental Margins*, edited by C. A. Burk and C. L. Drake, pp. 261–284, Springer-Verlag, New York, 1974.
- Lajoie, K. R., Coastal tectonics, in *Active Tectonics*, pp. 95–124, National Academy Press, Washington, D. C., 1986.
- Lund, E. H., Landforms along the coast of southern Coos County, Oregon, *Ore. Bin*, **35**, 189–210, 1973.
- Machida, H., Pleistocene sea level of south Kanto, Japan, analyzed by tephrochronology, *Bull. R. Soc. N. Z.*, **13**, 215–222, 1975.
- McInnelly, G. W., H. M. Kelsey, and A. R. Nelson, Late Pleistocene and Holocene tectonic deformation of the Whisky Run wave-cut platform in the Cape Arago-Coos Bay area, coastal Oregon, *Geol. Soc. Am. Abstr. Prog.*, **21**, 115, 1989.
- Mesolella, K. J., R. K. Matthews, W. S. Broecker, and D. L. Thurber, The astronomical theory of climatic change: Barbados data, *J. Geol.*, **77**, 250–274, 1969.
- Muhs, D. R., and C. A. Bush, Uranium-series age determinations of Quaternary eolianites and implications for sea-level history, New

21

- Providence Islands Bahamas, *Geol. Soc. Am. Abstr. Prog.*, 19, 780, 1987.
- Muhs, D. R., G. L. Kennedy, and T. K. Rockwell, Uranium-series ages of corals from marine terraces, Pacific coast of North America: Implications for the timing and magnitude of late Pleistocene sea level changes, in *Programs and Abstracts of 10th Biennial Meeting*, p. 140, Illinois State Water Survey, Urbana, 1988.
- Muhs, D. R., H. M. Kelsey, G. H. Miller, G. L. Kennedy, J. F. Whelan, and G. W. McInelly, Age estimates and uplift rates for late Pleistocene marine terraces: Southern Oregon portion of the Cascadia forearc, *J. Geophys. Res.*, this issue.
- Nelson, A. R., Apparent gradual rise in relative sea level on the south-central Oregon coast during the late Holocene—Implications for the Great Cascadia earthquake hypothesis, *Eos Trans. AGU*, 68, 1240, 1987.
- Nelson, A. R., S. F. Personius, and S. Rhea, Earthquake recurrence and Quaternary deformation in the Cascadia subduction zone, coastal Oregon, *U.S. Geol. Surv. Open File Rep.*, 88-673, 492-497, 1988.
- Newton, V. C., Jr., L. P. Kulm, R. W. Couch, D. Braman, G. S. Pitts, R. O. Van Atta, and D. R. McKeel, Prospects for oil and gas in the Coos Basin, western Coos, Douglas, and Lane counties, Oregon, *Oil Gas Invest.* 6, 74 pp., Oreg. Dep. of Geol. and Miner. Ind., Portland, 1980.
- Ota, Y., Marine terraces as reference surfaces in late Quaternary tectonic studies: Examples from the Pacific rim, *Bull. R. Soc. N. Z.*, 24, 357-375, 1986.
- Peterson, C. D., and M. E. Darienzo, Episodic, abrupt tectonic subsidence recorded in late Holocene deposits of the South Slough syncline: An on-land expression of shelf fold belt deformation from the southern Cascadia margin, *Geol. Soc. Am. Abstr. Programs*, 21, 129, 1989.
- Peterson, C. D., G. W. Gleeson, and N. Wetzel, Stratigraphic development, mineral sources, and preservation of marine placers from Pleistocene terraces in southern Oregon, USA, *Sediment. Geol.*, 53, 203-229, 1987.
- Peterson, C. L., L. D. Kulm, and J. J. Gray, Geologic map of the ocean floor off Oregon and the adjacent continental margin, scale 1:500,000, *Oreg. Dep. Geol. Miner. Ind., GMS-42*, 1986.
- Plafker, G., Tectonics of the March 27, 1964 Alaskan earthquake, *U.S. Geol. Surv. Prof. Pap.*, 543-I, 74 pp., 1969.
- Plafker, G., Alaskan earthquake of 1964 and Chilean earthquake of 1960: Implications for arc tectonics, *J. Geophys. Res.*, 77, 901-925, 1972.
- Rockwell, T. K., E. A. Keller, and G. R. Dembroff, Quaternary rate of folding of the Ventura Avenue anticline, western Transverse Ranges, southern California, *Geol. Soc. Am. Bull.*, 100, 850-858, 1988.
- Shackelton, N. J., and N. D. Opdyke, Oxygen isotope and palaeomagnetic stratigraphy of equatorial Pacific core V28-238: Oxygen isotope temperatures and ice volumes on a 10^5 year and 10^6 year scale, *Quat. Res.*, N. Y., 3, 39-55, 1973.
- Spence, W., Stress origins and earthquake potentials in Cascadia, *J. Geophys. Res.*, 94, 3076-3088, 1989.
- Stein, R. S., G. C. P. King, Seismic potential revealed by surface folding: 1983 Coalinga, California, earthquake, *Science*, 224, 869-872, 1984.
- Uyeda, S., and H. Kanamori, Back arc opening and the mode of subduction, *J. Geophys. Res.*, 84, 1049-1061, 1979.
- Weast, R. C., (Ed.), *CRC Handbook of Physics and Chemistry*, 49th ed., pp. A-166 and A-167, CRC Press, Boca Raton, Flor., 1979.
- West, D. O., and D. R. McCrumb, Coastline uplift in Oregon and Washington and the nature of Cascadia subduction-zone tectonics, *Geology*, 16, 169-172, 1988.
- Yeats, R. S., M. N. Clark, E. A. Keller, and T. K. Rockwell, Active fault hazard in southern California: ground rupture versus seismic shaking, *Geol. Soc. Am. Bull., Part 1*, 92, 189-196, 1981.
- Yonekura, N., Late Quaternary vertical crustal movements in and around the Pacific as deduced from former shoreline data, in *Geodynamics of the Western Pacific-Indonesian Region, Geodyn. Ser.*, vol. 11, edited by T. W. C. Hilde and S. Uyeda, pp. 41-50, AGU, Washington, D. C., 1983.
- H. M. Kelsey, Department of Geology, Western Washington University, Bellingham, WA 98225.
- G. W. McInelly, Geo Engineers, 2405 140 Avenue NE, Suite 105, Bellevue, WA 98005.

(Received July 14, 1989;
revised November 20, 1989;
accepted December 27, 1989.)

by Paul D. Komar, College of Oceanography, Oregon State University, Corvallis, Oregon

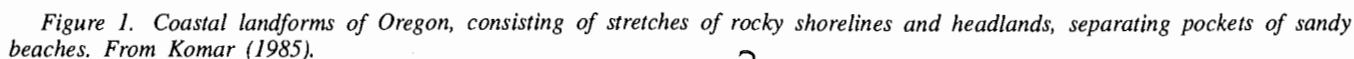
Early explorers of the Oregon coast (Figure 1) were impressed by the tremendous variety of its scenery. Today, visitors can still appreciate those same qualities. The low rolling mountains of the Coast Range serve as a backdrop for most of the length of its ocean shore. In the south, the Klamath Mountains extend to the coast, and the edge of the land is characterized by high cliffs being slowly cut away by ocean waves. The most resistant rocks persist as sea stacks scattered in the offshore. Sand and gravel are able to accumulate only in sheltered areas where they form small pocket beaches within the otherwise rocky landscape.

tween the headlands. Portions of these beaches form the ocean shores of sand spits such as Siletz, Netarts, Nehalem, and Bayocean. Landward from the spits are bays or estuaries of rivers that drain the Coast Range.

The first western explorers and settlers were attracted to the Oregon coast by the potential richness of its natural resources. Earliest were the traders who obtained pelts of ocean otter and beaver from the Indians. Later came prospectors who sought gold in the beach sands and coastal mountains but in many cases were content to settle down and "mine" the fertile farm lands found along the river margins. Others turned to fishing, supporting themselves by harvesting the abundant Dungeness crab, salmon, and other fish in the coastal waters. Also important to the early economy of the coast were the vast tracts of cedar and sitka spruce, a significance that continues to the present.

In contrast, today the most important "commodity" for the Northwest coast economy is the vacation visitor. Vacationers arrive in thousands during the summer months, but in spite of their numbers it is still possible to leave coastal Highway 101 and find the seclusion of a lonely beach or the stillness of a trail through the forest.

However, there is cause for concern that the qualities of the Oregon coast we cherish are being lost. Like most coastal areas,



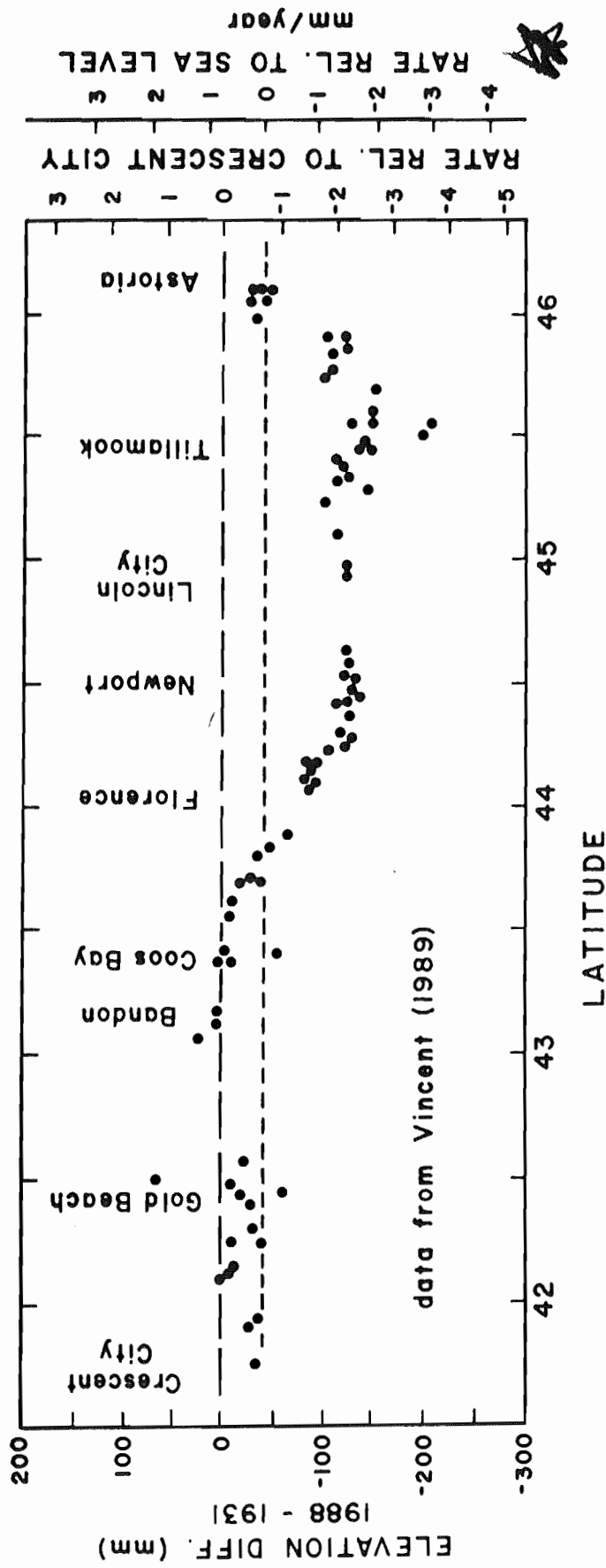


Figure 3. Elevation changes and the relationship to sea-level rise along the length of the Oregon coast from Crescent City in California north to Astoria on the Columbia River, based on repeated geodetic surveys along the coast. After Vincent (1989).

ernmost portion of the coast toward Astoria and the Columbia River. The first scale on the right of Figure 3 indicates the equivalent rates, the elevation changes divided by the lapsed time between surveys, 1988-1931 = 57 years. The differential rates are significant, for example amounting to 2-3 mm/year when comparing Astoria and the south coast with the Newport and Lincoln City areas.

It is possible to use the tide gauge data

coasts of the United States (Figure 2). The global rise in sea level has been estimated by various workers to be on the order of 1-3 mm/year (4-12 in. per century). The large range is due to the difficulty of separating that worldwide component from local tectonic and isostatic effects included in records from tide gauges. Assuming that the eustatic rise in sea level is on the order of 2 mm/year

in from even for due the of re the dro wh side is a upl gau tim day upli acc futu atur 1.5° sear turn acc glaci

River, part of which moves southward until it is blocked by Tillamook Head. However, the bulk of sand derived from the Columbia River moves northward along the coast of Washington. The quantities of this northward sand transport can be only roughly estimated, but the primary evidence for this sand supply is that many of the beaches along the southern half of the Washington coast are growing (Phipps and Smith, 1978). The highest rates of beach growth tend to be in the south, closest to the Columbia River, decreasing to the north until, beyond Copalis Head, net erosion prevails.

On many coastlines, sand spits grow in the direction of the net littoral drift. The Long Beach Peninsula extends northward from the Columbia River and likely reflects the net sand movement along the Washington coast. It is unclear whether this northward growth has continued within historic times, since there have been many cycles of growth and erosion at the tip of the Peninsula. There are several sand spits along the northern coast of Oregon, some pointing north, while others point to the south (Figure 1). Those spits are located within the beach cells where zero net littoral drift prevails, and their directions do not provide testimony as to net longshore sand movements.

In view of the pocket-beach nature of the Oregon coast, the question arises as to the sources of beach sand contained within those littoral cells. These sources are reflected in the small quantities of heavy minerals contained within the beach sand. On the Oregon coast, the beach sand generally consists of grains of quartz and feldspar minerals. Those particles are transparent or a light tan, and this is what governs the color of most beaches. However, the sands also contain small fractions of heavy minerals that are black, pink, various shades of green, and other colors. These grains are readily apparent as specks in a handful of beach sand and are sometimes concentrated by the waves into black-sand placer deposits on the beaches. Of importance is that these heavy minerals are indicative of the rocks they came from and in many cases can be traced back to specific rocks and therefore geographical sources. That is the case for the heavy minerals in the sands of the Oregon coast. Most distinctive are the minerals derived from the Klamath Mountains: a variety of ancient metamorphosed rocks is found in those mountains of southern Oregon and northern California. As shown in the diagram of Figure 14, sands derived from the Klamath Mountains contain such minerals as glaucophane, staurolite, epidote, zircon, hornblende, hypersthene, and the distinctive pink garnet that, in particular, can often be seen concentrated on the beach. In contrast, the rivers that drain the Coast Range transport sand containing almost exclusively two heavy minerals: dark-green augite and a small amount of brown hornblende (Figure

14). Augite comes from volcanic rocks and is contributed to the rivers by erosion of the ancient sea-floor rocks uplifted into the Coast Range. With the sand of the Columbia River comes a diversity of heavy minerals because the river drains a vast area that contains many types of rocks (Figure 14).

The presence of sand derived from the Klamath Mountains in beaches along almost the entire length of the Oregon coast is at first surprising—in view of the many headlands that prevent any longshore sand transport for that distance. However, thousands of years ago, during the maximum development of glaciers, the sea level was considerably lower, the shoreline was then on what is now the continental shelf, many miles to the west of its present position, and the beaches were backed by a smooth coastal plain. At that time, sand derived from rivers draining the Klamath Mountains could move freely northward as littoral drift without being blocked by headlands. Studies of heavy minerals contained within continental-shelf sands demonstrate that this was indeed the case (Scheidegger and others, 1971): the metamorphic minerals from the Klamaths can be found in the shelf sands nearly as far north as the Columbia River. As the Klamath-derived sand moved north, additional sand was contributed to the beaches by rivers draining the Coast Range, so there is progressively more augite and a smaller proportion of metamorphic minerals from the Klamaths in these beach sands. The Columbia River was a large source of sediment, but most of that sand

moved to the north and dominates the mineralogy of ancient beach sands found on the Washington continental shelf. Some Columbia River sand did move south along the Oregon beaches during lowered sea levels and mixed with the sand from the Klamath Mountains and the Coast Range.

Therefore, the absence of headlands during lowered sea levels permitted an along-coast mixing of sands derived from multiple sources, principally from the Klamath Mountain metamorphics, the Coast-Range volcanics, and the Columbia River sands. Varying with the location along this former shoreline of the Oregon coast, the beach consisted of various proportions of mineral grains from those sources. Although a portion of the beach sand was left behind during the rapid rise in sea level and now can be found on the continental shelf, some of it migrated landward with the transgressing shoreline. The beaches would have been low in relief so that storm waves were able to wash over them, transporting sand from the ocean shores to the landward sides of the beaches and thereby producing the migration. Additional sand was contributed by the various river sources and from sediments eroded from the coastal plain.

About 5,000-7,000 years ago, the rate of rise in sea level decreased as the water approached its present level. Just about at that time, the beaches of Oregon came under the influence of headlands that segmented the formerly continuous shoreline. At some stage several thousand years ago, the headlands extended into sufficiently deep water to hinder further along-coast transport of the beach sands. This is shown by a study of the mineralogy of sand found on the present-day beaches (Clemens and Komar, 1988a,b). The pattern of along-coast mixing of sand from the various sources, established during lowered sea levels, is still partly preserved within the series of pocket beaches now separated by headlands. Therefore, one can still find minerals derived from the Klamath Mountains in virtually all of the beaches along the Oregon coast, even though it is certain that the sand can no longer pass around the many headlands that separate those beaches from the Klamath Mountains. In most cases, the Klamath-derived sand could have reached the modern beach only by along-coast mixing during lowered sea levels and subsequent on-shore transport with the rise of the sea. However, there has been some modification of the beach-sand mineralogy from that along-coast mixing pattern, as local sources have contributed sand to the beaches during the last few thousand years. Such beach-sand sources include eroding sea-cliffs and some sand from the rivers and streams entering the isolated pocket beaches.

There can be distinct changes in beach-sand mineralogies on opposite sides of headlands, that is, within adjacent but isolated

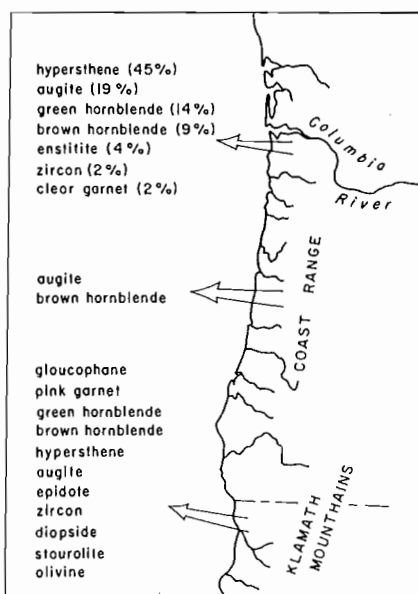


Figure 14. Principal sources of sand to Northwest beaches are the Columbia River and rivers draining the Coast Range and the Klamath Mountains. Each source supplies different suites of heavy minerals to beach and estuarine sands. From Clemens and Komar (1988b).

OTHER FACTORS

1. rain wash on cliff face
2. ground-water flow and pore pressures
3. vegetation cover
4. burrowing by rodents, etc.
5. people
 - walking on cliff and talus
 - carving graffiti on cliff face
 - watering lawns
 - culverts, etc.
 - protective structures (sea walls, etc.)

OCEAN FACTORS

1. waves
 - heights and periods (energy or energy flux)
 - approach angle (longshore currents and littoral drift)
 - set-up and run-up
2. cell circulation with rip currents
3. tidal variations
4. storm surge
5. sea level (seasonal and long-term net changes)

CLIFF FACTORS

1. composition
 - "hardness" (e.g., compressive strength)
 - talus production
 - source of beach sediments
2. layering (bedding), joints, and fractures
3. inclination of rock layers
4. height and slope of cliff face

BEACH FACTORS

1. volume of beach sediments (buffering ability)
2. composition and grain size
 - control on beach morphology
 - sand "blasting"
3. presence of drift logs

Figure 29. Schematic diagram illustrating the many factors and processes in

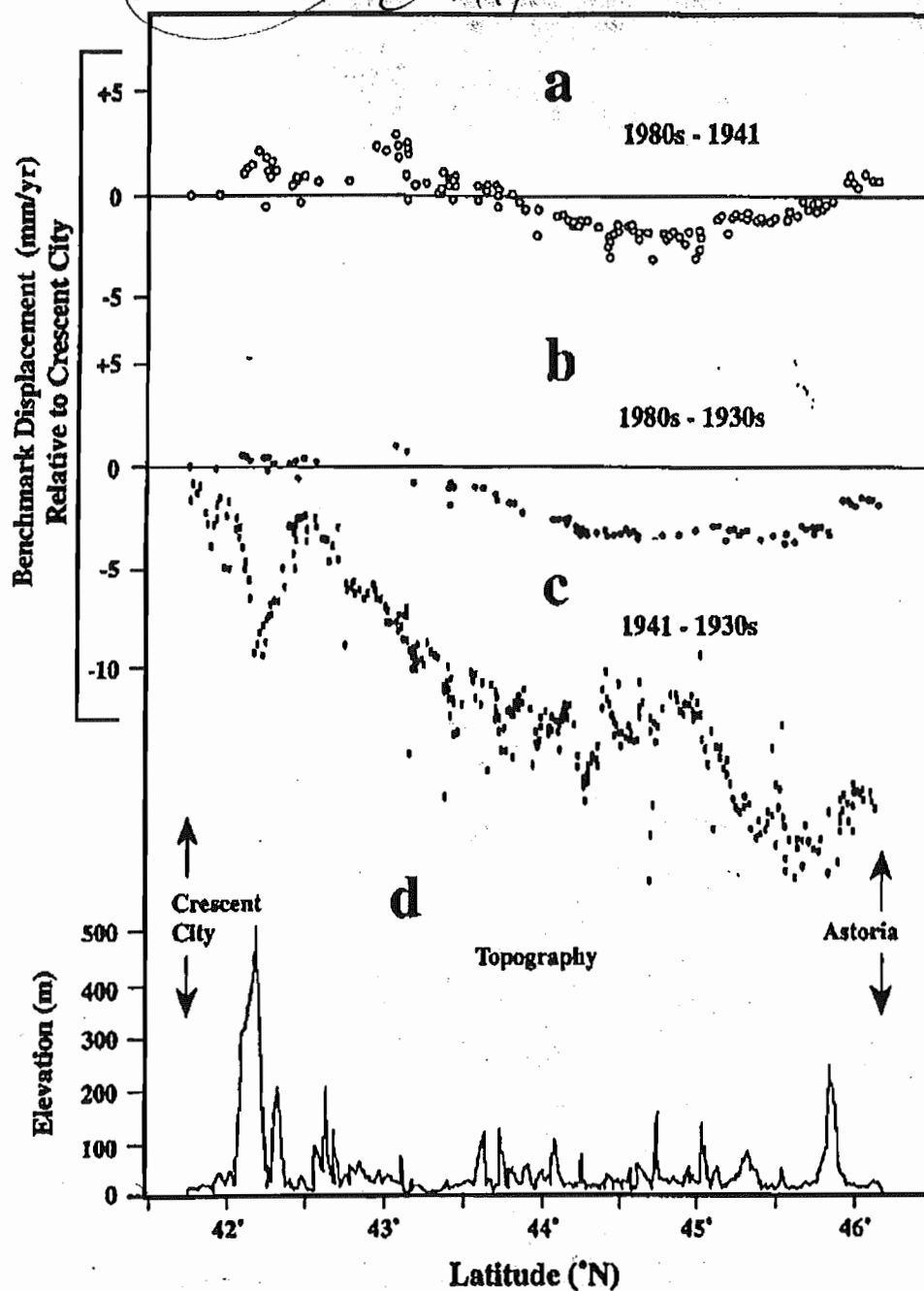


Figure 10. Uplift rates relative to Crescent City calculated from repeated first-order leveling along the Cascadia coast. Rates are calculated by differencing the heights determined by three epochs of leveling. Note similarity in the shape of the 1980s-1930s and 1980s-1941 profiles. The 1941-1930s profile probably contains minor systematic error that is amplified by plotting as rate of change because of the short time interval between surveys. Also note that several sharp cusps in the data correlate with peaks in topography, suggestive of local errors.

level route reaches an elevation of 500 m, and the other is at Tillamook Head (45.9°N) where the level route reaches an elevation of 250 m. Both locales show a relatively sharp change of inferred rate associated with relatively high local relief. Also, both anomalies are about the same wavelength as their corresponding local topographic highs, suggesting that these signals might be related to topography. The 1941 coastal survey is possibly questionable, a conclusion support-

ed below by consideration of loop misclosure. Topography does not, however, appear related to some of the other short wavelength anomalies nor to the longer wavelength tilt signals along the coast (Figure 10).

Loop Closure

Loop closure analysis is done to determine the accuracy of leveling data. Elevation differences between beginning and

27

1923 north	-99.00	626	-3.96	-0.16
54 south				
30s Sly E-W				
1980s inland	43.0	626	1.72	0.07
<i>Loop V</i>				
1919, 1920,	-85.00	798	-3.40	-0.11
1930s from	15.76	798	0.63	0.02
y to				

b for loop locations and locales.

Its, based on three surveys, it with time suggesting a static error. Third, the tilts Newport-to-Albany line are static error there unlikely. The Portland-to-Albany leg is not surveyed in 1941) and close to acceptable values. Errors during that epoch. Suspected systematic error on Portland segment. This Astoria-to-Portland line is the Newport-to-Albany line land valley profile in this sure around the loop is

ing data set are very poor. Loop V have a very large bench mark F56 at Grants et for two reasons. First, by tide gauges are quite influence of errors on the ss time between surveys ns. Figure 10c illustrates e between surveys, as in usable results from this at with independent tidal

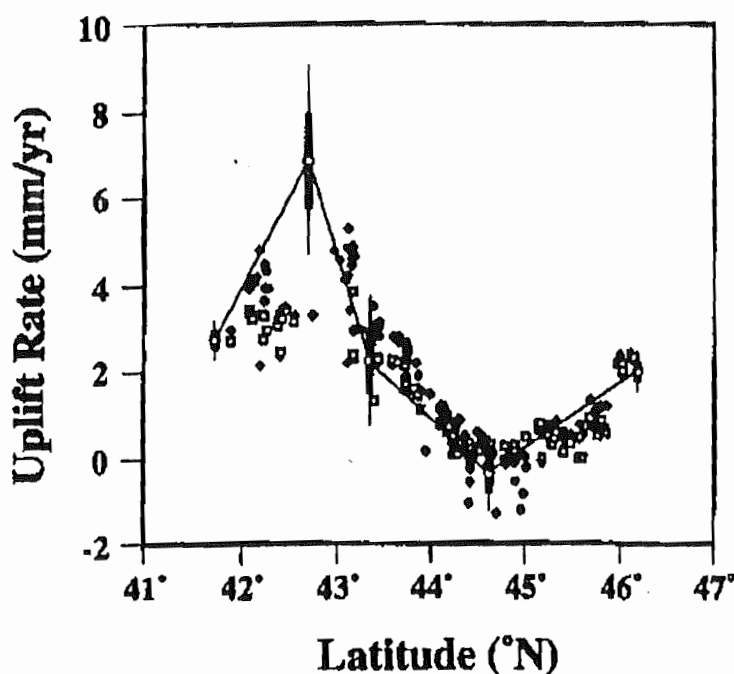


Figure 12. The Crescent City-to-Astoria uplift rate profiles derived from leveling (Figures 10a and 10b) are arbitrarily referenced to the tidally indicated uplift rate at each end of the Crescent City-to-Astoria portion of the uplift rate profile (Figure 9) determined from tidal data. Shapes of uplift rate profiles from leveling compare quite well to the uplift profile from tidal data.

MITCHELL ET AL.: CASCADIA PRESENT-DAY VERTICAL DEFORMATION

agment (Rainier-to-Portland, Portland-to-Al-
some later relevelings have different starting
ints) is attached to east-west lines, and then a
is drawn through the entire profile. The
ts of the various north-south and east-west
sonably consistent, suggesting very crude rate
the network of leveling lines. For example,
a low on the coastal profile (Figure 13c), as is
inland profile (Figure 13b); the flat slope in
ween them (Figure 14c) is therefore consistent.

of Regional Uplift Rates

the uplift rate data in map view, we use the
through the tidally adjusted uplift rate profiles
ata (Figures 12 through 14) and pick off integer
are plotted and hand-contoured to produce a
f uplift rates (Figure 15). To complete the map
state, inland from the region of rapid uplift, we
ier uplift rate contouring [Ando and Balazs,
et al., 1989], first correcting for different rates
e used in those studies. We extend the map
Mendocino, beyond the tide gauges which
train the north-south coastal uplift rate profile
auges. Cape Mendocino is no farther from tide
me portions of the inland valley north-south
file but lacks the constraint of fitting to tidally
eling results from more than one direction.
nations of leveling epochs near Cape Mendo-
lightly varying results, just as along the coast to
e adjustment of a freely floating end is not great
example), but the internal detail of the uplift
the Cape Mendocino vicinity is of interest.

ring approach is fairly crude and locally
we do not believe the data justify more detailed
d the overall regional pattern is well-resolved.
eling data are not confirmed by independent
al Positioning System (GPS) observations of
nch marks and level line junctions have been
d will be analyzed to determine vertical posi-
comparison (M. Murray, personal communi-
Nonetheless, comparable uplift rate patterns
the independent data sets of tidal records and
ng the coast constitute a test of consistency
There is, however, distortion of the uplift rate
ography-related error where the inland N-S
cross the Siskiyou Mountains in the vicinity of
rapid present-day uplift and several connecting

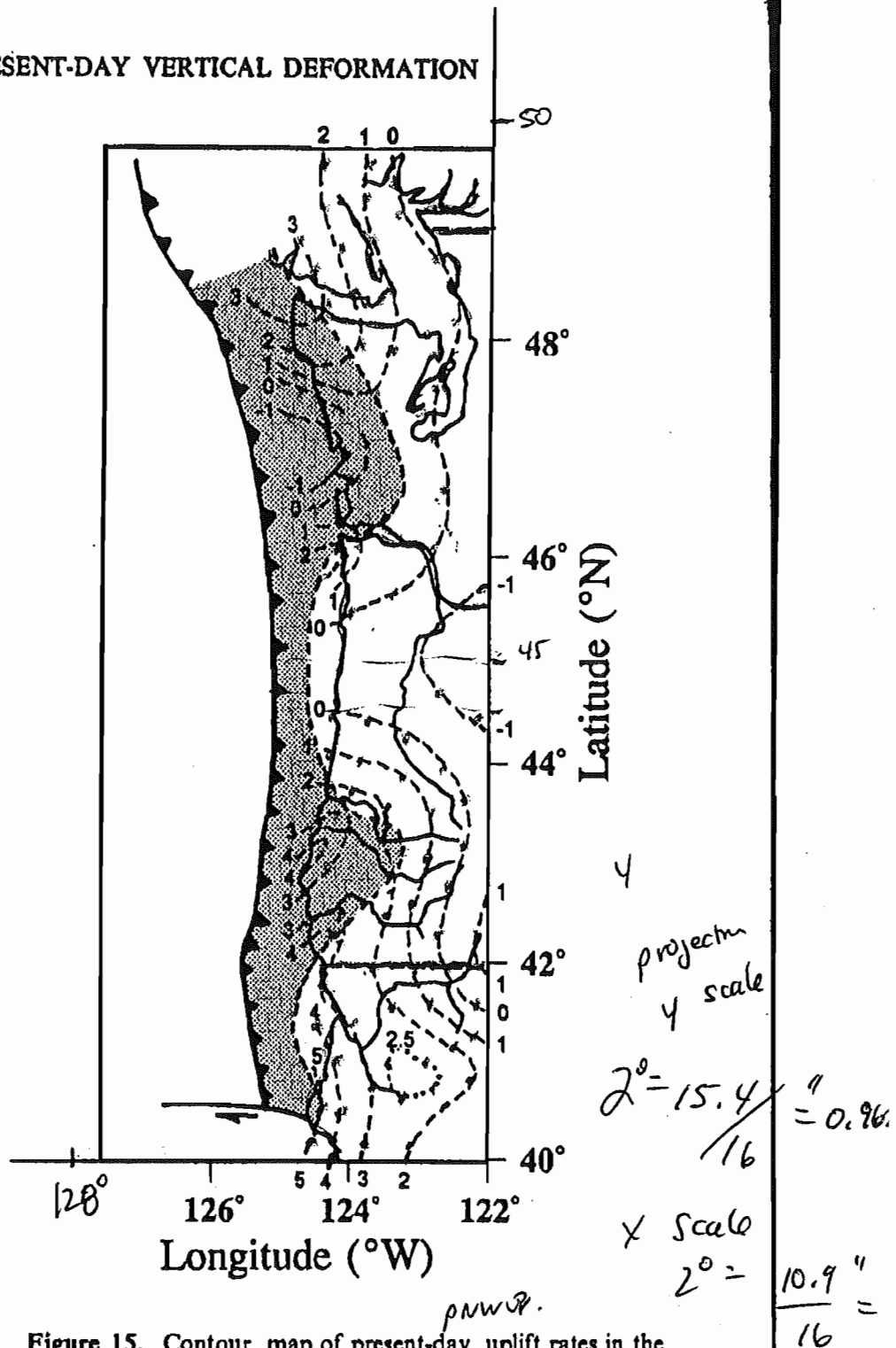


Figure 15. Contour map of present-day uplift rates in the Pacific Northwest, west of the Cascade Range and south of Canada. Contours are generated from tidal records and leveling profiles, with much of Washington state recontoured from Ando and Balazs [1979] and Holdahl et al. [1989], as discussed in the text. The stippled area is an interpretation of the region of elastic strain accumulation, assuming that the most rapid uplift at the surface approximately overlies the downdip edge of that portion of the subduction interface [Savage, 1983].

Grays Harbor/Willapa Bay. In southwestern Oregon, an axis of rapid uplift extends northeasterly from the Cape Blanco region (42.2-43.2°N). The overall shape of the uplift rate

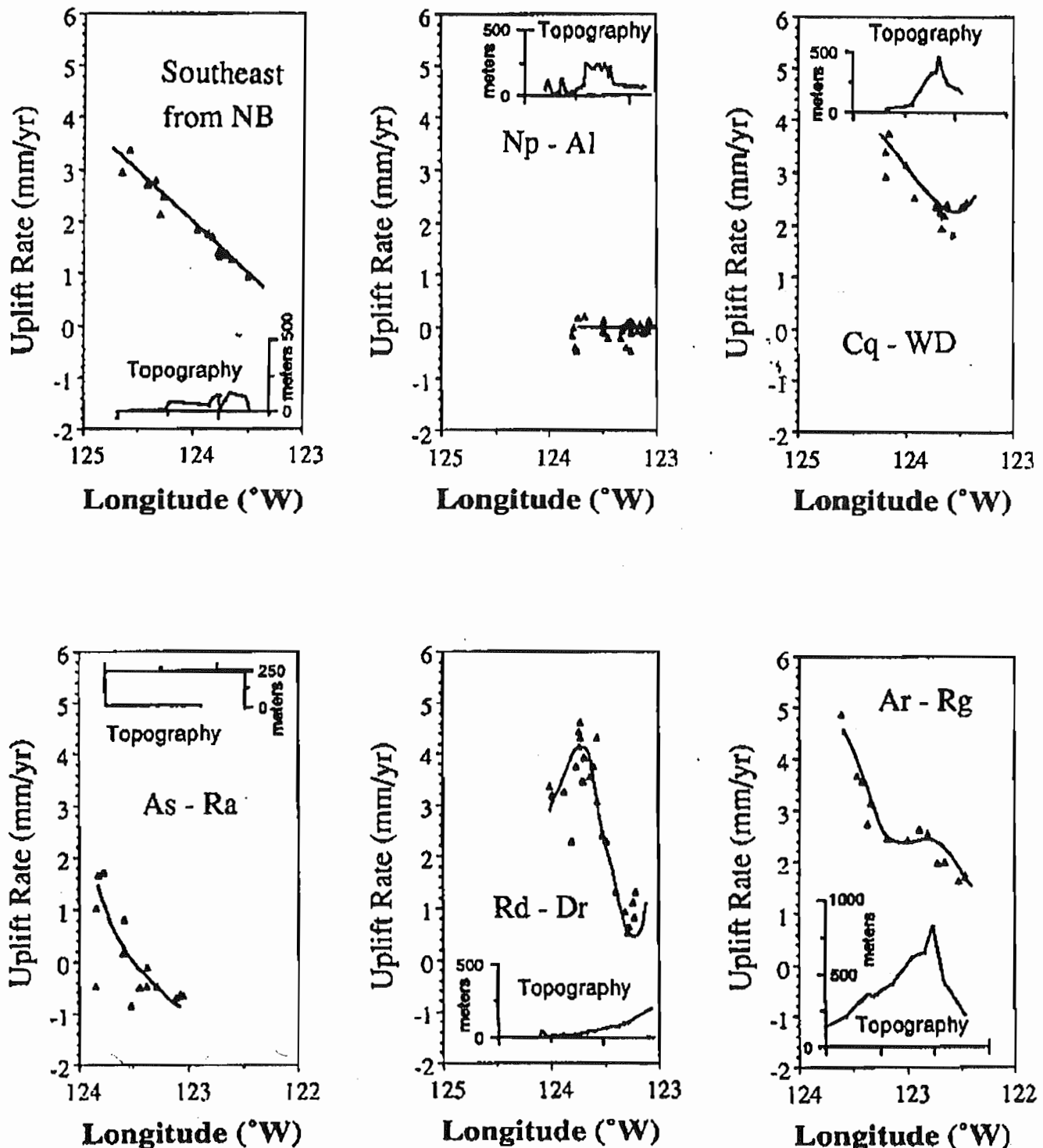


Figure 14. East-west uplift rate profiles connect the tidally adjusted north-south coastal profile (Figure 13a) to the north-south inland valley profile (Figure 13b). Refer to Figure 1b for locations. Notice that most of the east-west profiles tilt to the east, though at different rates. An exception is the Newport-to-Albany profile, which is essentially flat. *Reillinger and Adams* [1982] report similar tilts, but the longer time intervals available due to releveling in the late 1980s allow the tilts to exceed their random error envelopes.

ties to tide gauges at Crescent City and Astoria arbitrarily force the ends to match, the internal shapes of the releveling profiles and tidal profile are entirely independent. There is

Astoria-to-Rainier profile to the Astoria tide gauge, the Newport-to-Albany profile to the South Beach/Newport tide gauges. The Reedsport-to-Drain, Coquille-to-Winston/Dil-

30

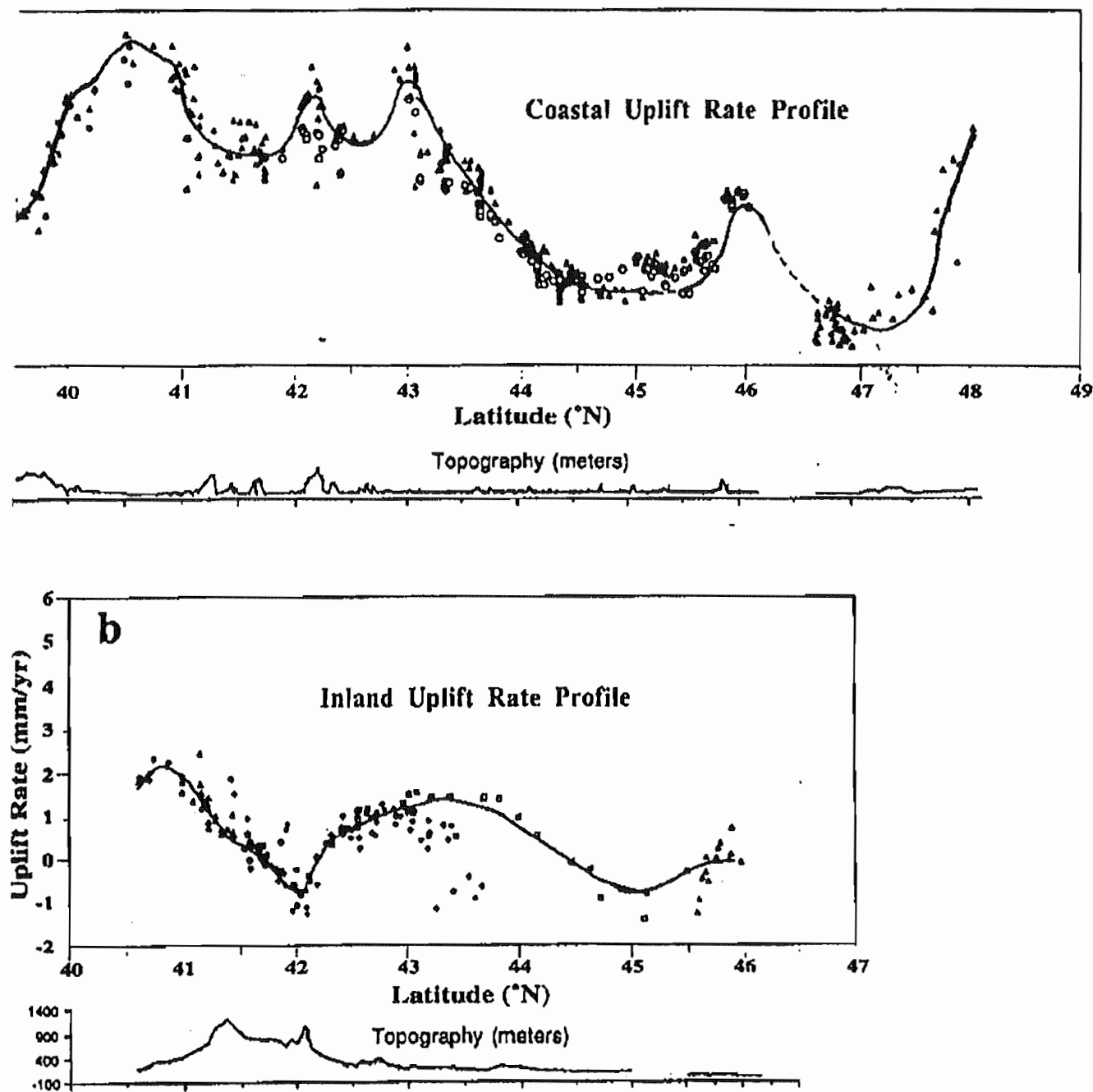


Figure 13. Detailed north-south uplift rate profiles from leveling: (a) along the coast and (b) through the north-south inland valleys. The shapes are similar, though the inland profile is more subdued and appears to be shifted slightly to the north, relative to the coastal profile. The coastal profile is in several pieces, which are tied to absolute rates indicated by tidal data (Table 2 and Figure 9) at Crescent City, Astoria, Toke Point, and Neah. The absolute rate of the inland valley profile is determined by adjusting it in segments to the east-west profiles in Figure 14. Small regions of subsidence, near Redding and south of Portland may be due to leveling lines crossing sediment filled basins, rather than tectonic motion.

12). Second, as *Wellman* [1972] points out, between independent data sets, such as leveling records as a specific example, are better and more useful internal tests for systematic and random

are defined. At the Astoria end, we get an uplift rate that is too rapid using the 1980s-1941 (Figure 10a) and too slow using the 1980s-1930s data (Figure 10b), compared to the tidally indicated difference in uplift rate, which is 0.9 ± 0.3

1994

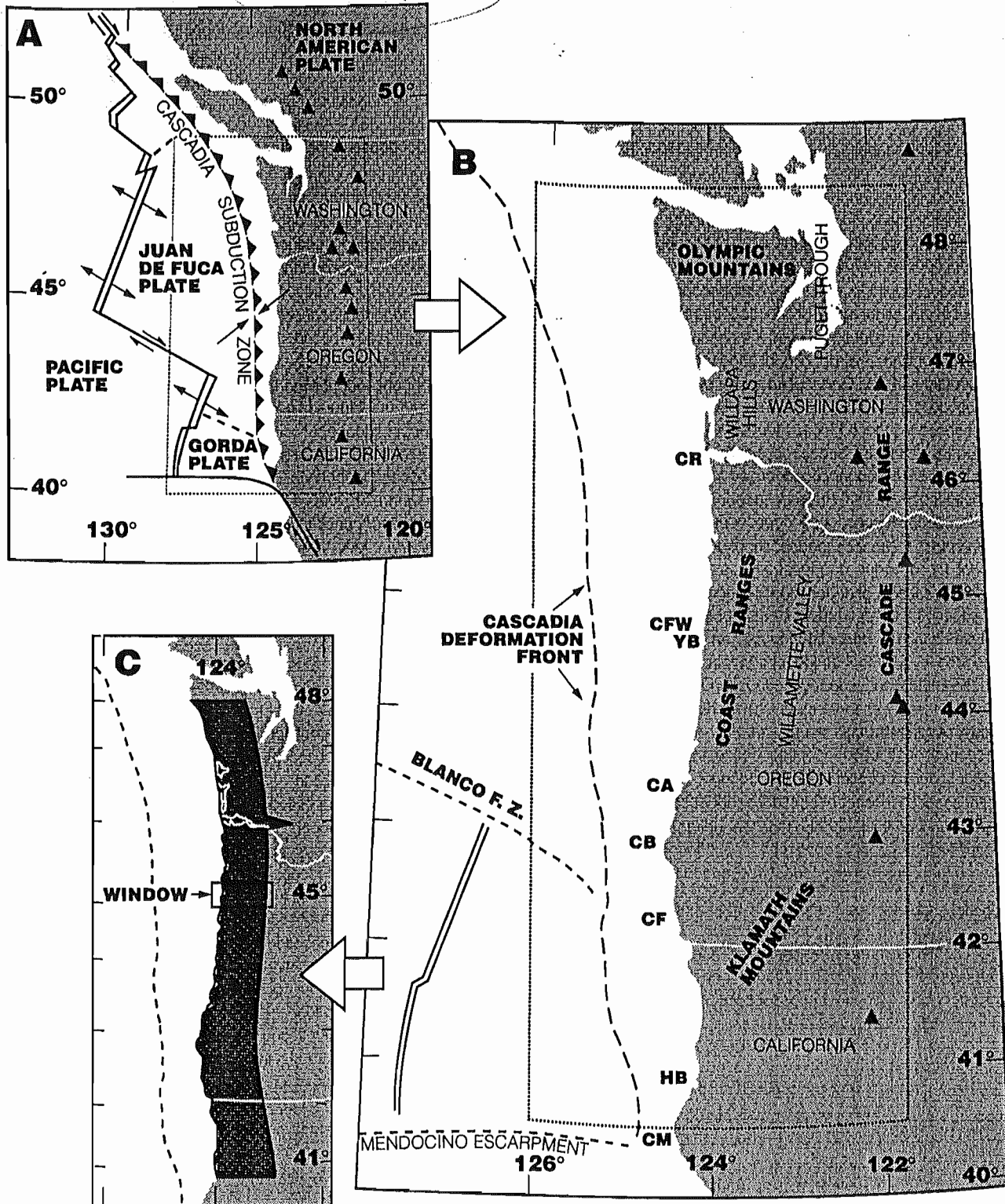


Figure 1. (a) Location map of the Pacific Northwest in the context of plate tectonics; triangles are Cascade volcanoes. (b) Location map of the coastal ranges situated on the leading edge of the North American plate between the Mendocino escarpment and the Canadian border. Triangles denote selected Cascade volcanoes. CR, mouth of the Columbia River; CFW, Cape Foulweather; YB, Yaquina Bay; CA, Cape Arago; CB, Cape Blanco; CF, Cape Ferrello; HB, Humboldt Bay; CM, Cape Mendocino. (c) Shading shows the area of the Coast Ranges, 65 arc min of longitude wide, for which the digital elevation model ETOPO-5 was employed to compute average topography. The box depicts the size of the computational window (65 arc min x 15 arc min) that was employed for each individual calculation of average topography. See text for further explanation.

32

sea level is an expression of Earth's geoidal surface. The geodetically derived uplift is in reference to present sea level and the shore platform uplift is in reference to the appropriate late Pliocene eustatic sea level high stand (see below). Because rock uplift relative to the geoid is equal to surface uplift minus exhumation [England and Molnar, 1990] and because there has been negligible erosion of either the shore platforms or the highway benchmarks, the coastal uplift rates that we discuss are both uplift rates of rock relative to the geoid as well as surface uplift rates. Subsequent use of the term "uplift rate" should thus be unambiguous. Using uplift rate data integrated over the last 45 years and that integrated over the last 80,000-125,000 years, we can compare interseismic uplift with long-term uplift at the coast along the Cascadia margin.

Average Topography Along the Crest of the Coast Ranges

We calculated average topography for the Coast Ranges (Figure 2) using the public domain 5 arc min digital elevation model ETOPO-5 [National Geophysical Data Center, 1988]. Using ETOPO-5, we calculated a running average for the topography of the Coast Ranges in a north-south trending swath extending from the coast inland for 65 arc min of longitude (Figure 1c). The swath extends between latitudes 41° and 47° N along the trend of the Coast Ranges, for a total length of 778 km. The average width of the swath is 86.6 km (90.9 km at latitude 41° and 82.2 km at latitude 47°). Each individual calculation of average topography at 5-arc min latitudinal intervals is the running average of the average altitude at 39 different grid points, 13 grid points from each of

three adjacent lines of latitude (computational window (Figure 1c) is 65 arc min of longitude \times 15 arc min of latitude on a 5 arc min grid), with 13 out of 39 of the grid points changing for each calculation. Thus each calculation of average topography represents an area of about 2400 km² (27.8 km \times 86.6 km).

Because we will subsequently compare uplift rates at the coast to trends in average topography for the Coast Ranges as a whole, we determined whether north-south trends in average topography for the coastal (western) side of the Coast Ranges are similar in form to trends of average topography for the Coast Ranges as a whole. Using the same computational technique but applied to narrower widths, we determined average topography for a 25-arc-min-wide swath on the west side of the Coast Ranges, and we also computed average topography for a nonoverlapping 25-arc-min-wide swath on the eastern side of the Coast Ranges. Comparing the western profile to the profile for the Coast Ranges as a whole (Figure 2), the profiles show that first, the highest average topography is between 41° and 45° , corresponding to the Klamath Mountains; second, average topography fluctuates around 200 m between 43.5° and 46° ; and third, a spike in average topography occurs at 47.5° - 48° , corresponding to the Olympic Mountains. The two profiles differ considerably along two segments where coastal plains or embayments are unusually wide, extending as much as 20 km inland. These segments include the southern Oregon coastal plain (Cape Blanco to Coos Bay; latitudes 43° - 43.3°) and the embayments of southern Washington (Columbia River, Willapa Bay, Grays Harbor; latitudes 46° - 47°). With the exception of these coastal lowlands, the western portion of the Coast Ranges has latitudinal trends in elevation similar to that of the Coast Range as a whole (Figure 2), albeit the average elevations

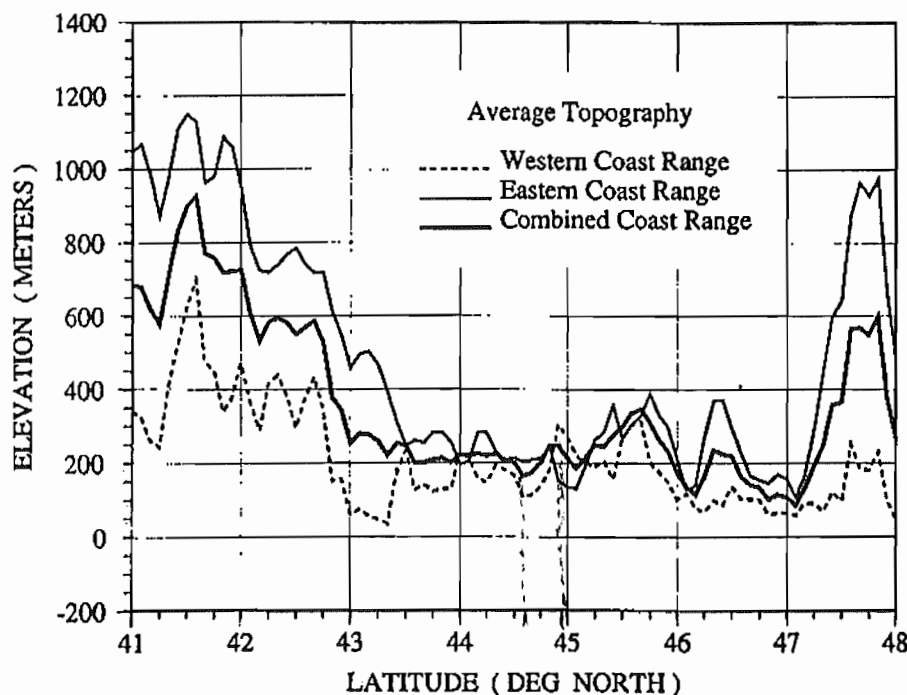


Figure 2. Latitudinal variation in average topography for the 25-arc-min-wide western portion of the Coast Ranges, for the 25-arc-min-wide eastern portion of the Coast Ranges and for the entire 65-arc-min-wide Coast Ranges. All longitudinal distances are measured eastward (inland) from the coast. The eastern and western data sets do not use overlapping data. General topographic trends are similar for the eastern, western, and combined data sets.

along the coast are lower because Coast Range drainages transport sediment to the west.

The error limit for the latitudinal variation in average topography of the Coast Ranges (Figure 3) is the standard error of the mean. Because of the running average, sequential standard errors are correlated, but every third standard error is independent. We also show an envelope curve depicting the upper bound of elevations used in the calculation at each latitude ("maximum elevation" in Figure 3). The maximum elevation is the average elevation of the crest of the Coast Ranges computed as a three-point running average. The maximum elevation profile shows the magnitude of surface uplift, or uplift of rocks minus exhumation, along the Coast Range crest.

Overlying Topography Versus Age of Subducted Juan de Fuca Plate

Subsidence, or change in elevation, of the ocean floor as it moves away from the spreading ridge is expressed by

$$e(t) = ct^{1/2}$$

[Parsons and Sclater, 1977], where $e(t)$ is the vertical distance in meters that the ocean floor has subsided in moving away from the spreading ridge and t is the age of the plate in millions of years. Constant c , the linear slope of the change-in-elevation versus $t^{1/2}$ relation, is 350 [Parsons and Sclater, 1977]. The use of this subsidence model, in conjunction with an approximate age distribution of the Juan de Fuca and Gorda

plates presently subducting at the Cascadia margin, yields latitudinal estimates of the relative elevation of the subducting plate at a position beneath the crest of the Coast Ranges (Figure 3).

The lithospheric subsidence model predicts that rapid density changes occur within the oceanic plate in close proximity to ridges. However, thick accumulations of young sediments along the Cascadia margin and a lack of seismicity near the trench axis preclude direct measurement of depths to the top of the subducting Juan de Fuca plate beneath the Coast Range. We acknowledge problems inherent in estimating slab morphology near subduction zones using the simple age-depth relationship cited above and emphasize that our interpretation focuses on the relative subsidence of the slab due to changes in slab age along the margin. When oceanic plates are loaded by subduction under continental crust, the differential subsidence would be enhanced over that caused by an increase in age of the plate alone. This enhancement is because a less dense, younger slab will subside less than an adjacent older, denser slab, if both are loaded by the same overlying continental plate. Thus the differential elevation of two adjacent subsiding slabs, as computed by the Parsons-Sclater relation in the case of no loading, is a minimum estimate for the amount of differential subsidence that must occur if both slabs are subsequently loaded by an overriding plate.

Approximations for the age of the subducting plates, needed to calculate relative subsidence, are made difficult by a complex pattern of spreading along the Juan de Fuca and Gorda ridges. These complications include propagating rifts, changes in relative motion poles, deformation within the

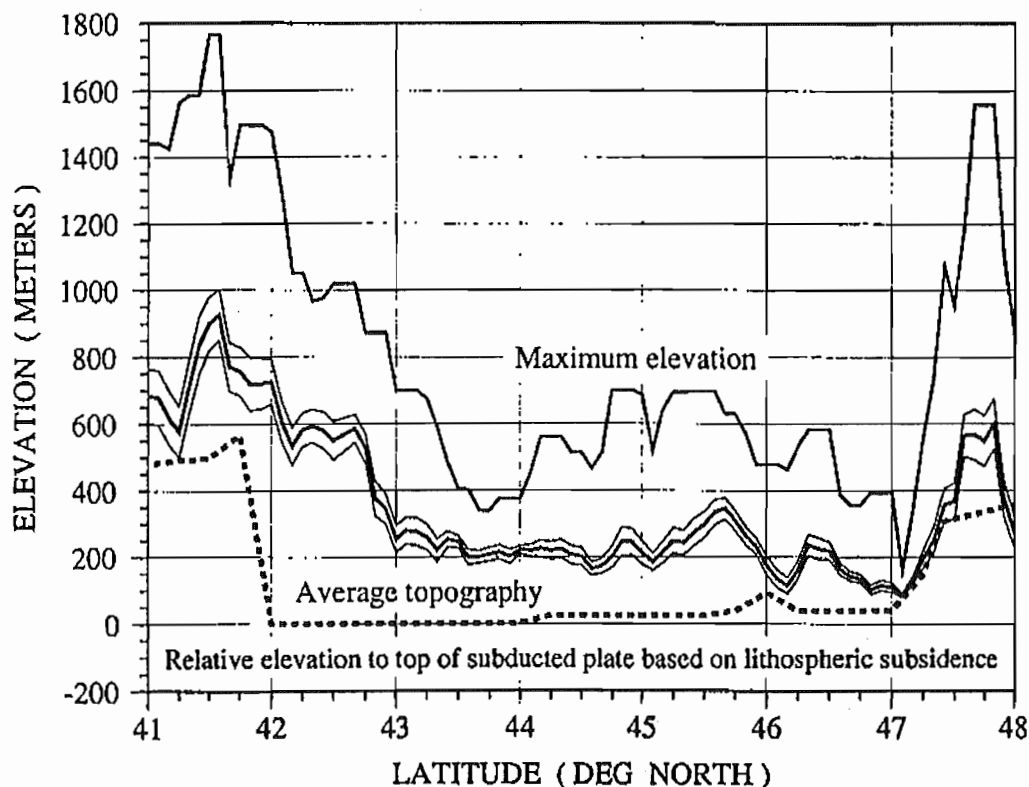


Figure 3. Latitudinal variation in average topography and age of subducted slab along the crest of the Coast Ranges. Top curve, maximum average elevation used in each topographic calculation; middle curves, average topography bounded by the standard error of the mean; bottom dashed line, relative elevation of the top of the subducted slab beneath the crest of the Coast Ranges.

34

Gorda plate, and an uncertain history for the development of the Blanco Fracture Zone [Wilson, 1986, 1990; Embley and Wilson, 1992]. Age estimates (Table 1) were determined by reflecting recognizable magnetic isochrons from the Pacific plate onto the Juan de Fuca and Gorda plates using the magnetic isochron map of Atwater and Severinghaus [1989]. A similar result is obtained through an eastward extrapolation of the isochron patterns observed immediately to the west of the Cascadia deformation front.

The age of the slab beneath the crest of the Coast Ranges is uniform except for markedly younger slab at the southern end beneath the Klamath Mountains, which form the Coast Ranges in southernmost Oregon and northernmost California (Figure 3). Younger slab also underlies the Olympic Mountains at the north end of the Coast Range. The age discontinuity in the subducted slab beneath the Klamath Mountains is due to subduction of the Blanco Fracture Zone (Figure 1b), which juxtaposes young crust to the south against older crust to the north (Table 1). The younger slab beneath the Olympic Mountains reflects subduction of progressively younger plate to the north as the Pacific-Juan de Fuca spreading center becomes closer to the leading edge of the North American plate (Figure 1b) (Table 1).

The most abrupt latitudinal change in average topography occurs above the subducted Blanco Fracture Zone (Figure 3).

Table 1. Age of the Subducted Juan de Fuca Plate as Projected through the Overlying Pacific Plate to the Crest of the Coast Ranges

Latitude* °N	Chron †	Age, Ma
48.0	5/5A	11.0
47.4	5A	12.0
47.25	5B	15.3
47.0	5D	17.86
46.75	5D	17.86
46.5	5D	17.86
46.25	5D	17.86
	<i>Pseudo Fault</i>	
46.0	5C	16.60
45.75	5D	17.86
45.5	5D	17.86
45.25	5D	17.86
45.0	5D	17.86
44.75	5D	17.86
44.50	5D/5E	18.2
44.25	5D/5E	18.2
44.0	5E	18.8
43.75	5E	18.8
43.5	5E	18.8
43.25	5E	18.8
43.0	5E	18.8
42.75	5E	18.8
42.5	5E	18.8
42.25	5E	18.8
42.0	5E	18.8
	<i>Blanco Fracture Zone</i>	
41.75	4	7.41
41.5	5E/4	8.5

*Latitude position is along crest of Coast Ranges

† Chron on the Juan de Fuca plate determined from reflection of chrons from Pacific plate to Juan de Fuca plate across the spreading center.

The top of the relatively young, more buoyant subducted crust south of the Blanco Fracture Zone has an elevation that is about 500 m higher relative to the top of the slab north of the Blanco Fracture Zone. The north facing scarp in the downgoing slab, with relatively higher slab to the south, is presently directly below the zone of maximum change in average topography along the Coast Range crest (Figure 3). This altitudinal change marks the topographic division between the Klamath Mountains to the south and the elevationally lower Oregon Coast Ranges to the north. Similarly, the topographically higher Olympic Mountains, at the northern end of the Coast Ranges in Washington, are underlain by relatively young subducted plate that is, in relative elevation, about 300 m higher than older subducted plate further south.

Geodetic Uplift Rates

Differences in the relative heights of bench marks reoccupied by successive first-order leveling surveys provide a data set of geodetically derived uplift rates along the coast for the past ~45 years, from 1941 to the period 1987-1988 (Figure 4) [Mitchell et al., 1991, 1992, this issue]. The trends in relative bench mark elevation changes between leveling surveys (Figure 4) are probably real and of tectonic origin because analysis of tidal records along the same segment of coast yields the same magnitudes and trends in uplift. The tidal gage records and the leveling survey records are two independent data sets; differencing the tidal records and differencing the leveling records yield similar relative differences in uplift rate between coastal localities [Mitchell et al., this issue].

The geodetically derived uplift rates are referenced to a contemporary sea level rise of 1.8 mm/yr [Douglas, 1991], with no correction for post glacial rebound. In magnitude and variability, the uplift rates are several times larger than the predicted magnitude of present-day post glacial rebound, and the regional variation of uplift rate is of a much shorter wavelength than that predicted for present-day post glacial rebound [Mitchell et al., this issue]. These geodetically derived uplift rates are uplift rates of rock relative to the geoid and thus are directly comparable to the shore platform uplift rates, described below.

Uplift Rates of Shore Platforms

Uplift rates are calculated for uplifted shore platforms in the latitude range 42° to 45°N. The magnitude of uplift, relative to present sea level, was determined for the junction of the paleo-sea cliff and the platform (the shoreline angle). Uncertainties in calculation of the magnitude of uplift of the shoreline angle are (1) the altitude of the shoreline angle at the time of its formation relative to altitude of the eustatic sea level high stand that eroded the shoreline angle (according to Wright [1970] and Trenhaile [1980], the two elevations are the same, ± 2 m); (2) altitude of paleo-sea level high stand, this altitude being a function of the age of the high stand and the sea level model employed (see below); (3) present-day altitude of shoreline angle, where the error in assigned altitude is a function of surveying accuracy; we used 7.5 arc min topographic maps for assigning altitude, where the error is ± 6 m, or one half the contour interval; and (4) original seaward tilt of the platform; this uncertainty only applies in cases of

35

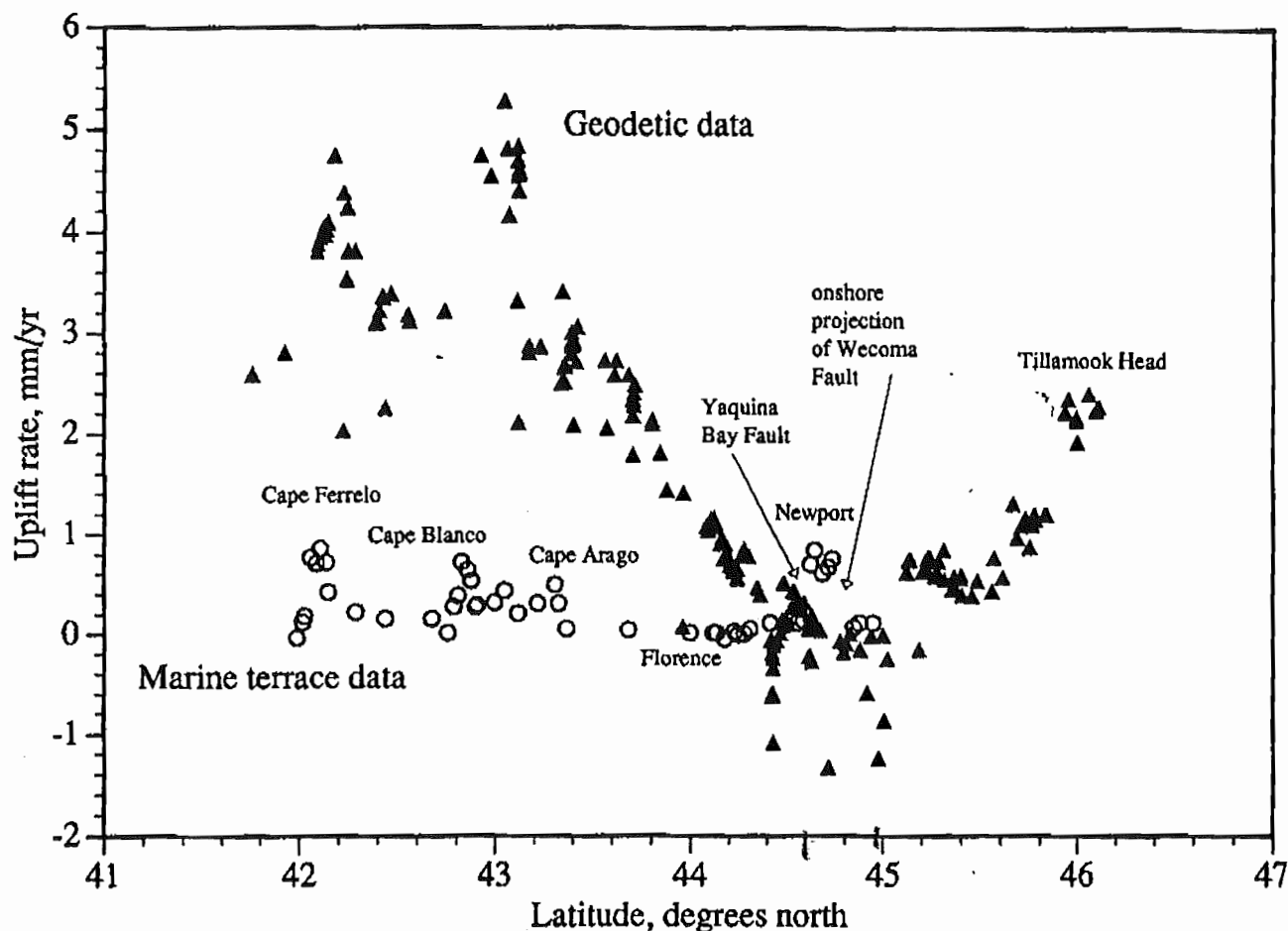


Figure 4. Latitudinal variation in uplift rates derived from resurveyed bench marks between 1941 and the 1987-1988 period, and from sea cliff/platform junctions of 80-125 ka shore platforms. Triangles, resurveyed bench marks; circles, shore platform data.

poor exposure where platform altitude is measured at a point seaward of the shoreline angle, necessitating calculation of shoreline angle elevation using the original slope of the platform [Bradley and Griggs, 1976].

Uplift rates can only be determined at localities where the shoreline angle elevation can be located on a terrace of a known age. The ages of the late Quaternary eustatic sea level high stands are well established at 80, 105, and 125 ka [Mesolella et al., 1969; Bloom et al., 1974; Chappell and Shackleton, 1986]. The 80 ka and 105 ka wave-cut platforms were identified based on terrace correlation, using soil development [Bockheim et al., 1992] and altitudinal surveys, to terraces of known age in the Cape Blanco [Kelsey, 1990] and Cape Arago [McInelly and Kelsey, 1990] areas. Marine terrace sediments of known age have age assignments based on a radiometric age from U-series dating of coral and amino-acid racemization-ratio correlation ages using molluscs [Muhs et al., 1990]. In central coastal Oregon, 125 ka platform ages were assigned [Ticknor, 1993] either based on terrace sequence (the terrace in question being the next one altitudinally above the 105 ka terrace) or based on correlation with a 125 ka age-assigned wave-cut platform near Yaquina Bay, Oregon [Kennedy et al., 1982].

We used paleo-sea level high stand elevations as determined from the coastal California sea level high stand elevation

model [Muhs et al., 1992], rather than the New Guinea sea level high stand model [Bloom et al., 1974; Chappell and Shackleton, 1986]. If the New Guinea model is more appropriate for the west coast of North America, uplift rates would be systematically higher for surveyed points on the 80 ka and 105 ka platforms but not for points on the 125 ka platform. The maximum increase in uplift rates would be about 0.1 mm/yr. Given all the above uncertainties in the magnitude of uplift of a shoreline angle formed at 80, 105, or 125 ka, the maximum error in the uplift rate calculation is about ± 0.2 mm/yr.

Shore platform uplift rates are for the most part <0.25 mm/yr and have a range of -0.04 to 0.87 mm/yr (Figure 4). Abrupt changes in shore platform uplift rate, in some cases by almost an order of magnitude, occur at several localities along the Cascadia margin. All abrupt changes in uplift rate can be related to a distinct structure, a fault or a fold, that displaces the shore platform. Uplift rates abruptly change across structures near Cape Ferrelo (CF, Figure 1b and Figure 4) [Kelsey and Bockheim, 1994], Cape Blanco (CB, Figure 1b and Figure 4) [Kelsey, 1990], Cape Arago (CA, Figure 1b and Figure 4) [McInelly and Kelsey, 1990] and Newport/Yaquina Bay (YB, Figure 1b and Figure 4) [Ticknor, 1993].

The platform offsets near Newport (Figure 4) are part of a regionally extensive upper plate fault zone at this latitude,

Quaternary upper plate deformation in coastal Oregon

Harvey M. Kelsey

Robert L. Ticknor

James G. Bockheim

Clifton E. Mitchell

Department of Geology, Humboldt State University, Arcata, California 95521

74 Russell Avenue, Watertown, Massachusetts 02172

Department of Soil Science, University of Wisconsin, Madison, Wisconsin 53706

Science Department, Lane Community College, Eugene, Oregon 97403-0640

ABSTRACT

The leading edge of the North American plate along the Cascadia subduction zone is deforming and rotating clockwise as a consequence of both underthrusting of the Gorda-Juan de Fuca plate and collision of the North American plate with the Pacific plate. The details of late Quaternary (≤ 125 ka) upper-plate deformation resulting from these plate interactions are largely obscured because the most recent deformation overprints earlier deformation in the Tertiary rocks of the Coast Range. However, by mapping uplifted wave-cut platforms formed during times of high sea level in the past ≈ 500 000 yr, we identify faults and folds active in the late Quaternary in central coastal Oregon. Through along-coast correlation of these platforms using elevation and soil development, we infer that several major faults have vertically offset platforms at rates as high as 0.6 m/k.y. for the past 125 k.y. We regionally extend our analysis by incorporating all known faults and folds in southern and central coastal Oregon that deform wave-cut platforms. Most platforms along the southern and central Oregon coast have been uplifted at rates of 0.1–0.3 m/k.y. since the late Pleistocene; however, platform uplift rates approach 1 m/k.y. in the vicinity of faults. The trend and distribution of these upper-plate coastal faults are consistent with their interpreted role as left-lateral, strike-slip, block-bounding structures accommodating clockwise rotation. We speculate that these upper-plate faults have a component of dip slip because of their association, in many instances, with localized uplift. If these faults bound rotating blocks, the dip-slip component of displacement may be either contractional or extensional, depending on the orientation of the fault relative to the north-south trend of the plate margin.

INTRODUCTION

Studies in Holocene tidal-wetland deposits along the Cascadia subduction zone in northern California, Oregon, Washington, and British Columbia have shown that the Cascadia margin has generated plate-boundary earthquakes of magnitude 8 or larger (Atwater, 1987, 1992; Darienzo and Peterson, 1990; Clarke and Carver, 1992; Clague and Bobrowsky, 1994; Darienzo et al., 1994; Atwater et al., 1995). Among the uncertainties concerning the nature of the plate boundary are the times and maximum size of plate-boundary earthquakes and the tectonic role of folds and faults in the upper plate. This paper addresses the second question by capitalizing on a unique late Pleistocene datum—the wave-cut platform—that records uplift, folding, and faulting of the upper plate in the past 100 000 yr. Wave-cut platforms provide a catalog of the location and movement history of upper-plate structures, thereby contributing to the development and assessment of kinematic models of upper-plate deformation.

In the first part of this report we describe geologic structures that have been active in the Holocene and/or late Quaternary within the upper plate in the onshore region of coastal central Oregon (Fig. 1). Onshore upper-plate structures active in the late Quaternary have been recognized elsewhere in coastal Oregon (Adams, 1984; Kelsey, 1990; Muhs et al., 1990; McInelly and Kelsey, 1990; Kelsey and Bockheim, 1994), but we focus on the central Oregon coast because these structures have not been described. In the latter part of the paper, we will address all active upper-plate structures in coastal Oregon, where we define “active” structures as those that deform surfaces cut in the past 125 k.y. or sediments deposited in the past 125 k.y. In our analysis of upper-plate deformation, we primarily consider the data set consisting of elevations of late Pleistocene (≤ 125 ka) wave-cut platforms and secondarily

a data set consisting of level-line surveys over an ≈ 45 yr period along western Oregon highways. We also draw from several other published data sets that document differential vertical displacement in the upper plate during the Quaternary.

This study attempts to demonstrate the youthfulness of several upper-plate structures, to constrain their style of deformation, and to relate this deformation to plate tectonics of the Cascadia margin. We hypothesize that upper-plate structures in central coastal Oregon are active, that they deform as part of the broad deformation zone that bounds the western margin of the North American plate, and that these structures are compatible with a prevailing upper-plate deformation model of dextral shear and clockwise rotation. We test these hypotheses through the following approaches. Upper-plate structures are recognized on the basis of deformation of marine terraces and geodetic leveling. Age assignments for marine terraces are determined through analyses of the degree of soil development on marine terraces and correlation of these soils to those on marine terraces elsewhere in coastal Oregon that have numerical ages. Fault style and fault-slip rate are constrained by mapping of fault trends and by evaluating magnitude of fault offset of marine platforms. Using all upper-plate active structures in coastal Oregon as a data base, we evaluate whether a model of dextral shear and clockwise rotation of the upper plate is compatible with late Pleistocene faulting and folding along the Oregon coast of the Cascadia margin.

UPPER PLATE GEOLOGY IN CENTRAL COASTAL OREGON

Regional Bedrock Geology of the Oregon Coast Range

The Oregon Coast Range consists of a tectonically elevated belt of crust lying 150–200 km

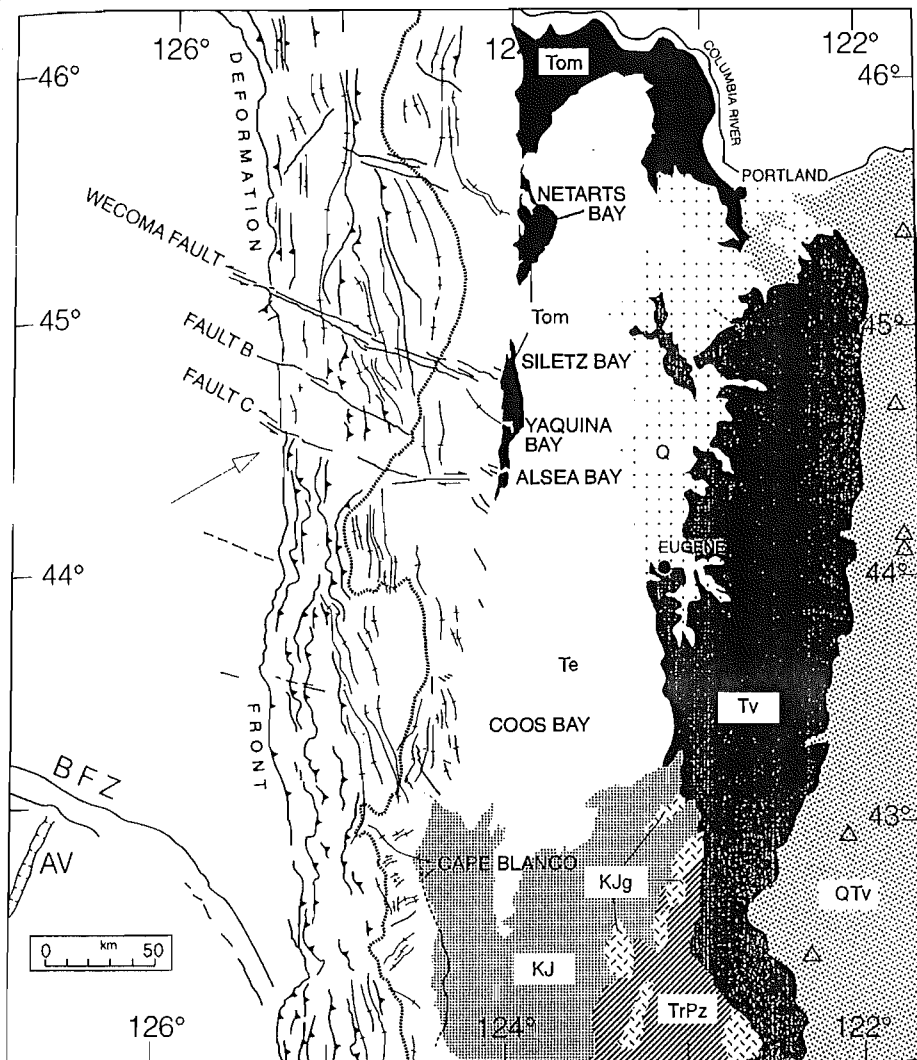


Figure 2. Tectonic map for continental shelf and rise of offshore Oregon and generalized geologic map for western Oregon west of the Cascade Mountains. Offshore data from Goldfinger et al. (1992b); onshore data from Walker and MacLeod (1991). All structures displace Pleistocene or younger sediments. This paper focuses on the late Quaternary deformation along the Oregon coast in the vicinity of Alsea, Yaquina, and Siletz Bays. Sites along the Oregon coast where late Holocene coseismic subsidence has been reported include, from north to south, Netarts Bay (Darienzo and Peterson, 1990), Siletz and Yaquina Bays (Darienzo et al., 1994), Coos Bay (Nelson, 1992), and the Sixes River at Cape Blanco (Kelsey et al., 1993). Bold dashed line is edge of continental shelf; bold solid line is steeply dipping fault; bold solid line with teeth is thrust fault with teeth on upper plate; thin solid lines with short cross bars are fold axes. AV is axial valley of the spreading ridge separating the Pacific plate to the west from the Gorda plate to the east. BFZ is Blanco fracture zone. The Juan de Fuca plate is bounded by the BFZ on the south and the deformation front on the east. The North American plate occurs east of the deformation front. The young (ca. 19 Ma) Juan de Fuca plate is obliquely subducting under the North American plate at ≈ 40 mm/yr (Riddiough, 1984). Explanation of geologic symbols: Q, Quaternary sedimentary fill in the Willamette valley; QTv, Quaternary and Tertiary volcanic rocks and volcaniclastic sediments of the Cascade Mountains; Tv, Tertiary volcanic rocks east of the Willamette valley and the Coast Range; Tom, Tertiary Oligocene and Miocene sedimentary and volcanic rocks of the Coast Range; Te, Tertiary Eocene volcanic and sedimentary rocks of the Coast Range; KJ, Cretaceous and Jurassic rocks of the Klamath Mountains; KJg, intrusive igneous rocks of the Klamath Mountains; TrPz, Triassic and Paleozoic rocks of the Klamath Mountains. Triangles denote volcanoes of the Cascade Range.

level highstands (Bloom et al., 1974) can serve as reference horizons from which to estimate late Quaternary deformation (Adams, 1984; Lajoie, 1986; Merritts and Bull, 1989; Kelsey, 1990; McInelly and Kelsey, 1990; Clarke and Carver, 1992). Such platforms are preserved along the central Oregon coast in the form of uplifted marine terraces. Each terrace is underlain by a thin (2–40 m) veneer of mostly marine sediment that covers the wave-cut platform.

We identified a set of six marine terraces on the central Oregon coast (Ticknor, 1993) (Fig. 3 and Table 1). Terraces are preserved discontinuously, range in elevation from sea level to 153 m and extend as much as 3 km inland. The younger and better preserved terraces typically form narrow strips ranging from <100 to ≈ 800 m in width. In the vicinity of Yaquina and Alsea Bays, the terraces are widest, attaining widths up to 2000 m.

Marine terraces were differentiated by terrace elevation, wave-cut platform elevation, terrace back-edge relief, and cover-bed stratigraphy (Table 1), as well as by degree of soil development. Platform elevations were measured wherever possible. Measurement sites were located on 1:24 000 maps using aerial photographs. Elevations were read off the maps with an accuracy of one-half the contour interval, which is ± 6 m. Altimeter surveys (error ± 3.3 m) were employed for the lowest wave-cut platforms, wherever ties to permanent benchmarks could be established.

Sediments that underlie the terraces are typically high-energy nearshore marine deposits capped by beach sand. Vegetated relict sand dunes commonly cover part of the beach deposits. These deposits are most prevalent in the vicinity of Alsea Bay, where hummocky dunal topography is characteristic of the surfaces of the lower terraces.

Previously reported ages for uplifted marine terraces in central coastal Oregon are limited to the vicinity of Yaquina Bay. Kennedy (1978) and Kennedy et al. (1982) assigned an age of 125 ka (oxygen isotope stage 5e) to cover sediments above the wave-cut platform at Hinton Point (also named Idaho Point) on the south side of Yaquina Bay (Fig. 3). This age assignment is based on a warm-water affinity of the fossil mollusk shells, in conjunction with amino acid enantiomeric (D:L) ratios for fossil shells. In contrast, amino acid D:L ratios for shells collected from terrace sediments above a wave-cut platform at Yaquina Bay State Park, on the north side of Yaquina Bay, correlate with amino acid D/L ratios from southern Oregon, and suggest an age of 80–85 ka (oxygen isotope 5a) (Kennedy, 1978; Kennedy et al., 1982). The difference in D:L ratios between

The oldest and highest terraces, the Fern Ridge and Alder Grove terraces, are preserved only in the vicinity of Alsea Bay on hill tops and ridge crests (Fig. 3). The platforms of both these terraces are tilted to the south.

Yachats to Heceta Head. South of Yachats, a single marine terrace crops out as a low bench, informally referred to as the Yachats Bench (Fig. 3). Platform elevations along the Yachats Bench decrease to the south and range from 13 to 0 m. The platform becomes submerged just north of Heceta Head (Fig. 1). Cover sediments on the Yachats Bench consist of beach sand that is in almost all instances overlain by eolian sand, debris flows, or both.

Marine Terrace Soils

We defined a soil chronosequence (a sequence of soils that differ in certain properties primarily as a function of time) for central Oregon coastal marine terraces and then used the chronosequence as a tool to correlate marine terraces across the three coastal reaches and to correlate the terraces to flights of marine terraces at other localities on the Cascadia margin. These correlations are the basis for identifying long-term, permanent vertical deformation along the coast. Ticknor (1993) provided more thorough discussion of soil properties, laboratory analyses of particle size, and aspects of pedogenesis for the central Oregon coast. The parent material for all the soils is unconsolidated Pleistocene beach or dune sand. Some soils described on the Yachats bench developed on basalt-rich debris flow deposits that overlie beach sand.

Field-identifiable soil properties that are both time dependent and can be used to distinguish the terraces include the depth to the Cox horizon (oxidized parent material), the thickness of the clay-enriched (Bt) horizon, the estimated maximum percent clay, and maximum clay skins. From these properties, we assigned development stages for the soils (Table 2) (Kelsey and Bockheim, 1994).

Soils were examined at 56 sites (Fig. 5) on the 6 marine terraces within the study area. Soil pits were excavated for 14 sites to a depth of 2 m, with continued augering down to the Cox horizon. Soils at 42 other sites were described from samples obtained with a 7.5-cm-diameter bucket auger. Soil data are presented separately for the three subregions: Siletz Bay to Newport (Table 3), Newport to Yachats (Table 4) and Yachats to Heceta Head (Table 5).

Soil properties change as a function of time for the six terraces (Fig. 6; Tables 3 and 4). Significant aspects of the Figure 6 data are: the average depth to the C horizon steadily increases (Fig. 6A); the Bt horizon thickness increases al-

TABLE 2. DEVELOPMENT STAGES OF SOILS ON ELEVATED MARINE TERRACES ALONG THE CENTRAL AND SOUTHERN OREGON COAST

Development stage	Depth to Cox (m)	B horizon hue	Bt (cm) thickness	Maximum B horizon texture* (% clay) [†]	Maximum clay films [§]
1	0.8–1.4	7.5–10YR	0	sil, l, sl (<30)	1–3npfpo
2	1.0–1.4	7.5YR	<50	sicl, cl, scl (30–40)	2–3n-mkpfpo
3	1.0–1.7	7.5YR	<50	sicl, cl, scl (30–40)	2–3mkpfpo
4	1.4–1.8	5–7.5YR	50–100	sicl, sic, cl, c (35–42)	3–4mkpfpo
5	1.9–2.8	5–7.5YR	100–200	sic, c (40–58)	3–4mk-kpfpo
6	2.6–4.5	5YR	>200	sic, c (40–65)	3–4mk-kpfpo
7	3.2–>4.5	2.5YR	>200	sic, c (45–65)	3–4mk-kpfpo

*S, sand; l, loam; sl, sandy loam; sil, silt loam; sicl, silty clay loam; sic, silty clay; cl, clay loam; c, clay. Abbreviations follow Soil Survey Staff (1975).

[†]We estimated percent clay for each horizon at each soil locality during field work. We have confidence in our ability to estimate clay content in the field because we obtained a significant correlation ($R = 0.81$; $p \leq 0.01$) between percent clay measured in the field and percent clay measured in the laboratory (28 samples).

[§]Notations for clay films: number denotes extent of ped faces covered by film: 1, 5%–25%; 2, 25%–50%; 3, 50%–90%; 4, >90%; n, thin; mk, moderately thick; k, thick; pf, film on ped face; po, film lines the pores. Abbreviations follow Soil Survey Staff (1975).

most linearly for the first five terraces (Fig. 6B); the average estimated percent clay increases along with Bt thickness from ≈30% on the youngest two terraces to slightly >40% on the next three older terraces (Fig. 6C); and the development stage increases almost linearly from 1.8 on the youngest terrace to 6.0 on the next to oldest terrace (Fig. 6D). It is also clear from Figure 6 that soils on the two oldest terraces cannot be distinguished from each other. Distinctions between these two terraces, however, were not critical for the platform correlations.

In the vicinity of Alsea Bay, development stages for soils on terrace sediments were conspicuously lower than the surrounding regions. Thirteen soil sites, which were notably underdeveloped, are not included in Table 4 or in Figures 5 and 6, and were not used for relative dating. Soils at these sites have developed on extensive sand dune deposits. Prolonged eolian activity on terrace surfaces in proximity to Alsea Bay is the likely explanation for the poorly developed soils.

In summary, the lowermost four marine terraces can be distinguished from one another on the basis of field-identifiable soil properties. The soils on Fern Ridge and Alder Grove terraces, in contrast, are old enough for the soils to have developed to such an extreme that distinguishing between the two is difficult (terrace 5 versus terrace 6 in Table 4). However, their relative ages are established based on elevation of the respective terraces.

Correlation of Marine Terraces on Either Side of Yaquina Bay Using Soils: The Yaquina Bay Fault

Matching of marine terraces across Yaquina Bay is necessary for evaluation of the hypothesis that a fault underlies the bay. A sequence of three terraces is preserved in the first 10 km north of the bay and a sequence of five terraces is preserved in the first 10 km south of the bay (Figs. 3 and 7A). We compared soil descriptions for the lowest three terraces 10 km south of the bay with the lowest three terraces 10 km north of the bay to evaluate the possible matches (Fig. 7B and Table 6). The best match based on soil properties (Fig. 7C and Table 6) indicates that the highest terrace north of Yaquina Bay can reasonably be matched with either the second- or third-highest terrace south of the bay. However, the only set of terrace matches entirely consistent with the soil data is the one that matches the highest (third) terrace north of the bay to the second-highest terrace south of the bay (Fig. 7D).

Matching of wave-cut platforms across Yaquina Bay shows that correlative platforms occur at different elevations on opposite sides of the bay, and the preferred match of terraces can only be accommodated if a fault beneath Yaquina Bay displaces the platforms up to the north (Figs. 7D and 8). A fault with the same sense of displacement, situated underneath

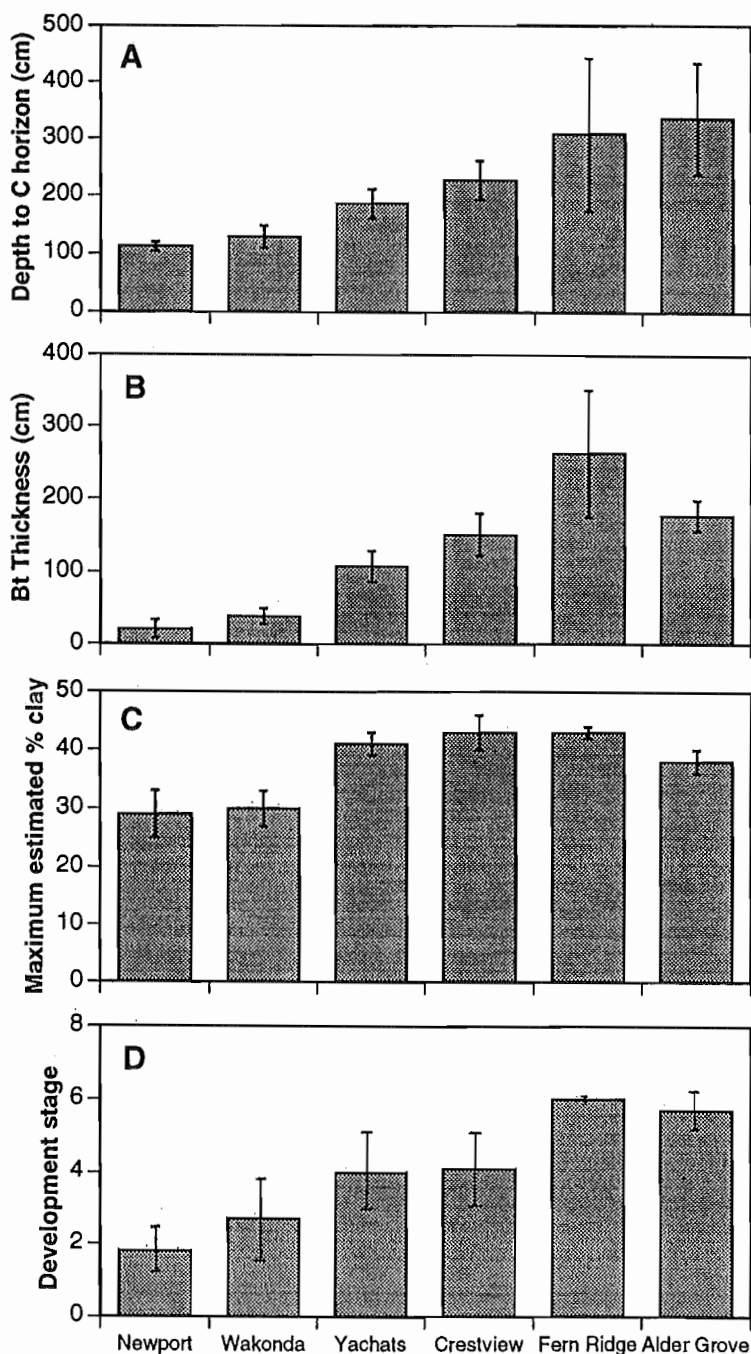


Figure 6. Charts showing average soil properties used as relative age indicators for soils developed on the six marine terraces. (A) Depth to C horizon. (B) Bt horizon thickness. (C) Estimated maximum percent clay in the Bt horizon. (D) Development stage (see Table 2). Vertical lines represent the standard error for the averages.

nated by deformation of the Crestview wave-cut platform, which is the only extensively preserved platform on the downthrown side of the Waldport fault zone. Shore-parallel profiles of platform elevation (Fig. 8) show that, in the vicinity of Alsea Bay, there is a crustal downwarp on the downthrown block of the Waldport

fault defined by an uplift minimum for the Crestview platform (no. 4 platform; Fig. 8). The Alsea Bay downwarp (ABD; Fig. 8) is ≈ 4 km in wavelength, and the amplitude of the downwarp, considering the ± 6 m elevation measurement error, is 14–37 m. Because the location of the downwarp is just east of the

Waldport fault (Fig. 8), we infer that the Alsea Bay downwarp is a product of displacement on the Waldport fault zone. The inference that the 14–37 m amplitude downwarp is associated with the fault zone is consistent with the time of formation of the surface (the Crestview platform was cut ca. 200 ka) and the minimum rate of vertical offset of the Waldport fault (0.1–0.15 m/k.y.) during the late Pleistocene.

In conclusion, both of the major embayments, Yaquina Bay and Alsea Bay, appear to be structurally controlled by faults that have been active in the late Quaternary. Alsea Bay appears to straddle a region of downwarping on the downthrown side of the Waldport fault zone and Yaquina Bay rests on the downthrown block of the Yaquina Bay fault (Fig. 9).

South of Alsea Bay, uplift rates decrease to the south. For the 12 km coastal reach south of Yachats (Yachats bench) (Figs. 3 and 8), there has been little vertical displacement of the Yachats platform in the past 125 k.y. (data for lat 44.23°N to 44.28°N in Table 8). Thus, the Yachats bench is one of the few coastal segments along the Oregon and northern California portion of the Cascadia margin that records negligible net vertical crustal displacement since the last interglacial (125 ka). At Searose Beach at the southern end of the study area (Fig. 1), uplift rates reach a minimum of 0.00 to 0.04 m/k.y., calculated for the 125 ka platform (lat 44.23°N in Table 8).

DEFORMATION SINCE THE LATE PLEISTOCENE IN CENTRAL COASTAL OREGON

Deformation since the formation of the wave-cut platforms (since the late Pleistocene) is the result of many hundreds of cycles of interseismic and coseismic deformation. However, the paleoseismicity of upper-plate faults cannot be addressed through marine terrace studies. Although we know that these faults offset datums that are on the order of 100 ka in age and that the faults have a vertical component of slip rate of 0.1–0.6 m/k.y., no earthquakes have occurred on these faults since ca. 1870, and we do not know if these faults have the capability of rupturing independently of ruptures on the underlying megathrust or if these upper-plate faults could play a role in segmenting ruptures on the subduction zone.

Differences in the relative heights of benchmarks reoccupied by successive first-order leveling surveys provide a data set of historic, geodetically derived uplift rates along the coast for the past ≈ 45 yr, from 1941 to the releveing epoch 1987–1988 (Fig. 10) (Mitchell et al., 1994). Although the data are noisy because of

40

Figure 9. (A) Summary tectonic map of the Oregon coast and offshore area (sources are Walker and MacLeod, 1991; Goldfinger et al., 1992b) showing more detailed tectonic maps for the following four coastal regions: (B) central Oregon coast; (C) Coos Bay–Cape Arago region (McInelly and Kelsey, 1990); (D) Cape Blanco region (Kelsey, 1990); and (E) southernmost coastal Oregon (Kelsey and Bockheim, 1994). All onshore structures have been active in the past 125 k.y. Bold lines are faults, and thin lines are synclines and anticlines.

ern continental margin, relative to stable North America, as a consequence of dextral shear and clockwise rotation.

Faults and folds that deform late Pleistocene wave-cut surfaces have been identified along three other segments of the Oregon coast, in addition to the central Oregon coast: Cape Arago–Coos Bay (McInelly and Kelsey, 1990); Cape Blanco (Kelsey, 1990); and Cape Ferrel–Brookings (Kelsey and Bockheim, 1994)

(Fig. 9, C, D, and E). Adjacent to the faults and folds, uplift rates are higher (≈ 0.4 – 1.0 m/k.y.) relative to the background rate of 0.0 – 0.2 m/k.y. (Kelsey and Bockheim, 1994).

The pattern of uplift and fault deformation in central coastal Oregon is the same as in the other coastal segments; wave-cut platforms between Yachats and Siletz Bay underwent a slow, long-term permanent uplift that averaged 0.1 – 0.3 m/k.y. in the late Pleistocene, with the exception of

the fault-bounded block extending from Yaquina Bay to Cape Foulweather, where uplift rates approached 1 m/k.y. (Table 8). The Yaquina Bay fault bounds this block to the south and the Cape Foulweather fault bounds it to the north (Fig. 8). The zone of coastal faulting associated with this block is ≈ 20 km to the east of the eastern end of an east-southeast–trending fault zone, described by Goldfinger et al. (1992a, 1992b), that extends from the Cascadia deformation front across the continental slope and shelf to the coast (Fig. 9). The on-land faults and the faults on the shelf and slope project toward each other, but there are no data to suggest that they connect.

Within the 2- to 10-km-wide zone of marine terrace deformation in coastal Oregon, fold axes are variable in trend and the faults are diverse in trend and style from one coastal segment to the next, as well as within a single seg-

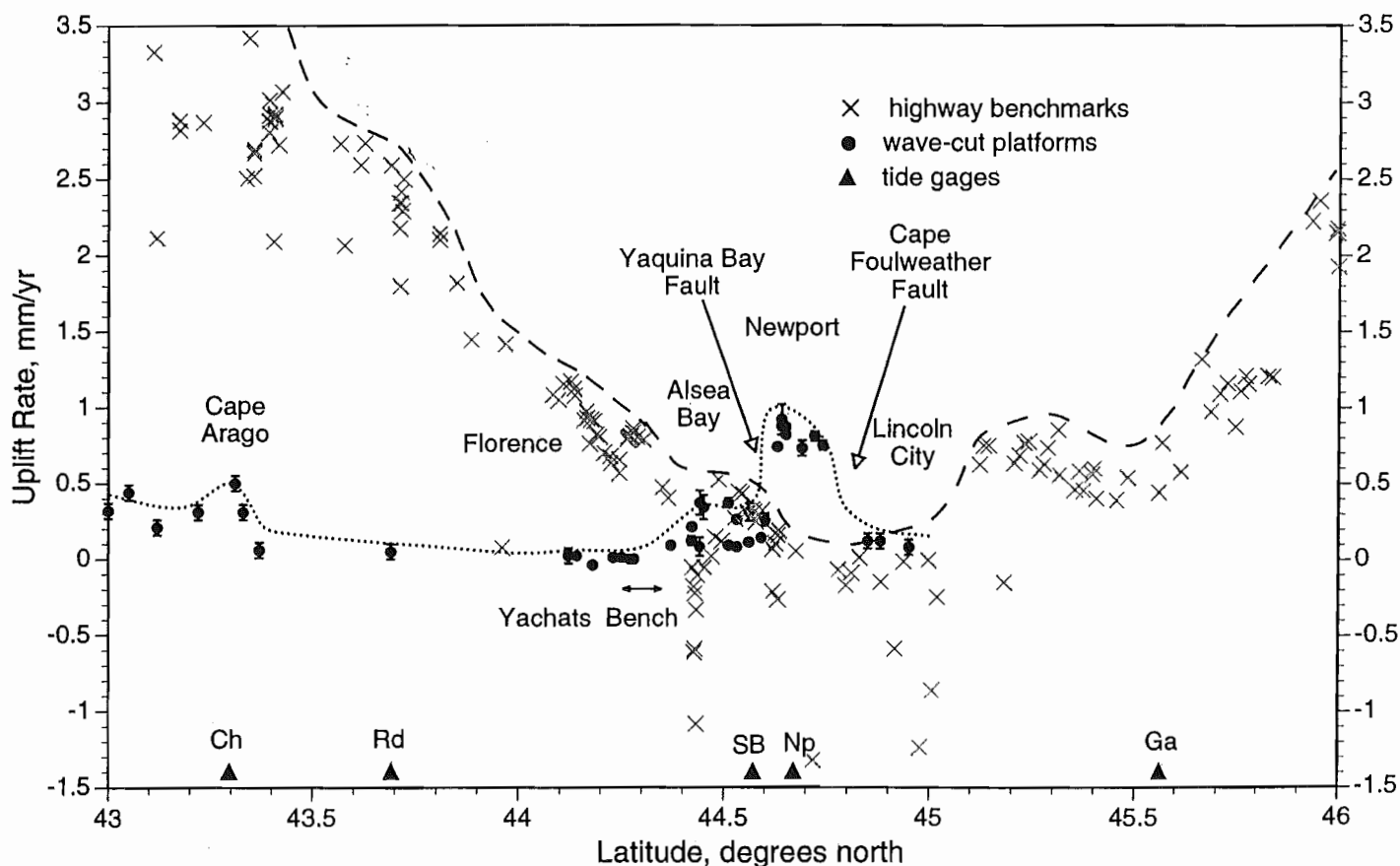


Figure 10. Along-coast variation in average uplift rates since 125 ka (solid dot symbol, derived from elevations and assigned ages for wave-cut platforms) versus uplift rates for 1941–1987 (\times symbol, derived from leveling of highway benchmarks; Mitchell et al., 1994) for the central Oregon coast. Dotted line tracks the variation in average platform uplift rates. Dashed line delineates the upper limit for benchmark uplift rates. Triangles show locations of the tide gages that provide an independent check on the historic uplift rates from leveling. Some benchmarks yield uplift rates significantly below the upper limit, probably because of local subsidence, or settling, of individual benchmarks. Vertical bars represent range of platform uplift rates determined for the shoreline angle of the 80, 105, and 125 ka platforms using the minimum and maximum platform gradients from Bradley and Griggs (1976) and North American sea-level model (Muhs, 1992; Muhs et al., 1992) (see Table 8).

41

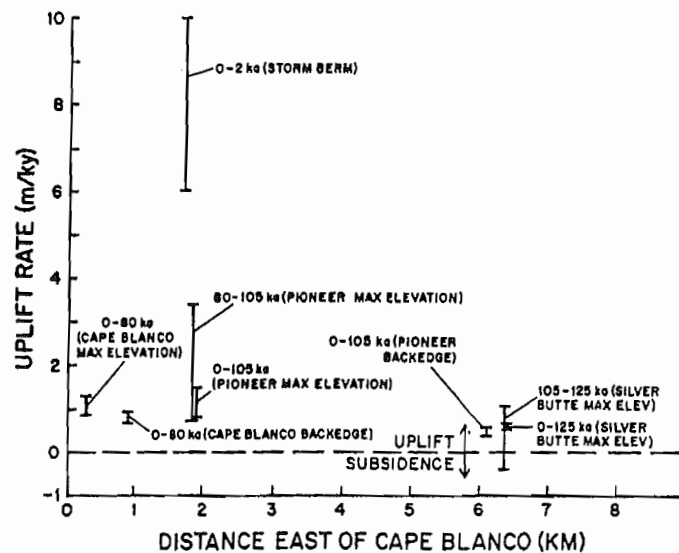


Fig. 12. Temporal and spatial variations in uplift rate for the three youngest wave-cut platforms near Cape Blanco, the Cape Blanco (80 ka), Pioneer (105 ka) and Silver Butte (125 ka) platforms. Uplift rate data are for points along the Cape Blanco anticline axis, except for the storm berm data, which are projected onto the axis from a point 1.3 km to the south. Uplift rates are from Tables 2 and 3, with the exception of the rate for 0-2 ka (see text).

of several coseismic uplift events at the apex of a fold growing in the accretionary margin in the late Holocene. The storm berm provides no data from which to infer the uplift mechanism. However, coseismic deformation of such a local structure as the Cape Blanco anticline is conceivable because only 55 km to the north in the Cape Arago-South Slough region, coseismic uplift and subsidence both have probably occurred during Holocene tightening of another fold, the South Slough syncline (Figure 1) [Nelson, 1987; Nelson et al., 1988; McInelly and Kelsey, 1990]. Nelson [1987] and Peterson and Darienzo [1989] describe stratigraphic evidence for as many as 7 or 8 abruptly buried salt marsh surfaces along the axial trace of the syncline. These abrupt subsidence events have all occurred during the late Holocene time span of the storm berm, and coseismic deformation of the synclinal fold is the most reasonable explanation for the buried surfaces.

Work elsewhere along the coast of Cascadia, including to the north of Cape Blanco at Netarts Bay in northwest Oregon [Darienzo and Peterson, 1990] and at

Willapa Bay in southwest Washington (Figure 1) [Atwater, 1987, 1988] and to the south of Cape Blanco at Humboldt Bay (Figure 1) [Carver and Burke, 1989] suggests at least four earthquakes on the Cascadia subduction zone during the time interval since the storm berm was deposited. The earthquake events that may have uplifted the berm would not necessarily be coincident in time with the earthquake events to the north and the south, but major earthquakes along the Cascadia zone are sufficiently frequent to accommodate several coseismic uplift events of the Cape Blanco anticline in the last two thousand years.

Cape Blanco Deformation in the Context of Observed Regional Strain and Inferred Regional Stress

The deformation observed in the marine terraces at Cape Blanco probably is an on-land expression of the north-northwest-trending fold belt on the continental shelf of the Cascadia margin (Figure 13) [Kulm and Fowler, 1974; Clarke et al., 1985; Peterson et al., 1986]. Structural

EPISODIC TECTONIC SUBSIDENCE OF LATE
HOLOCENE SALT MARSHES, NORTHERN
OREGON CENTRAL CASCADIA MARGIN

Mark E. Darienzo and Curt D. Peterson

Geology Department, Portland State University,
Oregon

Abstract. Salt marsh subsurface deposits (0-4 m depth) in Netarts Bay, a small coastal lagoon of northern Oregon, record six events of marsh burial in the last several thousand years. Five of the buried marsh surfaces show sharp, nonerosional upper contacts with either anomalous sand layers (tsunami deposits) or tidal flat mud deposits. These sequences indicate episodic, abrupt subsidence of the marsh surfaces to low intertidal levels. In contrast, lower marsh contacts with underlying intertidal muds are gradational, indicating gradual uplift and development of the marsh. Three independent measures of deposit elevation relative to mean tidal level (percent organics, diatom assemblages, and percent eolian sand) have been used to estimate vertical displacements of marsh surfaces. Abrupt subsidence displacements of 1-1.5 m alternate with gradual uplift displacements of the order of 0.5-1.0 m. The vertical tectonic movements are interpreted to reflect coseismic strain release (abrupt subsidence) following interseismic strain accumulation (gradual uplift), associated with interplate coupling between the Juan de Fuca Plate and the North American plate in the Cascadia subduction zone. Recurrence intervals between subsidence events range from possibly less than 300 years to at least 1000 years, with the last dated event likely occurring 300-400 radiocarbon years before present (RCYBP). Significant ^{14}C age overlaps of at least four subsidence events recorded at Netarts and reported for southern Washington and other northern

Oregon bays (at 300-500, 1000-1300, 1400-1800, and 3000-3300 RCYBP) suggest the potential for event synchronicity over at least 200 km of the central part of the Cascadia subduction zone. Additional work is needed to test the synchronicity of these episodic events of coseismic subsidence.

INTRODUCTION

The Oregon continental margin extends along 450 km of the central part of the Cascadia subduction zone. However, this segment, along with the Northern California, Washington, and British Columbia segments, has not experienced a substantial subduction zone earthquake in historical time (Figure 1). The absence of large thrust earthquakes has been attributed to terminated subduction or to aseismic subduction associated with a shallow angle of subduction, excessive sediment lubrication or malleability of the young, subducting Juan de Fuca plate [Ando and Balazs, 1979; Acharya, 1981]. However, the historical record (<200 years) might be too short to rule out coseismic subduction processes [Heaton and Kanamori, 1984; Heaton and Hartzell, 1986]. Studies of relative plate motion and of recent oceanic plate seismicity indicate an oblique subduction and north-south compression of the southern Juan de Fuca plate, in accord with the northward migration of the Mendocino triple junction [Riddihough, 1984; Kelsey and Carver, 1988; Spence, 1989]. Yet Pliocene-Pleistocene imbricate thrusts and shelf fold and fault belts that dominantly trend north-south off the Oregon coast demonstrate a significant component of east-west convergent strain [Kulm and Fowler, 1974; Clarke et al., 1985]. Recent studies of deep, small-scale seismicity along the northern Cascadia

Copyright 1990
by the American Geophysical Union.

Paper number 89TC01268.
0278-7407/90/89TC-01268 \$10.00

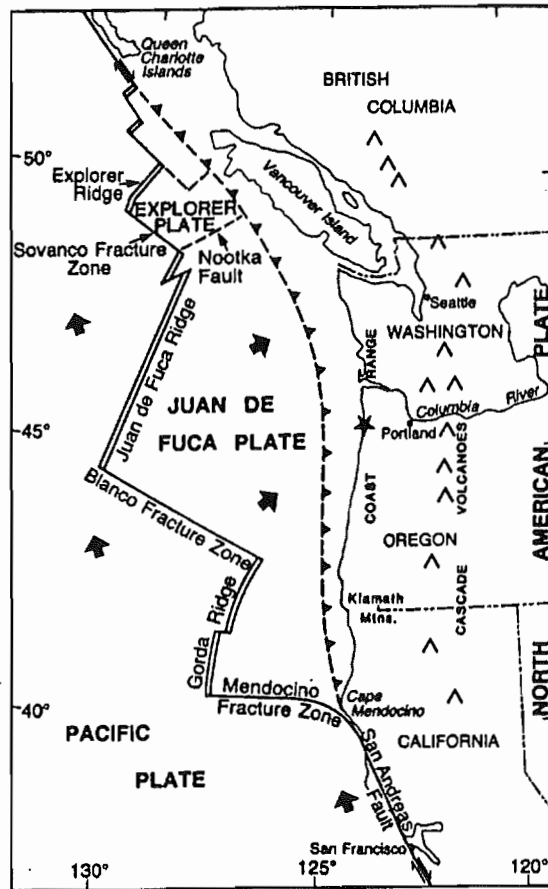


Fig. 1. Tectonic map of the Cascadia Margin. Star marks the study site. The approximate location of the trench axis, marking the boundary between the North American plate and the subducting Juan de Fuca Plate, is shown by a thrust boundary (dashed line).

margin, north of 46° latitude, indicate tensional forces associated with trench normal subduction of the northern Juan de Fuca plate [Taber and Smith, 1985; Weaver and Baker, 1988].

One test of active subduction tectonics in the Cascadia margin would be the evidence of cyclic uplift and abrupt subsidence of coastal areas. Such vertical tectonics are forced by the alternation of interseismic coupling (strain accumulation) and coseismic shear dislocation (strain release) of the subducting oceanic plate and overlying continental plate [Fitch and Scholtz, 1971]. When the subducting plate and overlying continental plate are coupled, the leading edge of the continental plate is dragged downward, producing an associated uplift on the opposite (landward) side of a flexure hinge line (Figure 2). When interseismic stresses overcome the frictional coupling, the coseismic strain release results in abrupt tectonic uplift (seaward of the hinge line) and corresponding abrupt subsidence (landward of

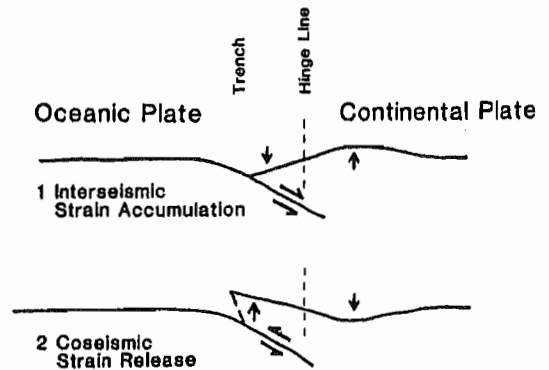


Fig. 2. Diagram of vertical coastal tectonics associated with (1) coupled strain accumulation and (2) coseismic shear dislocation between a subducting oceanic plate and an overriding continental plate [after Ando and Balazs, 1979].

the hinge line). Significantly, such abrupt vertical displacements of the sea floor produce large tsunamis [Heaton and Hartzell, 1986]. The alternation of coastal uplift and abrupt coastal subsidence together with tsunami deposition provides a potentially unique record of interplate paleoseismicity in strongly coupled subduction zones.

Such events of abrupt coastal subsidence (1-3 m) on the landward side of trench parallel hinge lines were observed in association with the 1946 Nankaido earthquake [Fitch and Scholz, 1971], the 1960 Chile earthquake [Plafker and Savage, 1970] and the 1964 Alaska earthquake [Savage and Hastie, 1966; Plafker, 1972; Owenshine et al., 1976]. Multiple events of abrupt submergence of late Holocene wetland surfaces have also recently been reported for the coast of southwest Washington [Atwater, 1987] and for northwestern Oregon (W. Grant, personal communication, 1988). These records of relative sea level change are interpreted as positive evidence for active subduction tectonics (including coseismic subsidence) along the central Cascadia margin. Similar field evidence of abrupt changes in relative sea level have been reported for Netarts Bay in northern Oregon [Peterson et al., 1988].

In this paper we describe in detail the stratigraphy and tectonic implications of buried marsh deposits from Netarts Bay, a coastal lagoon in northern Oregon (Figure 3). The small marsh of Netarts Bay was chosen for a detailed study of late Holocene records of relative sea level change on the basis of its protection from ocean storm waves and its negligible fluvial influence. These conditions are important to insure as complete and uncomplicated a record of relative sea level change as possible. In addition, its central position in the Cascadia margin (45° N) allows for the comparison of neotectonic processes in northwestern Oregon with reported marsh burial events in larger estuaries of southwestern Washington

Magnitude and frequency of subduction-zone earthquakes along the northern Oregon coast in the past 3,000 years

by Mark E. Darienzo and Curt D. Peterson, Department of Geology, Portland State University, P.O. Box 751, Portland, Oregon 97207

ABSTRACT

Similarities in number, depth, sequence stratigraphy, and radiocarbon ages characterize buried peats of seven estuaries along 175 km of the northern Oregon coast. We use these peats to infer the extent of earthquake-induced subsidence, earthquake magnitudes, and average recurrence intervals for late Holocene earthquakes at the Cascadia Subduction Zone. Synchronicity of earthquake-induced subsidence from Alsea Bay to the Necanicum River over a coastal distance of 175 km is inferred most confidently for the most recent (first) event and the third through sixth events. In contrast, earthquake-induced subsidence for the second event was lacking in at least three of the seven estuaries. However, tsunamis generated by the second event deposited sands in the unsubsided estuaries. Therefore, the second event is also considered synchronous between Alsea and Necanicum. A segment boundary between Yaquina and Netarts is inferred for the second event.

From these findings of synchronicity, we estimated the length of rupture for the late Holocene earthquakes. The corresponding magnitudes are at least 8.0, based on a rupture length of 175 km, a rupture width of at least 60 km, an average recurrence interval of 400 years, an average convergence rate of 4 cm/yr, and a shear modulus of 3×10^{11} dynes/cm². Using a range of convergence rates (3.5–4.5 cm/yr) and average recurrence intervals (300–500 years), rupture lengths (105–175 km), and rupture widths (60–90 km), calculated magnitudes for five of the last six earthquakes are greater than 8.0 for the central 175 km of the Cascadia Subduction Zone.

Average recurrence intervals between earthquakes for the estuaries on the northern Oregon coast range between 200 and 600 years. The wide range is due to the uncertainties associated with radiocarbon ages. Although more accurate recurrence intervals are desirable, these average recurrence intervals provide a useful estimate for assisting coastal communities with their disaster planning and for determining probabilities for future subduction-zone earthquakes off the northern Oregon coast.

INTRODUCTION

In the past ten years, several geophysicists have called attention to the potential for great earthquakes (greater than magnitude 8) related to the Pacific Northwest subduction-zone known as the Cascadia Subduction Zone (Heaton and Hartzell, 1987; Savage and Lisowski, 1991; Hyndman and Wang, 1993) (Figure 1). Although there have been large (up to magnitude 7.5) earthquakes in the region during historic times (last 150 years), there is no historical record of Pacific Northwest subduction-zone earthquakes, which are often greater than magnitude 8—with the possible exception of the 1992 Cape Mendocino earthquake (G. Carver, personal communication, 1994). However, evidence for subduction-zone earthquakes in the late Holocene has been found in the deposits of coastal wetlands of estuaries in British Columbia, Washington, Oregon, and northern California (Atwater, 1987, 1992; Darienzo and Peterson, 1990; Peterson and Darienzo, 1991; Clarke and Carver, 1992; Nelson, 1992a; Clague and Bobrowsky, 1994; Darienzo and others, 1994).

Now that subduction-zone earthquakes have been recognized in the stratigraphic record, questions arise as to what are the magnitudes of these Holocene earthquakes and the frequency with which they occur. Knowledge of the magnitudes and frequency is necessary to calculate the probability of the next earthquake and to help communities with disaster planning and the building of new and upgrading of existing structures.

In this study, we compare the stratigraphy and associated radiocarbon ages of seven estuaries along the northern Oregon coast: at Alsea Bay, Yaquina Bay, Siletz Bay, Nestucca Bay, Netarts Bay, Ecola Creek, and Necanicum River—an along-coast distance of 175 km (Figure 1). We selected these estuaries because we have made detailed studies of marsh stratigraphy at each of them. Results have been published for Alsea by Peterson and Darienzo (1991); for Netarts by Darienzo and Peterson (1990) and Darienzo (1991); for Yaquina, Siletz, Nestucca, and Necanicum by Darienzo (1991), Darienzo and others (1993), and Darienzo and others (1994); and for Ecola by Gallaway and others (1992). Stratigraphic patterns and radiocarbon ages were used to calculate possible ranges for paleo-magnitudes and average recurrence intervals. These results can potentially be compared with similar patterns and ages of paleoseismic events recorded in estuaries of other segments of the Cascadia Subduction Zone.

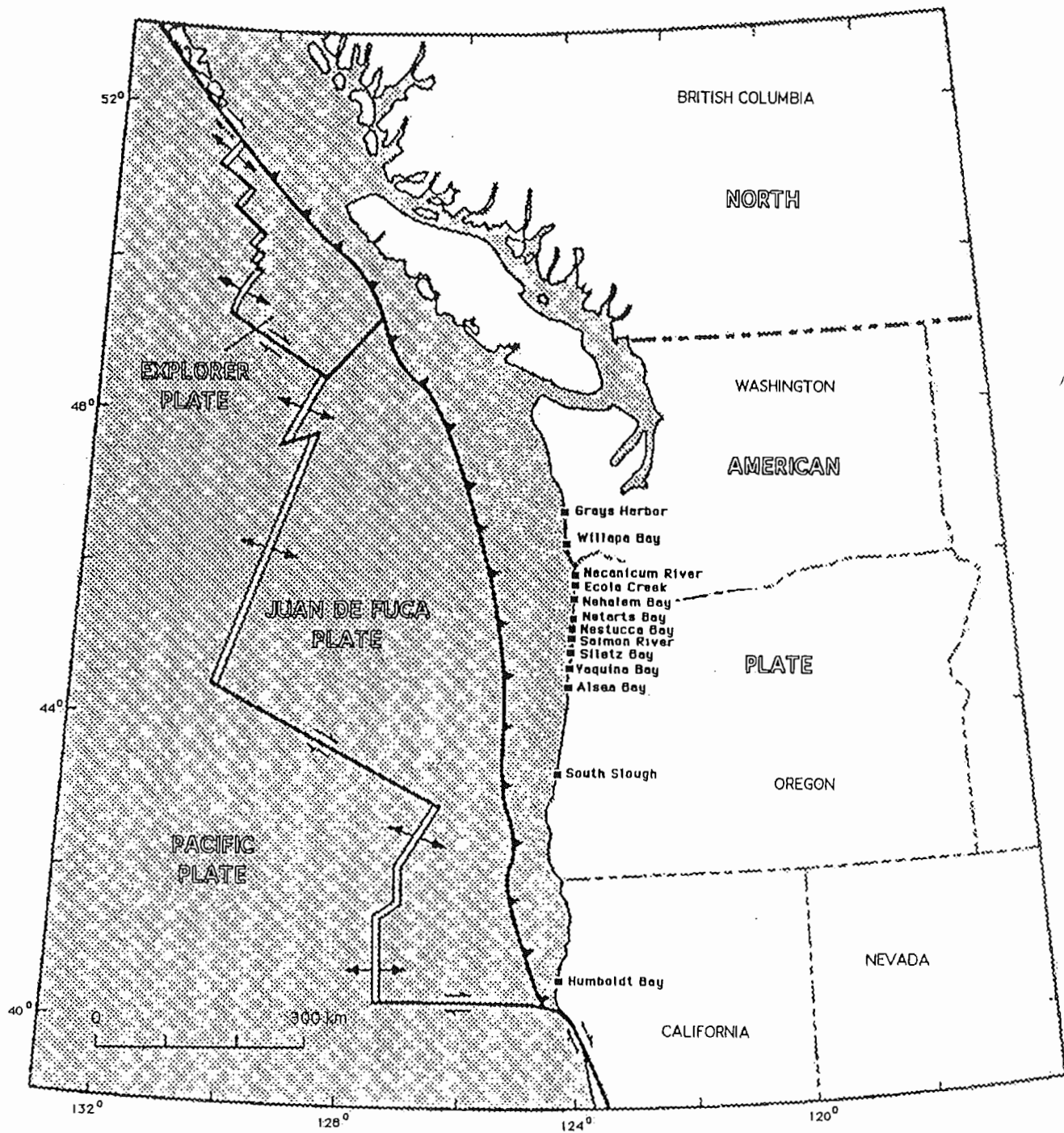
ESTIMATION OF MAGNITUDE

Establishment of event synchronicity

We used the late Holocene stratigraphic records in individual estuaries to assess the synchronicity of the paleoearthquakes among the estuaries along the northern Oregon coast. In this study, we examined and compared the following stratigraphic patterns in the paleoseismic record: the number and stratigraphic location of inferred tsunami deposits and the number, age, and stratigraphic position (depth) of earthquake-buried peats recorded within a specific period of time. If the events are synchronous, the magnitudes of the Holocene earthquakes can be estimated for rupture segments of at least the length of the northern Oregon coast. Synchronicity of coseismic events between estuaries provides information on the length of earthquake rupture along the coast. Therefore, the rupture length, as determined by synchronicity of events, would be a key parameter in paleomagnitude determinations. Formulas that use rupture length (coastline distance of event synchronicity) and estimates of rupture width and seismic slip could then be used to describe paleoearthquakes (Kanamori, 1977; Abe, 1981, 1984; Rogers, 1988; Byrne and others, 1990; Geomatrix, 1993).

A possible alternative to synchronicity of events along the northern Oregon coast is segmentation. In other words, ruptures occur along smaller segments of the locked subduction zone at different times, producing earthquakes of lesser coastline extent and magnitude. For example, a pair of earthquakes off Japan in the Nankai Trough resulted from rupture of adjacent segments in 1944 and 1946, while the 1707 Nankai Trough earthquake resulted from rupture of both segments simultaneously (Ando, 1975). The use of prehistoric dating, no matter how sensitive the dating technique, could not conclusively prove earthquake synchronicity because of the range of possible ages associated with conventional radiocarbon (± 100 yrs), high-precision radiocarbon (± 10 years), or dendrochronology (± 10 years) (Yamaguchi and others, 1989). However, synchronicity of the 300-yr-B.P. (before present) paleoseismic event between widely separated estuaries is suggested by similarities between high-precision radiocarbon ages and tree-ring ages of buried trees in coastal wetlands of Washington, Oregon, and northern California (Yamaguchi and others, 1989; Atwater and others, 1991; Carver and others, 1992; Nelson and Atwater, 1993). Further evidence for synchronicity has come from similarities in stratigraphic patterns of marsh deposits. For example, Atwater (1992) inferred correlations largely on the basis of appear-

45




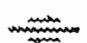

-  Seaward edge of plate boundary--Barbs show direction of dip
-  High-angle fault--Arrows show strike slip
-  Spreading ridge

Figure 1. Cascadia Subduction Zone and northern Oregon estuaries. Distance between the Necanicum and Alsea estuaries is approximately 175 km.

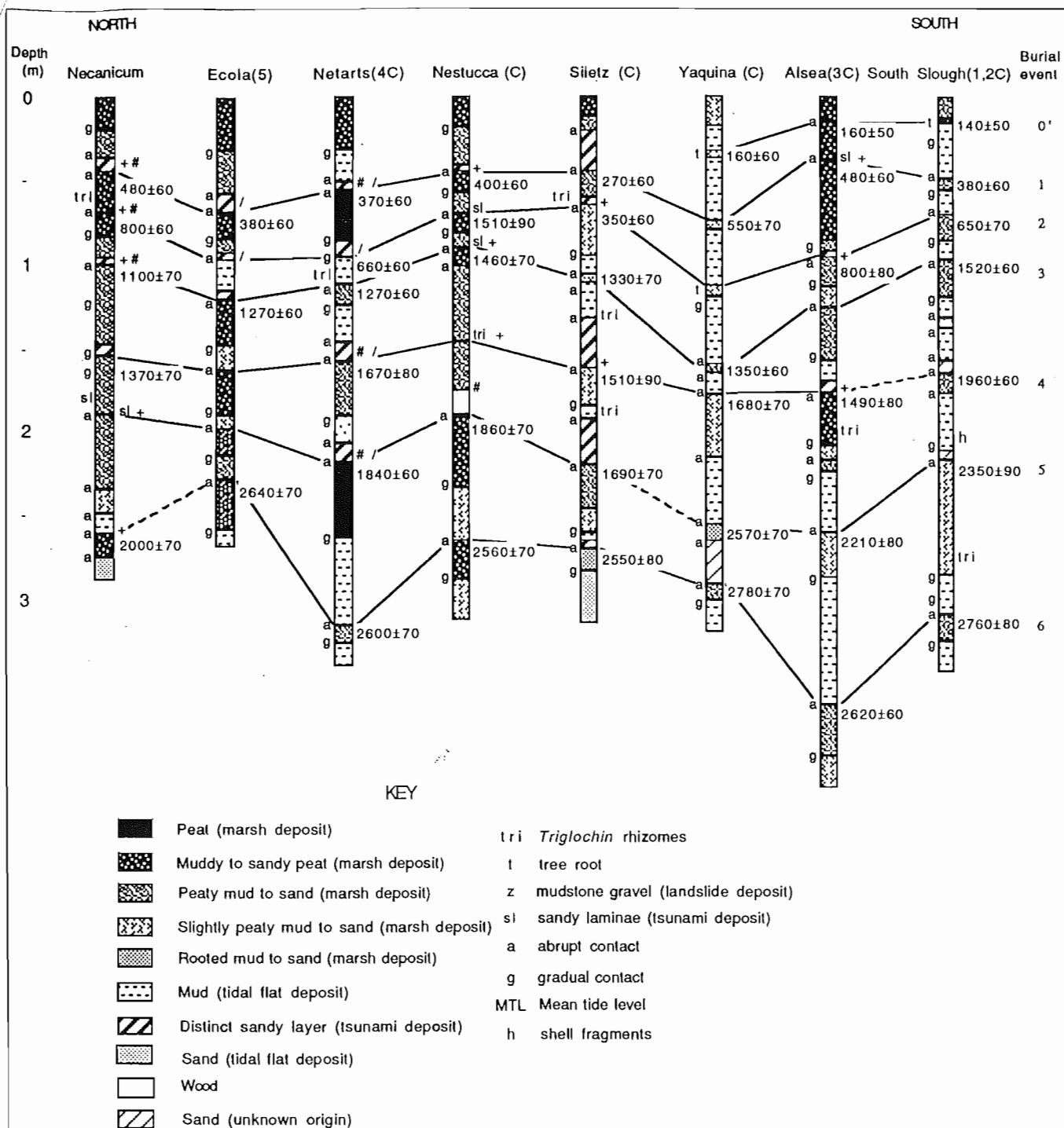


Figure 2. Representative stratigraphic columns with evidence for subduction-zone earthquakes and radiocarbon ages for all estuaries studied along the northern Oregon coast as well as South Slough, an estuary at Coos Bay on the south-central Oregon coast. Necanicum, Nestucca, Yaquina, and South Slough stratigraphic columns are composites. "#" indicates an increase or first appearance of brackish or marine diatoms from the buried peat to overlying sediments; "+" indicates an increase or first appearance of beach sand from the peat to overlying sediments; "/" indicates >50 percent beach sand in a probable tsunami deposit above the peat. Unnumbered stratigraphic columns are from Darienzo (1991) and Darienzo and others (1994). Columns numbered 1–5 are from (1) Nelson (1992b), (2) Peterson and Darienzo (1989), (3) Peterson and Darienzo (1991), (4) Darienzo and Peterson (1990), and (5) Gallaway and others (1993). "C" indicates that column is a composite of two or more sites.

Table 1. Radiocarbon ages of materials (peats unless otherwise noted) from estuaries along the northern Oregon coast that have produced evidence for Holocene subduction-zone earthquakes

Estuary (sources)	Site, location	Depth in cm (burial event no.)	Age in radiocarbon yrs B.P.	Age range in yrs B.P. 2 error multiplier (Cal. age range at 2 σ)	Laboratory no. (Beta)
Necanicum (Darienzo and others, 1994)	Neawanna 2, UTM428900, 5092300, zone 10, N	48 (1)	480 \pm 60	240-720 (300-680)	42112
		70 (2)	800 \pm 60	560-1,040	42113
		111 (3)	1,100 \pm 70	820-1,380	42088
		158 (4)	1,370 \pm 70	1,090-1,650	44595
		268 (6)	2,000 \pm 70	1,720-2,280 (1,610-2,340)	42114
	Neawanna 5, UTM 428900, 5092600, zone 10, N	78 (2) 167 (6)	680 \pm 80 2,200 \pm 90	360-1,000 1,840-2,560	43127 42115
Ecola (Gallaway and others, 1992)	115-R, UTM 426000, 5083300, zone 10, N	70 (1)	380 \pm 60	140-620 (0-590)	56402
		120 (3)	1,270 \pm 60	1,030-1,510	56401
		230 (6)	2,640 \pm 70	2,360-2,920 (2360-3050)	56404
Netarts (Darienzo and Peterson, 1990; Darienzo, 1991)	5, UTM 424400, 5024200, zone 10, N	55 (1)	370 \pm 60	130-610 (0-578)	24933
		111 (3)	1,270 \pm 60	1,030-1,510	24934
		157 (4)	1,670 \pm 80	1,350-1,990	24520
		220 (5)	1,840 \pm 60	1,600-2,080 (1490-2030)	24521
		316 (6)	2,600 \pm 70	2,320-2,880 (2360-3050)	41668
	Oyster farm, UTM 426800, 5029900, zone 10, N	97 (2)	660 \pm 60	420-900	41638
Nestucca (Darienzo and others, 1994)	Nestucca Duck, UTM 425500, 5004200, zone 10, N	80 (1)	400 \pm 60	160-640 (0-620)	43123
		70 (2)	1,510 \pm 90	1,150-1,870	42000
		90 (3)	1,460 \pm 70	1,180-1,740	42084
		190 (5)	1,860 \pm 70	1,580-2,140 (1,460-2,110)	41637
	Little Nestucca 5, UTM 426800, 5000500, zone 10, N	266 (6)	2,560 \pm 70	2,280-2,840 (2,320-2,920)	41671
Siletz (Darienzo and others, 1994)	Salishan House, UTM 418700, 4971500, zone 10, N	47 (1)	270 \pm 60	30-510 (0-520)	42089
		67 (2)	350 \pm 60	110-590	42090
		163 (4)	1,510 \pm 90	1,150-1,870	42001
		220 (5)	1,690 \pm 70	1,410-1,970 (1,310-1,900)	42091
		273 (6)	2,550 \pm 80	2,230-2,870 (2,200-2,970)	42002
	Millport Slough 1, UTM 421500, 4970800, zone 10, N	48 (1) 135 (3) 159 (4) 210 (5)	480 \pm 60 1,330 \pm 70 1,630 \pm 70 1,850 \pm 70	240-720 (300-680) 1,050-1,610 1,350-1,910 1,570-2,130 (1,440-2,100)	42085 43126 43125 42086
Yaquina (Darienzo and others, 1994)	Hatfield, UTM 417400, 4940200, zone 10, N	30 (0')	160 \pm 60	0-400	41991
	Outcrop B, UTM 428300, 4938400, zone 10, N	77 (1)	550 \pm 70	270-830 (310-720)	38862 (wood)
	Slack 1, UTM 427800, 4938000, zone 10, N	62 (3)	1,350 \pm 60	1,110-1,590	42092
		81 (4)	1,680 \pm 70	1,400-1,960	42093
		160 (5) 196 (6)	2,570 \pm 60 2,780 \pm 70	2,330-2,810 (2,340-2,890) 2,500-3,060 (2,530-3,260)	42094 42095
Alsea (Peterson and Darienzo, 1991)	Outcrop, UTM 419500, 4918700, zone 10, N	50 (1)	480 \pm 60	240-720 (300-680)	39181 (wood)
	AB 8, UTM 419000, 4918800, zone 10, N	87 (2)	800 \pm 80	480-1,120	27184
		177 (4)	1,490 \pm 80	1,170-1,810	26791
		242 (5)	2,210 \pm 80	1,890-2,540 (1,830-2,710)	27185
		327 (6)	2,620 \pm 60	2,380-2,860 (2,370-2,960)	26792
South Slough	Winchester 12, UTM 3931000, 4792400, zone 10, N (Nelson, 1992b)	47 (1)	380 \pm 60	140-620 (0-590)	26289
		15 (0')	140 \pm 50	0-340 (0-450)	41639 (wood)
		72 (2)	650 \pm 70	370-930	27675
		98 (3)	1,520 \pm 60	1,280-1,760	34280
		167 (4)	1,960 \pm 60	1,720-2,200	27744
	Day Creek, UTM 393800, 4796500, zone 10, N (Peterson and Darienzo, 1989)	220 (5) 310 (6)	2,350 \pm 90 2,760 \pm 80	1,990-2,710 (1,920-2,800) 2,440-3,080 (2,440-3,300)	27743 34278

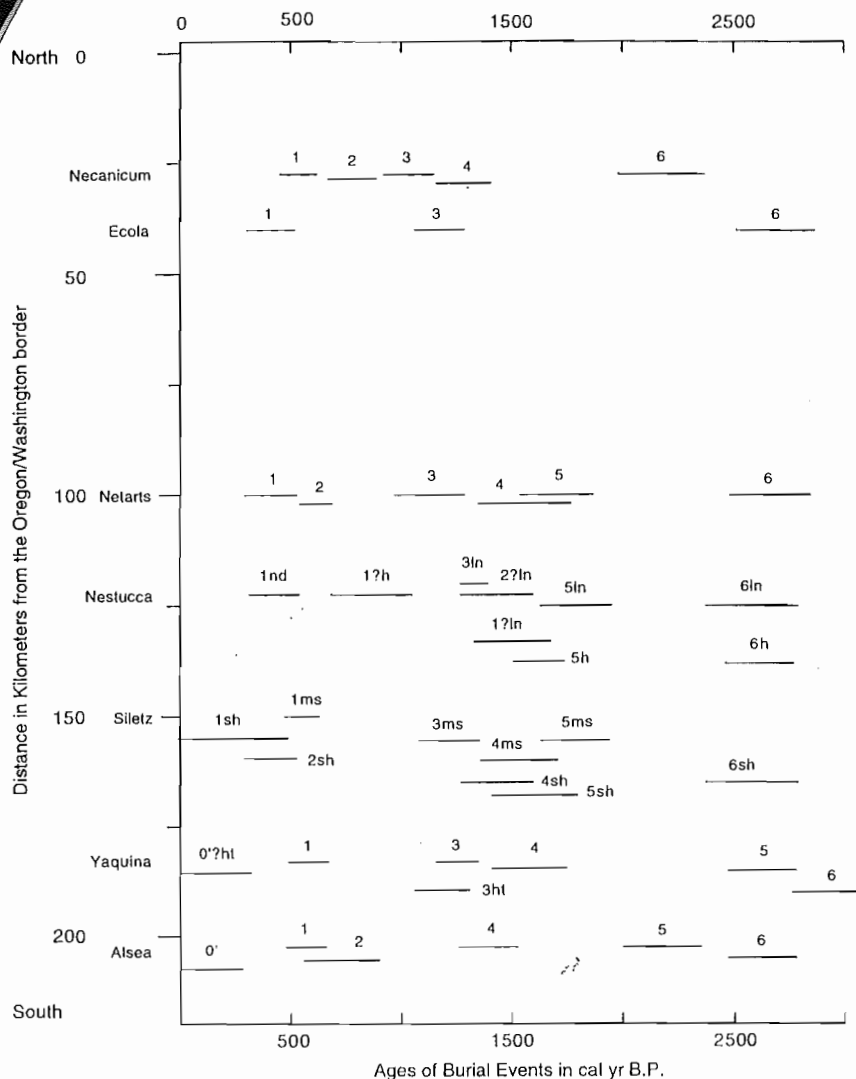


Figure 4. Ranges of calibrated radiocarbon ages with two deviations (2σ) of the last six earthquake events for all estuaries. Numbers designate events. Question marks indicate event designation uncertainties. Lower-case initials designate specific sites within the estuary where materials were radiocarbon dated (nd = Nestucca duck; ln = Little Nestucca; h = Hurliman; sh = Salishan House; ms = Millport Slough; ht = Hatfield). See Darienzo and others (1994) for stratigraphy of the Nestucca and Siletz cores.

dence in Netarts, Ecola, and possibly Necanicum; (2) tsunami sand and subsidence in Alsea, Nestucca, and Yaquina; and (3) tsunami sand at several sites and possible evidence of subsidence at a few sites in Siletz Bay (Figure 2) (Darienzo and others, 1994; Peterson and Darienzo, 1994; Peterson and Priest, in preparation). Age control for the second event is weak. The ages of the buried peats for the second event overlap at 2σ for Necanicum, Netarts, and Alsea (Figure 4). However, the age from Nestucca is much older than these, and it is not clear if this event, documented at four estuaries in northern Oregon, affected Nestucca Bay. The age of the second buried peat at Nestucca might be suspect and require additional dating to solve this problem (Darienzo and others, 1994).

In contrast to Nestucca, the age of the second peat from Siletz is younger and does not overlap at 2σ with the peats from Necanicum, Netarts, and Alsea. The young age is perhaps due to root contamination from above. The second buried peat at Ecola and Yaquina was not dated. The sands without accompanying subsidence stratigraphy that record the second event at the three northernmost estuaries

suggest deposition by a tsunami generated by an offshore subduction-zone earthquake off an adjacent segment of the Oregon coast to the south. The lack of evidence for this second event along the Washington coast further supports a segment rupture limited to the southern Oregon coast (Atwater, 1992). Possible segment boundaries are located either between the Netarts and Nestucca bays or between Siletz and Yaquina (Figure 1). Supporting a segment boundary between Netarts and Nestucca is the fact that there is evidence of subsidence for the second earthquake burial event at Nestucca but no such evidence at Netarts. Support for a segment boundary between Yaquina and Siletz includes evidence of subsidence at Yaquina, weak subsidence evidence at Siletz, and a possible segment boundary at this same location for the fifth earthquake burial event. Further work is necessary to accurately locate the boundary. Nevertheless, all estuaries were affected by this second paleoearthquake either directly, by subsidence and a tsunami, or indirectly, by a tsunami only. Therefore, the record of the second event could be considered synchronous among the estuaries on the northern Oregon coast.

The **third burial event** is recognized in all estuaries, and the ages of the buried peats at nearly all estuaries overlap at 2σ (Alsea was not dated) (Figure 4). The exception is the age of the third buried peat at Nestucca, which overlaps all estuaries except Necanicum. A distinct sandy layer is present over the third buried peat at four of the seven northern estuaries but absent at Alsea, Siletz, and Netarts (Figure 2). The Hatfield site in the lower reaches of Yaquina Bay had tsunami sand deposited over what is considered the third buried peat, based on radiocarbon age (Figure 4). However, the third buried peat at other sites in Yaquina Bay is not capped by tsunami sands (Peterson and Priest, in preparation). The tsunami sand in the lower reaches of Yaquina Bay is not shown in Figure 2, because the representative stratigraphy for Yaquina in Figure 2 is from the upper reaches of the estuary (Darienzo and others, 1994). Based on ages, evidence of subsidence, and one-to-one correspondence of tsunami sand from the Hatfield site with subsidence, this third event possibly occurred synchronously from the Necanicum River to Alsea Bay.

The **fourth burial event** is recognized in all seven estuaries. At five of the estuaries, the ages of the event overlap at 2σ (no age from Ecola or Nestucca). Tsunami sands overlie peats in four out of seven estuaries but are absent at core sites in Ecola and Nestucca. Based on ages, evidence of subsidence, and one-to-one correspondence of tsunamis with subsidence, this fourth event possibly occurred synchronously from the Necanicum River to Alsea Bay (Figures 2 and 4) (Darienzo and others, 1994; Peterson and Priest, in preparation).

The **fifth burial event** is recognized in all estuaries. Only three of the seven estuaries were observed to record tsunami sands above buried peats (Figure 2), and the age ranges for the fifth event overlap in only three out of the five estuaries dated (Figure 4). The ages of the event at Alsea and Yaquina, the two southernmost estuaries, are greater than at the other dated estuaries. This suggests a separate event (or more) for them and a segment boundary between Yaquina and Siletz. Or, buried peats with similar ages have not been identified in adjacent estuaries because of nondeposition or erosion. Ages of

49

Episodically buried forests in the Oregon surf zone

by Roger Hart, *College of Oceanic and Atmospheric Sciences, Oregon State University, Hatfield Marine Science Center, Newport, Oregon 97365;* and Curt Peterson, *Department of Geology, Portland State University, Portland, Oregon 97207*

ABSTRACT

Severe winter storms, especially in ENSO¹ years, expose rooted tree stumps in the surf zone of the central Oregon coast. Root mats up to 6 m in diameter are anchored in the Tertiary rocks of the late Holocene wave-cut platform. We studied more than 275 stumps at 14 localities between Neskowin and Coos Bay. Forest soil preserved beneath some roots can be traced landward, where it overlies creek mouth marsh and paleo-sand dune deposits. The stump fields and the forest soil are remnants of a continuous forest or series of forests that extended farther seaward than present-day temperate coniferous rain forest. Litter in the soil indicates that the forest soil was rapidly buried. Ages of the rooted stumps range from $1,970 \pm 50$ to $4,340 \pm 70$ radiocarbon years before the present (RCYBP).

Eustatic change of sea level and migration of sand barriers are considered as explanations for preservation of rooted stumps at some sites. However, large-diameter stumps rooted on continuously active late Holocene wave-cut platforms depleted of littoral sand are indicators of tectonic movements on the central Oregon coast. A necessary history requires six stages: (1) wave cutting of platform at sea level, (2) tectonic uplift of the platform, (3) growth of the forest on the wave-cut platform, (4) rapid burial and preservation of the forest, (5) inundation of the forest at sea level, and (6) renewed erosion of the beach platform. These results corroborate salt-marsh evidence of late Holocene vertical tectonic displacements associated with local or regional earthquake sources along the Oregon coast. Further radiocarbon dating of annular rings in the rooted stumps and preserved litter in the soil can potentially constrain the nature, age, and extent of the tectonic displacements.

INTRODUCTION

For several decades, scientists have reported tree stumps rooted on the wave-cut platforms of the surf zone along Oregon beaches (Kelley and others, 1978; Peterson and others, 1993; oral communications from R. Bayer, Yaquina Birders and Naturalists, 1985; E. Zoebel, Department of Botany, Oregon State University,

1995; and R. Loeffel, Fisheries Manager, retired, 1996). However, no systematic study of these rooted stumps has been published. The stumps stand upright, with broad root mats spread parallel to the wave-cut platform (cover photo). They have been observed in place for over ten years, even during periods when the surrounding sand has been stripped from the beach. Although some stumps may be rooted in submerged late Pleistocene stream channels, most are rooted in the Tertiary bedrock of the late Holocene wave-cut platforms. Similar roots associated with currently living trees are found only inland from the surf zone. The live trees that left the stumps on the beach must have grown on the wave-cut platform after regression of the surf zone. Following at least several hundred years of growth, transgression of the surf zone must have invaded the tree growing zone. These observations led to early concepts of late Holocene seismic activity along the central Oregon coast (Darienzo and Peterson, 1990).

We report on a study of 1.9- to 4.4-ka (kilo-annum = 10^3 years) trees rooted on the wave-cut platforms of the central Oregon coast, lat 43.23° – 45.00° N. (Figure 1). We document the association of forest soils, debris flows, and liquefaction features with the buried stumps. In the discussion, we evaluate three mechanisms for regression and transgression of the surf zone: (1) growth and removal of sand barriers, (2) eustatic change of sea level, and (3) vertical tectonic displacement of the Cascadia margin. We use observed stratigraphic relations to rule out mechanisms 1 and 2 at most localities.

BACKGROUND

The beaches of the central Oregon coast occupy late Holocene wave-cut platforms, at least several hundred meters in width, that are carved in late Pleistocene marine terrace deposits or in Tertiary sedimentary rocks. South of Newport, the surf zone may have reoccupied late Pleistocene platforms (Ticknor, 1993). North of Newport the youngest apparent Pleistocene platform is elevated as much as 30 m above present sea level.

In general, elevated wave-cut platforms underlie a series of inland marine terraces composed mainly of Pleistocene beach and dune sand (Kelsey and others, 1994; Ticknor, 1993).

Ticknor (1993) used the uplifted platforms to calculate average vertical displacement rates for the past 105 ka and found 0.85 ± 0.06 mm/year north of Newport and -0.01 ± 0.03 mm/year for the area around Yachats.

¹ El Niño Southern Oscillation. El Niño refers to the equatorial Pacific warm water anomaly. The Southern Oscillation traditionally refers to associated variations in atmospheric circulation in the south Pacific. Recently, teleconnection links to enhancement of the Aleutian low-pressure system off the Oregon coast have been documented and are thought to cause an increase in storminess and associated coastal erosion.

Rooted Stumps on Beaches of the Central Oregon Coast

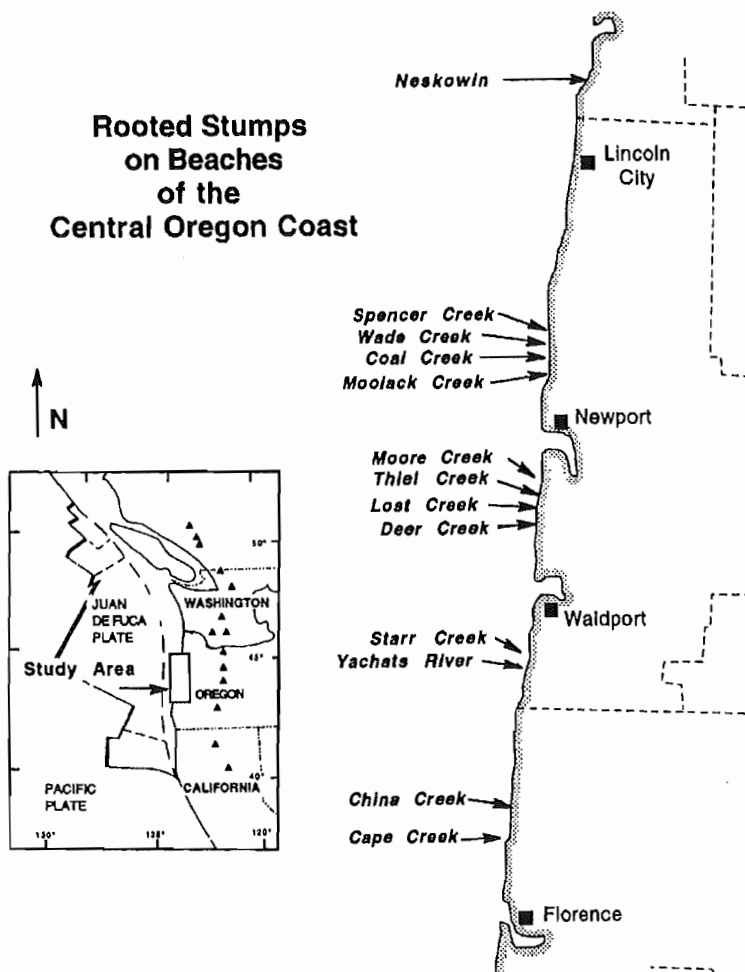


Figure 1. Location of the study area where rooted stumps have been mapped. The stump field at Sunset Bay discussed in the text and referred to in Table 1 is south of the enlarged area.

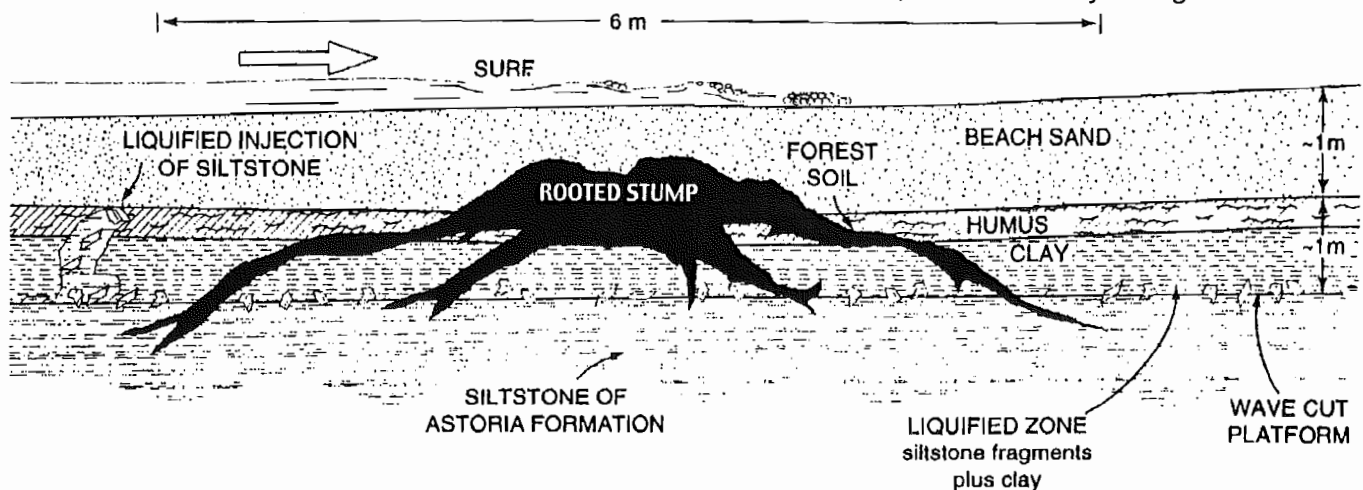


Figure 2. Diagrammatic figure of the principal features of the buried stumps beneath beach sand. The roots extend into the Tertiary siltstone on which the platform was cut. Some of the stumps have erosional remnants of forest soil with fresh litter, humus, and gray clay directly on the wave-cut platform. The inferred liquefied injection of siltstone fragments into the soil was probably coseismic but not necessarily synchronous with burial of the rooted stump.

Mitchell and others (1994) calculated present-day vertical displacement rates from repeated leveling surveys and tide gauge records. Their results indicate that, at the present time, the area around Newport is stationary or subsiding, whereas the area around Yachats is being uplifted.

The wave-cut platforms in the vicinity of Newport terminate landward in wave-cut cliffs; whereas, the wave-cut platforms north and south of Yachats most frequently terminate landward in Holocene foredunes.

RESULTS

More than 288 rooted stumps were mapped at 14 localities between Coos Bay and Neskowin, a distance of 206 km (Figure 1). Additional rooted stumps and soil profiles were studied and sampled at seven localities in creek mouths and backshore deposits. We collected 26 wood samples and 59 soil samples from beaches, creek mouths, and soil run-ups and examined them under the microscope. Over 60 km of beaches, marine cliffs, and creek mouths were photographed and mapped on either U.S. Geological Survey 1:24,000-scale (7½-minute series) topographic maps or on 1:4,800-scale aerial orthophoto maps used by Priest and others (1994). Details of the mapping and sampling are given in Table 1.

Rooted stumps

Normally, 1–5 m of beach sand covers the stumps in the surf zone (Figure 2), but they are exposed during periods of extreme beach sand erosion, most commonly during the winters of

Table 1. *Rooted stumps and forest soil localities, continued*

Locality	Access	Stump field	Soil	Samples
19 Ten Mile Creek	Rooted stump, forest soil, and marsh soil at top of beach 75 m S. of beach access from Stonefield Beach State Wayside.	1 rooted stump at the top of the beach.	Creek mouth marsh soil and forest soil at top of beach. Forest soil runs up marine cliffs S. Separated from modern soil by dune sands and shell midden 390 m S. of beach access.	3 sections measured. Wood sample TMC-1.
20 China Creek	Access beach from Muriel O. Ponsler Memorial Wayside. 3 rooted stumps on beach 50 m N. of access. Extensive stump field and forest soil horizon on beach S. across China Creek continues 1.2 km S.	3 rooted stumps in beach high-water zone exposed 6/96, 50 m N. of wayside. First noted 1982/83 by E. Zoebel. 5 rooted stumps exposed in higher high-water zone of beach S. of China Creek. 1 stump continuously exposed in bank at top of beach 500 m S. of Creek (Figure 4).	Forest soil on beach with litter S. of China Creek runs up to bank at top of beach and underlies dune field continuously 0.9 km to S. (Figures 5 and 8). Exposed 3/25/95–8/4/95. Extensive fire-scorched layers.	Wood samples from rooted stumps CCs-1, to -5. Cones of <i>Tsuga heterophylla</i> from beach S. of China Creek. Soil samples CC-1, CC-2, and CC-5. 3 sections measured.
21 Blowout Creek	Forest soil in bed of Blowout Creek 200 m S. of picnic area beach access at Carl G. Washburne Memorial State Park.	1 rooted stump in marine cliff 12 m S. of Blowout Creek.	Forest soil runs up from Blowout Creek and continues 2.1 km to Heceta Head. Runs up 12 m over large dune form (Figure 7). Litter exposed south of dune form.	Litter sample BC-1. Wood sample BC-1 from stump rooted in soil runoff.
22 Cape Creek	1 rooted stump on top of beach near picnic area of Devil's Elbow State Park.	1 rooted stump.	None observed.	Wood sample CaC-1.
23 Sunset Bay	18 rooted stumps and buried soil horizons on beach and in bed of Big Creek at Sunset Bay State Park.	18 stumps from Big Creek to fault line on N. end of beach. Intermittently exposed since 1983 ENSO.	Laminated soil of uncertain origin underlies beach sand.	Wood samples SSB-1 to -6; soil samples SSB-1 to -17.

(Continued from page 136)

clay underlying a horizon of forest soil. The clay layer, 1–3 m thick, is characterized by rooted stumps, layers of peat, marsh grass fragments, and clasts of siltstone. The forest soil, 0.5–2 m thick, is characterized by humus, litter, and rooted stumps. At some sites, two or more forest soil layers are divided by layers of beach sand and/or cobbles. The bottom forest layer is thickest and contains cones, bark, and needles. The top forest layer is sandy and contains a zone of fire-scorched material with red iron oxide minerals and possible charcoal.

Soil horizons stratigraphically equivalent to the surf zone soil ascend creek mouth valley walls and cross-cut Pleistocene sand-dune deposits of the marine terraces at seven localities (Figures 5, 6, 7; Table 1). The ascending forest horizons are characterized by Podzol profiles similar to the present day profile formed on top of Holocene dune deposits (Corliss, 1973). The top layer of undecomposed forest litter, shredded bark, cones, and twigs in a matrix of sandy loam varies in thickness from 2 in. to 20 in. This layer grades down into the humus layer which is 10–54 in. thick. The humus is friable with a few firm aggregates, slightly sticky, and nonplastic. Woody debris is locally abundant, and in places 10-cm-thick mats of bark and shredded bark are present. The gray leached zone, which varies from 0.1 to 1 m in thickness, is underlain by an orange-red B horizon 0.5–2 m thick and with well-developed laminae of sesquiox-

ides. The forest soil horizons terminate abruptly upward and are capped by Holocene debris flows, backshore beach sands, or dune sands that separate them from the present-day soil horizon.

Debris flows up to 5 m thick cover creek mouth and ascending forest horizons at nine sites (Table 1). The debris flows contain fragments of the underlying forest soil, angular dune-paleosol fragments, semiangular siltstone fragments, and woody debris mixed in with gravel and mud. The high abundance of angular and unconsolidated fragments suggests that the flows did not travel long distances. At Coal Creek, a debris flow covers a rooted stump at the backshore edge of the beach, which suggests a possible coincidence between platform subsidence and the debris flow. The debris flows probably extended onto the wave-cut platform.

DISCUSSION

The location and abundance of the tree stumps and associated soil indicate that they are erosion remnants of extensive forests that grew on Holocene wave-cut platforms. Several questions are raised by the data: (1) what caused regression of the surf zone off the late-Holocene wave-cut platform? (2) what caused inundation and burial of the established forests? and (3) what was the extent and timing of the burial events? In this section, we discuss each of these questions in turn.

(Continued on page 141)

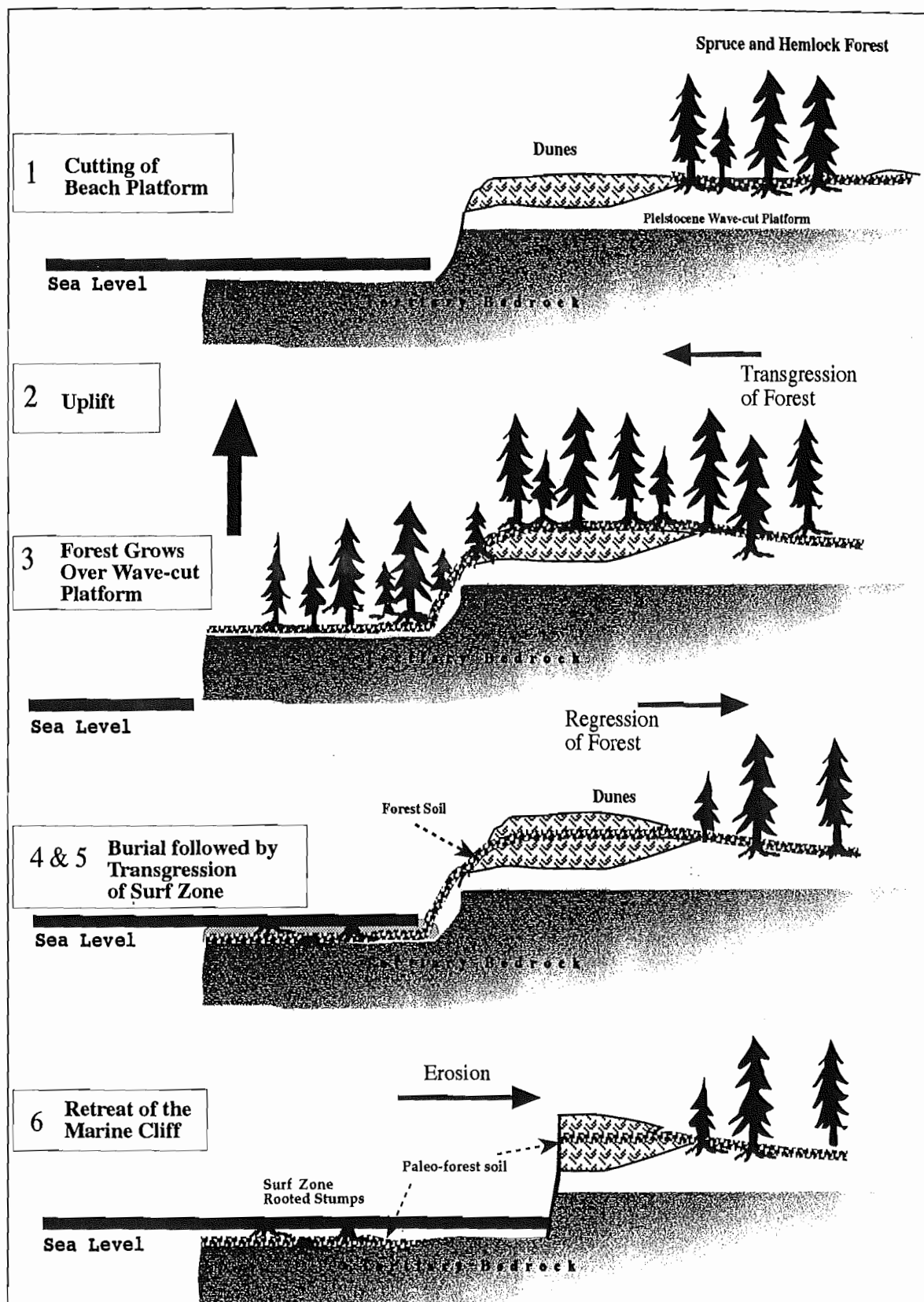


Figure 9. The six stages necessary to explain the occurrence of rooted stumps in the Oregon surf zone. Regression of the surf zone off the platform was probably the result of vertical tectonic displacement. Burial is inferred from the presence of nondecomposed forest litter. Transgression of the surf zone was not necessarily synchronous with burial and could have been the result of eustatic sea level rise, removal of sand barriers, or vertical tectonic displacement or any combination of the three.

Continued from page 141)

Forest soil at Deer Creek appears buried in beach sand. Trees growing near beaches can be buried in wet, salty sand if there is a rapid seaward growth of the beach. Growth of the beach can be caused by an abrupt increase of littoral sand supply induced by shifting nearshore currents or by an increase in sediment supply to the littoral cell (Peterson and others, 1990). Sudden vertical tectonic displacement could also induce burial of trees in beach sand if the displacement is great enough.

The ascending forest soil horizons are covered by dune sand at China Creek and Blowout Creek. Rapid migration of dunes over the trees as a result of an abrupt increase in littoral sand supply is a possible agent for burial and protection of the forest. Vertical tectonic displacement could also induce migration of dunes over forests by introducing the forest to areas of active dune formation at lower elevations.

Debris flows cover forest soil at nine localities north of Thiel Creek. A nearly continuous apron 15 mi wide may have covered the beaches between Spencer Creek and Lost Creek and could have buried the forest on the beach platform. Although it is nearly impossible to determine whether or not debris flows are coseismic, debris flows are commonly associated with earthquakes. For example, over 10,000 debris flows occurred during the 1976 Guatemalan earthquake (M_s 7.5) (Harp and others, 1981).

Additional work is needed to verify whether deposits currently covering the forest soils reflect the initial burial of the forests.

Inundation of the forest

Inundation of the forest in the surf zone was not necessarily synchronous with burial. Preservation of litter by burial in beach sand or in a peat bog would have required a synchronous drop to sea level. However, burial by debris flows or eolian dunes could have taken place above sea level before inundation. At any rate, the forest was inundated by a transgressing surf zone that could have been the result of eustatic rise of sea level and/or removal of sand barriers and/or tectonic subsidence.

In this paper we do not attempt to discriminate between the possible mechanism of inundation. Possibly all are involved. For example, even though eustatic rise of sea level was a factor, it was less than 1 mm per year at 1.9–4.4 ka (Berger, 1983). Some parts of the coastline were tectonically uplifted faster than this. Others were probably tectonically submerging.

Sequence of events

Although we cannot assume the same sequence of events for all sites, we propose a six-step sequence (Figure 9) as the most likely one for the majority of sites of rooted stumps and associated forest soil. First, the

wave-cut platform was cut at sea level prior to growth of the trees. Second, sea level regressed off the platform due to tectonic uplift. In the third stage, the forest grew over the platform. In the fourth stage, the forest was rapidly buried and the litter preserved. In the fifth stage, the forest was inundated by the surf zone. In the sixth and final stage, the forest soils and overlying deposits were eroded during the retreat of the marine cliffs.

CONCLUSIONS

The rooted stumps and forest soils on Oregon's beaches are remnants of forests similar to present-day coastal temperate rain forest that grew on the Holocene wave-cut platform and adjacent creeks, dune fields, and marine terraces. The paleo-forest soils exposed in the surf zone, in creek mouths, and on valley walls are probably contemporaneous with rooted stumps in the surf zone, but this cannot be established without further mapping, coring, and radiocarbon dating. The abrupt upward termination of the forest soil and the preservation of undecomposed litter indicates rapid burial by debris flows, dunes, or beach sands. The burial may have been coseismic and synchronous with inundation, but this cannot be established with the data set on hand. The preliminary ages of the stumps, 1.9–4.4 ka, show that the growth and burial of some of the trees took place after the time of major eustatic sea level rise in early mid-Holocene time. The rapid colonization and deterioration of the stumps and exposed soils in the surf zone indicate that these forest remnants were exposed only during short-lived erosion events or have not been previously exposed. The full cycle of platform cutting, uplift, forest growth, burial, inundation, and renewed platform cutting may have taken place over a period upward of 1,000 years. Additional platform-forest site coring/mapping and radiocarbon dating are necessary to test the extent, duration, and possible cyclicity of these processes. For example, do other forest remnants exist landward under Holocene dune fields or offshore on the inner shelf?

ACKNOWLEDGMENTS

Radiocarbon dating was supported by the Portland State University Department of Geology. This work was partially supported by grant No. NA36RG0451 from the National Oceanic and Atmospheric Administration to the Oregon State University Sea Grant College and by appropriations made by the Oregon State Legislature. The views expressed herein are those of the authors and do not necessarily reflect the views of NOAA or any of its subagencies. Author Hart is grateful to Ian Hart, Cathy Heflin, and Bob Shivers for their assistance in the field and to Cathy Heflin for her assistance in preparation of the manuscript and figures. The field work and manuscript benefited from discussions with Alan Niem and Paul Komar.

54

FIELD TRIP ROAD LOG FOR THE
CENOZOIC STRATIGRAPHY OF COOS BAY AND CAPE BLANCO,
SOUTHWESTERN OREGON

John M. Armentrout
1107 Wiltshire Drive
Carrollton, Texas 75006

INTRODUCTION

This two-day field trip is concerned with the Cenozoic stratigraphy of the southwestern Oregon Coast at Coos Bay and Cape Blanco (Fig. 2). The log is presented as two separate mileage sequences. Twelve rock units of early Eocene to Pleistocene age will be examined (Fig. 3).

The reader is referred to Baldwin (1966, 1974) and Baldwin and others (1973) for a description of the Cenozoic formations of Coos Bay and to Beaulieu (1971), Roth (1979), and Addicott (in preparation) for Cape Blanco. The molluscan paleontology of Coos Bay is discussed by Dall (1909), Turner (1938), Weaver (1945), and Armentrout (1967). Foraminiferal paleontology of Coos Bay is reviewed by Bird (1967), Rooth (1974), and Tipton (1975). The molluscan paleontology of Cape Blanco has recently been restudied by Addicott (in preparation) and Roth (1979). Foraminiferal paleontology of Cape Blanco is being restudied and initial results are presented in this paper.

CAUTION: Several of the stops are intertidal areas along sea cliffs. Participants are urged to be aware of the time of high and low tides. Caution is urged as onshore winds can significantly alter the timing and amplitude of the tide and the size of individual waves. The stop sequence should be adjusted to fit the tide and weather situations at the time of the field excursion. Many of the stops are at sea cliff view points. These areas are underlain by Pleistocene terrace sands and are often undercut. Approach all bluffs with great caution.

Overnight accommodations are available at Coos Bay, Bandon, and Port Orford. Campgrounds at Sunset Bay, Bullard's Beach near Bandon, and Cape Blanco are operated by the State of Oregon. Contact the State Parks and Recreation Section, 525 Trade Street, S.E., Salem, Oregon 97310, for information on the seasonal schedule and availability of camp sites.

ACKNOWLEDGEMENTS

The author is indebted to those Pacific Northwest geologists who shared their ideas and field data, in particular: Ewart Baldwin, University of Oregon; Ken Bird, Warren Addicott, Kristin McDougall, and Richard Janda, U.S. Geological Survey; Barry Roth, California Academy of Sciences; and Bruce Welton, Los Angeles County Museum of Natural History. Time has not permitted review of this guide by the above geologists: all interpretations as presented are the responsibility of the author.

55



Figure 1. Aerial View of Cape Arago Area. a) Assembly area - Stop 1: Flagpole View Point. b) Middle Cove. c) South Cove overlook - Stop 2. d) North Cove overlook - Stop 3. e) Channel-fill sequence of figure 11. f) Sea Lion View Point - Stop 4. g) Shore Acres State Park - Stop 5. h) Sunset Bay State Park - Stop 6. i) Gregory Point. j) Mouth of Coos Bay. Photograph courtesy of Oregon State Highway Division.

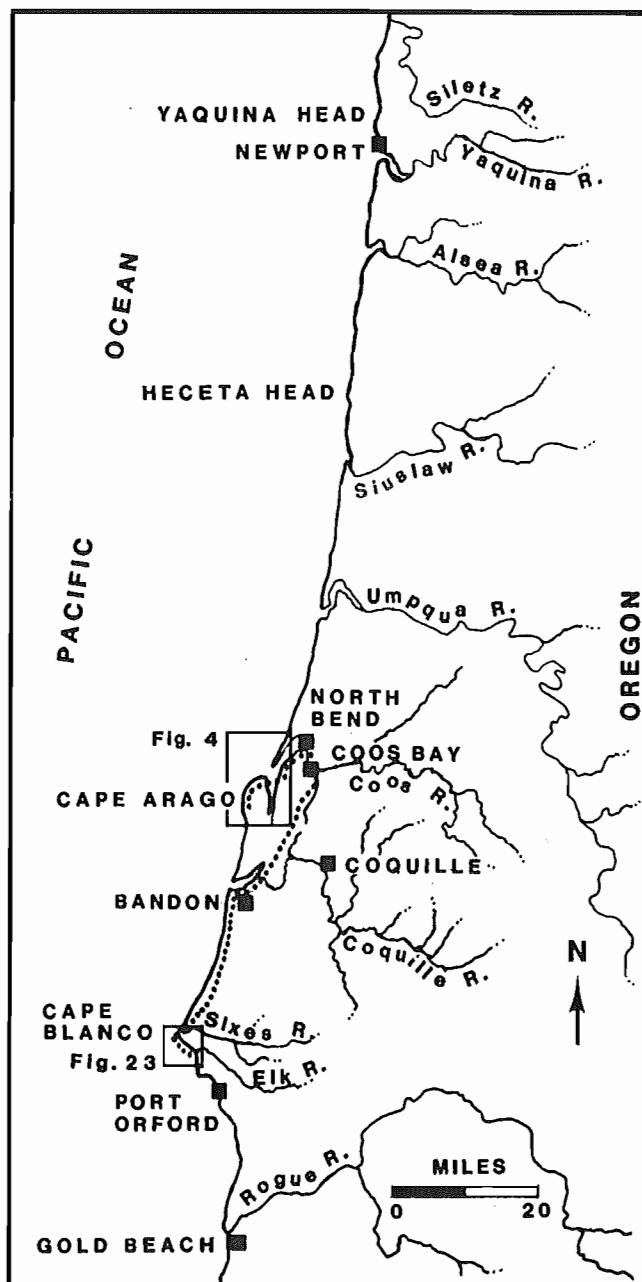


Figure 2. Index map to the field trip area.

SERIES		WEST COAST FORAM. STAGES	ORE./WASH. MOLLUSCAN STAGES	COOS BAY SECTION	CAPE BLANCO SECTION
NEOGENE	QUAT.	UNNAMED	UNNAMED	TERRACES	TERRACES
	PLEISTO.				ELK RIVER BEDS
		QUINAULT. ASSEM.	MOCLIPSAN		PORT ORFORD FM.
	MIOCENE	UNDIFF. ASSEM. MONTESANO FM.	GRAYSAN		
			-?-?-?-?- WISHKAHAN	EMPIRE FORMATION	EMPIRE FORMATION (RESTRICTED)
	MIDDLE	LUISIAN RELIZIAN	-?-?-?-?- NEWPORTIAN		
	EARLY	SAUCESIAN	PILLARIAN	MIOCENE BEDS	SANDSTONES OF FLORAS LAKE
	OLIGOCENE		JUANIAN		
		ZEMORRIAN	MATLOCKIAN		
	LATE	REFUGIAN	GALVINIAN	TUNNEL PT. FM.	
PALEOGENE	EOCENE		UNDIFF. ASSEM. COWLITZ & COALEDO FMS.	BASTENDORFF FORMATION	
		NARIZIAN		COALEDO FORMATION	
	EARLY	ULATISIAN	UNDIFF. ASSEM UMPQUA & TYEE FMS.	?-?-?-? ELKTON SILTSTONE	
	LATE	PENUTIAN			ROSEBURG FM. ?-?-?-?-?
		?	?		

Figure 3. Correlation of provincial time scale, biochronologies and formations at Coos Bay and Cape Blanco. Usage of Foraminiferal Stages follows W. W. Rau (pers. commun., 1979); molluscan stages follows Armentrout (1975) and Addicott (1976).

COOS BAY SEGMENT

The Coos Bay field trip segment consists of a one-day excursion of 9.8 miles with 13 stops (Figs. 1, 4, and 11).

The Cenozoic geology of Coos Bay consists of Paleocene to Pleistocene continental margin marine rocks which were folded into the Coos synclinorium during Oligocene and early Miocene time (Baldwin and others, 1973). Subsequent Neogene deposition in the area was confined to the axis of this synclinorium, along the South Slough Syncline (Figs. 4 and 5). The Coos Bay Cenozoic section measures more than 12,000 feet thick (Fig. 6). Paleocene units crop out in the Coast Range around the perimeter of the Coos synclinorium but will not be visited on the field trip. The Seven Cenozoic units that will be visited are separated into four unconformity bound sequences of rocks: (1) Eocene to lower Oligocene (Elkton Siltstone, Coaledo Formation, Bastendorff Formation, and Tunnel Point Formation); (2) upper lower to middle Miocene (Miocene Beds); (3) upper Miocene (Empire Formation); and (4) Pleistocene (terrace deposits).

MILEAGE DESCRIPTION

Cumulative (Interval)

Drive to Cape Arago State Park from either North Bend or Coos Bay. The route is well marked. Cumulative mileage will be started at Stop 4.

0.0 Begin interval mileage at the entrance to Cape Arago State Park. Drive counterclockwise around the park road.

(0.5)

0.0 STOP 1: FLAG-POLE AREA: Cape Arago State Park. Park along the roadway and walk out to the stone observation area at the western edge of the Cape overlooking Middle Cove on the south (Fig. 1-a).

Cape Arago consists of Eocene sedimentary rocks folded into a north-trending anticline which is now truncated by a coastal terrace. The anticline extends from North Cove to South Cove, and is cut by a normal fault with downdropped strata on the west. A secondary fault trends through Middle Cove and may intersect the primary fault in North Cove. Resistant sandstone of the downfaulted middle Eocene Coaledo Formation form the seaward face of Cape Arago. North Cove and South Cove are eroded into the early Eocene Elkton Siltstone Member of the Tyee Formation (Beaulieu, 1971). The Elkton Siltstone is discordantly overlain by the Coaledo Formation (Dott and Bird, 1979). The Elkton Siltstone is abundantly microfossiliferous (Bird, 1967; Dott and Bird, 1979). Sandstone of the Coaledo Formation contains megafossils, particularly at Middle Cove where sand dollars are moderately abundant along with numerous mollusks (Turner, 1938). Shale interbeds of the Coaledo Formation are microfossiliferous (Rooth, 1974).

Return to the roadway and proceed eastward.

(0.4)

0.0 STOP 2: SOUTH COVE OVERLOOK: Park along the road and walk southwest on the terrace surface to the bluff overlooking South Cove.

South from Cape Arago the coastline follows the cliff area of the Seven Devils area southward along Sacchi Beach, Agate Beach, and Merchant's Beach to Five Mile Point. Beyond Five Mile Point is the long sandy area near Whisky Run and Bullard's Beach and finally the rocky headland of Coquille Point at Bandon. On a very clear day Cape Blanco can also be seen far to the south.

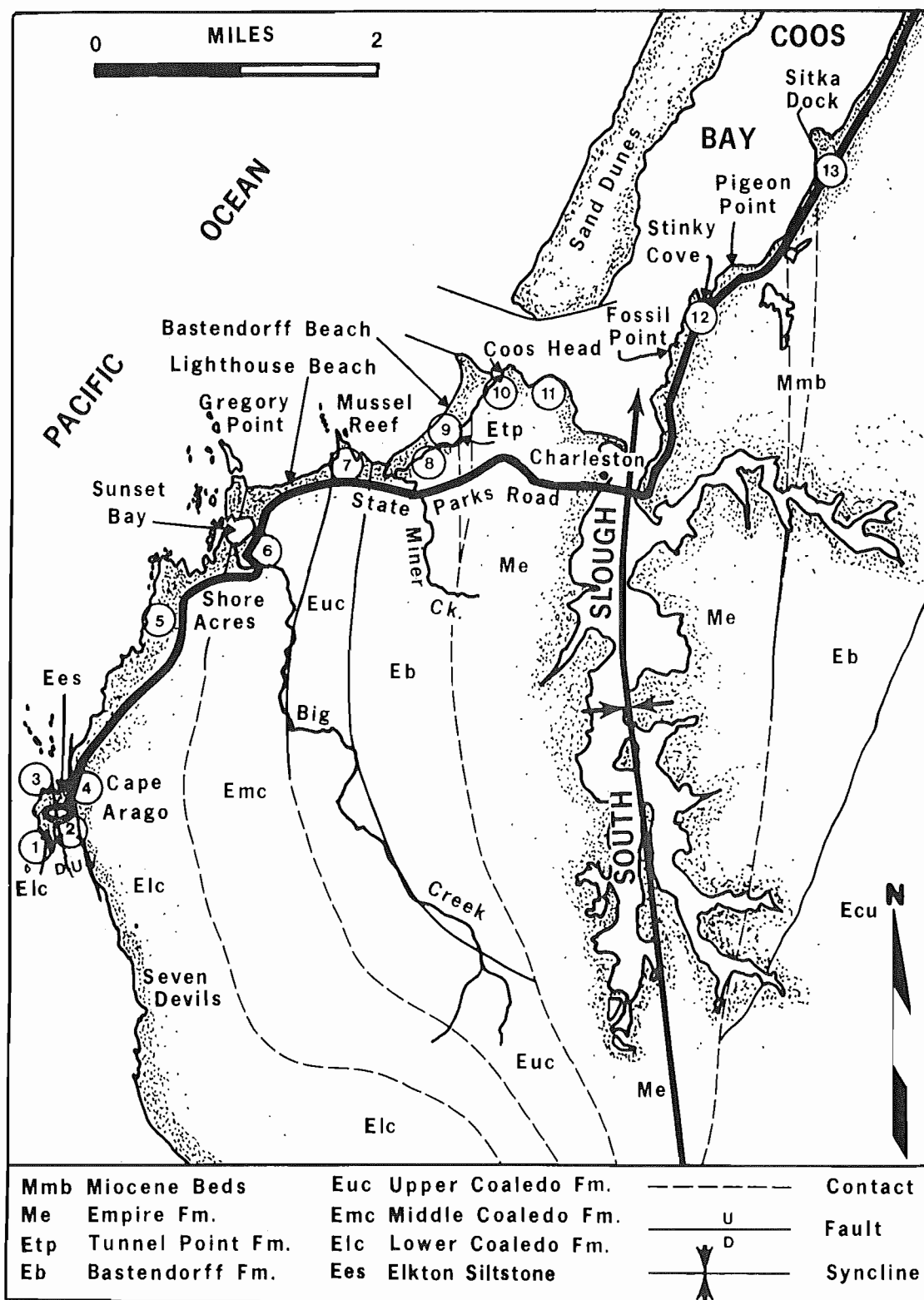


Figure 4. Geologic map for Coos Bay area (modified from Baldwin and others, 1973). Circled numbers indicate field trip stops.

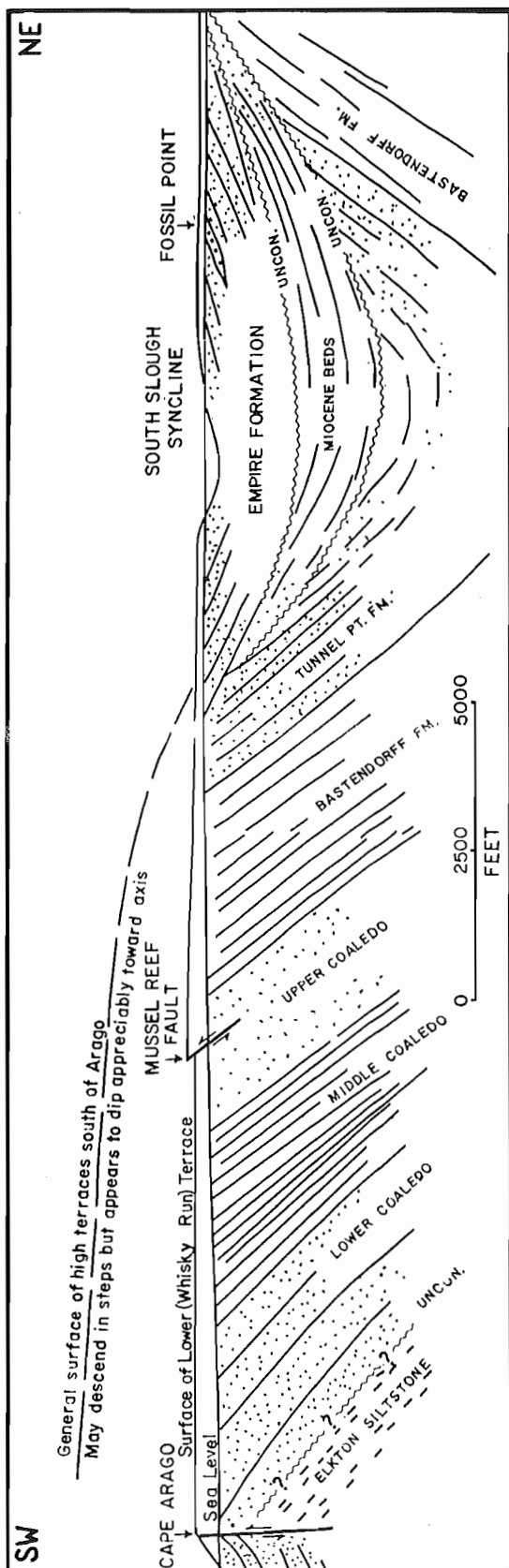


Figure 5. Geologic cross section of South Slough Syncline (modified from Baldwin 1966).

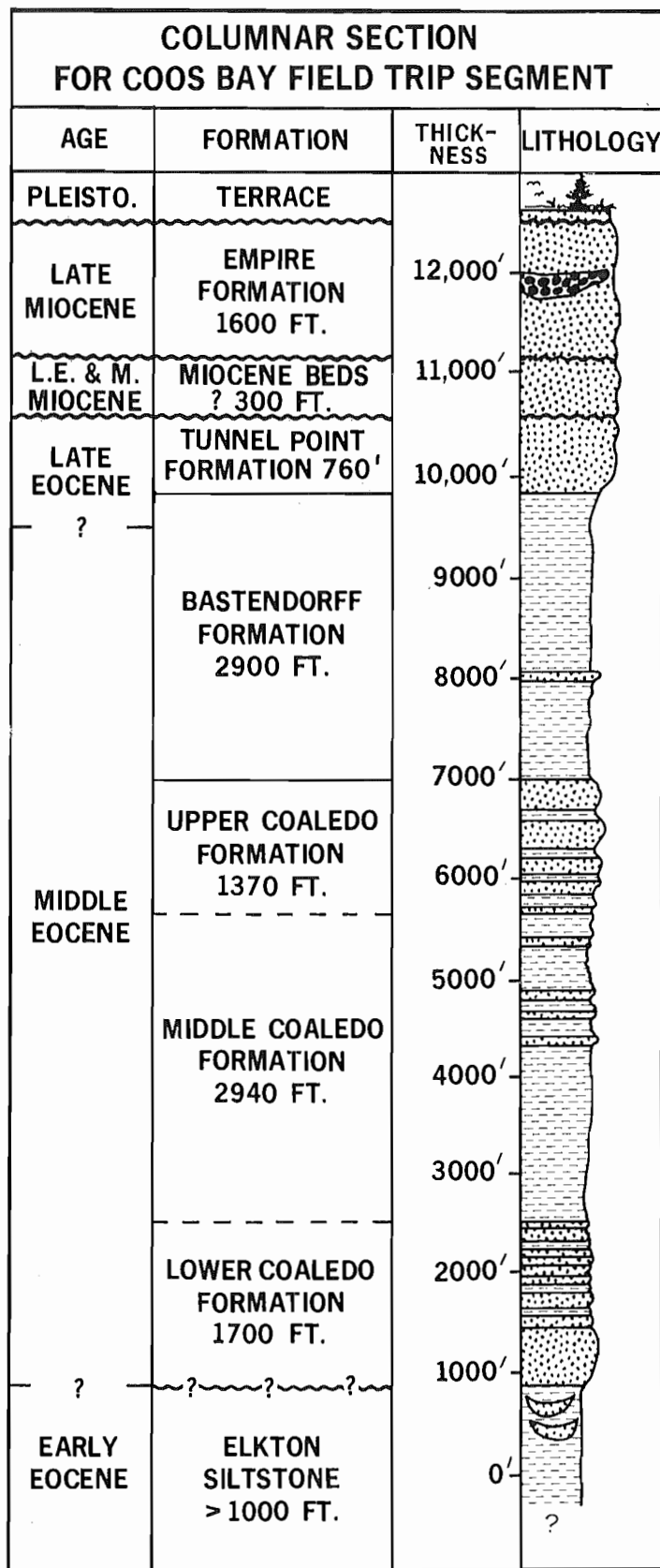
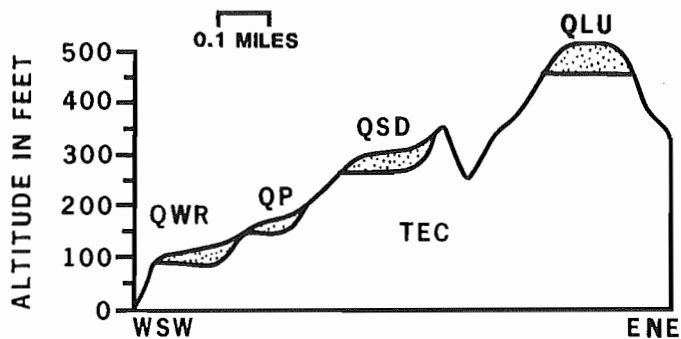


Figure 6. Stratigraphic column for Coos Bay Cenozoic formations.



QWR WHISKY RUN TERRACE
 QP PIONEER TERRACE
 QSD SEVEN DEVILS TERRACE
 QLU LOWER UNNAMED TERRACE
 TEC EOCENE COALEDO FORMATION

Figure 7. Coastal Terrace Sequence: STOP 2. Griggs (1945) has mapped five coastal terraces in the vicinity of Cape Arago. This diagram shows the relative relationship of the four lower and more visible terraces which can be seen from STOP 2. The cross section is drawn trending east-northeast.

A sequence of five coastal terraces can be seen from this vantage point (Fig. 7). Griggs (1945) mapped, named, and cursorily described these terraces. Baldwin (1945, 1966) and Armentrout (1967) have made observations at selected key localities. Cape Arago is capped with 10 to 40 feet of colluvium and marine sands and gravels of the Whisky Run terrace. At Cape Arago the paleoshoreline of the Whisky Run terrace is at an altitude of about 95 feet. Southward along the Seven Devils area the prominent bench of the Seven Devils terrace occurs at an altitude of about 300 feet. Farther south, the Pioneer terrace is well developed at about 150 feet above the valley at Two Mile Creek which is just north of Five Mile Point. The Whisky Run terrace at 100 feet elevation forms the flat surface of Five Mile Point. The break between the Pioneer and Whisky Run terraces is visible in the coastal bluffs between Five Mile Point and Two Mile Creek. Two prominent high terraces at altitudes of 730 and 500 feet were unnamed by Griggs (1945), and are difficult to identify at Cape Arago.

Large channels filled with lenticular sequences of massive sandstone and mudstone can be seen in the eastern cliffs of South Cove (Figs. 8-9). These rocks of the Elkton Siltstone are transitional stratigraphically from thick-bedded, mid-fan sandy turbidites of the underlying Tyee Formation to the overlying coal-bearing deltaic Coaledo Formation (Dott and Bird, 1979). Foraminifers suggest a shoaling sequence from upper bathyal Tyee faunas to inner neritic, upper Elkton faunas. Channel fills are either laminated mudstone-siltstone identical with the channelized deposits or massive to faintly parallel-laminated and rarely graded light-colored sandstones.

Dott and Bird (1979) interpret the Elkton Siltstone at Cape Arago as shelf and slope deposits cut by an array of sea gullies which range in size up to 300 feet wide and 75 feet deep. These gullies may have acted as conduits of sand from a sandy littoral and deltaic zone (Coaledo Formation-like facies) across a narrow shelf and slope feeding deeper marine turbidity currents and other gravity flows (Tyee Formation-like facies), which built subsea fans (Dott and Bird, 1979).

Return to roadway and proceed north and west back through the main entrance of Cape Arago State Park, stopping at the drinking fountain at the north end of the main parking area.

(0.3)

62

- 0.0 STOP 3: NORTH COVE OVERLOOK: Walk along the paved trail to the north end of the picnic area. (Fig 1-d). From vantage points along this trail the geology of North Cove can be seen.

The geology of North Cove is similar to that of South Cove. The eastern cliffs of the Cove are Elkton Siltstone while the seastacks farthest to the west are Coaledo Formation sandstone. The traverse along the North Cove beach is passable even at normal high tide. The trail from the Cape Arago-North Cove picnic area descends to the beach. A major Elkton Siltstone channel crops out at the eastern margin of North Cove (Figs. 1-e and 10). The channel axis has been reoccupied by a modern stream which cascades down a prominent rib of sandstone. The sandstone rib stands in marked relief compared to exposures of the same sandstone on either side of the waterfall. The constantly wet sandstone may be more erosionally resistant than alternately wet and dry cliff faces to either side (Ehlen, 1967). The major "waterfall" channel is only one of several Elkton Siltstone channels which occur along the cliffs to the north of the waterfall. Sedimentary structures in the Elkton Siltstone are exposed on the wave-cut terrace just north of the lobate beach north of the waterfall. Primary sedimentary structures include flame structures, rill-type solemarks, load features, groove and flute casts, interclast conglomerates, climbing ripple laminations, flaser bedding, cross-trough stratification, laminated mudstone and sandstone, and clastic dikes. Paleocurrents are to the northwest. Northward, past the area of Sea Lion View Point (STOP 4), the Elkton Siltstone is overlain by massive tan conglomeratic sandstones of the Coaledo Formation.

Return to the North Cove parking area and leave Cape Arago State Park on State Parks Road.

- (0.4)
0.0 STOP 4: SEA LION VIEW POINT: From this view point (Fig. 1-f) one can see the seastacks of North Cove and Simpson's Reef. Shell Island is the largest sea stack of the North Cove group.

Simpson's Reef, the farthest offshore and most elongate reef, dips landward. Most of the North Cove sea stacks dip seaward. These structural attitudes define Simpson's Reef Syncline (Ehlen, 1967).

- 0.0 START CUMULATIVE MILEAGE. Continue north on State Parks Road. Road cuts along this area are in alluvium and colluvium on the back of Whisky Run terrace.

- (1.0)
1.0 Shore Acres State Park: turn left into the park. Proceed to and park in the main viewpoint parking area. Walk out to the view area at the sea cliff.

- (0.2)
1.2 STOP 5: SHORE ACRES STATE PARK: Shore Acres (Fig. 1-g) was developed as an estate by the Louis Simpson family, prominent in lumbering and ship-building in the Coos Bay area. The manor house burned in the late 1930's and the estate (including the land of Cape Arago State Park) was donated by the Simpson family to the State of Oregon in 1942.

Shore Acres is underlain by the lower sandstone member of the Coaledo Formation. These strata dip eastward at about 40° and are part of the east limb of the Cape Arago Anticline (Ehlen, 1967). Numerous down to the south normal faults trend northwest. The five coves in the park area are eroded along zones of weakness associated with faults. The lower sandstone member of the Coaledo Formation is about 1,300 feet thick in the coastal section (Ryberg, 1978) and thickens to 1,800 feet to the southeast (Allen and Baldwin, 1944) where the outcrop area of the Coaledo Formation wraps around the south end of the South Slough Syncline. The lower sandstone member is predominantly fine- to medium-grained, cross-bedded and

laminated sandstones with minor interbeds of siltstone and mudstone. At Shore Acres the sandstones stand out as erosionally resistant, concretionary ribs where the interbedded fine-grained rocks have been differentially eroded. Large iron-cemented concretions are characteristic features of the lower Coaledo Formation. Fossils are abundant in some intervals of the lower Coaledo. Ophiuroids (brittle stars) are moderately common within one bed which crops out in both the northern and southern coves at Shore Acres State Park.

Shore Acres State Park is developed upon the Whisky Run terrace (Fig. 7). Four to nine feet of littoral sand rest upon this terrace platform. Whisky Run terrace sands can best be viewed from the north end of the viewpoint area.

Proceed back to State Parks Road.

- (0.4)
- 1.6 Turn left toward Sunset Bay State Park.
- (0.4)
- 2.0 View at 11:00 o'clock of Gregory Point and Cape Arago Lighthouse (Fig. 1-i and 11-b). Gregory Point is underlain by lower Coaledo Formation sandstone. These sandstones dip northeastward and strike increasingly more westward around the northern end of the Cape Arago Anticline (Ehlen, 1967).
- (0.5)
- 2.5 Bridge across Big Creek. Big Creek heads in shales of the Bastendorff Formation to the east and cuts through the upper and middle Coaledo Formation.
- (0.2)
- 2.7 STOP 6: SUNSET BAY STATE PARK: Park in the beach parking area. Traverses along either the north or south margins of Sunset Bay afford access to outcrops of lower Coaledo sandstone and middle Coaledo siltstone and mudstone. Access is best at low tide when outcrops of the surf-cut terrace are exposed over large areas along the north side of the cove. Trails along the north bluff of the bay provide excellent views of the faulting of the wave-cut terrace (beware of undercutting of the trails along the bluff).

Sunset Bay is an arcuate bay formed along a complex set of northwest-trending faults transverse to the strike of bedding (Fig. 11-a). Sunset Bay is offset 450 feet in a right lateral sense, between the north side and south side of the bay. Whether this displacement is along a single fault, or a series of smaller faults such as those exposed along the bay margins, is unknown. Orientation of drag folds suggests that the fault motion was oblique slip (Ehlen, 1967) (Fig. 12).

Ryberg (1978) identified several lithofacies in coarsening upward sequences within the lower Coaledo Formation. Outcrops exposing these coarsening upward sequences occur along the shores of Sunset Bay. The top of each sequence is generally identified by dark-brown, concretionary, coarse pebbly sandstone which forms erosionally resistant ribs. The typical sequence from bottom to top includes interdistributary siltstone and fine-grained sandstone, overlain by coarser distributary channel (and possibly fluvial) sandstone with interbedded lagoon or swamp coal and carbonaceous siltstone. These coarsening upward sequences are interpreted by Ryberg (1978) as representative of the outbuilding of individual distributary channels during progradation of a delta. This agrees with Dott's (1966) deltaic model for the Coaledo Formation.

Sedimentary structures are well developed and beautifully exposed in outcrops along the north side of Sunset Bay and on the cliffs and terraces beyond the southwest edge of the bay entrance. Primary sedimentary structures include tabular, trough, wedge and hummocky cross-stratification, ripple cross-stratification, and rare flute and groove sole marks. Secondary

64



Figure 12. Coaledo Formation: STOP 6. View of drag-folds along faults in the Coaledo Formation. Photo taken at low tide from bluffs above the north side of Sunset Bay.

structures resulting from gravity deformation of the sediments include contorted bedding and flare, and ball and pillow structures. Clastic dikes and isolated sandstone "load-balls" represent liquification structures. Bioturbation includes both vertical and horizontal burrows.

The lower Coaledo is abundantly fossiliferous (Turner, 1938; Rooth, 1974). Mollusks and Foraminifera dominate the fauna but echinoids, shark teeth, and rare crustacean fossils also occur. The mollusks suggest deposition in middle to lower neritic depths (Rooth, 1974).

Paleocurrents are predominantly to the northwest and mineralogic studies suggest a mixed andesitic (e.g., Cascade-like) and metaplutonic (e.g., Klamath Mountains-like) provenance (Dott, 1966; Ryberg, 1978). This fits well with Dott's (1966) paleogeographic reconstruction for middle Eocene time which consists of a broad coastal plain prograding westward across a narrow shelf and slope. The coastal plain was flanked by highlands on the southeast. The highland included both volcanic and metaplutonic terrains.

Outcrops of the middle member of the Coaledo Formation in Sunset Bay consist of interbedded laminated siltstone and mudstone with minor amounts of sandstone. Ryberg (1978) considered this lithofacies to represent intertidal flat and delta front deposits. The abundant molluscan (Turner, 1938) and foraminiferal faunas (Detling, 1946; Cushman and others, 1947; Rooth, 1974) represent deepening conditions from outer neritic just above the lower Coaledo sandstones to upper bathyal conditions above. The best outcrops and a complete section of the middle Coaledo siltstones and mudstones occurs along Lighthouse Beach at STOP 7.

The steeply dipping beds of the Coaledo Formation are truncated by the Pleistocene Whisky Run terrace. The Whisky Run terrace platform and presumably the shoreline angle are at an altitude of about 50 feet at the rear of the north side of Sunset Bay. The terrace platform along the south side of the bay is at 70 feet. The terrace has probably been offset by movement along a fault hidden beneath the water of Sunset Bay.

Tree stumps with root spreads up to 35 feet are exposed along Big Creek and in the intertidal zone of Sunset Bay beach. One set of root systems occurs in association with peat toward the north end of the beach. The trees could have been growing on the Holocene flood plain of Big Creek and drowned as the sea carved out the Sunset Bay amphitheater long after sea level attained its present position. Previously unpublished carbon

14 data on one root from along Big Creek yields an estimated age of about 1,200 years B.P. (Southern Methodist University Radiocarbon Laboratory Sample 593-B8/12-Count 1439: 10/11/78; Armentrout, unpub. data).

Return to the parking area and proceed north on State Parks Road. The road climbs from the Big Creek Holocene flood plain to the top of the Pleistocene Whisky Run terrace.

- (0.4)
- 3.1 Road to the left provides access to the Cape Arago Lighthouse on Gregory Point. Steeply dipping beds of the lower Coaledo sandstone underlie the point.
- (0.6)
- 3.7 STOP 7: YOAKAM POINT - MUSSEL REEF: Park along State Parks Road and walk northwest along a dirt road; about 150 feet from the main road, bear right (north) at the Y-junction, and continue to the sea cliff overlook area.

STOP 7A: Looking westward from Yoakam Point the three members of the Coaledo Formation can be observed. The lower sandstone member underlies Gregory Point to the west (Fig. 11-b). The middle mudstone and siltstone member has been eroded back forming Lighthouse Beach (Fig. 11-c). Yoakam Point and its seaward extension, Mussel Reef, consists of the upper sandstone member of the Coaledo Formation (Fig. 11-d). The cove immediately east of Yoakam Point is eroded in a siltstone of the upper sandstone member of the Coaledo Formation. The small point at the east side of this cove is the uppermost Coaledo Formation sandstone.

The platform of the Gregory Point-Yoakam Point area is formed by the Whisky Run terrace and is veneered by about 11 feet of littoral sand. At Yoakam Point the terrace is faulted with the eastern block offset about 10 feet above the western block. The fault trends north-northwest, parallel to the strike of the underlying Coaledo Formation and appears to be a high-angle reverse fault (Baldwin, 1966) (Fig. 5). The fault is best observed from the beach where the offset of a coal seam delineates the fault motion.

Griggs (1945) has mapped the eastward continuation of the Whisky Run terrace at the back of Bastendorff Beach where it forms the platform as far northeast as Tunnel Point (Fig. 11-g). The Pioneer terrace surface forms the platform at Coos Head, the northernmost point at the mouth of Coos Bay (Griggs, 1945) (Fig. 11-h).

Descend to Lighthouse Beach along the trail just south of Yoakam Point and walk to Gregory Point. Stop 7B consists of a traverse from Gregory Point to Yoakam Point.

STOP 7B: Gregory Point is formed of uppermost lower Coaledo sandstone interpreted to be deltaic distributary channel deposits (Ryberg, 1978). The sandstone is conformably overlain by middle Coaledo siltstone, mudstone and thinly bedded sandstone interpreted by Ryberg (1978) as intertidal flat to delta front deposits. Thick channelized massive sandstone occurs at several intervals within the finer grained sequence and is interpreted as prodelta front slump deposits (proximal turbidite or grainflow gravitite). A white tuff 3- to 6-feet-thick occurs just above the middle part of the middle Coaledo member at Lighthouse Beach.

At several points along Lighthouse Beach the truncated ends of middle Coaledo sandstone beds at the abrasion surface of Whisky Run terrace are bored by rock-boring clams. These features will be examined in detail at STOP 11.

The middle Coaledo Formation mudstone and siltstone is gradational with the overlying upper Coaledo sandstone. Upper Coaledo sandstone units are very similar to those of the lower Coaledo, representing fluvial and

6413



Figure 21. Aerial View of Cape Blanco Traverse. a) Jurassic Otter Point Formation. b) Late Miocene Empire Formation. c) Cape Blanco Coast Guard facility. d) Eocene Shales - Stop 4. e) Miocene Sandstones - Stop 6. f) Fin Rock Miocene Sandstones - Stop 7. g) Terrace Fossil Beds - Stop 3. h) View Point - Stop 2. i) Cape Blanco State Park Campground. j) Goldwasher's Gully - Stop 11. k) Cliff at Stop 12. l) Cliffs at Stops 13-15. m) Mouth of Elk River. n) Port Orford. o) Humbug Mountain. Photograph courtesy of Oregon State Highway Division.

64C

Soil
BASICS

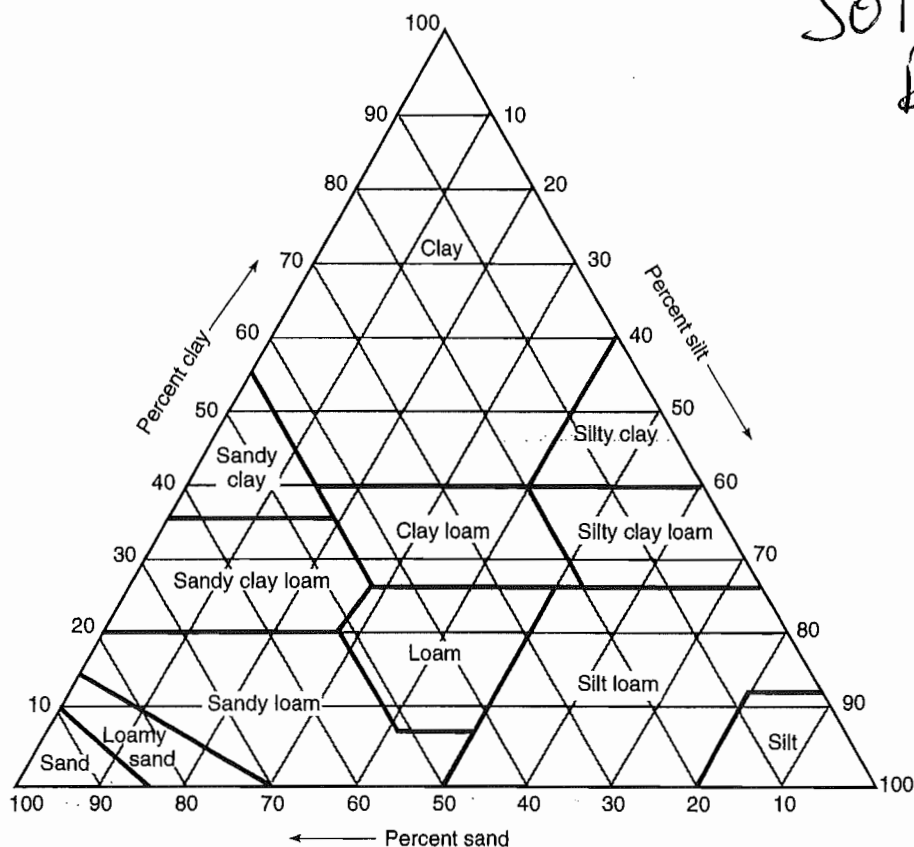


Figure 3.12

Percentages of clay (< 0.002 mm), silt (0.002–0.05 mm), and sand (0.05–2.0 mm) in basic soil textural classes as defined by the U.S. Department of Agriculture.

(Soil Survey Staff, 1951)

ganic content are typically black to dark brown, whereas the presence of ferric iron is indicated by yellow-brown to red colors. Light gray to white colors are associated with a concentration of SiO_2 or CaCO_3 . It should be recognized, however, that small amounts of a pigment can cause rather intense discoloration, and so color alone may be a poor index of the total quantity of the pigmenting substance. *Texture* is simply the relative proportions of different particle sizes in a soil horizon, and is somewhat analogous to the property of sorting as used by geologists. However, it is based only on the particles that are less than 2 mm in diameter (fig. 3.12). *Structure* in soils is a unique characteristic in that it designates the shape developed when individual particles cluster together into aggregates called *peds* (fig. 3.13). In clay-rich soils, the openings between peds may play an extremely important geomorphic role by providing the primary avenues for downward percolation through an otherwise impermeable soil. *Organic matter* in soils consists mainly of dead leaves, branches, and the like, called *litter*, and the amorphous residue, called *humus*, that develops when litter is decomposed. Litter may form at mean annual temperatures as low as freezing,

but its optimum production occurs at about 25° to 30° C and decreases rapidly above those levels. Microorganisms that convert litter to humus begin to function at temperatures slightly above freezing (5° C), but the optimum temperature for their life activities may be as high as 40° C (fig. 3.14). It is significant that at temperatures between 0° and 25° C, humus is produced in abundance, but above 25° C little if any humus is accumulated. Humus has an important effect on soil formation because it includes chelators that promote the leaching of iron and aluminum, and increases water absorption. In addition, the development of humus releases CO_2 in high concentrations, leading to unusual amounts of carbonic acid within the humic zone and an associated lowering of the pH.

The total quantity of water that can be held in a soil is the *available water capacity* (AWC). By combining this parameter with the bulk density (dry weight of soil/unit volume), an estimate of the depth of wetting can be made (see Birkeland 1999). Such information is significant in that it relates to many soil properties, especially those affected by the redistribution of material during the downward percolation of water.

105

102

4.1 SOIL COLOR¹

When we examine a soil, the first thing we are likely to notice is its color. In and of themselves, soil colors have little effect on the behavior and use of soils. An important exception to this statement is the fact that dark-colored surface soils absorb more solar energy than lighter-colored soils, and therefore may warm up faster.

The main reason for studying soil colors is that color provides valuable clues to the nature of other soil properties and conditions. Because of the importance of accurate color description in soil classification and interpretation, a standard system for color description has been developed using Munsell color charts (Figure 4.1). In this system, a small piece of soil is compared to standard color chips in a soil color book. Each color chip is described by the three components of color: the **hue**, the **chroma** (intensity or brightness), and the **value** (lightness or darkness).

Causes of Soil Colors

Soils display a wide range of reds, browns, yellows, and even greens (see Plate 13). Some soils are nearly black, others nearly white. Some soil colors are very bright, oth-

¹For an excellent collection of papers on the causes and measurement of soil colors, see Bigham and Ciolkosz (eds.), 1993.

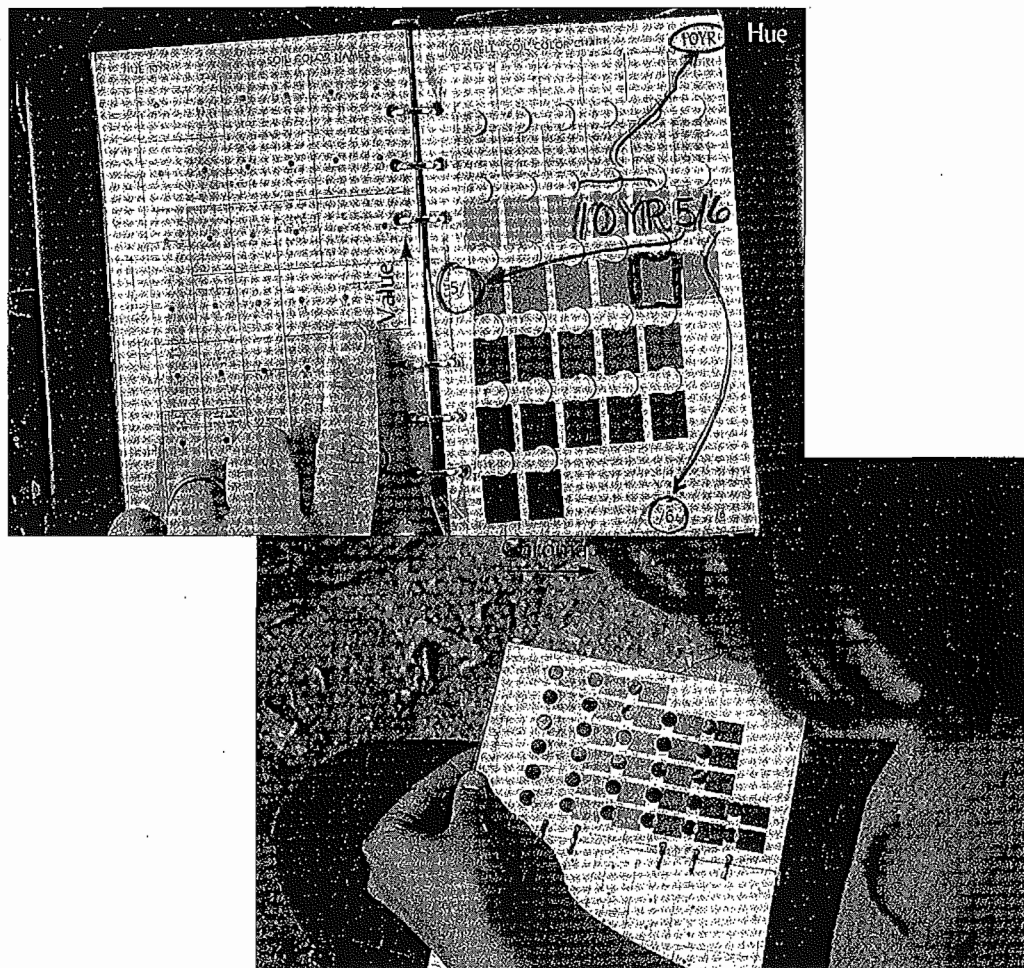


FIGURE 4.1 Determining soil color by comparison to color chips in a *Munsell Color Book*. Each page shows a different hue, ranging from 5R (red) to 5Y (yellow). On a single page, higher-value (lighter) colors are nearer the top and lower-value (darker) colors are near the bottom. Higher-chroma (brighter) colors are nearer the right-hand side and duller, grayish (low-chroma) colors are near the left-hand side. The complete Munsell color description of the soil pictured is 10YR 5/6 (yellowish brown), moist. (Photos by R. Weil)

105A

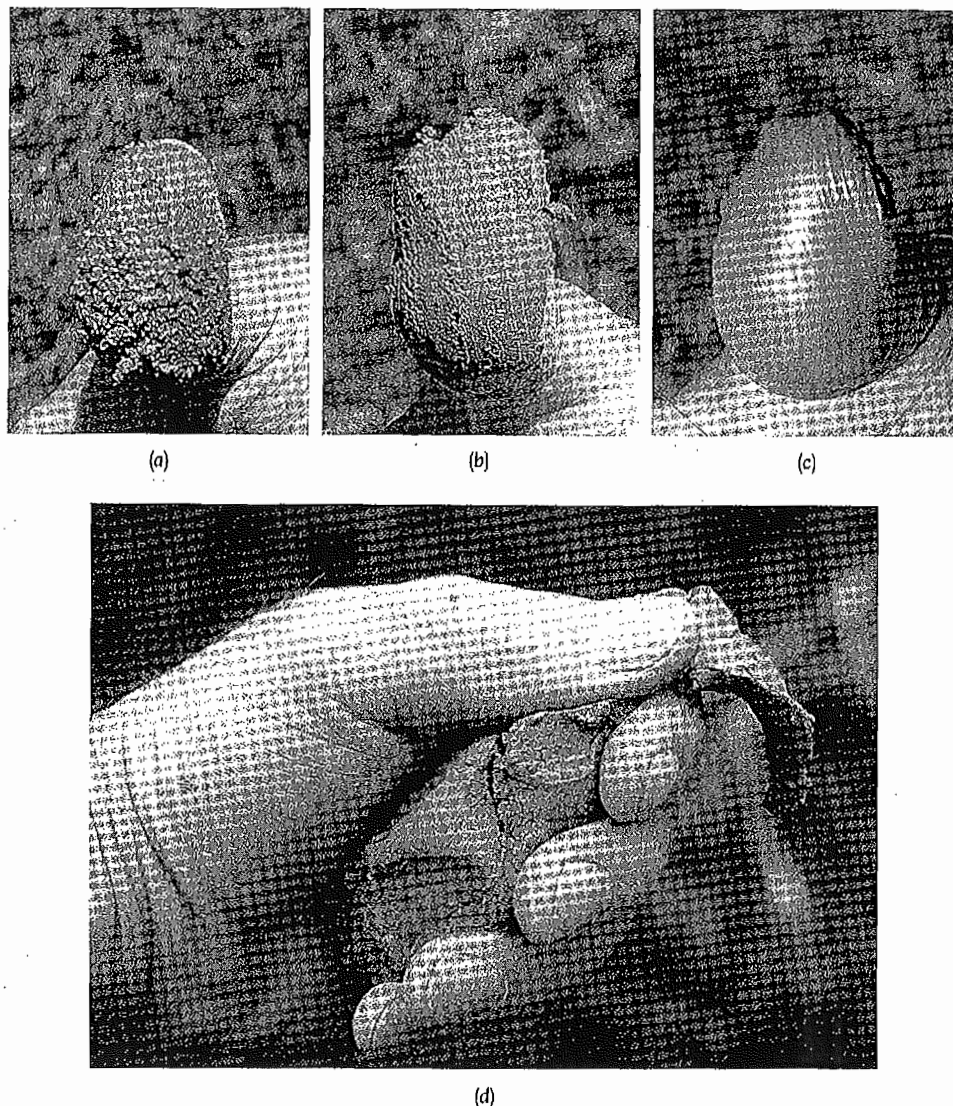


FIGURE 4.9 The "feel" method as used to distinguish between a sand (a), a silt loam (b), and a clay (c) soil. Moist samples are rubbed between the thumb and forefinger. Note the shiny appearance for the clay (c), the lack of cohesion in the sand (a), and the intermediate status of the silt loam. An estimate of percent clay is often a very useful first step in determining textural class by feel. Percent clay in a sample is best estimated by squeezing a ribbon of moist soil (d).

TABLE 4.4 Criteria Used with the Field Method of Determining Soil Texture Classes

Criterion	Sand	Sandy loam	Loam	Silt loam	Clay loam	Clay
1. Individual grains visible to eye	Yes	Yes	Some	Few	No	No
2. Stability of dry clods	Do not form	Do not form	Easily broken	Moderately easily broken	Hard and stable	Very hard and stable
3. Stability of wet clods	Unstable	Slightly stable	Moderately stable	Stable	Very stable	Very stable
4. Stability of "ribbon" when wet soil rubbed between thumb and fingers	Does not form	Does not form	Does not form	Broken appearance	Thin, will break	Very long, flexible

10513

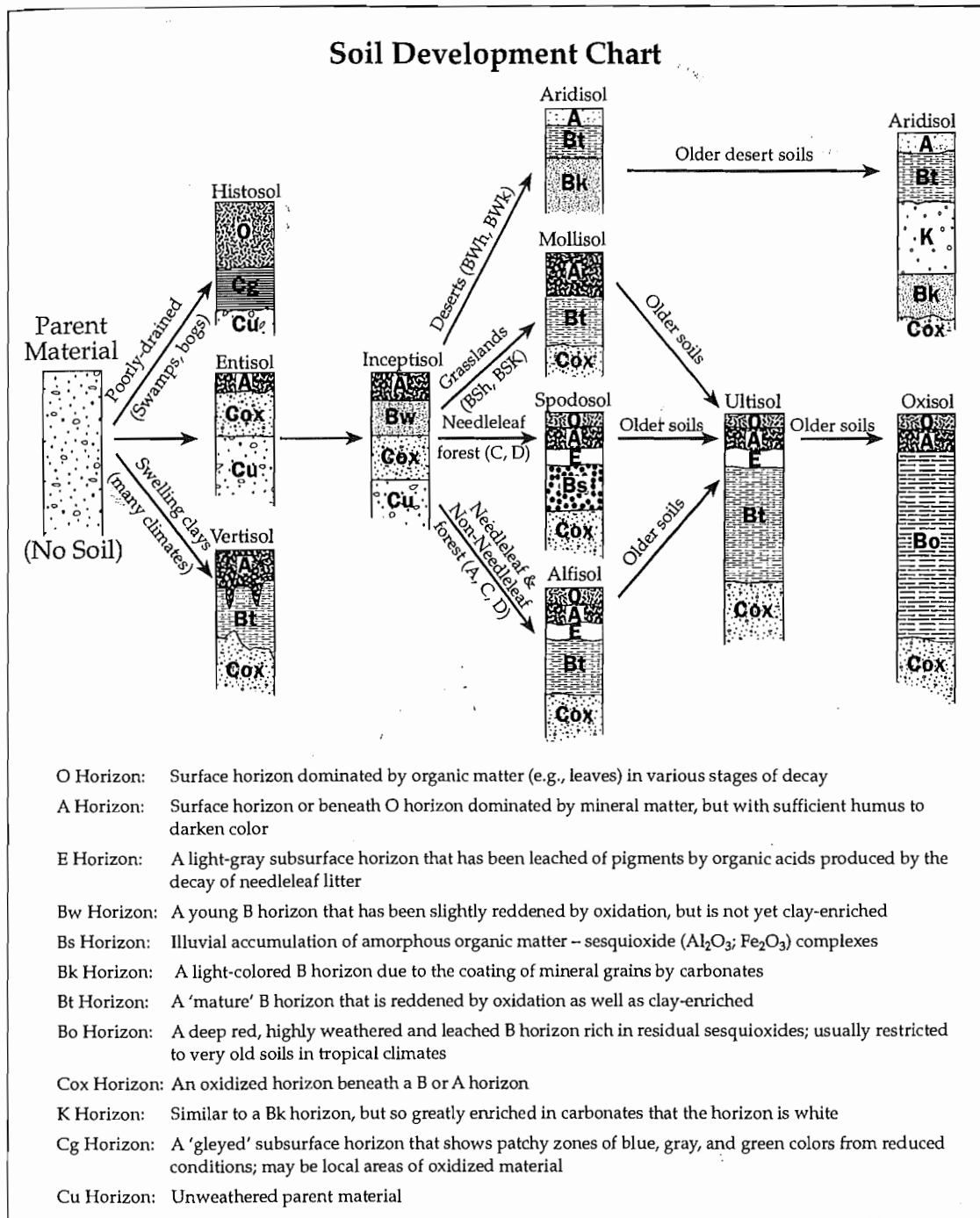


Figure 2.7 Soil orders arranged into a development scheme, with greater development (and age, in most cases) to the right. Parent material controls the first step in the development, and time and bioclimate beyond that. Letters in parentheses depict climate classification of Köppen. (Courtesy of Dennis Netoff, 1997.)

106

103

Table 1.1 Soil-Horizon Nomenclature**Description of master horizon and subhorizons**

- O horizon**—Surface accumulations of mainly organic material; may or may not be, or has been, saturated with water. Subdivided on the degree of decomposition as measured by the fiber content after the material is rubbed between the fingers.
- Oi horizon**—Least decomposed organic materials; rubbed fiber content is greater than 40% by volume.
- Oe horizon**—Intermediate degree of decomposition; rubbed fiber content is between 17 and 40% by volume.
- Oa horizon**—Most decomposed organic materials; rubbed fiber content is less than 17% by volume.
- A horizon**—Accumulation of humified organic matter mixed with mineral fraction; the latter is dominant. Occurs at the surface or below an O horizon; Ap is used for those horizons disturbed by cultivation.
- E horizon**—Usually underlies an O or A horizon, and can be used for eluvial horizons within or between parts of the B horizon (e.g., common above fragipan, x). Characterized by less organic matter and/or fewer sesquioxides (compounds of iron and aluminum) and/or less clay than the underlying horizon. Many are marked by a concentration of sand and silt. Horizon is light colored due mainly to the color of the primary mineral grains because secondary coatings on the grains are absent; relative to the underlying horizon, color value will be higher or chroma will be lower.
- B horizon**—Underlies an O, A, or E horizon, and shows little or no evidence of the original sediment or rock structure. Several kinds of B horizons are recognized, some based on the kinds of materials illuviated into them, others on residual concentrations of materials. Subdivisions are:
- Bh horizon**—Illuvial accumulation of amorphous organic matter-sesquioxide complexes that either coat grains or form sufficient coatings and pore fillings to cement the horizon.
- Bhs horizon**—Illuvial accumulation of amorphous organic matter-sesquioxide complexes, and sesquioxide component is significant; both color value and chroma are three or less.
- Bk horizon**—Illuvial accumulation of alkaline earth carbonates, mainly calcium carbonate; the properties do not meet those for the K horizon.
- Bt horizon**—Illuvial concentrations primarily of silt (Forman and Miller, 1984). Used when silt cap development reaches stages 5 and 6.
- Bo horizon**—Residual concentration of sesquioxides, the more soluble materials having been removed.
- Bq horizon**—Accumulation of secondary silica.
- Bs horizon**—Illuvial accumulation of amorphous organic matter-sesquioxide complexes if both color value and chroma are greater than three.
- Bt horizon**—Accumulation of silicate clay that has either formed in situ or is illuvial (clay translocated either within the horizon or into the horizon); hence it will have more clay than the assumed parent material and/or the overlying horizon. Illuvial clay can be recognized as grain coatings, bridges between grains, coatings on ped or grain surfaces or in pores, or thin, single or multiple near-horizontal discrete accumulation layers of pedogenic origin (clay bands or lamellae). In places, subsequent pedogenesis can destroy evidence of illuviation. Although Soil Survey Division Staff (1993) does not include this, clay accumulation that lacks evidence for illuviation is included (could have been formed in situ, for example).
- Bw horizon**—Development of color (redder hue or higher chroma relative to C) or structure, or both, with little or no apparent illuvial accumulation of material.
- By horizon**—Accumulation of secondary gypsum.
- Bz horizon**—Accumulation of salts more soluble than gypsum.
- K horizon**. A subsurface horizon so impregnated with carbonate that its morphology is determined by the carbonate (Gile and others, 1965). Authigenic carbonate coats or engulfs nearly all primary grains in a continuous medium. The uppermost part of a strongly developed horizon is laminated, brecciated, and/or pisolithic (Machette, 1985). The cemented horizon corresponds to some caliches and calcretes.
- C horizon**—A subsurface horizon, excluding R, like or unlike material from which the soil formed, or is presumed to have formed. Lacks properties of A and B horizons, but includes materials in various stages of weathering.
- Cox and Cu horizons**—In many unconsolidated deposits, the C horizon consists of oxidized material overlying seemingly unweathered C. The oxidized C does not meet the requirements of the Bw horizon. In stratigraphy, it is important to differentiate between these two kinds of C horizons. Here Cox is used for oxidized C horizons and Cu for unweathered C horizons. Cu is from the nomenclature of England and Wales (Hodson, 1976). Alternatively the Cox can be termed BC or CB.
- Cr horizon**—In soils formed on bedrock, there commonly will be a zone of weathered rock between the soil and the underlying rock. If it can be shown that the weathered rock has formed in place, and has not been transported, it is designated Cr. Such material is the saprolite of geologists; in situ formation is demonstrated by preservation of original rock features, such as grain-to-grain texture, layering, or dikes. If such material has been moved, however, the original structural features of the rock are lost, and the transported material may be the C horizon for the overlying soil. Those Cr horizons with translocated clay, as shown by clay films, are termed Crt.
- R horizon**—Consolidated bedrock underlying soil.

(continued)

107

107

tographs, so one can become familiar with the classification criteria. However, to avoid becoming overwhelmed, one should read Buol and others (1997). This readable text covers all the orders, chapter by chapter, and each is subdivided into the central concept and geographic distribution of the order, the setting, pedogenic processes, uses, and classification. The reader should be aware, however, that the classification has gone through many revisions, so consult Soil Conservation Service (1994) for the latest (watch for still more recent keys).

The new classification has much appeal for geomorphologists and ecologists, at least down to the suborder level. This is because soil profile development is included in the classification, as well as base saturation, amount of organic matter, and properties indicative of relative wetness and dryness. Most geomorphological soil studies deal with climatic and time factors, and the above properties will later be shown to be related to both.

Eleven orders are now recognized in the new classification; these are subdivided into 55 suborders, and the latter into over 200 great groups. One should be impressed with the magnitude of this task as it begins at the lowest level of classification, the approximately 12,000 soil series in the United States. The orders are basically differentiated by a particular horizon or horizon combinations that occur in the soil profile. These usually can be recognized in the field without recourse to laboratory analysis. One criticism of Soil Taxonomy, from a geomorphological point of view, is the overem-

phasis on classification at the order level by surface horizon (e.g., Mollisol). In contrast, horizons beneath the A horizon commonly are more important to geomorphologists. Classification into suborders requires an increasingly quantitative knowledge of soil properties and soil-moisture and soil-temperature regimes. However, it is often not necessary to take these measurements because, with experience, soil classification can be estimated from properties recognizable in the field (e.g., thin Av horizon with a calcic horizon at depth points toward aridic moisture regime).

To classify a soil at the order and suborder level, one must be able to identify the diagnostic horizons as well as the soil-moisture and -temperature regimes. The reader will find that some of these definitions are exceedingly complicated, but in time they will make some sense. Diagnostic horizons are so named because they are essential to classify the soil. Epipedons are the surface diagnostic horizons. The diagnostic horizons are somewhat similar to the field-designated soil horizons, although in places they can encompass several different field-designated soil horizons. In an extreme example of the latter, the mollic epipedon can include both the A and B horizons, as long as mollic properties are obtained. For some diagnostic horizons, the criteria are so complex that one has to read the defining criteria in detail using both the field and laboratory data (e.g., spodic horizon). Only the main discriminating criteria are given here (Table 2.1); Soil

Table 2.1 Common Diagnostic Horizons Used in Soil Taxonomy

Diagnostic Horizon	Defining Criteria	Probable Field Horizon Equivalent
Epipedons		
Mollic epipedon	Must be 10 cm thick if on bedrock, otherwise a minimum of 18 or 25 cm thick depending on subhorizon properties and thicknesses; color value darker than 3.5 (moist) and 5.5 (dry); chroma less than 3.5 (moist); organic carbon content at least 0.6%; structure developed and horizon not both massive and hard; base saturation $\geq 50\%$	A, A + E + B, A + B
Umbric epipedon	Meets all criteria for mollic epipedon, except base saturation $< 50\%$	A
Ochric epipedon	Epipedon that does not meet requirements of either mollic or umbric epipedons	A
Histic epipedon	Complex thickness requirements, but > 20 cm thick; $> 12\%$ organic carbon, with some adjustment for percent clay; saturated with water for 30 consecutive days or more per year, or artificially drained	O
Subsurface Horizons		
Albic horizon	Light colored with few to no coatings on grains—light color is that of grains; if color value (dry) is 7 or more, or color value (moist) is 6 or more,	E

(continued)

Table 2.1

Diagnosti

Argillic

Kandic

Natric

Spodic

Cambic

Oxic h

Calcic

Petroc

Gypsic

Petrog

Salic t

Durip

Fragip

Taken fr

108

Table 2.1 (continued)

Diagnostic Horizon	Defining Criteria	Probable Field Horizon Equivalent
Argillic horizon	chroma is 3 or less; if color value (dry) is 5 or 6, or color value (moist) is 4 or 5, chroma is closer to 2 than to 3 Complex thickness requirements, but at least 7.5 or 15 cm thick depending on texture and thickness of overlying horizons; must have these greater amounts of clay relative to overlying eluvial horizon(s) or underlying parent material: (a) if the latter horizons have <15% clay, argillic horizon must have a 3% absolute increase (10 vs. 13%); (b) if the latter horizons have 15 to 40% clay, the ratio of clay in argillic horizon relative to them must be 1.2 or more, and (c) if the latter horizons have >40% clay, the argillic horizon must have an 8% absolute increase (42 vs. 50%); in most cases, evidence for translocated clay should be present (clay as bridges between grains or clay films in pores or on ped faces)	Bt
Kandic horizon	Minimum thickness is either 15 or 30 cm; complex clay increase requirements relative to overlying eluvial horizon(s) or underlying parent material: if the latter horizons have <20% clay, the kandic horizon must have a 4% absolute increase; if the latter horizons have 20–40% clay, the kandic horizon must have at least 20% more clay; if the latter horizons have >40% clay, the kandic horizon must have at least 8% absolute increase; complex depth-texture relations; CEC <16 meq/100 g clay	Bt
Natric horizon	In addition to properties of argillic horizon: prismatic or columnar structure; 15% or more exchangeable sodium; exchangeable magnesium and sodium exceed exchangeable calcium and exchange acidity	Btn
Spodic horizon	Minimum thickness is 2.5 cm, and contains >85% spodic materials: the latter are amorphous materials composed of organic matter and Al, with or without Fe; usually beneath an albic or Ej horizon	Bh, Bs, Bhs
Cambic horizon	Base usually at least 25 cm deep; stronger chroma or redder hue relative to underlying horizon; soil structure or absence of rock or sediment structure; weatherable minerals present; carbonates removed if originally present; no cementation or brittle consistence	Bw
Oxic horizon	At least 30 cm thick; >15% clay and sandy loam or finer; cation exchange capacity ≤16 meq/100g soil; few weatherable minerals	Bo
Calcic horizon	At least 15 cm thick; 15% CaCO ₃ ; relative to underlying horizon, has at least 5% more CaCO ₃ , or at least 5% by volume secondary carbonate	Bk
Petrocalcic horizon	Horizon continuously cemented with CaCO ₃	Km
Gypsic horizon	At least 15 cm thick; at least 5% more gypsum than underlying horizon; product of thickness(cm) times content (%) is 150 or more	By
Petrogypsic horizon	Strongly cemented gypsic horizon, commonly with greater than 60% gypsum	Bym
Salic horizon	At least 15 cm thick; at least 2% salts more soluble than gypsum; product of thickness (cm) times content (%) is 60 or more	Bz
Duripan	Silica cementation is strong enough that fragments do not slack in water	Bqm
Fragipan	Horizon of high bulk density relative to overlying horizons; formed in loamy material; although seemingly cemented with a brittle appearance, slacks in water; slowly permeable to water, so usually mottled; very coarse prismatic structure, usually with some bleached faces	Bx, Cx

Taken from Soil Conservation Service (1994).

ntinued)

109

109

Available water capacity can be calculated if the moisture content at an upper limit (*field capacity*) and a lower limit (*permanent wilting point*) are known. Field capacity is determined by allowing a saturated sample to drain by gravity for at least 48 hours, by which time the remaining water content is held by adhesion to mineral and organic particles. After field capacity is reached, water can still be taken from the soil by plants until the tensional stresses holding the water in place become too great for the plants to break. At that point, the vegetation wilts. The water remaining in the soil is defined as the permanent wilting point. Both field capacity and permanent wilting point are expressed as a weight percentage according to the following equation:

$$P_w = \frac{W_s - W_d}{W_d} \times 100$$

where P_w is moisture percentage, W_s is total soil weight, and W_d is weight of soil after drying at 105°C. The available water capacity is simply the difference between the moisture content at field capacity and that at the permanent wilting point.

Soil Horizon Nomenclature and Description

Assuming that the vertical arrangement of the properties described above are distinct enough to identify a soil horizon, the pertinent consideration then becomes what nomenclature should be used to convey that information. In the United States, two systems of soil nomenclature are now in use. One is outlined in the *Soil Survey Manual* and is used in field descriptions of soil profiles (Soil Survey Division Staff 1993). The second is designed for the systematic classification of soils, and is based on the definition of diagnostic horizons, which, in many cases, can only be delineated following detailed laboratory analyses. The soil classification system used in the United States will be discussed in the next section. We will concentrate here on the nomenclature used to describe soils in the field.

Three kinds of symbols are used to denote horizons and layers in a soil profile. Capital letters, as shown in table 3.5, designate master horizons. Lowercase letters are used as suffixes to indicate specific characteristics of layers in the master horizon (table 3.6), and numbers are used as suffixes to connote vertical subdivision within a horizon or layer. In addition, numbers are prefixed to the master horizon designations to indicate a significant change in particle size or mineralogy within the soil. These signify a difference in the material from which the horizons have formed. In 1975 the Soil Conservation Service (S.C.S.) used Roman numerals as the prefix but have since changed to Arabic numerals (Soil Survey Division Staff 1993) (Note that the S.C.S. is now referred to as the National Resources Conservation Service). The number 1 is never used because it is implied to represent

TABLE 3.5 Nomenclature of Soil Horizons.

Horizon ^a	Characteristics
O	Upper layers dominated by organic material above mineral soil horizons. Must have > 30% organic content if mineral fraction contains > 50% clay minerals, or > 20% organics if no clay minerals.
A	Mineral horizons formed at the surface or below an O horizon. Contains humic organic material mixed with mineral fraction. Properties may result from cultivation or other similar disturbances.
E	Mineral horizons in which main characteristic is loss of silicate clay, iron, or aluminum, leaving a concentration of sand and silt particles of resistant minerals.
B	Dominated by obliteration of original rock structure and by illuvial concentration of various materials including clay minerals, carbonates, sesquioxides of iron and aluminum. Often has distinct color and soil structure.
C	Horizons, excluding hard bedrock, that are less affected by pedogenesis and lack properties of O, A, E, B horizons. Material may be either like or unlike that from which the solum presumably formed.
R	Hard bedrock underlying a soil.

Adapted from the Soil Survey Staff, 1960, 1975, 1981.

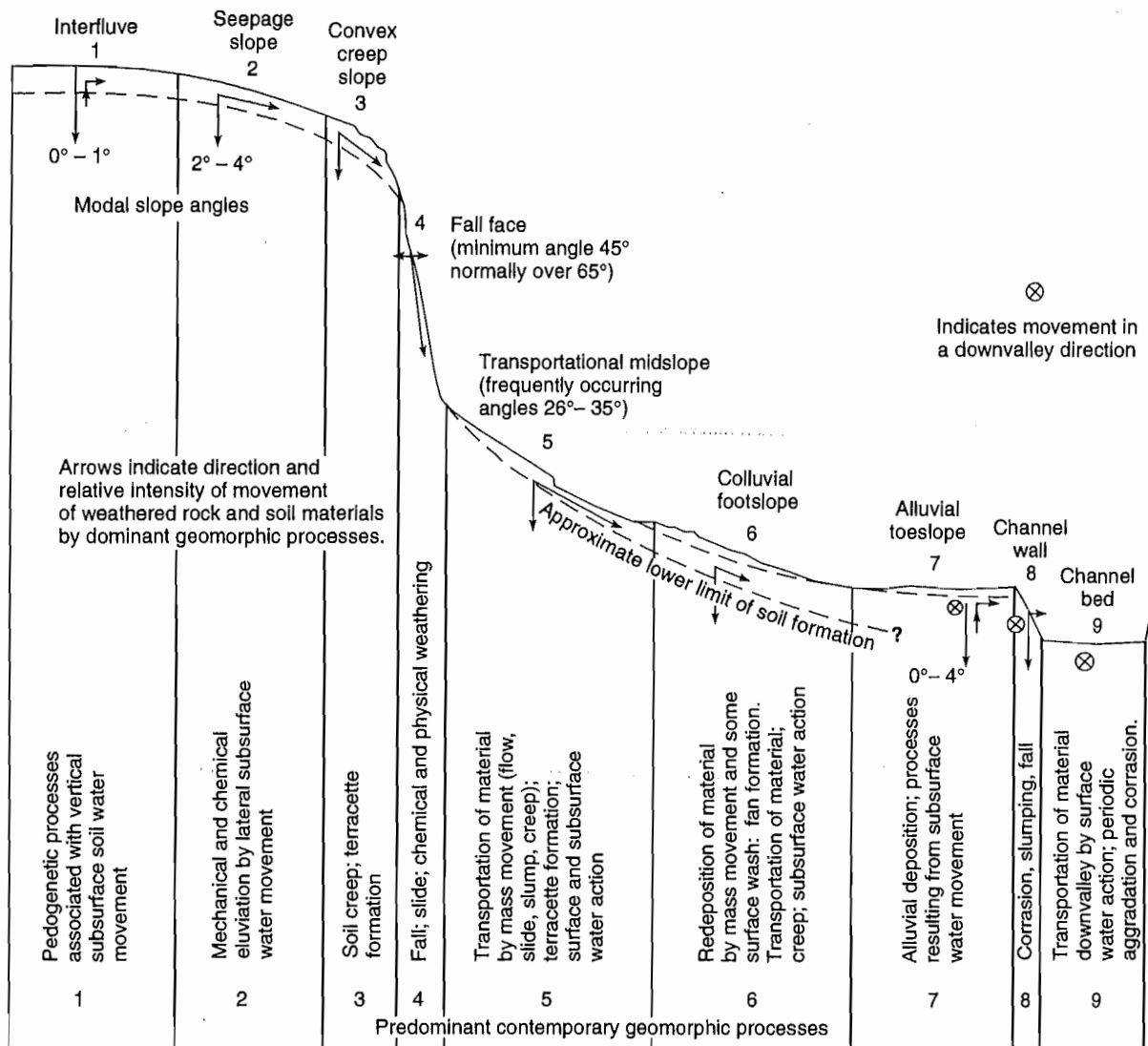
^aHorizons can be divided into subhorizons by adding Arabic numbers.

the material in the surface zones. Therefore, if no changes occur downward into the profile, prefix numbers are not needed.

The master horizons are designated by the capital letters O, A, E, B, C, and R (table 3.5). Horizons at the ground surface are called either O or A depending on the nature and amount of organic constituents they contain. The O horizon is dominated by undecomposed or partially decomposed materials, such as leaves, needles, lichens, or fungi. Mineral fragments represent only a small fraction (generally less than 50 percent) of the horizon by weight. In contrast, the A horizon is dominated by mineral grains and is normally considered to be the thin, dark-colored surface layer where decomposed organic matter is concentrated and where clays and mobile components are continuously leached downward, or *eluviated*. The E horizon underlies the O or A horizon. It is characterized by intense leaching that removes Fe⁺³ or organic coatings from the mineral grains, a process that usually imparts a bleached gray color to the horizon. The C and R horizons exist at the base of the profile. The C horizon is usually thought of as the underlying, unconsolidated parent materials that have been unmodified, or only very slightly modified, by soil-forming processes. The R horizon is simply consolidated bedrock beneath the soil.

112

101

**Figure 4.53**

Diagrammatic representation of the hypothetical nine-unit landsurface model.

(Redrawn from J. B. Dalrymple, et al., "A Hypothetical Nine-Unit Landsurface Model," *Zeitschrift für Geomorphologie* 12:60-76, 1968. Used by permission of Gebrüder Borntraeger Verlagsbuchhandlung, Stuttgart.)

mountainous terrain where erosion is rapid, and are normally characterized by thin, weakly developed rocky soils. The rate of physical weathering tends to be at a maximum when the thickness of the residuum (the soil and colluvium) is minimal (fig. 4.54). Chemical weathering, which proceeds most efficiently under a significant cover of residuum, will be slowed, however, when the residuum becomes so thick that it interrupts the movement of water to the bedrock weathering front (an example of negative feedback). Numerous examples of weathering-limited slopes can be seen on slick-rock slopes developed in sandstones of the Colorado Plateau (Oberlander 1977; Howard and Kochel 1988). In contrast, **transport-limited slopes** are formed where the rate of weathering is more rapid than erosion. Slopes

produced under this regime normally develop on any unconsolidated parent material regardless of environment, but they are typically dominant in humid-temperate zones where vegetation cover is continuous. These profiles are less affected by parent rock and more dependent on the type and rate of slope processes.

Selby (1982) has made a cogent argument that weathering-limited slopes are directly dependent on the relative resistance of the underlying parent rocks. As evidence, he has demonstrated a high correlation between rock mass strength (see table 4.4) and the angle developed on various slope segments (fig. 4.55). A line drawn around the data points shown in figure 4.55 creates what Selby calls the *strength equilibrium envelope*, and the slopes represented by points within that envelope are

115

112

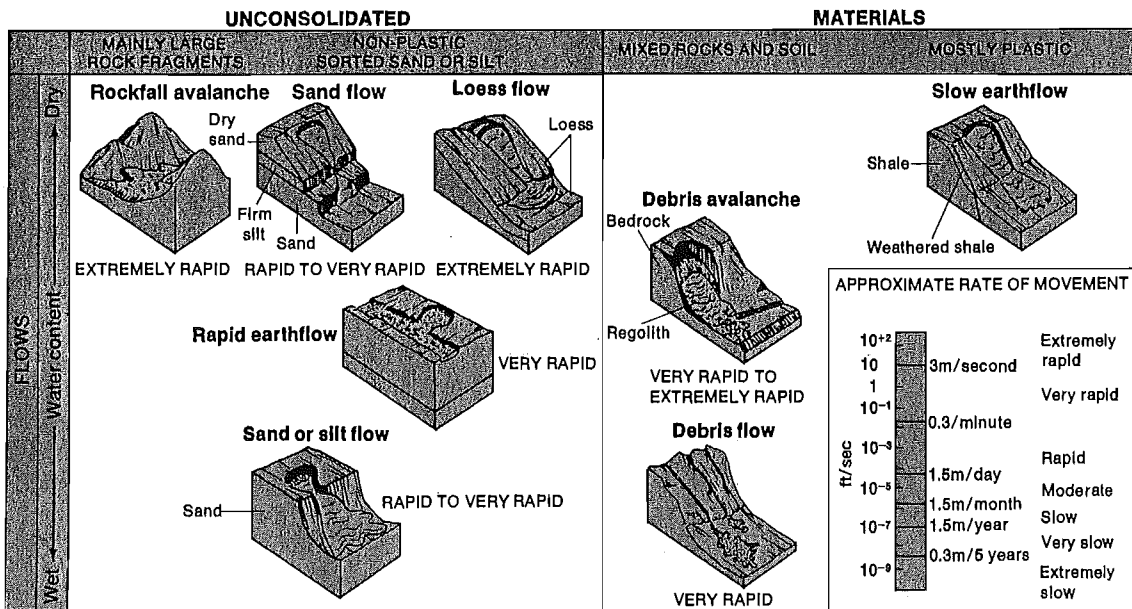
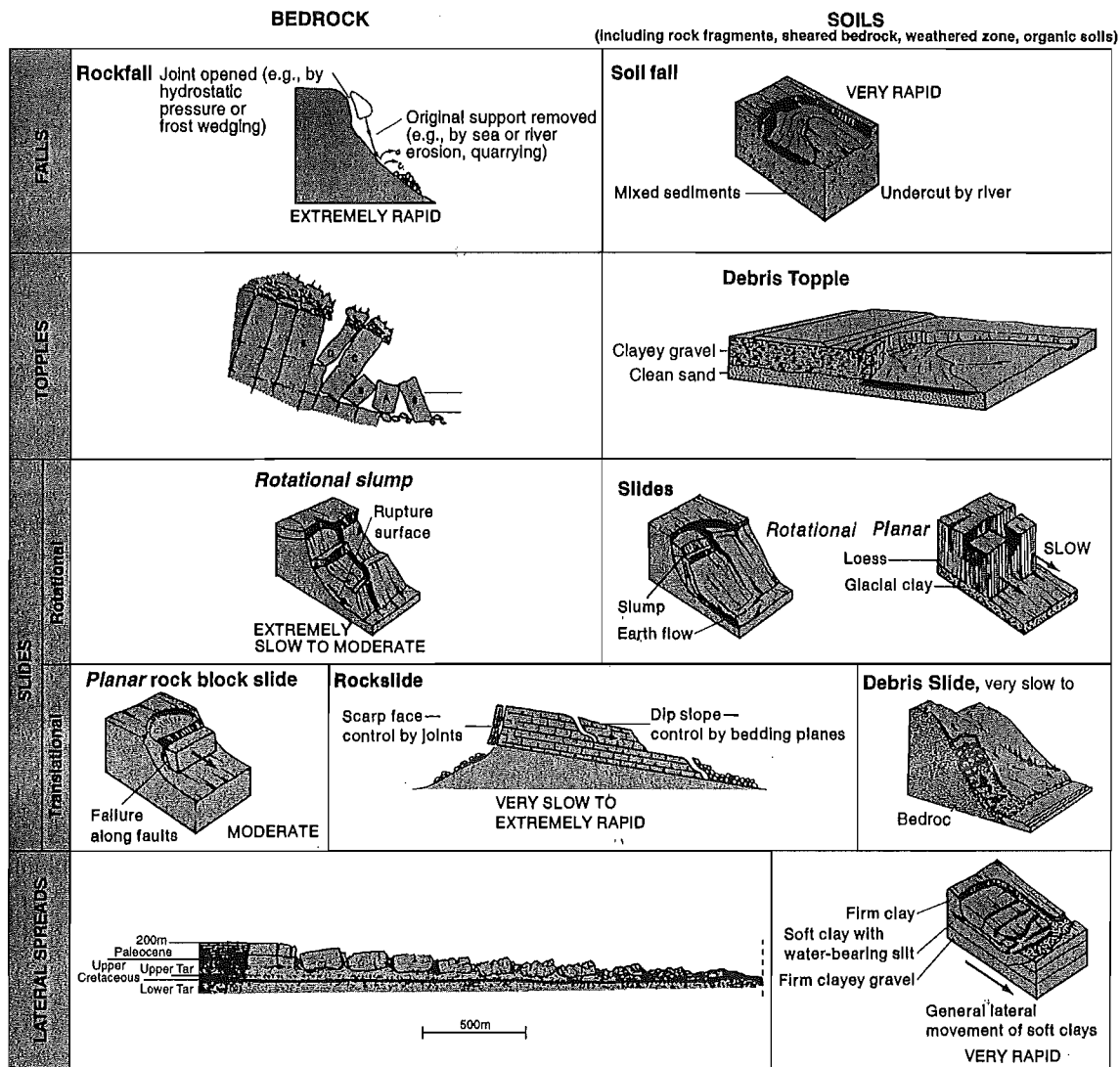


Figure 4.36

Classification of landslides.

(From D. J. Varnes, 1978, "Landslides: Analysis and Control," *TRB Special Report 176*, Transportation Research Board, National Research Council, Washington, D.C. Used by permission.)

SURFICIAL MAPPING methodology

A. Type I Criteria: Age, Origin, Landform, Material.

1. Age of Surficial Material

H = Holocene (< 10,000 years old)
W = Wisconsin (ca. 89 to 10 ka)
I = Illinoian
P = Pleistocene Undifferentiated
EP = Early Pleistocene
MPI = Middle Pleistocene
LP = Late Pleistocene
Q = Quaternary Undifferentiated
CZ = Cenozoic Undifferentiated

2. Origin / Surficial Process

A. Hillslope
r = residuum (in situ regolith)
c = colluvium (mass wasting)
ds = debris slide
rf = rock fall or topple
B. Valley Bottom
a = stream alluvium (normal flow)
hcf = hyperconcentrated flow
df = debris flow
sw = slackwater deposition
C. Lacustrine
l = lacustrine deposit, undiff.
lb = lake-bottom deposit
ld = lacustrine deltaic
D. Other
g = glaciofluvial, undifferentiated
go = glacial outwash
e = eolian
co = collapse (solution)
cr = cryoturbation
x = anthropogenic disturbance
f = artificial fill
rk = bedrock (process n/a)

3. Landform Units

A. Hillslope
n = nose
sl = side slope
h = hollow
vener = < 2m of regolith
blanket = > 2 m of regolith
bf = boulder field
bs = boulder stream
pg = patterned ground
tis = talus deposits

Table 5-2. Surficial Map Criteria for the Central Appalachians (after Kite, 1994).

3. Landform Units (Cont.)

B. Valley Bottom
ch = channel
fp = floodplain (RI < 2-3 yr)
t = terrace (t₁, t₂ ... t_n; height AMRL)
f = fan
f-t = fan terrace (t₁, t₂ ... t_n; height AMRL)
a = apron (footslope deposit)
lo = lobe
lv = levee
ox = oxbow, abandoned channel
C. Other
ft = flow track (debris flows)
hm = hummocky topography
rb = rock-block slide deposits
x = excavated, fill, disturbed ground
d = delta
du = dune

4. Material (Composition and Texture)

b = boulders (>256 mm; clast supported)
c = cobbles (64-256 mm; clast supported)
p = pebbles (4-64 mm; clast supported)
g = gravel (>2 mm; clast supported)
sg = mixed sand and gravel
s = sand (0.05-2.0 mm)
st = silt (0.002-0.05 mm)
cy = clay (<0.002 mm)
l = loam (mix of sand, silt, clay)
d = diamiction undifferentiated
bbd = very bouldery diamiction
bd = bouldery diamiction
cd = cobbly diamiction
pd = pebbly diamiction
ds = sandy matrix diamiction
dt = silty matrix diamiction
dy = clayey-matrix diamiction
rk = bedrock (modify with lithology)
rs = rotten stone, saprolite
tr = travertine
tu = tufa
ma = marl
og = organic-rich sediment
w = water
u = unknown

B. Type II Criteria: 2-D Surface Features

1. Karst

bv = blind valley
ca = cave (human entry)
Active cave passage
Abandoned cave passage
dv = dry valley
kw = karst window
sk = sinkhole (doline)
skst = sinking stream
ks = karst spring
2. Hillslope

hs = headscar
ds = debris-slide scar
ls = landslide scar undifferentiated
rs = rotational slide (slump) scar
ts = translational slide scar
rb = rock-block slide scar
tc = terracettes

3. Other

wf = water fall
w = water, lake, reservoir
Spring
wt = wetland, undifferentiated
wh = wetland, heath
wm = wetland, marsh
ws = swamp
quarry (with highwall)
gravel pit
deep mine opening
strip mine (with highwall)
mine subsidence zone
rc = rock city
Scarp
Meander scroll on floodplain
Lacustrine strandline

C. Type III Criteria: - Data Reference Points

Sandwich symbols showing stratigraphy
Depth to bedrock (drilling or seismic data)
Minimum depth to bedrock (log data)
Test hole / boring
Well
RE = refusal (in test boring)
Hand-auger hole, shovel hole,
Fossil locality
Paleocurrent direction
Observation Point

Hillslope Units after Hack and Goodlett (1960)

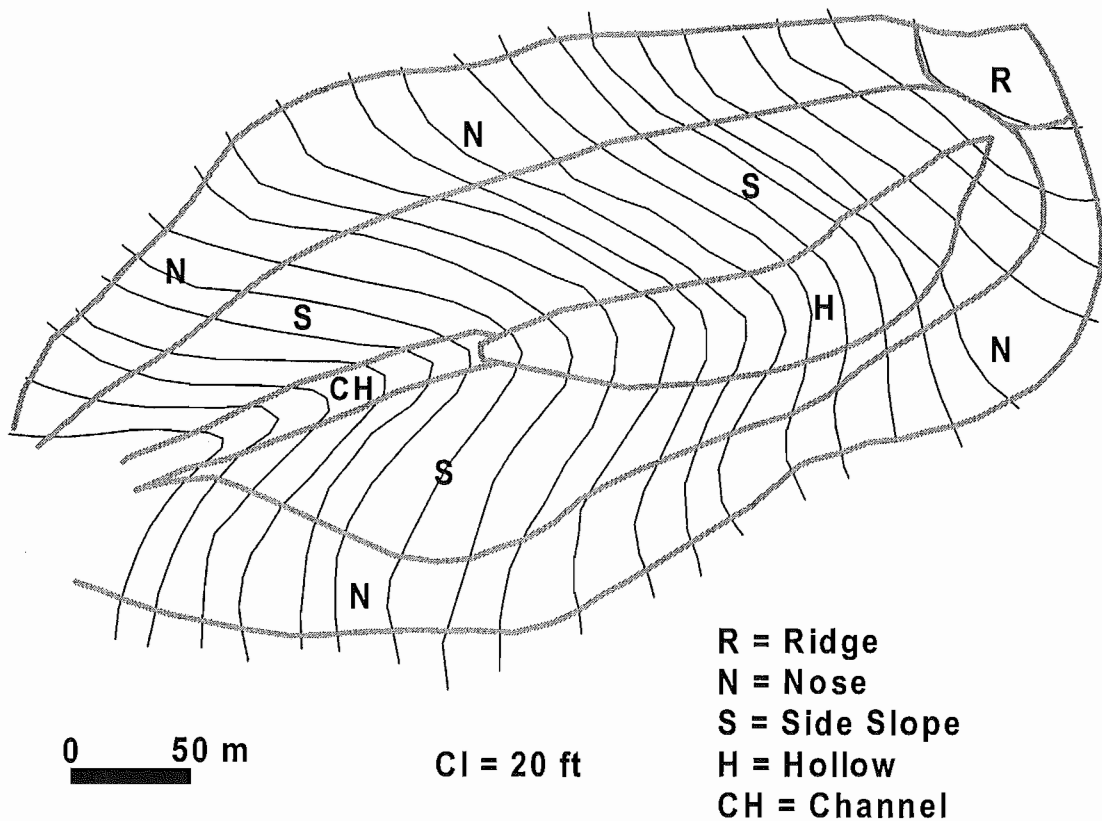
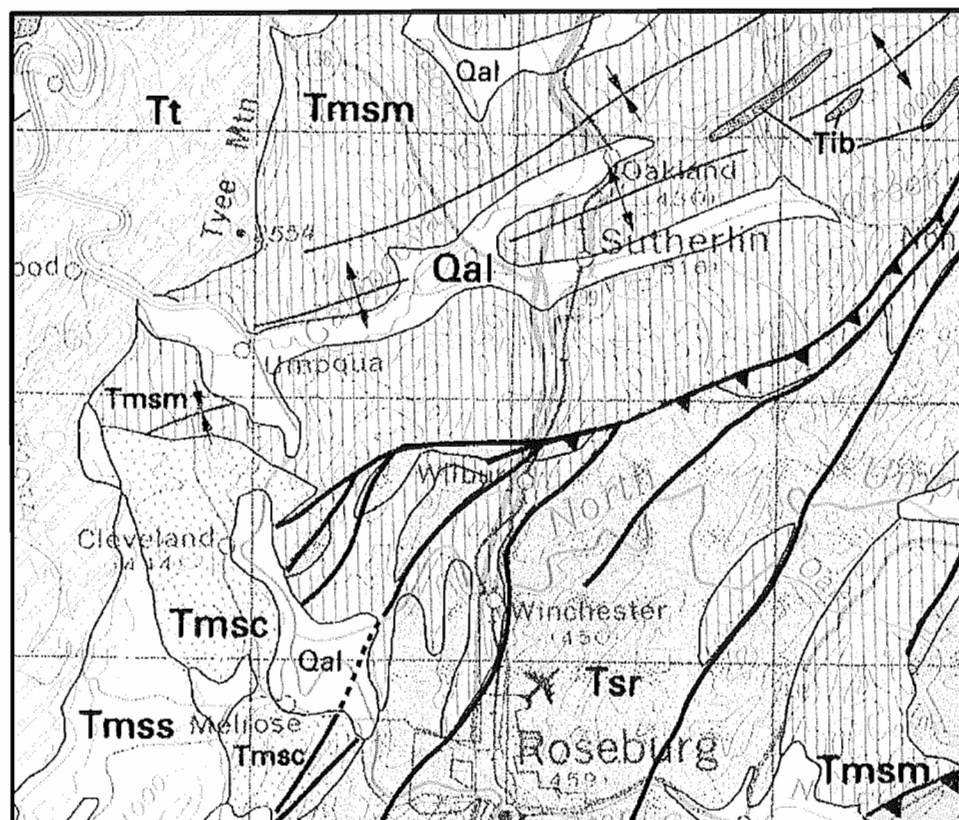
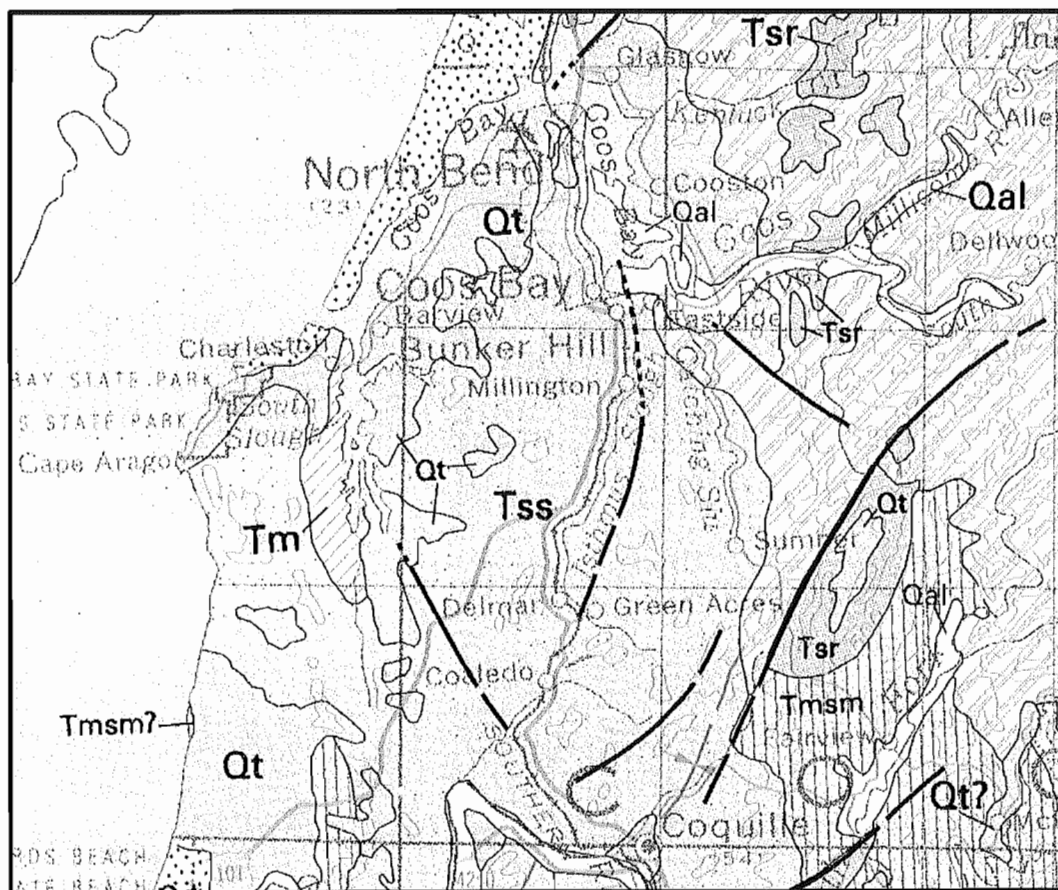
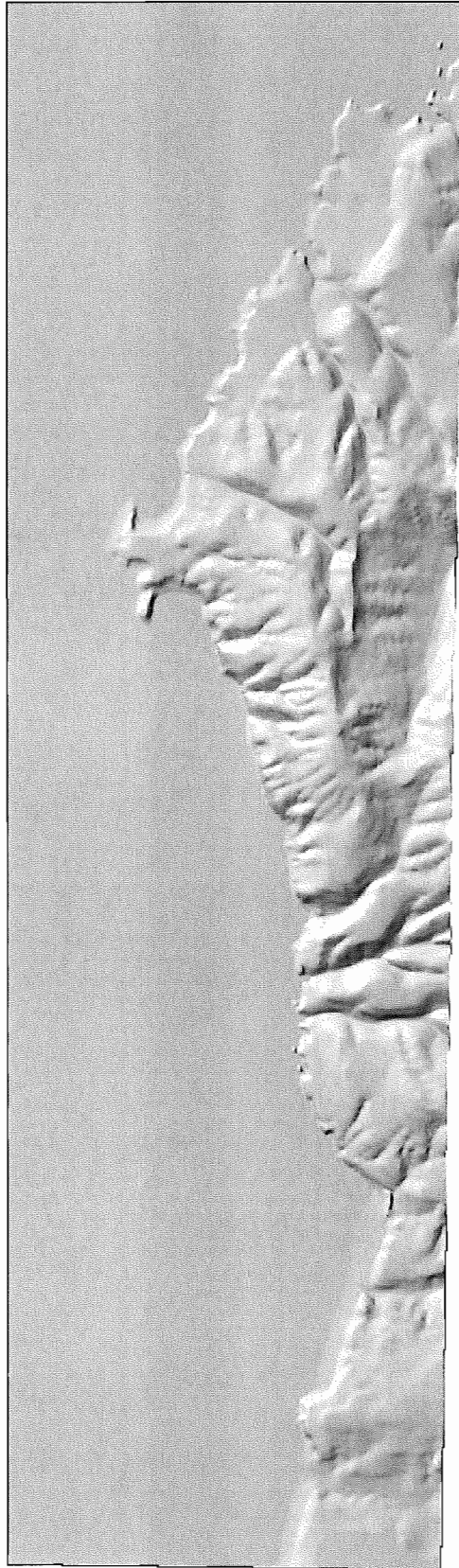


Figure 5-1. Hillslope landform elements after Hack and Goodlett (1960). Net transport flow paths are divergent on nose, convergent in hollows, and parallel on side slopes (Reneau and others, 1989). Noses represent drainage divides between zero- to first-order tributaries. Ridge crests serve as drainage divides between higher-order watersheds.

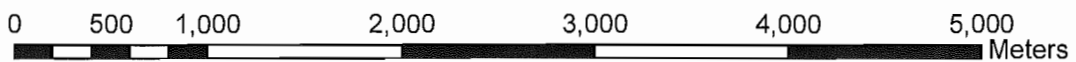
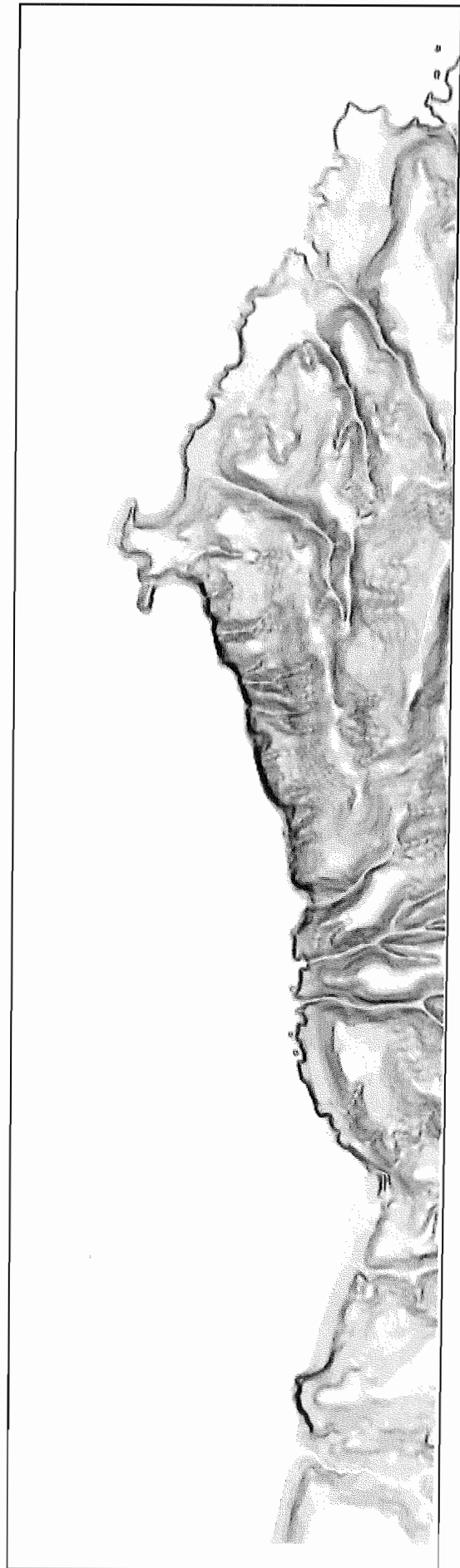
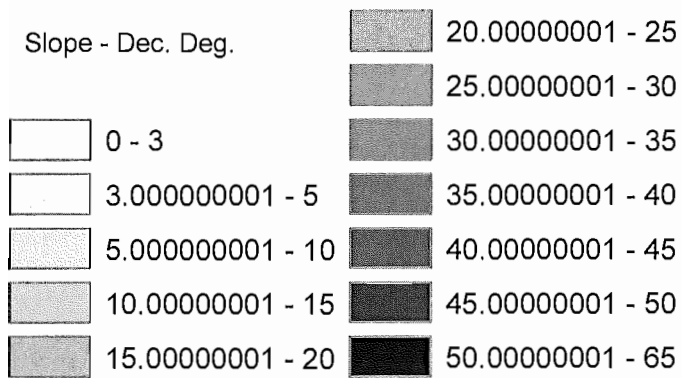
Geologic Maps of the Sunset Bay-Garden Valley Field Stops (from Walker and McLeod State Map)



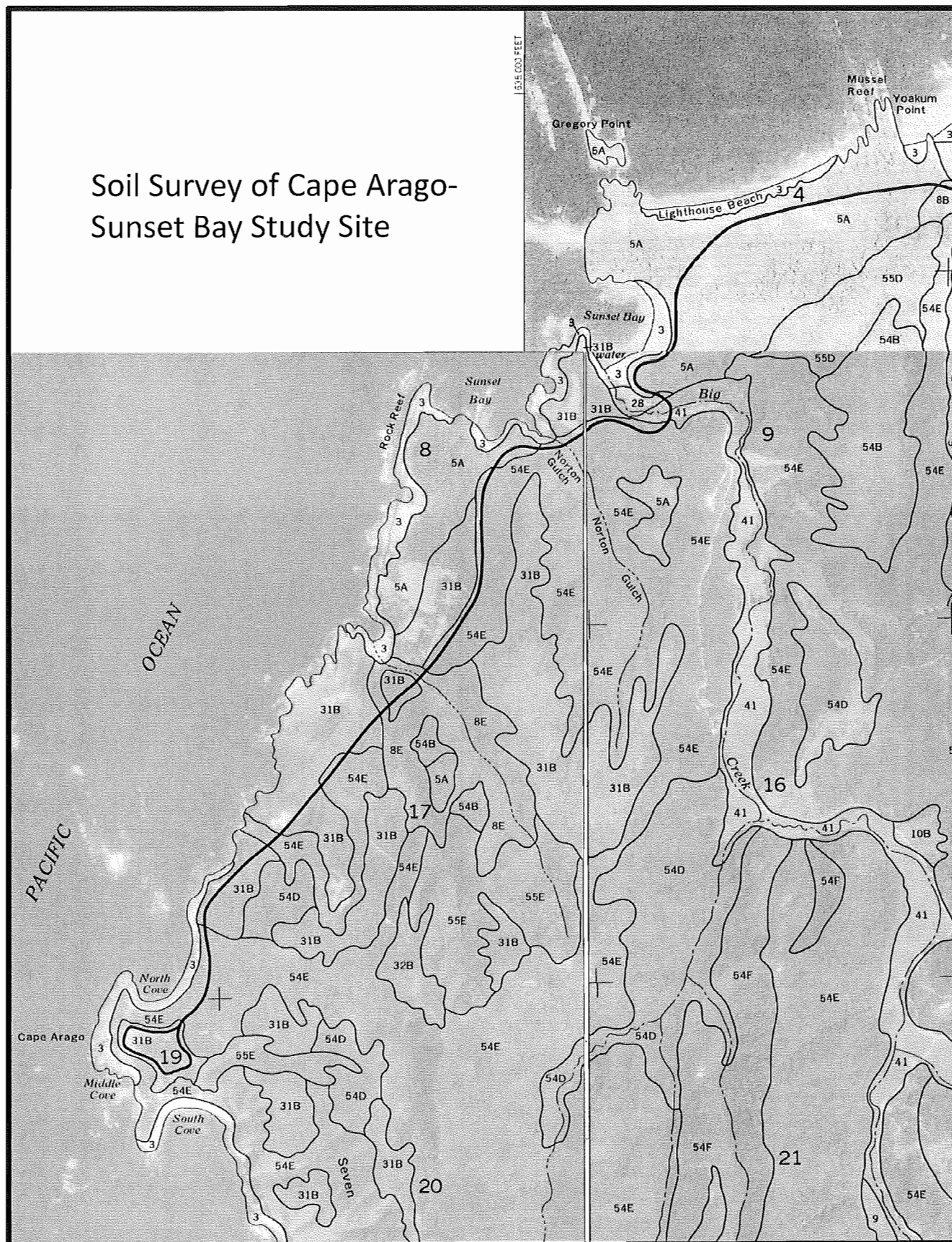
10-M Hillshade Model of Cape Arago-Sunset Bay



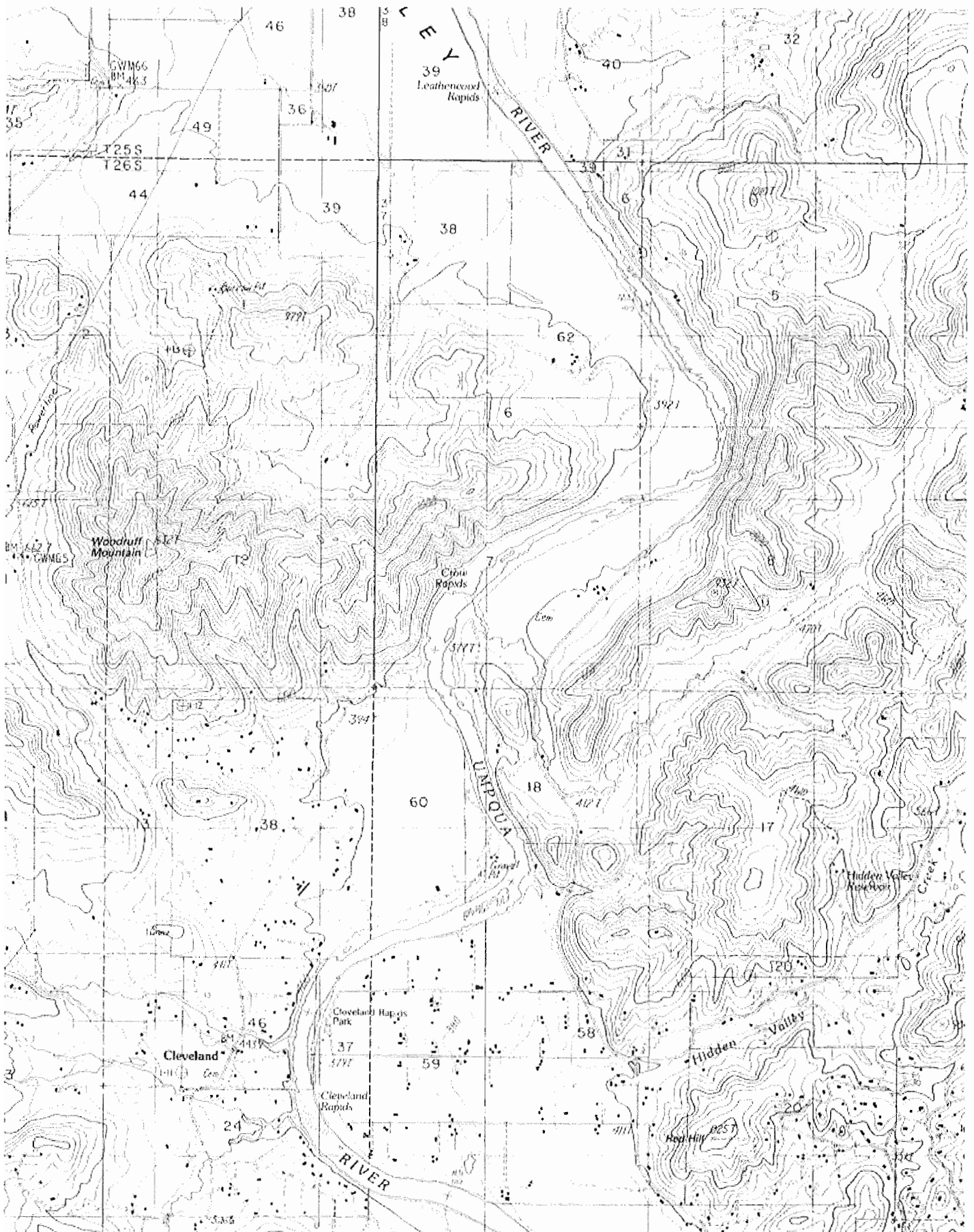
Cape Arago-Sunset Bay Slope Map



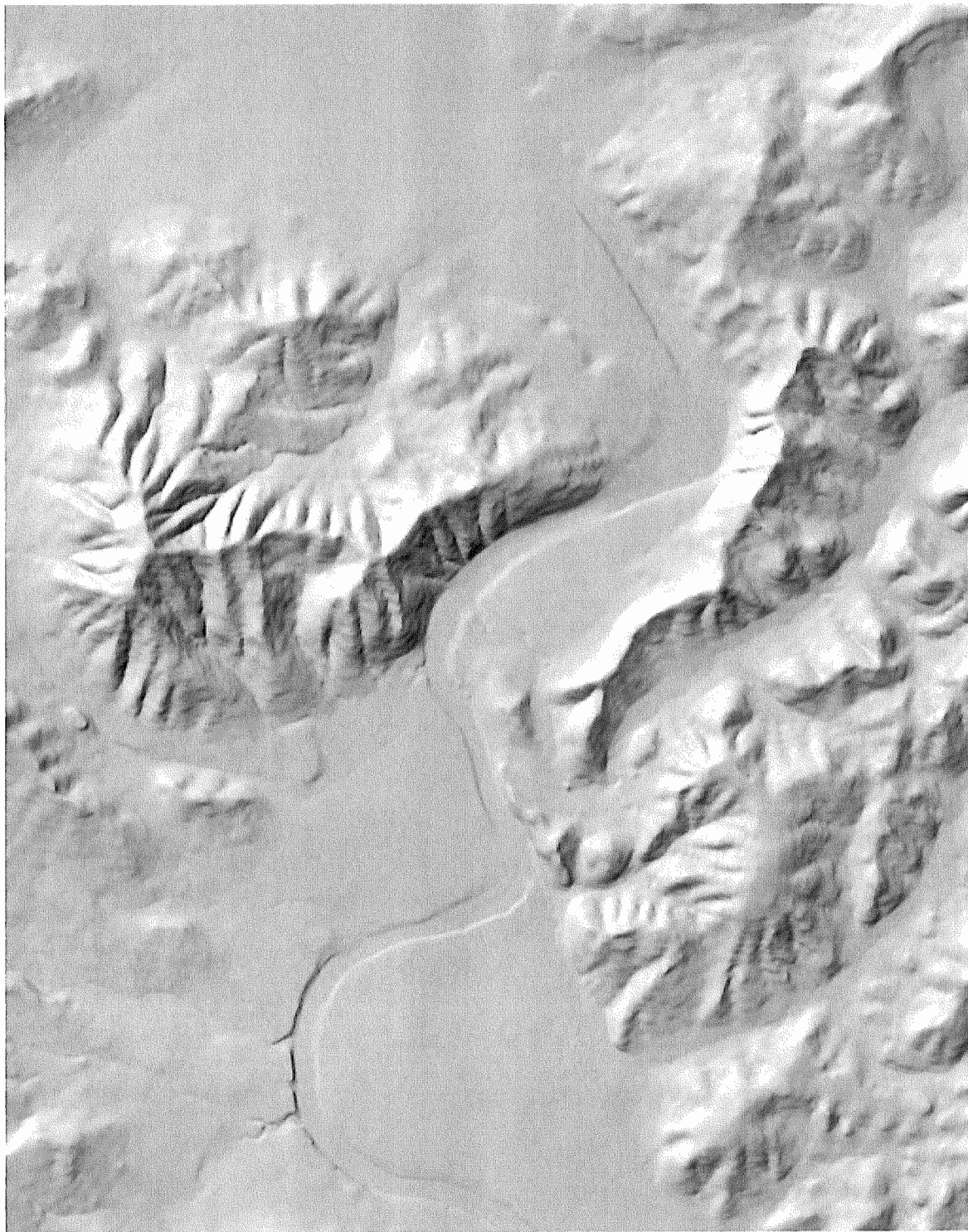
Soil Survey of Cape Arago-Sunset Bay Study Site



Garden Valley Road-Cut DRG



Hillshade Model of Garden Valley Outcrop



Slope Model of Garden Valley Outcrop



0 500 1,000 2,000 3,000 4,000 5,000 Meters

Slope dec. deg.

	10.00000001 - 15	35.00000001 - 40
	15.00000001 - 20	40.00000001 - 45
0 - 3	20.00000001 - 25	45.00000001 - 50
3.000000001 - 5	25.00000001 - 30	50.00000001 - 55
5.000000001 - 10	30.00000001 - 35	

SUNSET BAY GEOMORPHIC MAPPING PROJECT

Dr. Taylor – ES322 Geomorphology

INTRODUCTION

Geologic mapping has a long tradition in the United States, dating to the western expeditions of Powell in the late 1800's (Powell, 1882; 1888). The National Geologic Mapping Act of 1992 recognized the importance of geologic mapping as a tool for resource evaluation, environmental protection, and natural hazards assessment. As a cartographic subset, surficial maps provide representation of the critical links between bedrock geology, climate, tectonics, vegetation, and surficial processes.

The purpose of this field-based exercise is to gain an understanding of mapping concepts as they are applied to the surficial deposits and landforms manifested at the Earth's surface. This exercise focuses on landforms and processes in the vicinity of Sunset Bay, Coos County, Oregon.

SURFICIAL MAPPING APPROACH

Surficial mapping will employ a four-fold scheme in which units are delineated on the basis of age, origin (process), landform, and material (texture). The technique emphasizes the link between landforms, materials, and processes in a landscape dominated by tectonic uplift, hillslopes, mass wasting, and fluvial/coastal erosion.

Large-scale landform units are classified into hillslope and valley-bottom features. Hillslope landforms are subdivided into ridges and side slopes. Valley-bottoms are subdivided into channels, floodplains, terraces, and fans. Hillslope deposits include residuum and colluvial diamicton. Fluvial deposits are typically clast supported, moderately sorted, and imbricated due to deposition by turbulent streamflow. Debris flows result in poorly-sorted diamictons with crude internal stratification. Dating of surficial deposits is problematic, hence traditional stratigraphy-based techniques are largely not applicable. The four-fold mapping protocol circumvents the need for formal stratigraphic nomenclature.

SOIL SURVEYS AS A REFERENCE FOR LANDSCAPE ANALYSIS

Soils represent the weathered mantle of unconsolidated surficial material that covers land surfaces. They are comprised of a mixture of mineral and organic matter derived from the physical, chemical, and biologic weathering of bedrock. The Natural Resource Conservation Service (NRCS) is the federal agency that is primarily responsible for the analysis and preservation of this valuable resource. As a result, county soil surveys and soil maps have been prepared for most regions of the U.S. These surveys provide an important data set for geomorphic analysis of landforms and surficial materials.

The main controlling factors that contribute to soil formation are: 1) climate, 2) organic activity (animals / plants), 3) relief / topography, 4) parent material, and 5) time (CLORPT). Climate refers to amount of rainfall and temperature. Organic activity refers to style of plant growth, microbial activity, and burrowing organisms. Relief / topography refers to the steepness of slope. Parent material refers to the source of weathered material upon which the soils are formed (e.g. bedrock = igneous, sedimentary, metamorphic; surficial regolith = colluvium). Time refers to the residence time of the soil material, essentially the length of time that the soil has been forming without physical interruption. All of these factors contribute to soil characteristics.

Soil surveys are conducted by using topographic maps, air photos, ground surveys, soils excavations, and geologic maps. Soil map units are delineated primarily on the basis of material composition (i.e. texture of the soil) and topographic configuration (steepness of slope, flood-prone

areas, etc.). Other parameters include color and soil chemistry. Soil maps are typically published on air photos and created for individual counties and conservation districts. A brief comparison of soils and topographic maps suggests that soils are not randomly distributed, but are intimately related to topography and geomorphic setting. Landforms and geomorphic processes often influence the physical and chemical properties of soils. Hence, if we know the soil and its characteristics we may be able to begin to understand the geomorphic system.

PROCEDURES AND TASKS

Part 1. Geomorphic Mapping

- (1) Drive to Sunset Bay, Coos County, Oregon... or take a class field trip as the case may be.
- (2) We will spend the afternoon at Sunset Bay. The following resources are available to support your observations: (a) topographic map of Cape Arago-Sunset Bay area, (2) 10-m hillshade model, (3) slope model, and (4) relevant excerpts from the NRCS Coos County Soil Survey.
- (3) The first step is to orient yourself to the area, examine all available maps and directly observe the landscape around you, answer the following questions:
 - a. List and describe the upland (ridge, hillslopes) and lowland (valley bottoms, beaches) landforms that you observe.
 - b. List and describe the dominant erosional processes evident in the area. Think of all the agents of erosion, and how they are working at this site.
 - c. List and describe the range of surficial deposits ("regolith") that occur in this area. In your description include texture (grain size) and sorting of surficial material). Make observations of material color as well.
- (4) Examine the topographic and slope maps. Using the topographic map as a base, use colored pencils to shade landform elements based on slope. Use the following color code and slope classes:

a. 0 to 10 degrees	Yellow
b. 10 to 20 degrees	Green
c. 20 to 30 degrees	Blue
d. > 30 degrees	Red

(USE topo map on p. 124)
- (5) Once you've color-shaded your map, use a heavy pencil or pen to draw "contacts" or black line land-unit boundaries between your shaded areas.
- (6) Compare your color-coded topographic slope map to the Coos County soil survey for the area. Fill in the following table combining observations from these two data sources:

A. Yellow Land-Unit Zone (0-10 degrees)

Soil Unit Code (number + name)	Landforms	Materials (texture, sorting)	Processes (transport agent)	Age
_____	_____	_____	_____	_____
_____	_____	_____	_____	_____
_____	_____	_____	_____	_____
_____	_____	_____	_____	_____
_____	_____	_____	_____	_____

B. Green Land-Unit Zone (10-20 degrees)

Soil Unit Code (number + name)	Landforms	Materials (texture, sorting)	Processes (transport agent)	Age
_____	_____	_____	_____	_____
_____	_____	_____	_____	_____
_____	_____	_____	_____	_____
_____	_____	_____	_____	_____
_____	_____	_____	_____	_____

C. Blue Land-Unit Zone (20-30 degrees)

Soil Unit Code (number + name)	Landforms	Materials (texture, sorting)	Processes (transport agent)	Age
_____	_____	_____	_____	_____
_____	_____	_____	_____	_____
_____	_____	_____	_____	_____
_____	_____	_____	_____	_____
_____	_____	_____	_____	_____

D. Red Land-Unit Zone (>30 degrees)

Soil Unit Code (number + name)	Landforms	Materials (texture, sorting)	Processes (transport agent)	Age
_____	_____	_____	_____	_____
_____	_____	_____	_____	_____
_____	_____	_____	_____	_____
_____	_____	_____	_____	_____
_____	_____	_____	_____	_____

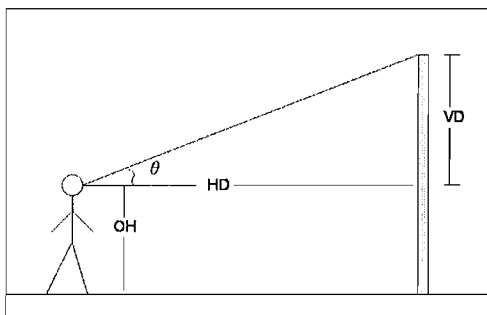
(7) Complete your draft geomorphic map by combining slope observations with soil-landform-material observations. Using a marker or dark pencil, refine your color-shaded areas to include subdivisions based on the soils-landform-process observations. Subdivide color zones with heavy dashed-lines, and label your geomorphic units within each color zone with one of the following designations:

- Qr – residuum, Quaternary in age, undifferentiated (ridge tops, in-place regolith)
- Qc - colluvium, Quaternary in age, undifferentiated (hillslopes and footslopes)
- Qal - alluvium, Quaternary in age, undifferentiated (river deposits, valleys, channels, floodplains)
- Qt – marine terrace, Quaternary in age, undifferentiated (abandoned, elevated beach zones)
- Hb – beach zone, Holocene in age (present day beach zones)
- Qd – dune deposits, Quaternary in age, undifferentiated (wind-blown, sand dunes)

Part 2 - Landform and Soil Sampling Exercise – North End of Sunset Bay

A. At the north end of Sunset Bay, there is an elevated upland bench that bounds the beach. Examine the area on the topographic map, on your geomorphic map, and on the slope-hillshade-soils maps. Working in teams, conduct the following tasks.

B. At the beach level, using a Brunton compass-pace-tape, and trigonometric techniques, determine the approximate height of the upland bench above active beach level **in meters and feet**. Refer to the figure below for a guide on how to complete this calculation.



OH = ocular height, VD = vertical distance from eyes to top of object, HD = horizontal distance from eyes to object, θ = angle of inclination between eyes and top of object:

	$\tan \theta = VD / HD$	Total Height of Object = OH + VD
Ocular Height _____		
HD _____		
θ _____		Total Height (ft) _____
VD _____		Total Height (m) _____

C. Hike up to the top of the bench, at the north end of Sunset Bay. Using the soil auger, collect a series of samples at about 20 to 25 cm increments, to a total depth of approximately 150 centimeters. See how far you can drive the auger into the regolith materials. Carefully empty the bucket auger samples out on the ground in organized, linear fashion, from top to bottom for observation. Keep track of the depth increments of each extraction using a meter stick and the sample rod.

Once we make field observations, we will ziplock-bag and label the samples for transport back to the Geology Lab. Depending on time, in the field, or follow-up in the lab, use your soil observation skills / tools to describe the soil samples for each increment. Refer to the soil-observation reference materials provided in the field guide. Fill in the table below.

Depth Interval (cm)	Color (moist)	Consistency (moist)	Texture	Other Observations
_____	_____	_____	_____	_____
_____	_____	_____	_____	_____
_____	_____	_____	_____	_____
_____	_____	_____	_____	_____
_____	_____	_____	_____	_____
_____	_____	_____	_____	_____
_____	_____	_____	_____	_____
_____	_____	_____	_____	_____
_____	_____	_____	_____	_____
_____	_____	_____	_____	_____
_____	_____	_____	_____	_____

D. Soil Interpretation

Question 1: Table 2 below is a summary of soils data collected for marine surfaces throughout the southern Oregon region. By comparing your soils observations to Table 2, what is your best approximation of soil development stage for the Sunset Bay surface soil?

TABLE 2. DEVELOPMENT STAGES OF SOILS ON ELEVATED MARINE TERRACES ALONG THE CENTRAL AND SOUTHERN OREGON COAST

Development stage	Depth to Cox (m)	B horizon hue	Bt thickness (cm)	Maximum B horizon texture* (% clay) [†]	Maximum clay films [‡]
1	0.8-1.4	7.5-10YR	0	sil, l, sl (<30)	1-3npfpo
2	1.0-1.4	7.5YR	<50	sicl, cl, scl (30-40)	2-3n-mkpfpo
3	1.0-1.7	7.5YR	<50	sicl, cl, scl (30-40)	2-3mkpfpo
4	1.4-1.8	5-7.5YR	50-100	sicl, sic, cl, c (35-42)	3-4mkpfpo
5	1.9-2.8	5-7.5YR	100-200	sic, c (40-58)	3-4mk-kpfpo
6	2.6-4.5	5YR	>200	sic, c (40-65)	3-4mk-kpfpo
7	3.2->4.5	2.5YR	>200	sic, c (45-65)	3-4mk-kpfpo

*l, loam; sl, sandy loam; sil, silt loam; sicl, silty clay loam; sic, silty clay; cl, clay loam; scl, sandy clay loam; c, clay. Abbreviations follow Soil Survey Staff (1951).

[†]Notations for clay films; number denotes extent of ped faces covered by film; v1, <5%; 1, 5%-25%; 2, 25%-50%; 3, 50%-90%; >90%; n, thin; mk, moderately thick; k, thick; pf, film on ped face; po, film lines the pores. Abbreviations follow Soil Survey Staff (1951).

[‡]We estimated percent clay for each horizon at each soil locality during field work. We have confidence in our ability to estimate clay content in the field because we obtained a significant correlation ($r^2 = 0.66$; $p \leq 0.01$) between percent clay estimated in the field and percent clay measured in the laboratory (28 samples).

Question 2: Based on your geomorphic mapping, soil sampling, and review of the Coos County Soil Survey, what is the type of landform that you sampled at the north end of Sunset Bay?

Question 3: Explain how this surface formed? How old is this surface, i.e. the time since it was eroded and formed at sea level?

Question 4: Using your surface height calculation in 8 B above and age estimate, calculate rate of surface elevation change in mm/yr. Calculate again in meters / thousand years. Show all of your work. (NOTE: 17m is the whiskey run surface at 80,000 yrs old)

Question 5: Is the Oregon coast at Sunset Bay uplifting or subsiding over time? What forces may be driving this phenomena?

Question 6: How does the Quaternary tectonic setting of the Oregon Coast relate to that manifested in the Tertiary bedrock outcrops and structured exposed on the beach at Sunset Bay? Are similar processes operating today as they did in the Eocene or Oligocene? What is your evidence one way or another?

G322 Lab Exercise
Neotectonic and Coastal Processes of Oregon

Part I. Pre-Lab Questions

Use your notes, textbook, wall maps, and reading assignments to answer the following questions.

A. Match the Following Coastal Locations with the terms on the Right. List all that apply.

_____	1. Oregon Coast	Passive Margin Tectonics (inactive)
_____	2. Washington Coast	Active Margin Tectonics - subduction
_____	3. Southern California Coast	Active Margin Tectonics - transform
_____	4. Northern California Coast	Active Margin Tectonics - rifting / spreading
_____	5. Aleutian Islands of Alaska	Emergent Coastline
_____	6. Southeast Alaskan Coast	Submergent Coastline
_____	7. Gulf of Mexico - Texas	Active Subsidence
_____	8. Central Atlantic / U.S.	Active Uplift

B. Thinking Questions

9. The last major glaciation (i.e. a pervasive cold-wet climate regime) in the northern hemisphere was at it's peak 18,000 to 20,000 years ago. 100's to 1000' of feet of Ice covered much of Canada and the northern tier of the U.S.

A. From what major hydrologic source does the precipitation that forms glacial ice originate?

B. Describe how this moisture is cycled into glacial ice (what are the processes associated with this part of the hydrologic cycle).

C. What happens to global sea level during a major glacial climate? What happens to global sea level during a major interglacial (i.e. warm / melting) climate?

D. What happens to land surface elevation at convergent tectonic boundaries (i.e. subduction zones), especially where accretionary tectonics is prevalent?

E. What happens to land surface elevation at passive tectonic boundaries, where sediment accumulates over time (think about what happens to water saturated sediment as it accumulates, becoming thicker over time, under increasing weight).

10. If global sea level is rising at a rate of 2 mm/yr, at a passive continental margin, how long will it take for sea level to rise 5 m? Show your math work.

11. If global sea level is rising at a rate of 5 mm/yr, and an active tectonic coastline is experiencing uplift at a rate of 5 mm/yr, what will be the net relative rate of sea level change at this location? Show your math work.
12. If global sea level is rising at a rate of 3 mm /yr, and a passive margin coastline is actively subsiding at a rate of 5 mm /yr, what will be the net relative rate of sea level change at this location? Show your math work. Is this coastline best characterized as "emergent" or "submergent"?
13. If global sea level is rising at a rate of 1 mm/yr and an active tectonic coastline is experiencing uplift at a rate of 5 mm/yr, what will be the net relative rate of sea level change at this location? Show your math work. Is this coastline best characterized as "emergent" or "submergent"?
14. List two dominant oceanic processes associated with the Oregon Coast.
15. List two dominant tectonic processes associated with the Oregon Coast.
16. List three geologic hazards that you can think of, associated with the Oregon Coast (think about the news reports that you hear every year).
17. In terms of temperature as related to the physics of volume expansion / contraction (think hot air balloon), which condition would have a greater volume, warm sea water or cold sea water?
18. In terms of density driven currents: warm sea water is _____ (more dense or less dense?) compared to cold sea water. Therefore, warm sea water will tend to _____ (rise or sink), and cold sea water will tend to _____ (rise or sink?).
19. Similarly, in terms of density-driven motion in rock material: hot, young oceanic crust is _____ (more dense or less dense?) compared to cold, old oceanic crust. Therefore, hot, young oceanic crust will tend to (rise or sink?), and cold, old oceanic crust will tend to _____ (rise or sink?).
20. Question for you: What would happen to global sea level under conditions of very rapid seafloor spreading? Why?

What would happen to global sea level under conditions of very slow seafloor spreading? Why?

Part 5. Neotectonics of the Oregon Coast

Western Oregon is the site of plate tectonic convergence, with subduction of the Juan de Fuca plate beneath the North American plate. This convergent zone is associated with accretionary tectonics, compressional strain, and Cascade arc volcanism. As such, neotectonic deformation, crustal motion, and differential uplift/subsidence of the Oregon coast must be reconciled with any geomorphic model of the region.

Historic crustal motion of the Earth is measured via re-leveling surveys of surface elevation (re-leveling = re-measurement of land surface elevation over time), or with satellite positioning systems (GPS = global positioning system). Longer term uplift of coastal areas is reconstructed by examination of wave-cut terraces and coast terrace deposits, with related application of geologic dating techniques.

Mitchell and others (1994) examined historic re-leveling data of surface elevations along a transect extending from northern California to Washington. They combined the re-leveling data with tide gauge measurements to determine net relative vertical ground motion velocities for coastal regions of the Pacific Northwest. Table 4 is a summary of historical ground motion velocity data for a south-to-north transect, arranged by latitude (degrees north); positive velocities = uplift, negative velocities = crustal subsidence.

Task 7 Using the data in Table 4, plot a south-to-north transect of historic ground motion velocity (y axis) vs. latitude (x axis). Use the blank profile paper provided in Figure 7 (alternatively, create the profile using the chart wizard in microsoft Excel). List the geographic names of the data localities above the profile, for reference.

Question 5-1. Identify regions of coastal PNW that are experiencing rapid historic uplift. Identify regions of coastal PNW that are experiencing no net uplift, or subsidence. Do you see any spatial patterns in terms of uplift / stability / subsidence along the south-to-north transect?

Question 5-2. Assuming that sea level is presently rising, what can you conclude about the rate of tectonic uplift, and rate of sea level rise for the Newport, OR area?

Question 5-3. Examine a tectonic map of the PNW (see the "fractured surface" map on the wall of the lab room). Identify the area of highest rates of tectonic uplift on your profile, and locate that area on the tectonic map. Comment on the relationship between the type of tectonic boundary(ies) and the highest rates of coastal uplift in the PNW.

Question 5-4. Which areas of the coastal transect would you expect to find the highest, and most well-developed flights of coastal terraces? Which areas would you expect to find the most well-developed coast-terrace soils? Why? Draw sketches to support your answer.

Task 8. Figure 8 is a map of interpolated uplift rates for select points in the Pacific Northwest (west of the Cascades). Draw contour lines on the map data connecting points of equal uplift rates. Use a contour interval = 1 mm/year. Using colored pencils, color code the neotectonic domains using the following classification scheme (i.e. color all regions of the map according to uplift rate):

uplift 0-1 mm /yr	blue
uplift 2-3 mm/yr	yellow
uplift 4-5 mm/yr	red

Question 5-5. Identify the zone of highest uplift. What type of tectonic process is occurring in this region.

Question 5-6. Locate Monmouth, OR on the map. What is our historic rate of uplift on campus? Which part of western Oregon is associated with the highest rates of uplift?

Question 5-7. What is the rate of uplift in the Puget Sound region? What other isostatic process(es) must be accounted for in the Puget Sound region, and to the north of that point.

Task 8. Table 5 is a listing of data collected from uplifted marine terraces in southern Oregon. The terraces are formed by wave-base erosion, at or below sea level. They are elevated along the Oregon coast through the process of relative uplift over time. The age of the terrace is derived by numerically dating preserved marine deposits. The original depth of the wave-cut platform is reconstructed from fossil organisms. Paleo-sea level (compared to modern sea level) is derived from the global marine sea level record.

Complete the data in Table 5 by using Microsoft Excel. Download the table from the class web site and use the spreadsheet math functions to determine parameters in columns e, f, and g (total tectonic uplift and average uplift rate). To help in resolving the parameters, draw a cross-sectional sketch of modern sea level, paleo-sea level, original depth of terrace, and present elevation. Calculate the total tectonic uplift that the terrace has experienced, combine that with the age data to determine the long-term average rate of uplift on the southern Oregon Coast.

Question 5-8. How do the long term average uplift rates in Table 5 compare with the historic uplift rates presented in Table 4, and Figures 7-8? Explain the differences or similarities that you observe.

Question 5-9. In looking at degree of soils development on the Whiskey Run, Cape Blanco, and Pioneer terraces; explain which terraces would have more well-developed soils, and which less. Describe the physical and chemical characteristics of the soils that you would expect to see when visiting all three of the localities.

Question 5-10. If you were asked to find these marine terraces on a map and in the field, what types of topographic and geologic evidence would you look for (how would you go about doing this from scratch)? Explain how county soils surveys would help in this process.

Table 3A. Reconstructed Global Sea Level Data for the Late Pleistocene (data reconstructed from coral assemblages in Tahiti, New Guindea, Barbados).

Calendar Age (kyr BP)	Reconstructed Relative Sea Level Compared to Modern (meters)
3.0	-0.07
5.8	-0.60
6.8	-4.19
7.3	-6.90
7.8	-11.43
8.2	-15.46
9.0	-22.71
9.5	-29.89
10.1	-39.79
10.5	-43.03
11.0	-48.90
11.5	-55.47
12.2	-61.60
12.8	-68.48
13.3	-74.56
13.9	-79.86
14.3	-93.12
14.6	-96.44
14.9	-98.87
16.8	-109.32
17.8	-112.38
18.4	-116.09
19.0	-118.24

Figure 5D. Reconstructed Global Sea Level Curve for the Late Pleistocene.

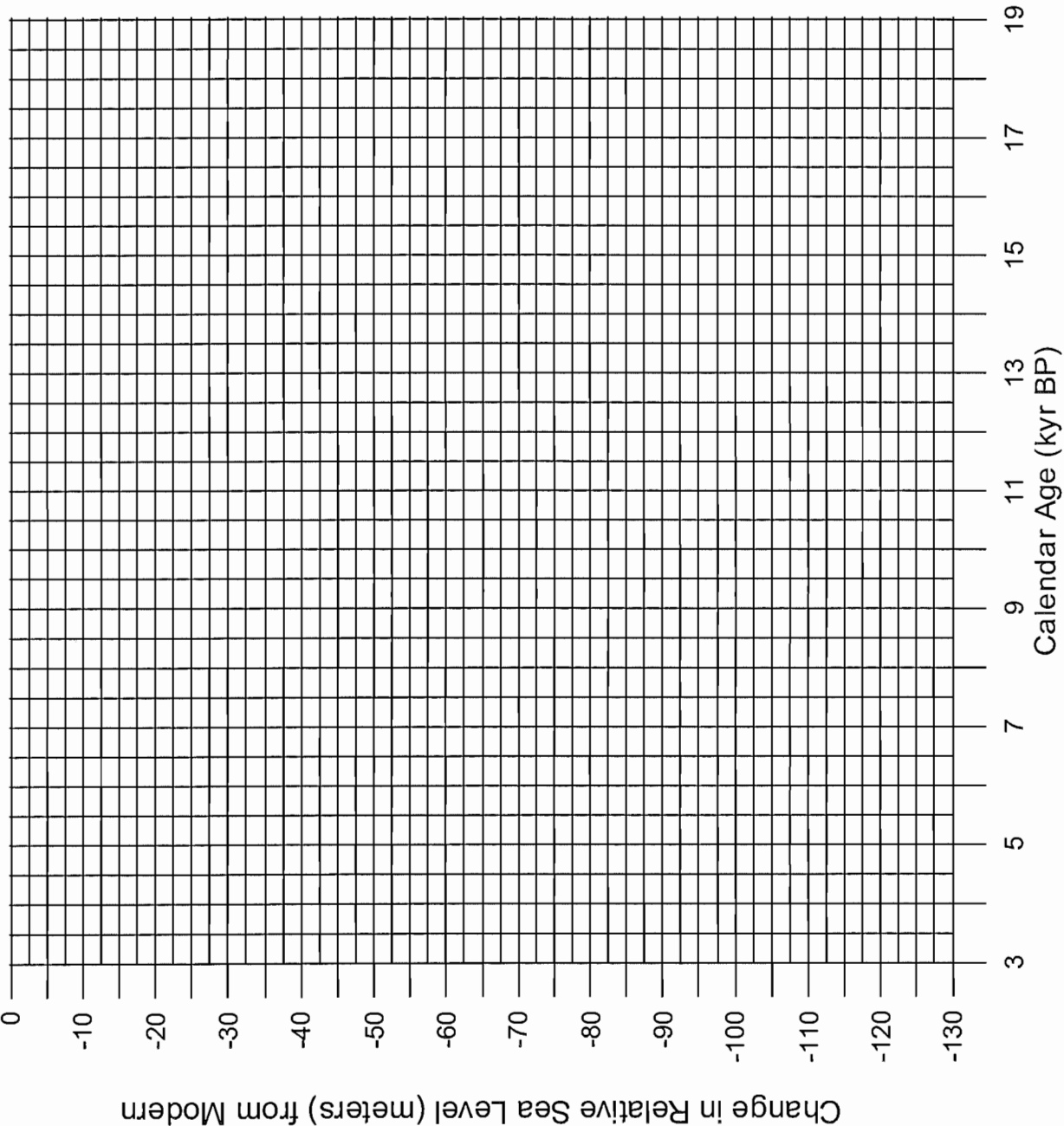


Figure 5E. Profile of the Continental Shelf, West of Newport Oregon.

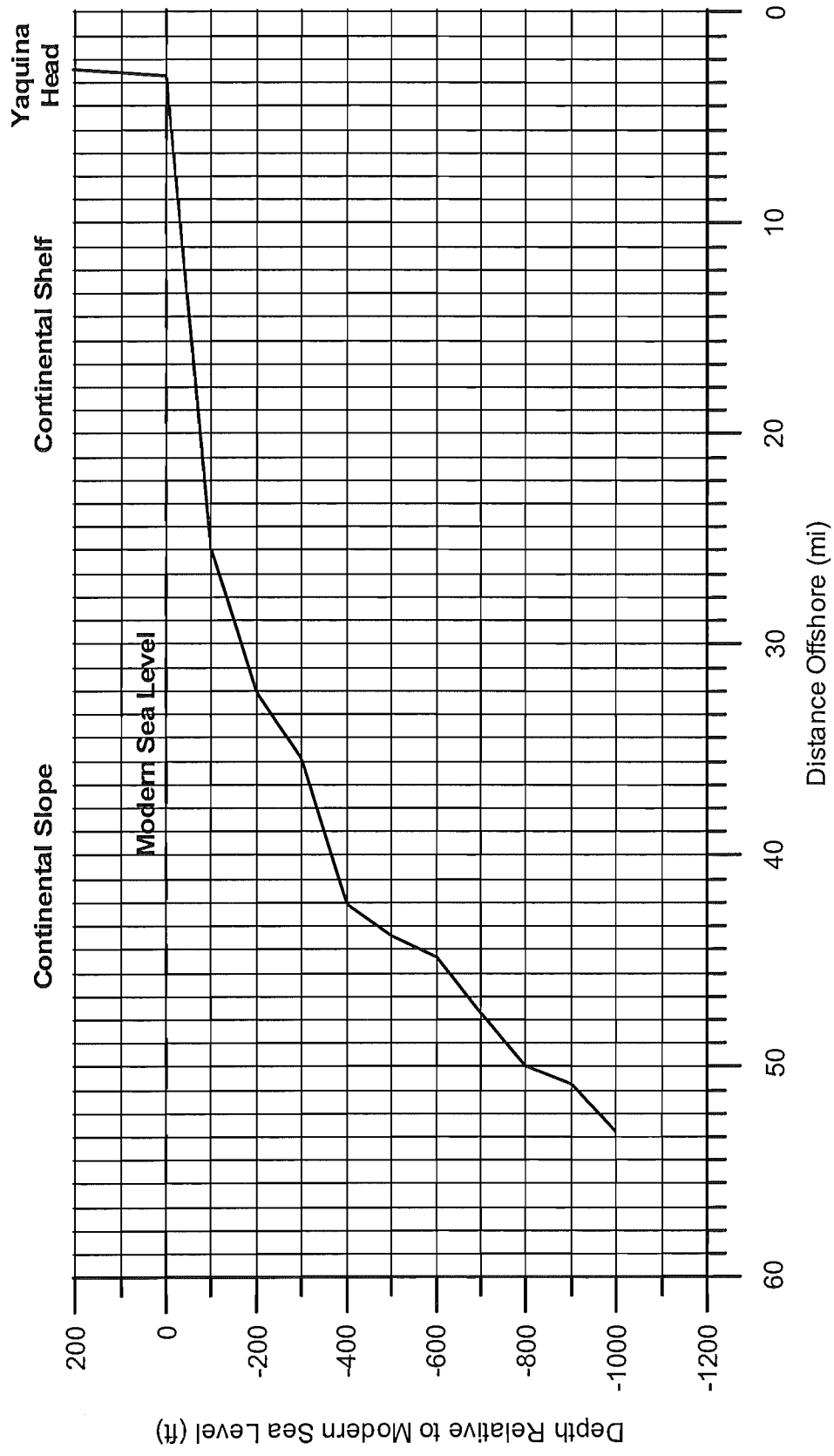


Table 4. Average Vertical Ground Motion Velocities for a South-to-North Transect Along the Coast of the Pacific Northwest

(Data derived from Mitchell et al., 1994 via releveling surveys).
 (Note: positive velocity = uplift, negative velocity = subsidence)
 c:wou:geomorph:f00:coastlab:neotect.xls / coastup

Latitude (degrees N)	Historic Average Vertical Ground Motion Velocity (mm/yr)	Approximate Geographic Location
39.5	1.2	Fort Bragg, CA
39.6	1.5	
39.7	1.8	
39.9	3.0	
40.0	4.1	
40.2	4.5	Garberville, CA
40.4	5.1	
40.6	5.4	
40.7	5.2	
40.9	4.9	Arcata, CA
41.0	4.8	
41.0	4.4	
41.0	3.8	
41.1	3.5	
41.2	3.3	
41.3	3.1	
41.4	2.8	
41.5	2.8	
41.7	2.8	
41.8	2.8	
41.9	2.9	
42.0	3.3	
42.1	3.8	Brookings, OR
42.1	4.0	
42.2	4.1	
42.3	4.1	
42.3	3.6	
42.4	3.3	
42.5	3.1	Gold Beach, OR
42.6	3.0	
42.7	3.0	
42.8	3.4	
42.9	3.7	
43.0	4.4	
43.1	4.4	
43.2	4.1	Bandon, OR
43.2	3.7	
43.3	3.4	
43.4	3.0	
43.5	2.5	
43.8	1.4	Reedsport, OR

Table 4. Average Vertical Ground Motion Velocities for a South-to-North Transect Along the Coast of the Pacific Northwest

(Data derived from Mitchell et al., 1994 via releveing surveys).
 (Note: positive velocity = uplift, negative velocity = subsidence)
 c:\wou\geomorph:f00:coastlab:neotect.xls / coastup

Latitude (degrees N)	Historic Average Vertical Ground Motion Velocity (mm/yr)	Approximate Geographic Location
44.0	0.9	Florence, OR
44.2	0.6	
44.3	0.2	
44.4	0.0	
44.6	-0.1	Newport, OR
44.7	-0.2	
44.9	-0.2	Lincoln City, OR
45.2	-0.3	
45.5	-0.4	Tillamook, OR
45.6	-0.1	
45.7	0.2	
45.9	0.5	
45.9	1.2	
46.0	1.5	Seaside, OR
46.1	1.6	
46.1	1.5	
46.2	1.0	
46.4	0.4	
46.5	0.0	Willapa, WA
46.7	-0.6	
46.8	-0.8	
47.0	-1.0	Aberdeen, WA
47.2	-1.1	
47.3	-1.2	
47.4	-1.1	Queets, WA
47.6	-0.7	
47.7	-0.4	
47.7	0.3	
47.8	1.1	
47.9	1.8	La Push, WA
48.0	2.6	
48.1	3.2	Lake Ozette, WA

Figure 7. Plot of South-to-North Average Uplift Rate Profiles Along the Coast of the Pacific Northwest

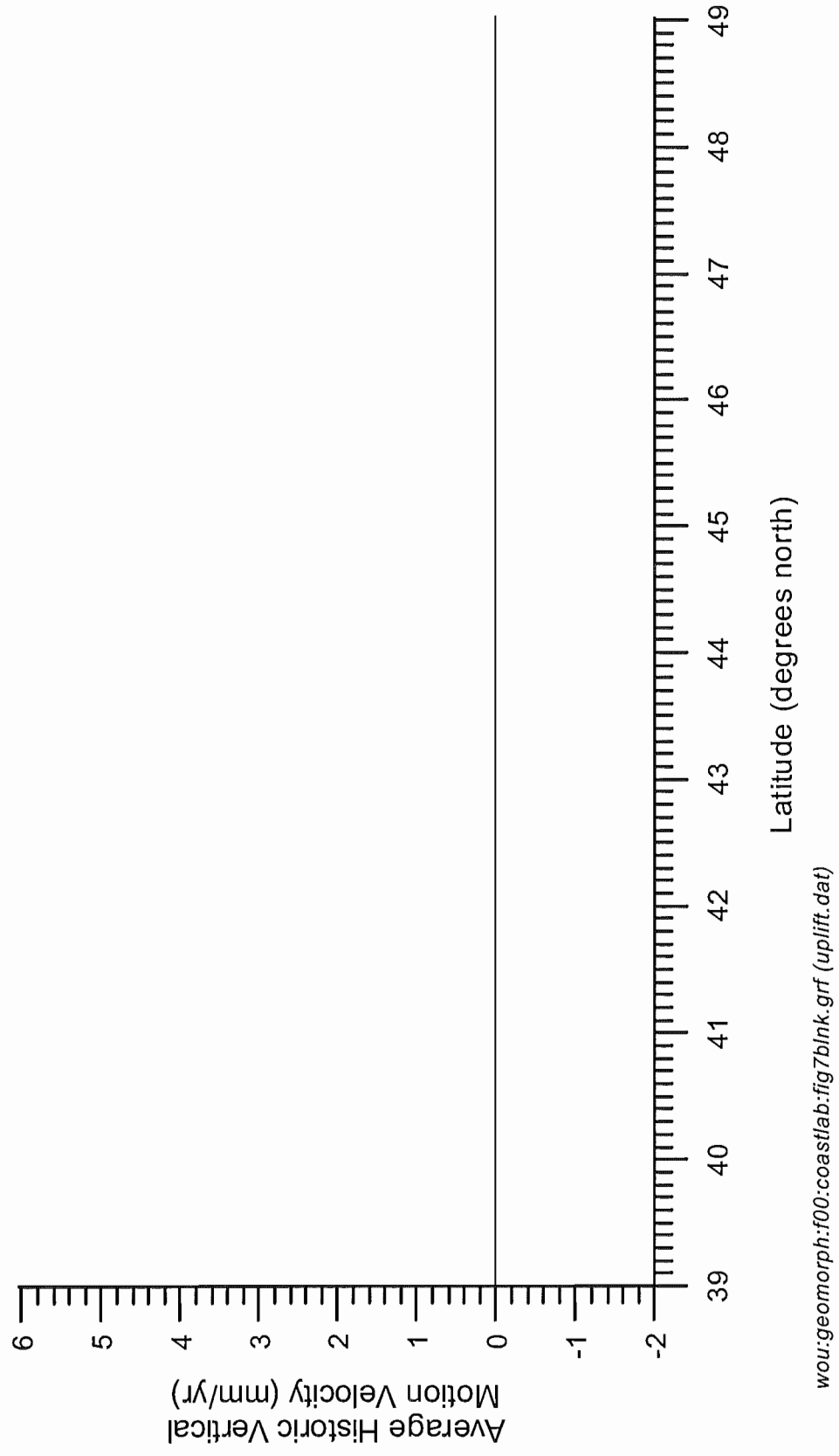


Figure 8. Map of Interpolated Uplift Rates for the Pacific Northwest, West of the Cascade Range (data derived from Mitchell et al., 1994)

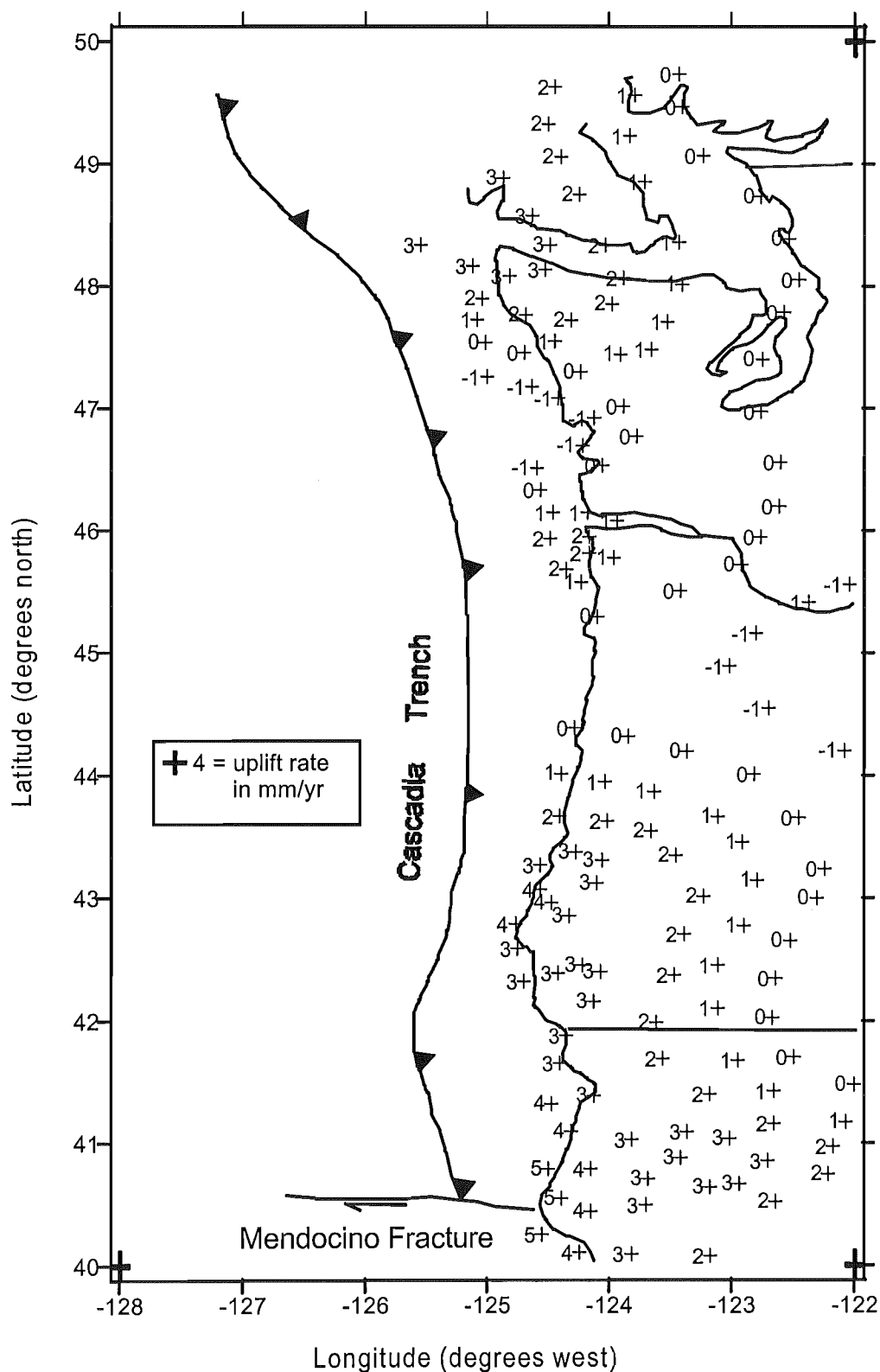


Table 5. Worksheet Calculation of Late Quaternary Uplift Rates in the PNW, as Derived from Marine Terrace Data (data derived from Muhs et al., 1990).

Terrace Name	Location	Terrace Age (ka)	Present Elevation (m)	Original Depth of Wave-Cut Platform (meters)	Paleo-Sea Level (meters)	Total Tectonic Uplift (meters)	Average Uplift Rate (m/kyr)	Average Uplift Rate (mm/yr)
		<i>a</i>	<i>b</i>	<i>c</i>	<i>d</i>	<i>e</i>	<i>f</i>	<i>g</i>
Whiskey Run	Coquille Point, OR	80	17	14	-19			
Whiskey Run	Coquille Point, OR	80	17	48	-19			
Whiskey Run	Coquille Point, OR	80	17	14	-5			
Whiskey Run	Coquille Point, OR	80	17	48	-5			
Cape Blanco	Cape Blanco, OR	80	53	10	-19			
Cape Blanco	Cape Blanco, OR	80	53	28	-19			
Cape Blanco	Cape Blanco, OR	80	53	10	-5			
Cape Blanco	Cape Blanco, OR	80	53	28	-5			
Pioneer	Cape Blanco, OR	105	57	26	-9			
Pioneer	Cape Blanco, OR	105	57	90	-9			
Pioneer	Cape Blanco, OR	105	57	26	-2			
Pioneer	Cape Blanco, OR	105	57	90	-2			

Explanation of Data:

Column a: "ka" = kiloans = 1000's of years ago (how long ago the wave-cut platform was formed)

Column b: "present elevation" = present day elevation of coastal terrace above sea level

Column c: "original depth" = original depth of wave-cut platform below sea level, at time of wave erosion

Column d: "paleo-sea level" = level of sea, relative to present, at time wave-cut platform was eroded

Column e: total tectonic uplift of wave-cut platform from time in column a to present.

Column f: tectonic uplift rate of terrace in meters per 1000 yrs

Column g: tectonic uplift rate of terrace in millimeters per yr

c:\wou\geomorph:f00:coastlab:neotect.xls / table 5 terrace data

REFERENCE TABLES

APPENDIX 7

Table for length conversion

Unit	mm	cm	m	km	in	ft	yd	mi
1 millimeter	1	0.1	0.001	10^{-6}	0.03937	0.00328	0.00109	6.21×10^{-7}
1 centimeter	10	1	0.01	0.0001	0.3937	0.0328	0.0109	6.21×10^{-6}
1 meter	1000	100	1	0.001	39.37	3.281	1.094	6.21×10^{-4}
1 kilometer	10^6	10^5	1000	1	39,370	3281	1093.6	0.621
1 inch	25.4	2.54	0.0254	2.54×10^{-5}	1	0.0833	0.0278	1.58×10^{-5}
1 foot	304.8	30.48	0.3048	3.05×10^{-4}	12	1	0.333	1.89×10^{-4}
1 yard	914.4	91.44	0.9144	9.14×10^{-4}	36	3	1	5.68×10^{-4}
1 mile	1.61×10^6	1.01×10^5	1.61×10^3	1.6093	63,360	5280	1760	1

APPENDIX 8

Table for area conversion

Unit	cm ²	m ²	km ²	ha	in ²	ft ²	yd ²	mi ²	ac
1 sq. centimeter	1	0.0001	10^{-10}	10^{-8}	0.155	1.08×10^{-3}	1.2×10^{-4}	3.86×10^{-11}	2.47×10^{-8}
1 sq. meter	10^4	1	10^{-6}	10^{-4}	1550	10.76	1.196	3.86×10^{-7}	2.47×10^{-4}
1 sq. kilometer	10^{10}	10^6	1	100	1.55×10^8	1.076×10^7	1.196×10^6	0.3861	247.1
1 hectare	10^8	10^4	0.01	1	1.55×10^7	1.076×10^6	1.196×10^5	3.861×10^{-3}	2.471
1 sq. inch	6.452	6.45×10^{-4}	6.45×10^{-10}	6.45×10^{-8}	1	6.94×10^{-3}	7.7×10^{-4}	2.49×10^{-10}	1.574×10^{-7}
1 sq. foot	929	0.0929	9.29×10^{-8}	9.29×10^{-6}	144	1	0.111	3.587×10^{-8}	2.3×10^{-5}
1 sq. yard	8361	0.8361	8.36×10^{-7}	8.36×10^{-5}	1296	9	1	3.23×10^{-7}	2.07×10^{-4}
1 sq. mile	2.59×10^{10}	2.59×10^6	2.59	259	4.01×10^9	2.79×10^7	3.098×10^6	1	640
1 acre	4.04×10^7	4047	4.047×10^{-3}	0.4047	6.27×10^6	43,560	4840	1.562×10^{-3}	1

APPENDIX 9

Table for volume conversion

Unit	mL	liters	m ³	in ³	ft ³	gal	ac-ft	million gal
1 milliliter	1	0.001	10^{-6}	0.06102	3.53×10^{-5}	2.64×10^{-4}	8.1×10^{-10}	2.64×10^{-10}
1 liter	10^3	1	0.001	61.02	0.0353	0.264	8.1×10^{-7}	2.64×10^{-7}
1 cu. meter	10^6	1000	1	61,023	35.31	264.17	8.1×10^{-4}	2.64×10^{-4}
1 cu. inch	16.39	1.64×10^{-2}	1.64×10^{-5}	1	5.79×10^{-4}	4.33×10^{-3}	1.218×10^{-8}	4.329×10^{-9}
1 cu. foot	28,317	28.317	0.02832	1728	1	7.48	2.296×10^{-5}	7.48×10^{-6}
1 U.S. gallon	3785.4	3.785	3.78×10^{-3}	231	0.134	1	3.069×10^{-6}	10^{-6}
1 acre-foot	1.233×10^9	1.233×10^6	1233.5	75.27×10^6	43,560	3.26×10^5	1	0.3260
1 million gallons	3.785×10^9	3.785×10^6	3785	2.31×10^8	1.338×10^5	10^6	3.0684	1

APPENDIX 10

Table for time conversion

Unit	sec	min	hours	days	years
1 second	1	1.67×10^{-2}	2.77×10^{-4}	1.157×10^{-5}	3.17×10^{-8}
1 minute	60	1	1.67×10^{-2}	6.94×10^{-4}	1.90×10^{-6}
1 hour	360	60	1	4.17×10^{-2}	1.14×10^{-4}
1 day	8.64×10^4	1440	24	1	2.74×10^{-3}
1 year	3.15×10^7	5.256×10^5	8760	365	1

Appendix 9.A. Continued Velocity

Unit	Equivalent ^{1,2}			
	feet per day	kilometers per hour	miles per hour	meters per second
feet per day	1	1.27×10^{-5}	1.157×10^{-5}	3.528×10^{-6}
kilometers per hour	7.874×10^4	1	0.6214	0.2778
feet per second	8.64×10^4	1.097	0.6818	0.3048
miles per hour	1.267×10^5	1.609	1	0.447
meters per second	2.835×10^5	3.6	2.237	1

Mass

Unit	Equivalent ^{1,2}					
	ounce	pound	kilogram	metric slug	short ton	long ton
ounce	1	6.25×10^{-2}	2.835×10^{-2}	2.891×10^{-3}	1.943×10^{-3}	2.835×10^{-3}
pound	16	1	0.4536	4.625×10^{-2}	3.108×10^{-2}	4.464×10^{-2}
kilogram	35.28	2.205	1	0.102	6.852×10^{-2}	9.842×10^{-2}
metric slug	345.9	21.62	9.807	1	0.0721	9.807×10^{-3}
slug	514.7	32.17	14.59	1.49	0.1	1.459×10^{-2}
short ton	3.2×10^3	2,000	907.2	92.51	1	0.8929
ton	3.529×10^3	2,205	1,000	102	1.103	1
long ton	3.584×10^3	2,240	1,016	103.7	1.12	1

Force

Unit	Equivalent ^{1,2}		
	dyne	newton	pound _{force}
dynes	1	1×10^{-5}	2.248×10^{-6}
newtons	1×10^5	1	0.2248
pound _{force}	4.448×10^5	4.448	1
kilogram _{force}	9.807×10^5	9.807	2.205

Density

Unit	Equivalent ^{1,2}			
	pounds per cubic inch	pounds per cubic foot	grams per cubic centimeter	grams per liter
pounds per cubic inch	1	1,728	27.68	2.768×10^4
pounds per cubic foot	5.787×10^{-4}	1	1.6×10^{-2}	16.02
pounds per gallon	4.33×10^{-3}	7.481	0.1198	119.8
grams per cubic centimeter	3.61×10^{-3}	62.43	1	1,000
grams per liter	3.61×10^{-3}	6.24×10^{-2}	0.001	1

APPENDIX 9.A. Conversion Tables

Length

Unit	Equivalent ^{1,2}					
	millimeters	inches	feet	meters	kilometers	miles
millimeters	1	3.937×10^{-2}	3.281×10^{-3}	1×10^{-3}	1×10^{-6}	6.214×10^{-7}
inches	25.4	1	8.33×10^{-2}	2.54×10^{-2}	2.54×10^{-5}	1.578×10^{-5}
feet	304.8	12	1	0.3048	3.048×10^{-4}	1.894×10^{-4}
meters	1,000	39.37	3.281	1	1×10^{-3}	6.214×10^{-4}
kilometers	1×10^6	3.937×10^4	3,281	1,000	1	0.6214
miles	1.609×10^6	6.336×10^4	5,280	1,609	1.609	1

Area

Unit	Equivalent ^{1,2}						
	square inches	square feet	square meters	hectares	acres	square kilometers	square miles
square inches	1	6.944×10^{-3}	6.453×10^{-4}	2.471×10^{-8}	1.594×10^{-8}	6.453×10^{-10}	2.491×10^{-10}
square feet	144	1	9.29×10^{-2}	2.471×10^{-5}	2.296×10^{-5}	9.29×10^{-8}	3.587×10^{-8}
square meters	1,550	10.76	1	2.471×10^{-4}	2.471×10^{-4}	1×10^{-6}	3.861×10^{-7}
acres	6.773×10^6	4.36×10^4	10,000	1	1	1×10^{-4}	3.861×10^{-5}
hectares	1.55×10^7	1.076×10^5	2.471×10^4	1	1	0.01	3.861×10^{-3}
square kilometers	1.55×10^9	1.076×10^7	1×10^6	100	259	1	0.3861
square miles	4.014×10^9	2.788×10^7	2.59×10^6	259	640	2.59	1

Volume

Unit	Equivalent ^{1,2}						
	cubic inches	liters	gallons	cubic feet	cubic yards	cubic meters	acre-ft
cubic inches	1	1.639×10^{-2}	4.329×10^{-3}	5.787×10^{-4}	2.143×10^{-5}	1.639×10^{-5}	1.329×10^{-8}
liters	61.02	1	0.2642	3.531×10^{-2}	1.308×10^{-3}	0.001	8.106×10^{-7}
gallons	231.0	3.785	1	0.1337	4.951×10^{-3}	3.785×10^{-3}	3.064×10^{-6}
cubic feet	1,728	28.32	7.481	1	3.704×10^{-2}	2.832×10^{-2}	2.296×10^{-5}
cubic yards	4.666×10^4	764.6	202.0	27	1	0.7646	6.191×10^{-4}
cubic meters	6.02×10^4	1,000	264.2	35.31	1.308	1	8.106×10^{-4}
acre-ft	7.527×10^7	1.233×10^6	3.259×10^5	4.356×10^4	1,613	1.233	1

Discharge (flow rate, volume/time)

Unit	Equivalent ^{1,2}				
	gallons per minute	liters per second	acres-foot per day	cubic feet per second	cubic meters per day
gallons per minute	1	6.309×10^{-2}	4.419×10^{-3}	2.228×10^{-3}	5.45
liters per second	15.85	1	7.005×10^{-2}	3.531×10^{-2}	86.4
acres-foot per day	226.3	14.28	1	0.5042	1,234
cubic feet per second	448.8	28.32	1.983	1	2,447
cubic meters per day	1.369×10^4	8.64×10^3	6.051×10^4	3.051×10^4	1

128

TABLE 4.1 English and SI Units

$$1 \text{ N} = 1 \text{ Kg} \cdot \text{m} / \text{sec}^2$$

Parameter	English Unit	SI Unit	Conversion Factor	Dimensional Formula
Force	pound (lb)	newton (N)	1 lb = 4.448 N	ML/T^2
Mass	slug	kilogram (kg)	1 slug = 14.594 kg	M
Length	foot (ft)	meter (m)	1 ft = 0.3048 m	L
Time	second (s)	second	1 s = 1 s	T
Density	slug/ft ³	kg/m ³	1 slug/ft ³ = 515.4 kg/m ³	M/L^3
Specific weight	lb/ft ³	N/m ³	1 lb/ft ³ = 157.1 N/m ³	M/L^2T^2
Pressure	lb/ft ²	N/m ²	1 lb/ft ² = 47.88 N/m ²	M/LT^2
Dynamic viscosity	lb-s/ft ²	N-s/m ²	1 lb-s/ft ² = 47.88 N-s/m ²	M/LT
Bulk modulus	lb/ft ²	N/m ²	1 lb/ft ² = 47.88 N/m ²	M/LT^2

$g = \text{Acceleration due to Gravity} = 9.8 \text{ m/sec}^2$

Equations for areas and volumes

Circumference of circle = $3.1416 \times \text{dia} = 6.2832 \times \text{radius}$

Area of circle = $0.7854 \times (\text{dia})^2 = 3.1416 \times (\text{radius})^2$

Area of sphere = $3.1416 \times (\text{dia})^2$

Volume of sphere = $0.5236 \times (\text{dia})^3$

Area of triangle = $0.5 \times \text{base} \times \text{height}$

Area of trapezoid = $0.5 \times \text{sum of the two parallel sides} \times \text{height}$

Area of square, rectangle, or parallelogram = $\text{base} \times \text{height}$

Volume of pyramid = $\text{area of base} \times 1/3 \text{ height}$

Volume of cone = $0.2618 \times (\text{dia of base})^2 \times \text{height}$

Volume of cylinder = $0.7854 \times \text{height} \times (\text{dia})^2$

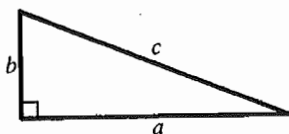
Pressure

Unit	Equivalent ^{1,2}										
	pounds per square inch	pounds per square foot	atmospheres	kilograms per square centimeter	kilograms per square meter	inches of water (68°F)	feet of water (68°F)	inches of mercury (32°F)	millimeters of mercury (32°F)	bars	kilo Pascals
pounds per square inch	1	144	6.805×10^{-2}	7.031×10^{-2}	703.1	27.73	2.311	2.036	51.72	6.895×10^{-2}	6.895
pounds per square foot	6.945×10^{-3}	1	4.73×10^{-4}	4.88×10^{-4}	4.882	0.1926	1.605×10^{-2}	1.414×10^{-2}	0.3591	4.79×10^{-4}	4.79×10^{-2}
atmospheres	14.7	2,116	1	1.033	1.033×10^4	407.5	33.96	29.92	760	1.013	101.3
kilograms per square centimeter	14.22	2,048	0.9678	1	1×10^4	394.4	32.87	28.96	735.6	0.9807	98.07
kilograms per square meter	1.422×10^{-3}	0.2048	9.678×10^{-3}	0.001	1	3.944×10^{-2}	3.287×10^{-3}	2.896×10^{-3}	7.356×10^{-2}	9.807×10^{-3}	9.807×10^{-2}
inches of water (68°F)	3.609×10^{-2}	5.197	2.454×10^{-3}	2.53×10^{-3}	25.38	1	8.333×10^{-2}	7.343×10^{-2}	1.865	2.49×10^{-3}	0.249
feet of water (68°F)	0.4328	62.32	2.945×10^{-3}	3.043×10^{-3}	304.3	12	1	0.8812	22.38	2.984×10^{-2}	2.984
inches of mercury (32°F)	0.4912	70.73	3.342×10^{-2}	3.453×10^{-2}	345.3	13.62	1.135	1	25.4	3.386×10^{-2}	3.386
millimeters of mercury (32°F)	1.934×10^{-2}	2.785	1.316×10^{-2}	1.36×10^{-2}	13.6	0.5362	4.468×10^{-2}	3.937×10^{-2}	1	1.333×10^{-3}	0.1333
bars	14.5	2,089	0.9869	1.02	1.02×10^4	402.2	33.51	29.53	750.1	1	100
kilo Pascals	0.145	20.89	9.869×10^{-3}	1.02×10^{-2}	102	4.022	0.3351	0.2953	7.501	0.01	1

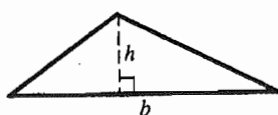
Appendix 9.A. Continued

1.779

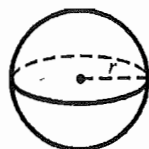
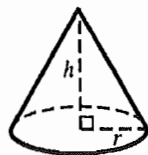
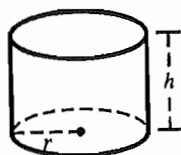
GEOMETRIC FORMULAS



Right Triangle



Any Triangle



● Triangles

Pythagorean Theorem $a^2 + b^2 = c^2$

Area $A = \frac{1}{2}bh$

● Circles

Area $A = \pi r^2$

Circumference $C = 2\pi r$

● Cylinders

Surface Area $S = 2\pi r^2 + 2\pi rh$

Volume $V = \pi r^2 h$

● Cones

Surface Area $S = \pi r^2 + \pi r \sqrt{r^2 + h^2}$

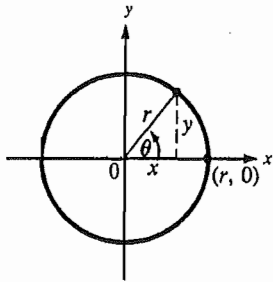
Volume $V = \frac{1}{3}\pi r^2 h$

● Spheres

Surface Area $S = 4\pi r^2$

Volume $V = \frac{4}{3}\pi r^3$

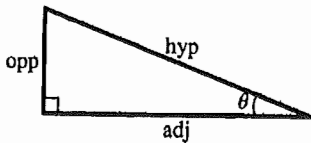
TRIGONOMETRIC FUNCTIONS AND LAWS



● Definitions Based on the Circle

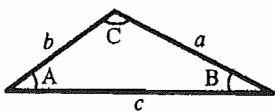
$$\begin{aligned}\cos \theta &= \frac{x}{r} & \sec \theta &= \frac{r}{x} \\ \sin \theta &= \frac{y}{r} & \csc \theta &= \frac{r}{y} \\ \tan \theta &= \frac{y}{x} & \cot \theta &= \frac{x}{y}\end{aligned}$$

For the unit circle, $r = 1$



● Definitions Based on the Right Triangle

$$\begin{aligned}\cos \theta &= \frac{\text{adj}}{\text{hyp}} & \sec \theta &= \frac{\text{hyp}}{\text{adj}} \\ \sin \theta &= \frac{\text{opp}}{\text{hyp}} & \csc \theta &= \frac{\text{hyp}}{\text{opp}} \\ \tan \theta &= \frac{\text{opp}}{\text{adj}} & \cot \theta &= \frac{\text{adj}}{\text{opp}}\end{aligned}$$



● Law of Sines

$$\frac{\sin A}{a} = \frac{\sin B}{b} = \frac{\sin C}{c}$$

● Law of Cosines

$$\begin{aligned}a^2 &= b^2 + c^2 - 2bc \cos A \\ \cos A &= \frac{b^2 + c^2 - a^2}{2bc}\end{aligned}$$

182

Stop 1. Bastendorff Beach

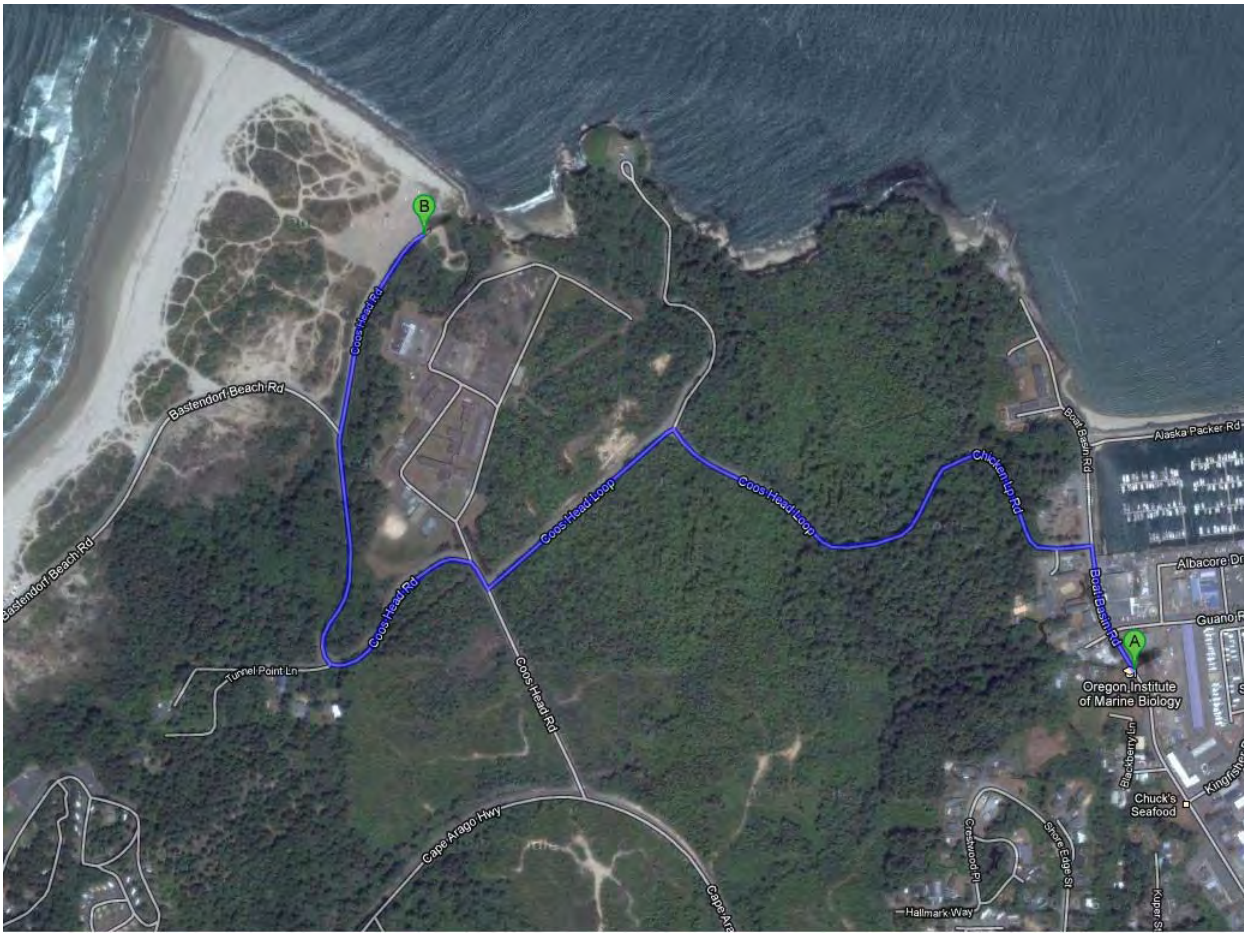


Figure 1-1. Navigation

Leaving OIMB, our first stop is Bastendorff Beach, a short drive over Coos Head.

Oregon Beach dynamics

The Oregon Coast is highly active, with one of the most energetic wave climates (Figure 1-2) in the world, and all of that energy pushes a lot of sand around. We all learned about longshore drift in Geo 101, but the pattern in Oregon is fundamentally different. Oregon's coast is broken into a series of "pocket beach" littoral cells, long stretches of dune or bluff-backed beach bounded by rocky headlands that extend into water that is deep enough to block sediment transport around the ends of the headlands. There are also large differences in the direction and energy of summer versus winter waves (Figure 1-3); highly energetic winter waves erode the beaches and move sand offshore to form sand bars, while gentler summer waves restore the sand to the beaches. Within each cell, sand also moves north or south depending on the prevailing wave directions and in response to climate events such as El Niño's. Here at Bastendorff beach we see evidence for this intra-cell movement in the form of dramatic accretion of the beach since the construction of the south jetty in the early 1900's. The beach rapidly accreted (Figure 1-3) until about 1967, and has reached some state of equilibrium since then. The abandoned sea cliff is now hidden behind the forest of shore pines, but is clearly visible on lidar. Also typical of the Oregon Coast, the backshore at Bastendorff beach has been rapidly and effectively stabilized by

European dune grass, a non-native species that have substantially changed dune characteristics in the last century.

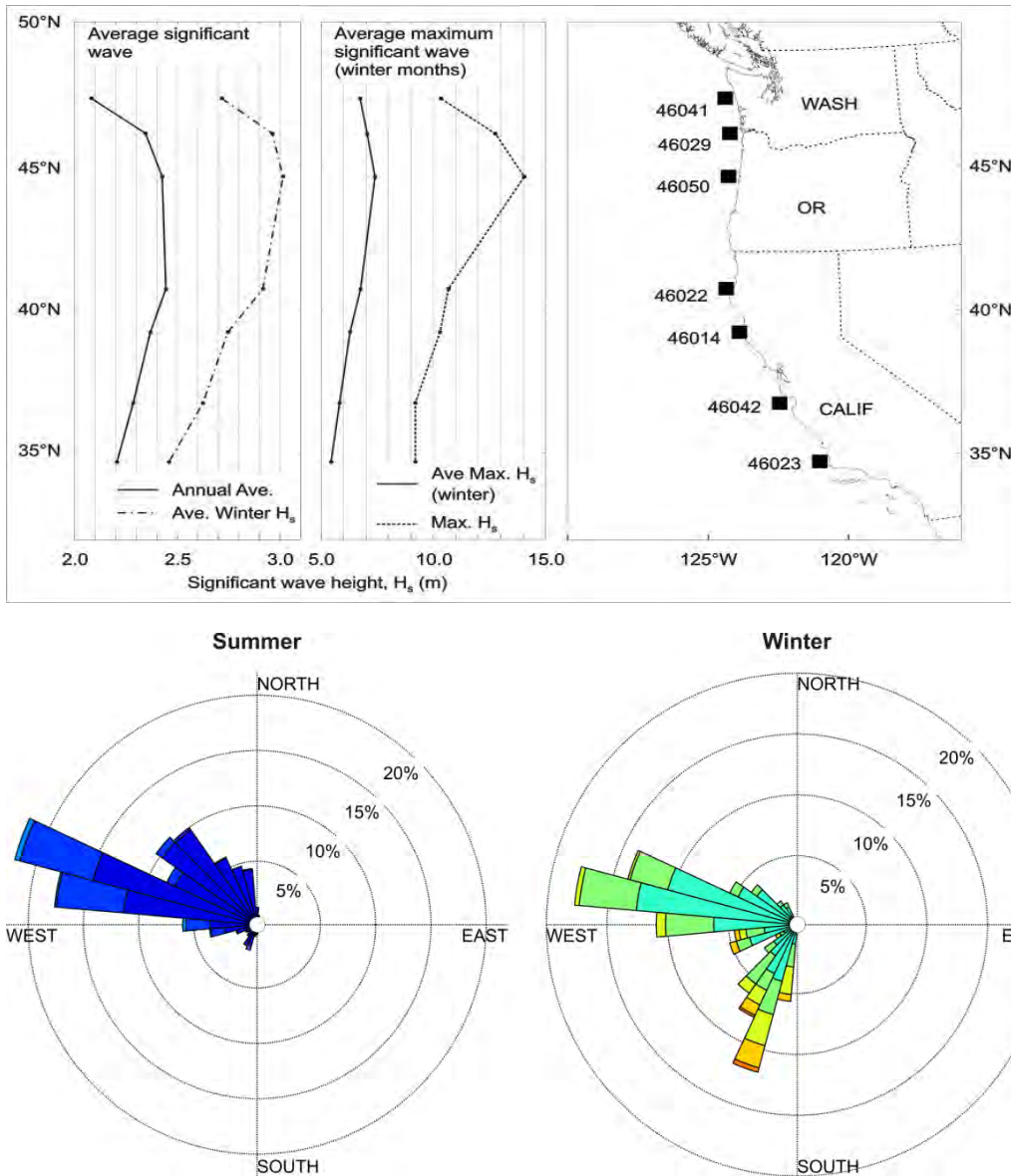


Figure 1-2. Top: Wave heights on the US west coast. Bottom: Winter vs summer wave directions offshore from the central Oregon coast. Colored scale indicates the wave height in meters.

The introduction of European beach grass, (*Ammophila arenaria*) in the early 1900s for the purposes of dune stabilization and its eventual proliferation along the coast, has without doubt single-handedly transformed the character of the coast, particularly since the late 1930s. For example, the first state-wide aerial photographic survey of the coast in 1939 clearly shows that the majority of the dunes and barrier spits on the coast were completely devoid of vegetation. At that time, the expanse of low lying hummocky dunes allowed sand to be transported significant distances inland, where the dunes piled up against marine terraces where present, or inundated forest communities. With the introduction of European beach grass, particularly in the late 1960s and early 1970s when extensive dune planting programs took place, the dunes and barrier spits have subsequently become stabilized, building foredunes that now range in height from 10- 16 m.

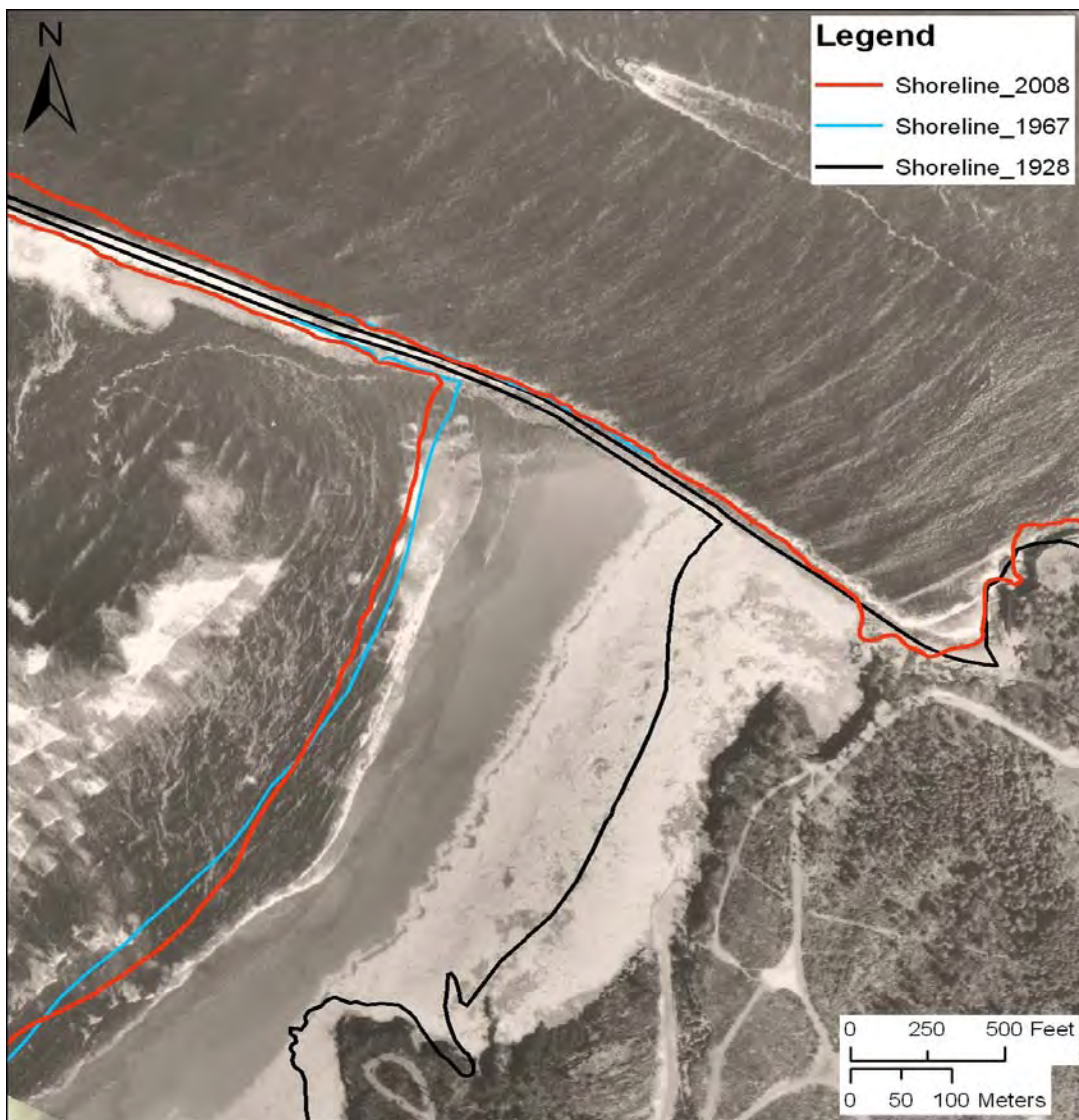


Figure 1-3. Historic shorelines at Bastendorf Beach, photo is from 1939.

Periodic extreme storms, such as occur during El Nino or La Nina events can cause dramatic erosion within littoral cells, and in some cases appear to actually move sand out of the cell, or into water so deep that summer waves cannot return it. Understanding beach erosion and dynamics therefore requires detailed quantitative data, so that one can begin to sort out the cyclic changes from the permanent changes. Jonathan Allan, DOGAMI's coastal geomorphologist, has pioneered this effort, using serial lidar and repeat RTK-GPS surveys to track beach changes. There are several iterations of coastal lidar currently available, and although the earlier data are much lower resolution and accuracy than current Oregon Lidar Consortium data, they are sufficiently accurate in the relatively flat and well-exposed beach areas to allow for quantitative comparison. However, beach changes take place at far shorter intervals than the time between lidar flights, and weather precludes lidar collection during most of the winter, when changes are greatest. To get around this, Jon has established a series of monitoring profiles up and down the coast where he does repeat RTK-GPS surveys with sufficient accuracy to detect changes in elevation of 4-5 cm, a small fraction of the typical 1-3m seasonal change in beach elevation.

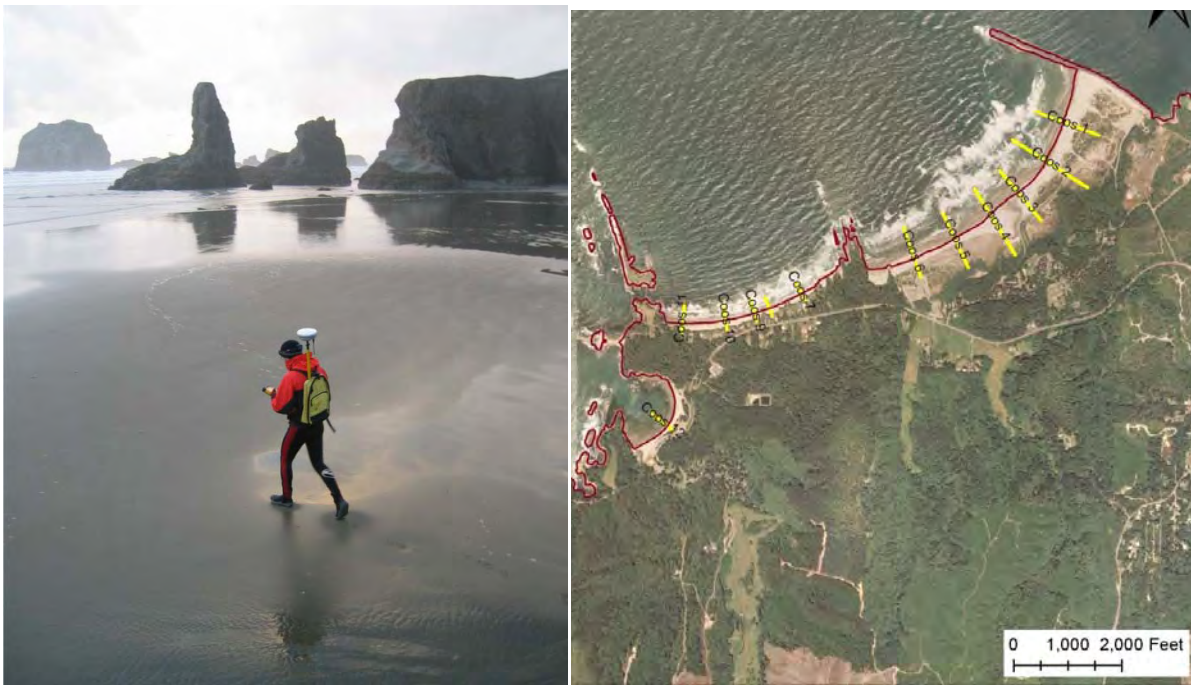


Figure 1-4. RTK-GPS beach profiling and location of transects at Bastendorf Beach. Data for these sites and many others are available at: <http://www.nanoos.org/nvs/nvs.php?section=NVS-Products-Beaches-Mapping>.

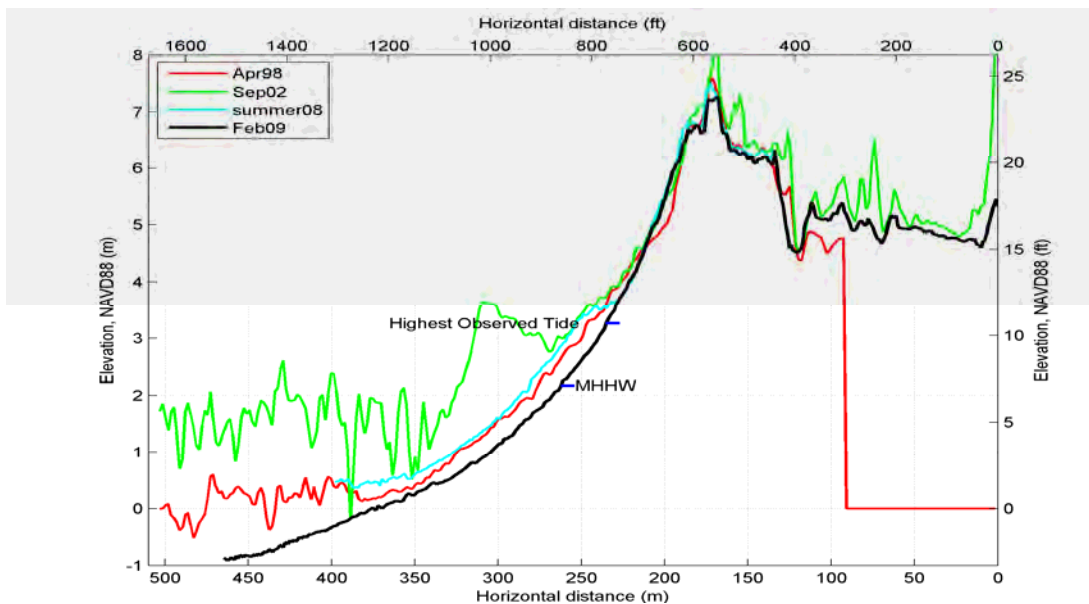


Figure 1-5: The Coos 2 profile site indicating the generally low backshore elevations that suggest that the beach probably prograded rapidly seaward following jetty construction, while the high contemporary foredune indicates that the shoreline has stabilized.

For those interested in rocks, the shoreline behind the beach is composed of a sequence of steeply E-dipping Eocene and Oligocene marine sedimentary rocks, overlain just at our stop by Miocene marine mudstone with a significant angular unconformity.

Stop 2: Shore Acres State Park

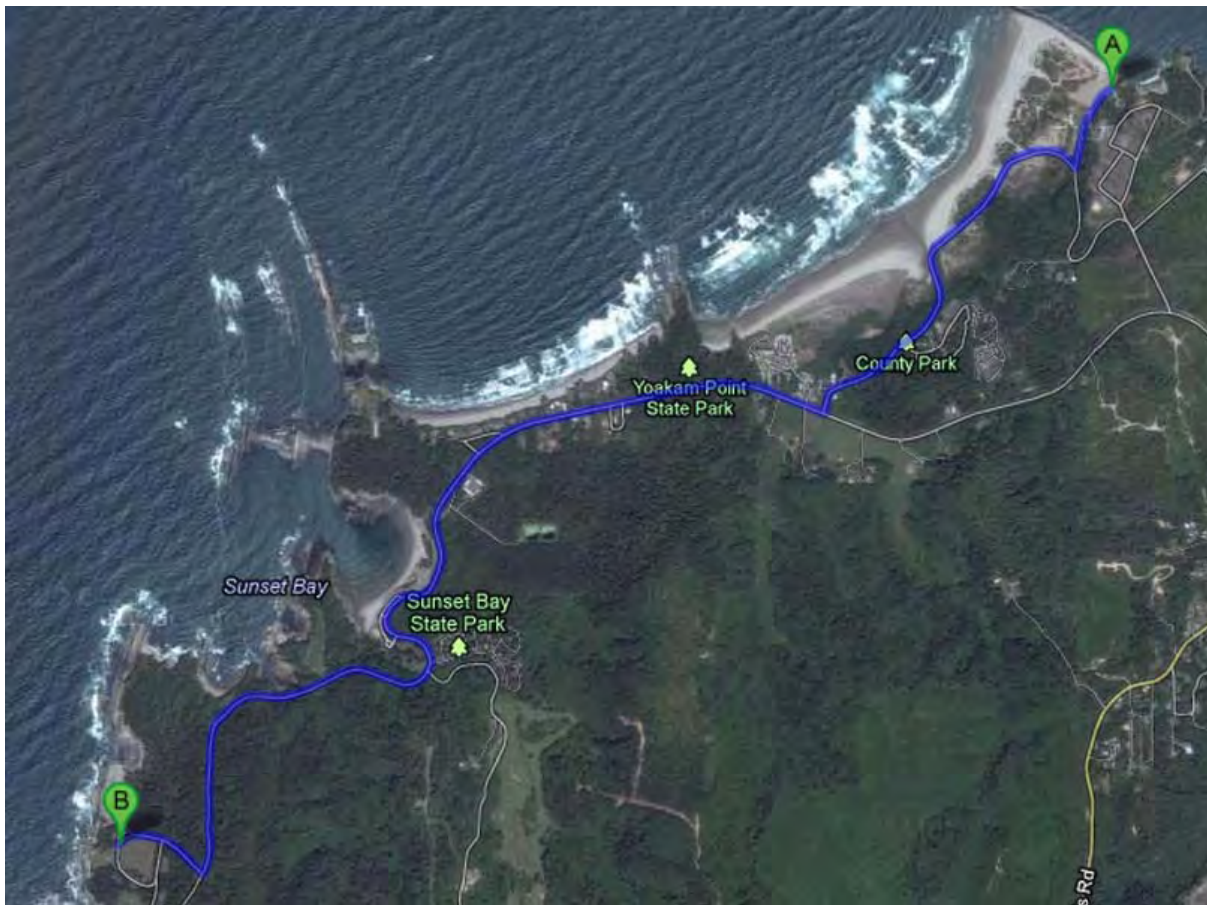


Figure 2-1. Navigation

Leaving Bastendorf Beach, Stop 2 at Shore Acres State Park is a short drive down the Cape Arago Highway. There is a \$5 per car day use/entry fee required at Shore Acres.

Shore Acres is an iconic bit of Oregon coastal scenery. Thick sandstone beds of the lower Coaledo Formation dip moderately inland, forming beautifully sculpted ramparts against which huge waves crash (Figure 2-2). The broad flat surface on which the park is located is the lowest of a well-defined sequence of marine terraces that are present in the Coos Head-Cape Arago region. As we all remember from Geomorph 101, marine terraces form during times of stable or slowly rising sea level, as waves erode the shoreline, carving a submarine wave-cut platform as erosion progresses inland. The platforms end at the paleo-sea cliff commonly referred to as the shoreline angle or backedge, and are covered with nearshore marine sediments of varying thickness. As sea level cycled during the Pleistocene, tectonically rising coasts preserved a stair step sequence of terraces like those we see here. These terraces were dated by McInnelly and Kelsey (1990) and then mapped in detail by Madin, McInnelly and Kelsey (1995). The terraces are:

- Whisky Run (80 ka, Stage 5a)
- Pioneer (105 ka, Stage 5c)
- Seven Devils (125 ka Stage 5 d or e?)
- Metcalf (200-250 ka, Stage 7)

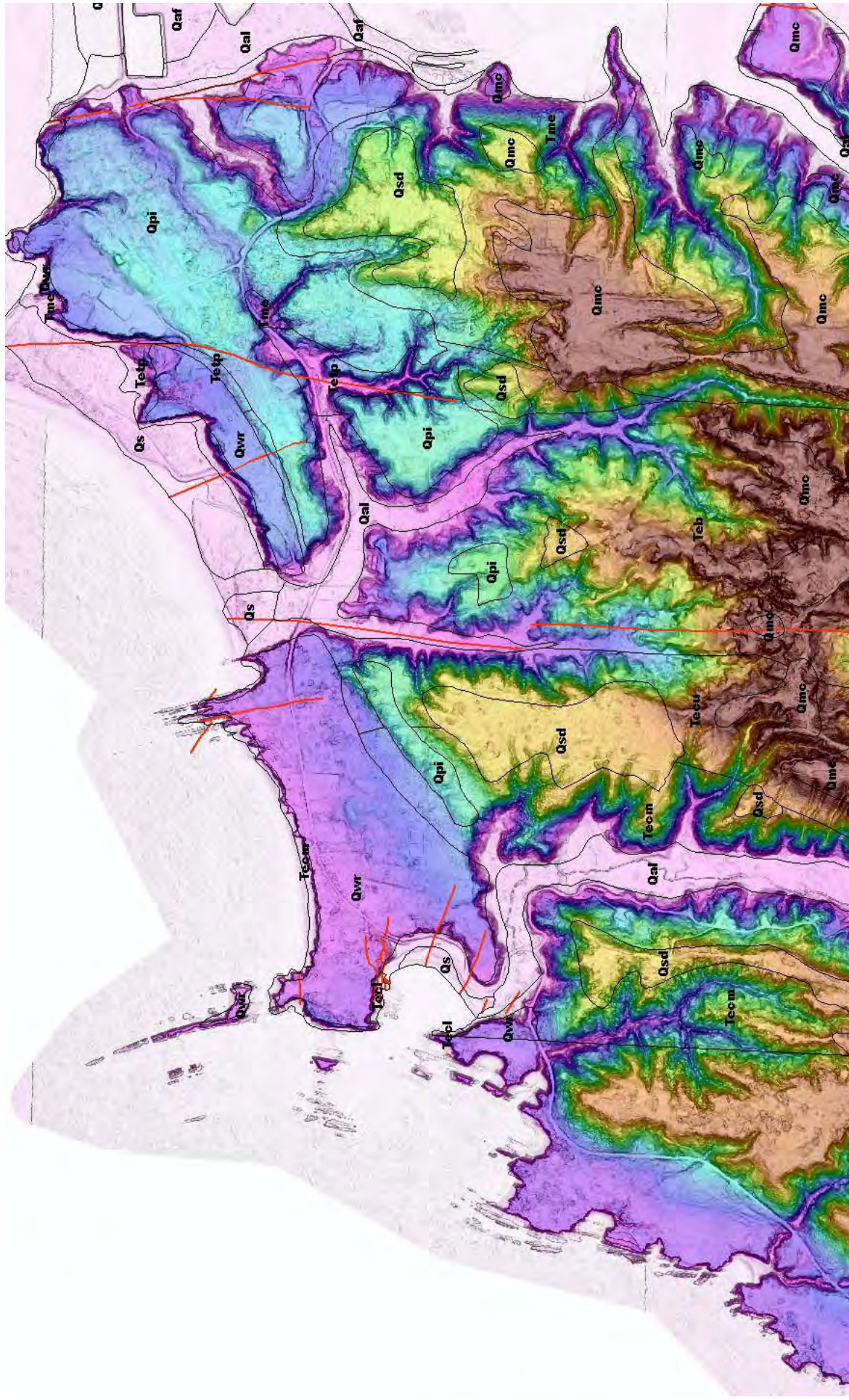
An older Arago terrace may or may not exist. On the lidar image (Figure 2-3) we can clearly see the flat Whiskey Run surface (Qwr, generally violet and blue elevation colors) and its well-defined backedge, the Pioneer Terrace (pale blue elevation tint) is quite dissected with little of the backedge preserved, as is the Seven Devils terrace (yellow elevation



Figure 2-2. Shore Acres Park, note people for scale.

tint), and the Metcalf terrace (brick red elevation tint) is even more deeply eroded (and tilted) and is largely preserved capping ridges

We are standing on the Whiskey Run terrace and all along the edge of the modern sea cliff you can see the exposed wave cut platform and the very thin terrace cover sediments. The marine terraces are rapidly formed planar surfaces that define sea level at a particular stage, so they are excellent markers for tectonic deformation. Figures 2-3 and 2-4 show a cross section of deformation through this area, as well as calculated uplift rates for the various terraces. Care must be taken to work with the wave-cut platform, not the terrace surface, because the thickness of the terrace cover sediments varies widely.



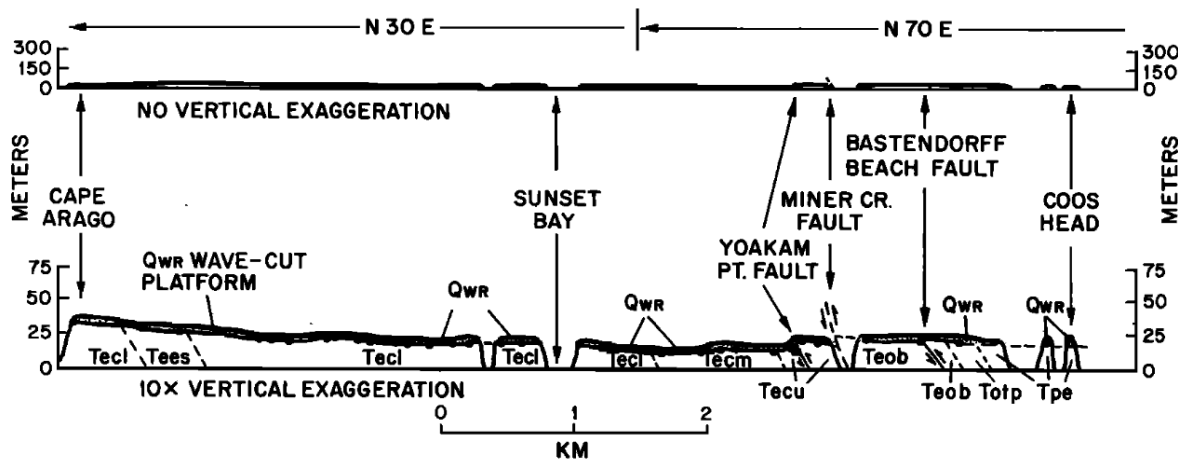


Fig. 7. Post-80 ka deformation of the Whisky Run wave-cut platform is illustrated in this coastwise transect from Cape Arago to Coos Head (view to northwest and north-northwest). Solid circles are altimeter survey locations. Data are projected onto a line that trends N30°E from Cape Arago to Sunset Bay, then N70°E to Coos Head. The gradual descent of the Whisky Run Wave-cut platform from Cape Arago to Coos Head is interrupted repeatedly by flexural-slip faults at Yoakam Point, Miner Creek, and Bastendorff Beach. Geologic units are same as previous figure.

Figure 2-4. Deformation of Whisky Run terrace between Cape Arago and Coos Head

TABLE 2. Marine Wave-Cut Platforms at Cape Arago: Ages, Uplift Rates, Tilt Rates, and Horizontal Strain Rates

Wave-Cut Platform	Estimated Age, ka	Maximum Elevation, m	Shore-Normal Distance From Shoreline Angle, km	Original Gradient of Platform, m/km	Original Depth of Platform, m	Paleo-Sea Level, m	Sea Level Model ^c	Maximum Uplift Rate, m/kyr	Elevation of Shoreline Angle, m	Uplift Rate at Shoreline angle, m/kyr	Maximum Observed Tilt, rad	Tilt Rate rad/yr	Horizontal Strain Rate, yr ⁻¹
Whisky Run	80	35	0.2	20	4	-19 ± 5	NG	0.73 ± 0.07	31	0.63 ± 0.07	2.3 × 10 ⁻³	2.9 × 10 ⁻⁸	0.44 × 10 ⁻⁷
	80	35	0.2	40	8	-19 ± 5	NG	0.78 ± 0.07	31	0.63 ± 0.07			
	80	35	0.2	20	4	-5 ± 2	CA-JP	0.55 ± 0.03	31	0.45 ± 0.03			
	80	35	0.2	40	8	-5 ± 2	CA-JP	0.60 ± 0.03	31	0.45 ± 0.03			
Pioneer	105	68 ^e	0	NA	0	-9 ± 3	NG	0.73 ± 0.03	68	0.73 ± 0.03	5.7 × 10 ⁻³	5.4 × 10 ⁻⁸	0.83 × 10 ⁻⁷
	105	68 ^e	0	NA	0	-2	CA-JP	0.67	68	0.67			
Seven Devils ^d	125	100	0.2	20	4	+6	both	0.78?	98 ^g	0.74?	8.1 × 10 ⁻³ ?	6.5 × 10 ⁻⁸ ?	1.0 × 10 ⁻⁷ ?
	125	100	0.2	40	8	+6	both	0.82?	98 ^g	0.74?			
Metcalf ^h	200?	169	0	NA	0	B+2		0.84?	169	0.84?	17 × 10 ⁻³ ?	8.5 × 10 ⁻⁸	1.3 × 10 ⁻⁷ ?

^aFor Whisky Run and Seven Devils platforms, the maximum elevation near Cape Arago is 200 m seaward (westward) of the paleoshoreline angle. For Pioneer and Metcalf platforms the maximum elevation near Cape Arago is at the paleoshoreline angle. All platforms are landward tilted at Cape Arago.

^bRelative to present sea level.

^cNG, New Guinea model [Chappell and Shackleton, 1986]; CA-JP, California-Japan model [Machida, 1975; Muhs et al., 1988]; B, Bermuda data for 200 ka high stand [Harmon et al., 1983].

^dUncertainties for Whisky Run and Seven Devils wave-cut platforms: (1) paleo-sea level, (2) paleo-water depth during the 80 and 105 ka sea level high stands for the present point of maximum elevation.

^eFor all terrace platforms, tilt is measured from the vicinity of Cape Arago N60°E to the vicinity of South Slough. Tilts measured parallel to the N60°E downwind direction.

^fSee assumptions for derivation of strain rate in text.

^gElevation is extrapolated from known distance measured in downdip direction and using average platform tilt.

^hThe estimated ages of the Seven Devils and Metcalf platforms are minimum ages and not constrained by isotopic data. Therefore all calculated rates based on these ages are maximum rates and are queried because of the large uncertainties.

MCINELLY AND KELSEY: TECTONIC DEFORMATION, COASTAL OREGON

Figure 2-5. Measured deformation rates for terraces between Cape Arago and Coos Head.

Note also that the offshore rocks here very clearly define the structure of the steeply dipping and folded marine strata. All along this stretch of coast, the geologic structure has a strong influence on the shape of the coastline, for instance Sunset Bay has formed where a series of scissor faults perpendicular to the bedding have weakened the resistant sandstone rips enough to allow wave erosion to penetrate inland and then spread where it encounters mudstone and siltstone.

Figure 2-6 shows a 2ft contour map of the Shore Acres area and the paleo sea cliff behind it. There are two large alluvial fans that emanate from very small gullies in the sea cliff, and are built out onto the Whisky Run terrace surface. George Priest from the DOGAMI Newport field office has been mapping the Oregon coast in detail for years, and he sees evidence that Western Oregon endured a much colder and wetter climate than today from shortly after the last high sea stand ~80,000 years ago until ~10,000 years ago. During much of this period sea level was ~200-400 feet lower than today with annual rainfall probably approaching that of southeast Alaska, hundreds of inches per year. Cascadia subduction zone earthquakes shook the region about every 500 years, sometimes occurring during winter when slopes

were least stable. As a result, numerous deep bedrock slides and debris flows covered most steep slopes. These old landslides and colluvial deposits now form a more or less continuous, semi-consolidated deposit in many areas. These unusual fans may be the result of that extremely wet and active period.

Finally, here is an opportunity to make a point about using lidar for geologic maps, and I can beat up on this map because it is mine (from 17 years ago). Compared to the lidar geomorphology, a few of the contacts in Figure 2-3 are pretty good, but most are off by tens of meters or more. I also completely missed the obvious extension of the Whisky Run terrace and backedge to the east of the fault that extends under Bastendorf Beach, and completely missed the landslide at the back of the beach, as well as two additional faults crossing the Whisky Run terrace near Sunset Bay. The moral of the story is that if you are making a geologic map, get lidar first, so future generations don't make fun of your work in field trip guides.

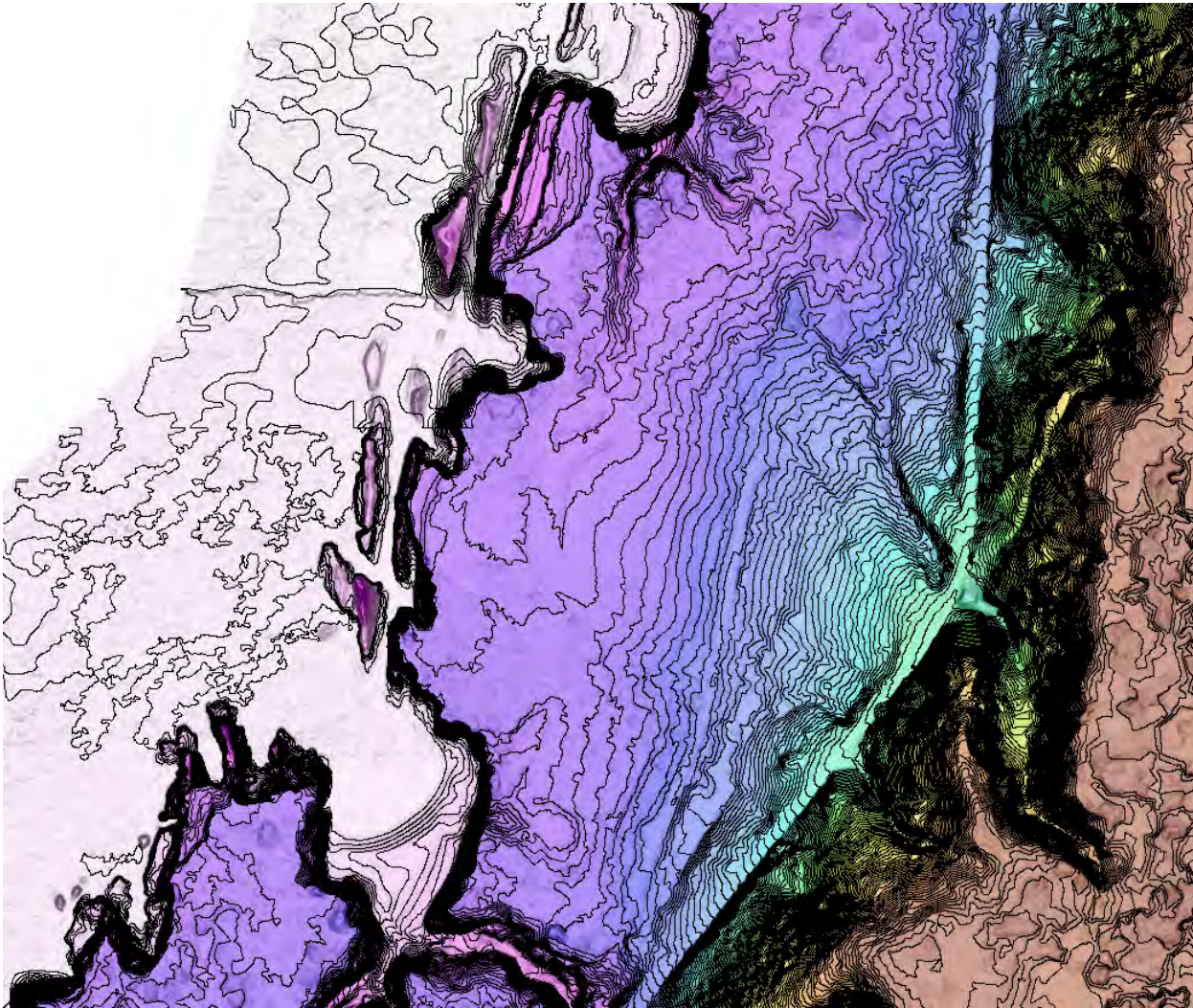


Figure 2-6. 2 ft lidar contours on color elevation gradient and slopeshade at Shore Acres State Park.

Stop 3: Seven Devils Road

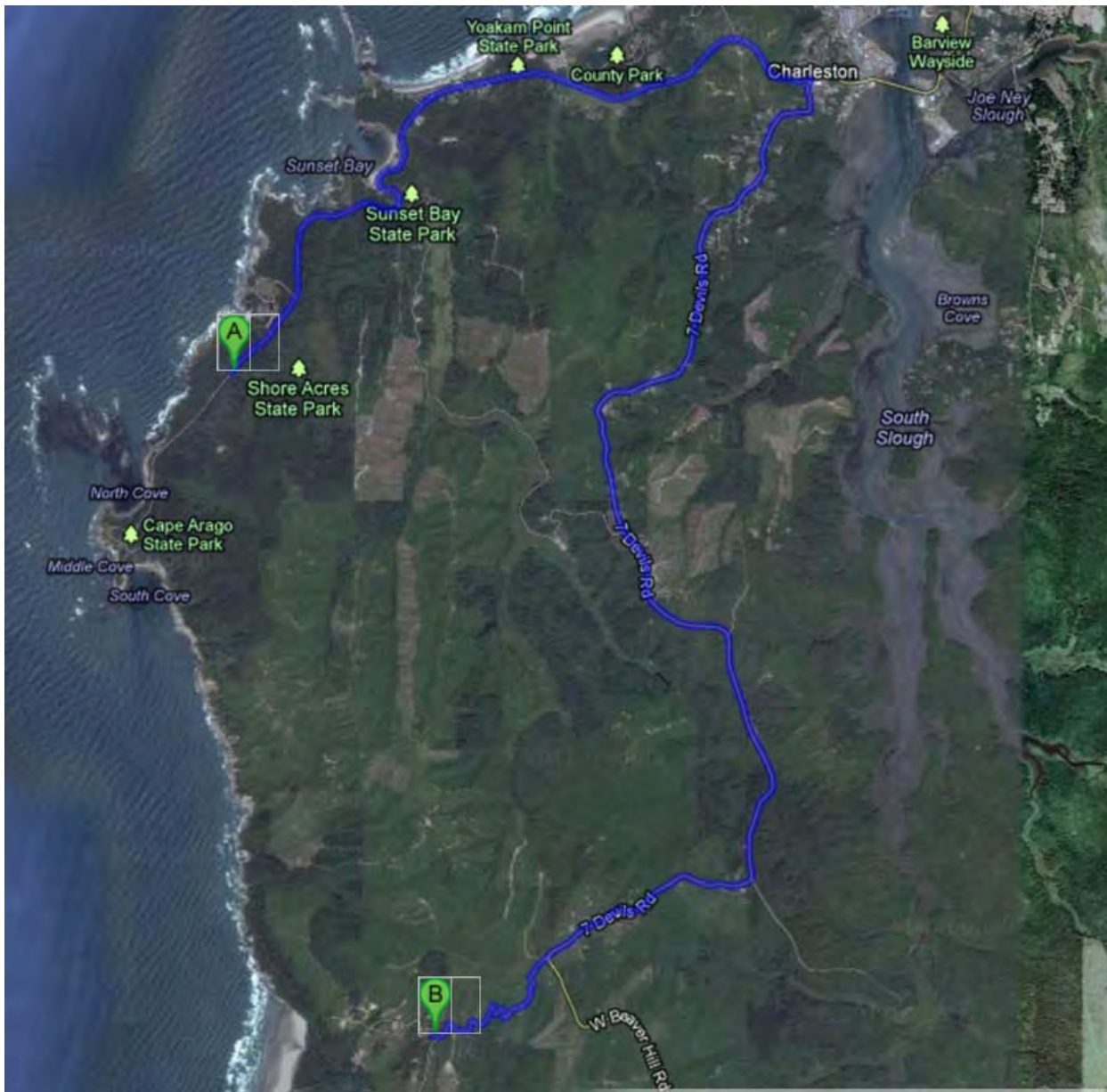


Figure 3-1. Navigation

From Shore Acres to stop 3 is about a half hour drive. We retrace our steps to Charleston then climb quickly up through the marine terrace sequence to get on top of a series of ridges that separate South Slough from the Pacific. These ridges (Figure 3-2) are all capped with Metcalf terrace, which appears as bleached or iron-stained weakly cemented sand. The ridges are all strike ridges held up by the same steeply E-dipping marine strata we saw at Bastendorf beach, with valleys occupying the mudstone intervals. South Slough was long believed to occupy the axis of a large N-trending syncline, but more recent geologic mapping, coupled with gas-exploration seismic shows that in fact there is a thrust fault up the Slough, and our route along Seven Devils road is actually on the anticline formed on the upper plate of the thrust sheet.



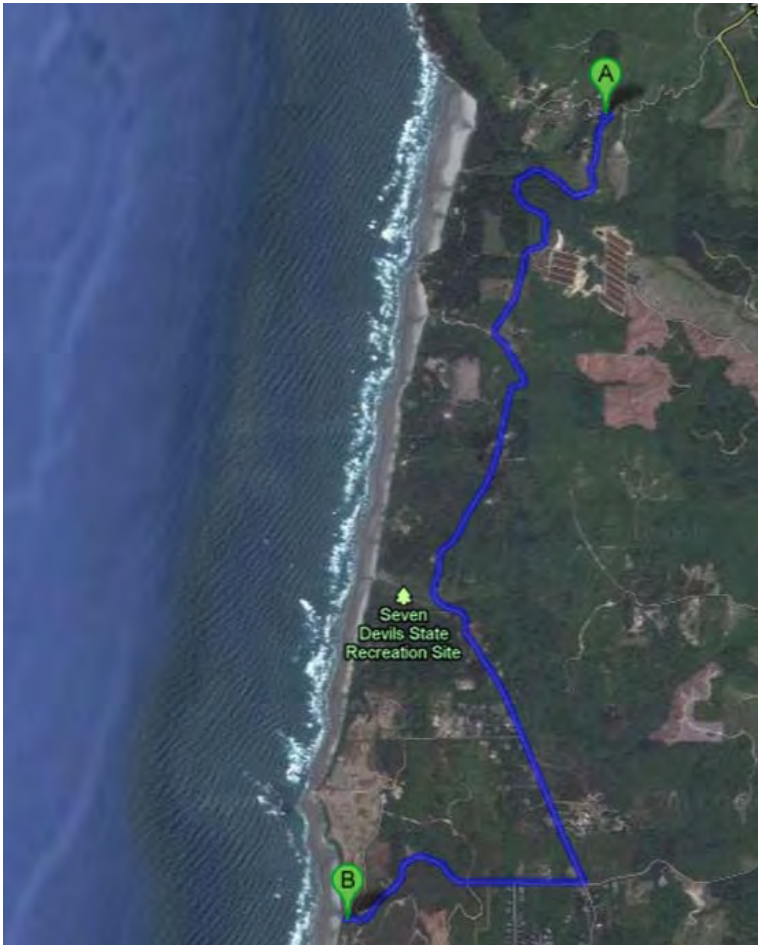
Figure 3-2. Topography along Seven Devils Road.

We turn off the pavement and descend the steep and winding section of Seven Devils road, drive carefully. Everyone but the driver can gawk at the excellent road cut exposures of lower Coaledo Formation sandstone. You may also be able to see the Metcalf wave-cut platform just as we start down; the Metcalf cover sediments here are quite thin.

We will descend to the Seven Devils Terrace and drive across it, stopping just where we start to descend again to look at good exposures of the Seven Devils wave cut platform. Here the platform is cut in lower Coaledo, which is a nearshore

sandstone, and the marine terraces are nearshore sands as well. Both are quite leached or stained with iron and weathered, and it can be very difficult to tell the Eocene from the Pleistocene.

Stop 4: Whiskey Run



Stop 4 is a 15 minute drive from stop 3. En route we will pass the Seven Devils wayside where there are restrooms if needed. We will proceed to the Whiskey Run beach parking lot. About 900 meters after we turn west on Whiskey Run road, we will descend across a scarp about 20 meters high. This has been mapped in the past as the backedge to the Whiskey Run terrace, making the upper surface the Pioneer terrace. We will focus on the scarp at this stop, but lack of good parking and sufficient shoulder (and the lure of the sunny beach!) means that we will discuss it down at the parking lot. McNally and Kelsey (1990) mapped this scarp as the Whiskey Run backedge, and the high surface to the east as the Pioneer Anticline, an area of warped Pioneer terrace surface, and the Pioneer anticline is actually a seismic source in the USGS NSHM model, with a slip rate of 0.2 to 1mm/year. This scarp is unusually straight and sharp for a Whiskey Run backedge, but the orientation and scale are certainly consistent. I propose new high resolution nearshore bathymetry provides evidence that this feature is in fact a fault scarp. Figure 4-3 shows

recently acquired offshore data along with the lidar, and there is a strong linear feature in the submarine bedrock that is exactly on strike with the scarp. The lidar also shows evidence that the scarp divides and steps (Figure 4-4) right, developing a small graben just before it goes offshore, which is not behavior consistent with a sea cliff.

If we take a wider look, the lidar reveals several other even more convincing fault scarps (Figure 4-5) in the marine terrace surface, two of which cannot be backedges because they face landward. Although many of these scarps are quite large, they are cutting a surface that is 80-105 ka in age, so their slip rates are modest. Given the proximity to the subduction zone, there is a question as to whether these faults have an independent seismogenic movement, or simple slip sporadically with subduction events.

This is not the first evidence for active faulting in the area. Back in the early 1990's, Mark Hemphill-Haley and I trenched an 8 m high scarp in the Seven Devils or Metcalf terrace on the Winchester Fault, located at the south end of South Slough (Figure 3-2). We found a beautiful west dipping fault (Figure 4-6) that thrusts Coaledo formation over the marine terrace cover sediments and soils. The wave cut platform is drag-folded on the upper plate, standing vertical, then overturning into the fault plane, dragging beach lag boulders on the platform with it. Three separate colluvial wedges suggest at least two earthquakes, but radiocarbon samples from all but the youngest unfaulted colluvium were carbon dead.

McInelly and Kelsey defined the Pioneer Anticline using the water wells that they could locate in the later 1980's to define the elevation of the wave cut platform. Development over the last few years has greatly increased the number of wells in the area, and offers an opportunity to revisit this problem with better data

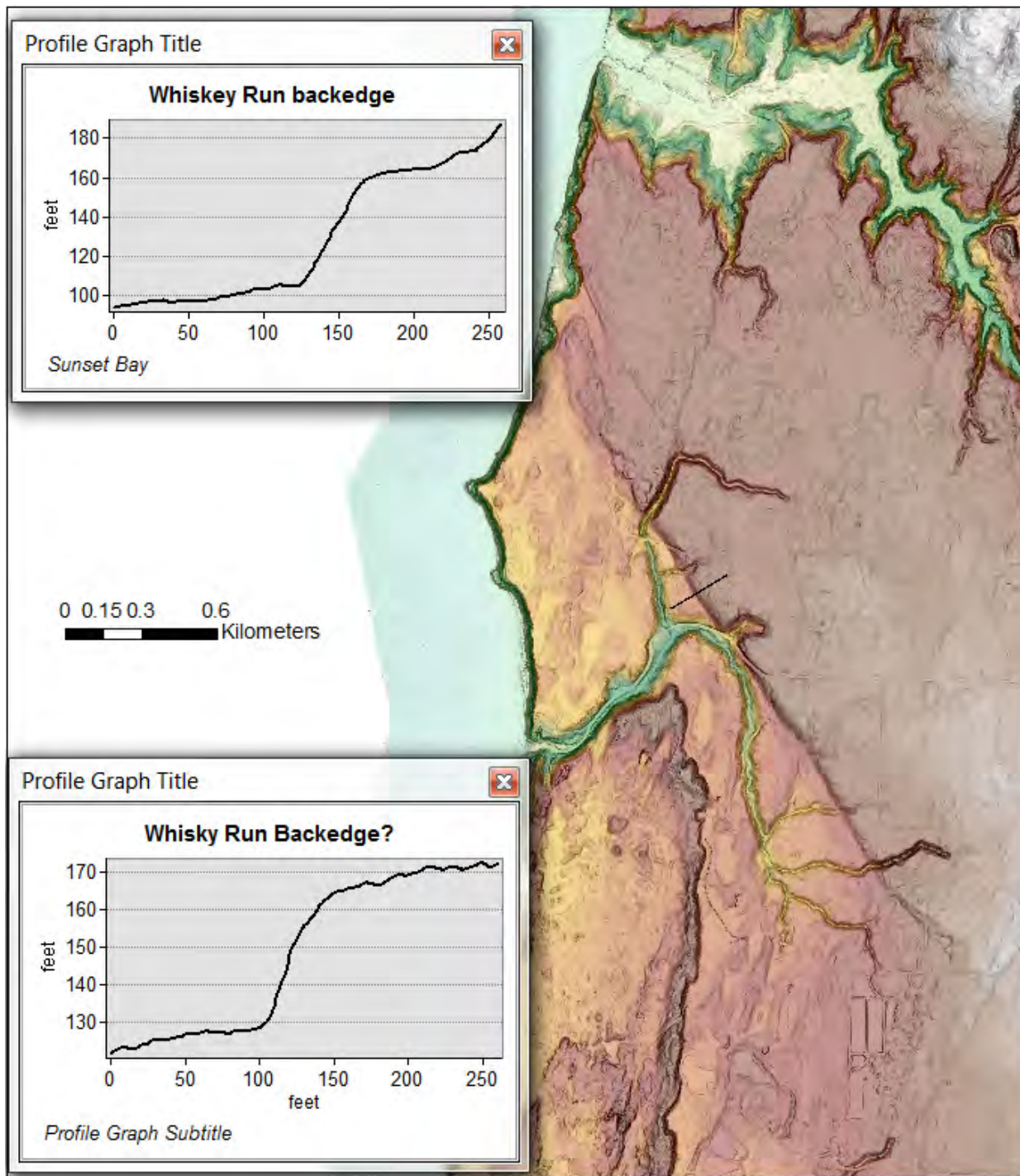


Figure 4-2. Whiskey Run backedge/fault?

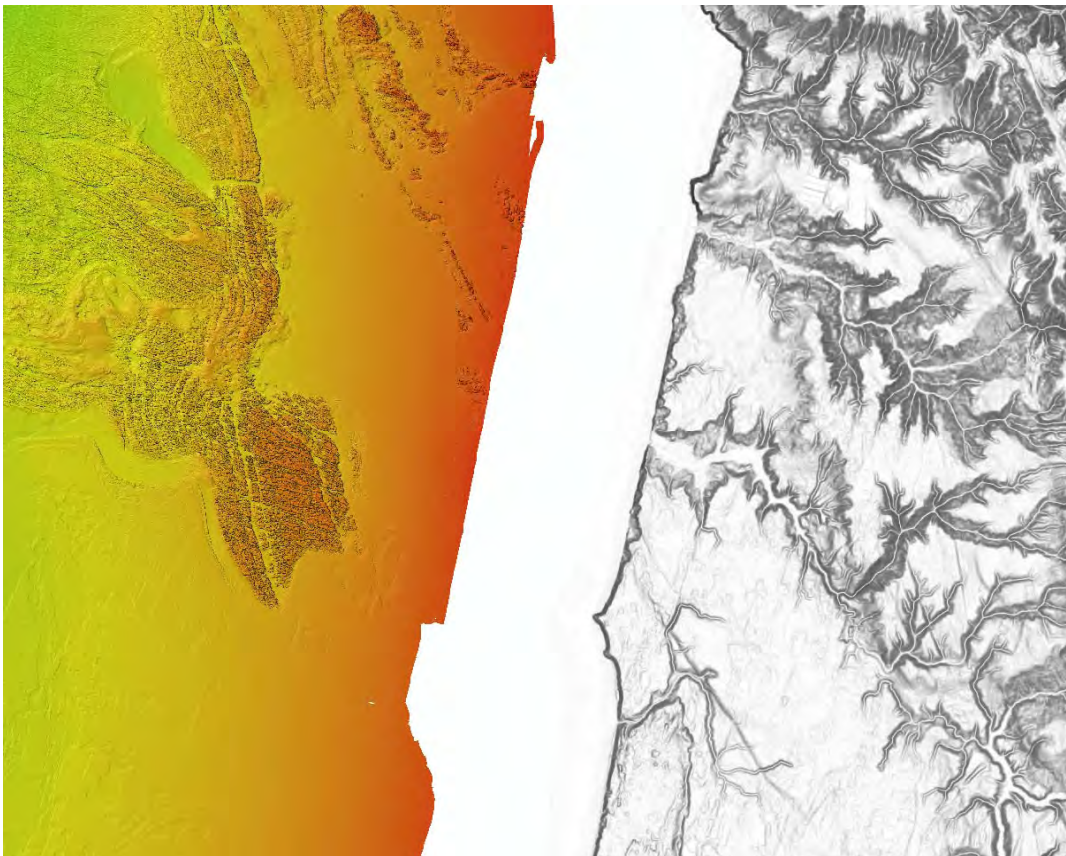


Figure 4-3. Lidar and high-res bathymetry

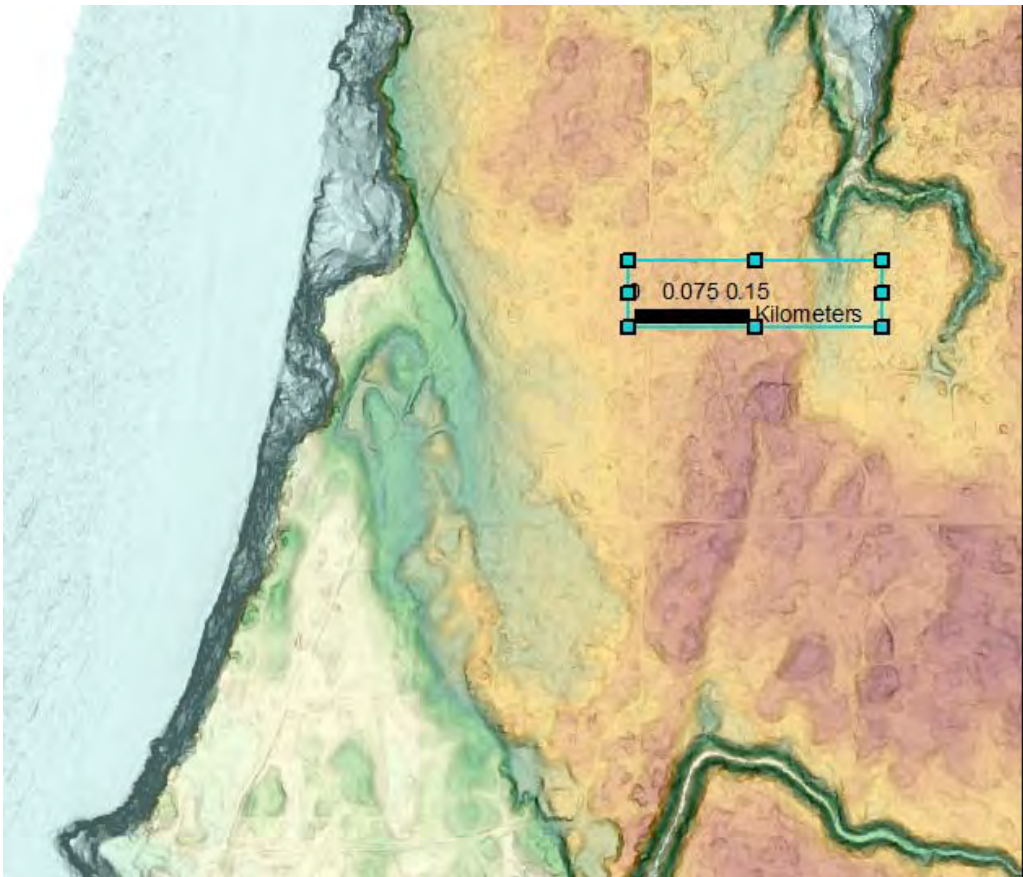


Figure 4-4. Detail of Whiskey Run backedge/scarp

Finally, a note about Whiskey Run. The name originated during the local gold rush in the late 1800's, when miners worked some placers in the marine terrace. Today, these same black sand placer deposits are being mined from the Seven Devils terrace just west of Whiskey Run by Oregon Resources Corporation. The primary product of the mine is refractory chromite for casting, but the black sands also contain ilmenite, garnet and minor gold and platinum. These minerals are absent in the local marine sedimentary rock, and are derived from the Jurassic accreted terrains to the south and southeast of here.

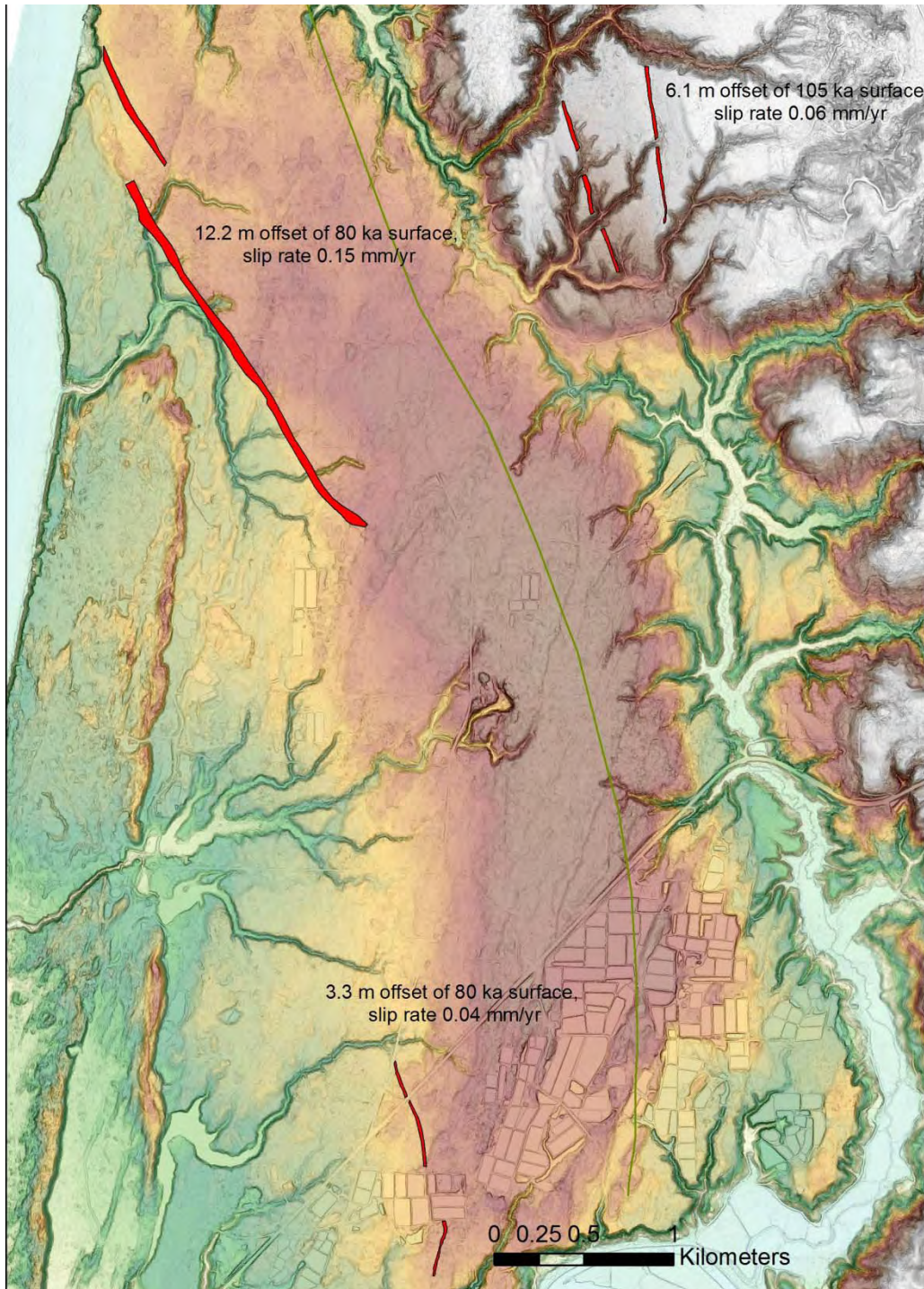
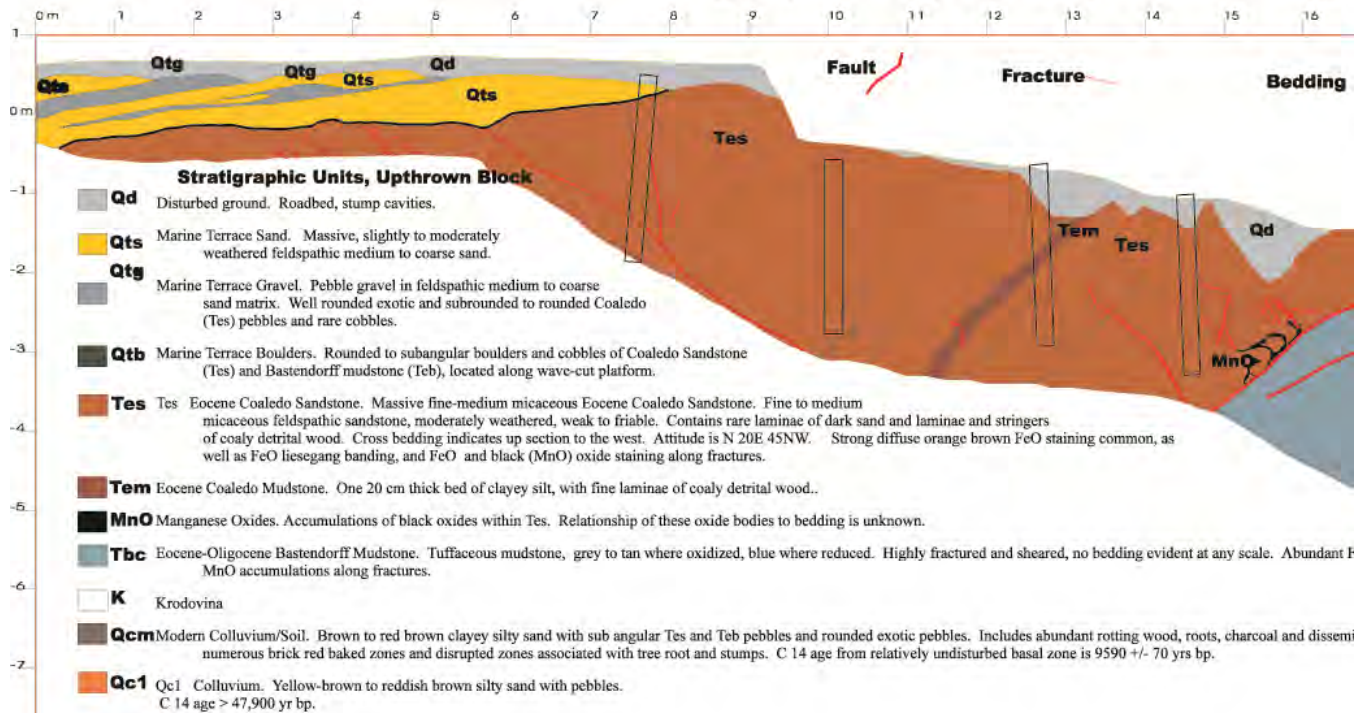


Figure 4-5. Scarps on the Pioneer Anticline

Winchester Fault Cox Canyon

N 85 W

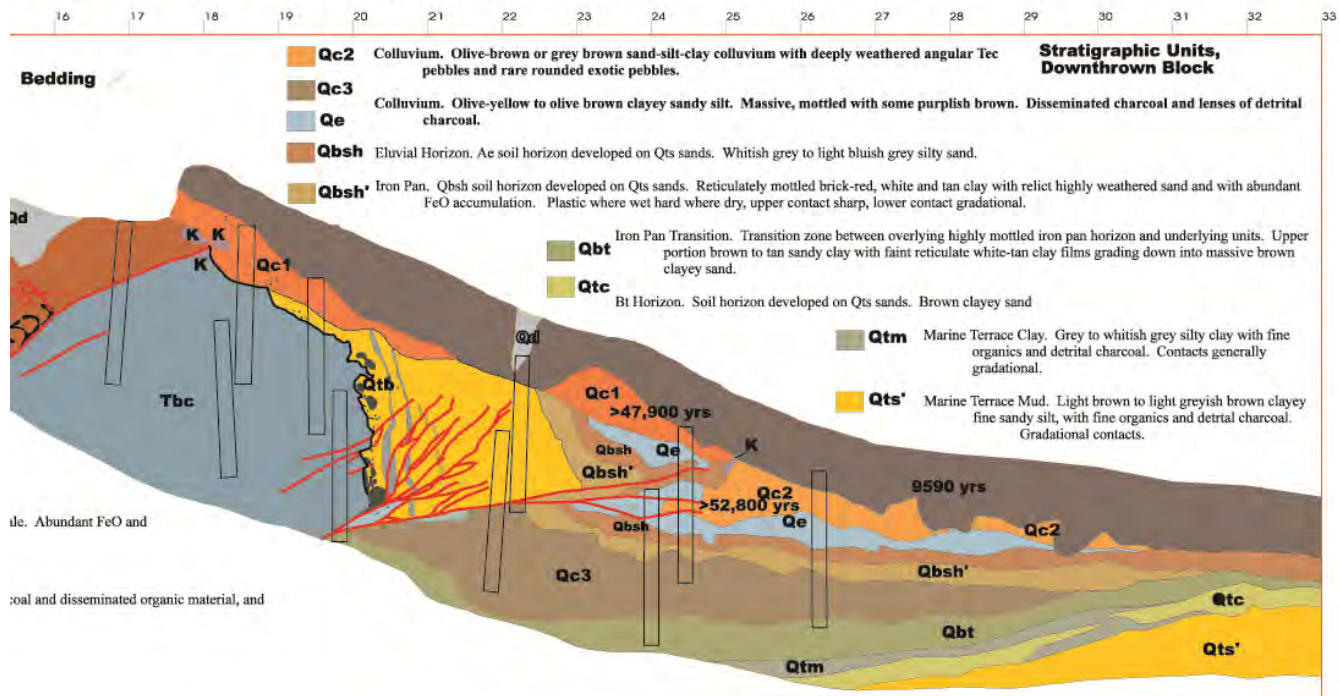
Logged September 1993 by Ian Madin (Oregon Department of Geology and Mineral Industries)



Canyon Scarp, Trench A, Coos County, Oregon

S 85

Geology and Mineral Industries) Mark Hemphill-Haley (University of Oregon) and Tim Roberts (Oregon State University)



Figure

4-6. Winchester Fault trench log.

GEOGRAPHIC AND GEOLOGIC SETTING

The coastal region of central Coos County, Oregon, is typically rugged, with a 1- to 4-km-wide (0.6 to 2.5 mi), wave-cut coastal bench that transitions abruptly into deeply incised, upland topography of uplifted marine terraces that ramp onto the Oregon Coast Range to the east. Topographic relief is moderate, ranging from sea-level to numerous ridges and mountains including, from south to north, Bill Peak (460 m [1,510 ft]), Grigsby Rock (412 m [1,352 ft]), Lampa Mountain (240 m [787 ft]), Schuck Mountain (293 m [962 ft]), Budd Mountain (136 m [447 ft]), Noble Hill (261 m [855 ft]), and Arago Peak (225 m [736 ft]) (Figure 1; map plates [note that elevations shown on map plates are lidar derived]). The Coast Range is drained in the map area by a number of west-flowing streams. Major stream drainages include Bear Creek, the Coquille River, Cunningham Creek, Beaver Creek, Sevenmile Creek, Whiskey Run, Twomile Creek, Threemile Creek, and Fivemile Creek. The rugged coastal relief is accompanied by a wet maritime climate (precipitation is ~188 cm/year [74 in/year]) and dense vegetation. Due to steep topography and thick, impenetrable forests, good outcrops of unaltered rock are generally limited to sea stacks, coastal bluffs, stream bottoms, roadcuts, and areas of active logging.

Bedrock geology along the central Coos County coast is composed of two complexly folded and faulted tectonostratigraphic terranes, the Sixes River and Siletz terranes, and a less deformed clastic overlap sequence. The two terranes record a history of oceanic and continental margin sedimentation, magmatism, and terrane accretion from the Late Jurassic into the Eocene (Dott, 1971; Roure and Blanchett, 1983; Blake and others, 1985; Diller, 1896, 1901, 1903). These terranes are now situated inboard of the active Cascadia subduction zone, where oceanic crust is presently being obliquely subducted beneath the North American continental plate (Figure 3). Jurassic to Eocene aged sedimentary rocks and mélangé (Hsü, 1968; Silver and Beutner, 1980; Cowan, 1985; Festa and others, 2010, 2012; Raymond, 1984) of the Sixes River terrane are in fault contact with Paleogene volcanic and sedimentary rocks of the Siletz terrane. South and east of the study area these two terranes are faulted against terranes of the Klamath Mountains province along the Canyonville fault to the south and unnamed thrust faults to the east. South of the Siletz terrane, six discrete terranes underlie the coastal area of southwestern Oregon (Blake and others, 1985) (Figure 4), all of which are separated by major faults or fault zones. Several of these fault zones are low-angle thrusts, so that the terrane assemblage represents stacks of subhorizontal

nappes. In addition to the Siletz and Sixes River terranes of the study area, terranes assembled nearby include the Gold Beach, Pickett Peak, Western Klamath (Elk subterrane), Snow Camp, and Yolla Bolly terranes (Blake and others, 1985; Giaramita and Harper, 2006). The terranes that lie south of the Canyonville fault are unconformably overlain by less deformed Upper Cretaceous and younger sedimentary sequences that constrain the minimum ages for terrane amalgamation.

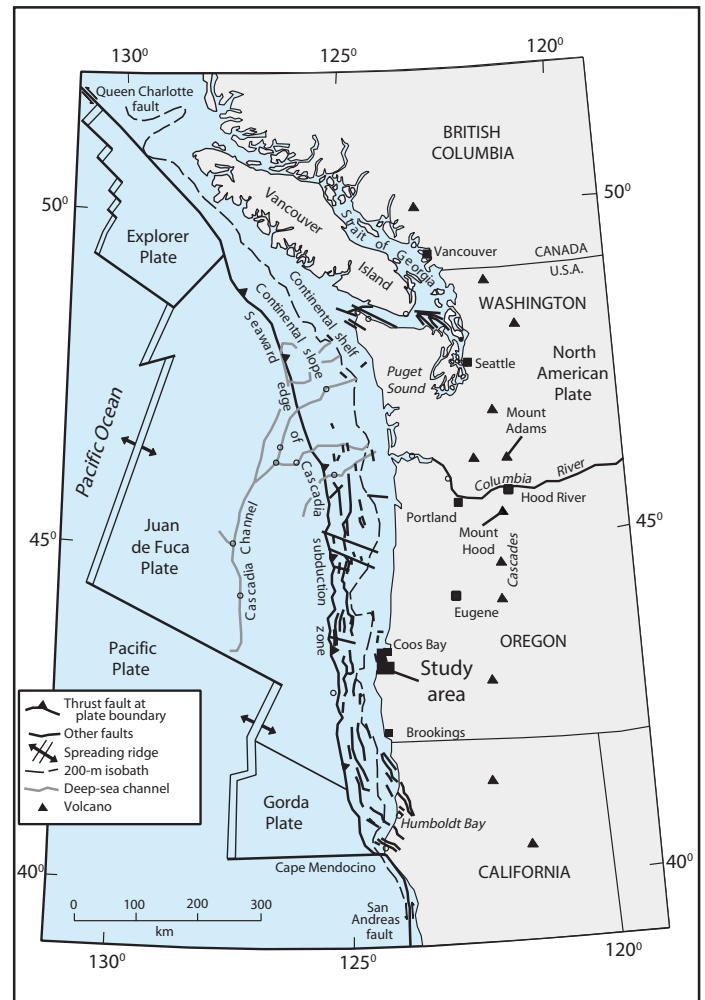


Figure 3. Tectonic setting of the United States Pacific Northwest region showing the Cascadia Subduction Zone and regional plate boundaries, selected Quaternary faults in the North American plate, and the location of the study area along the southern Oregon coast (modified from Nelson and others, 2004). The deformation front (barbed line) is defined by bathymetry where the abyssal plain meets the continental slope and is inferred to represent the surface projection of the Cascadia thrust fault. Triangles depict major Cascade Range volcanoes/

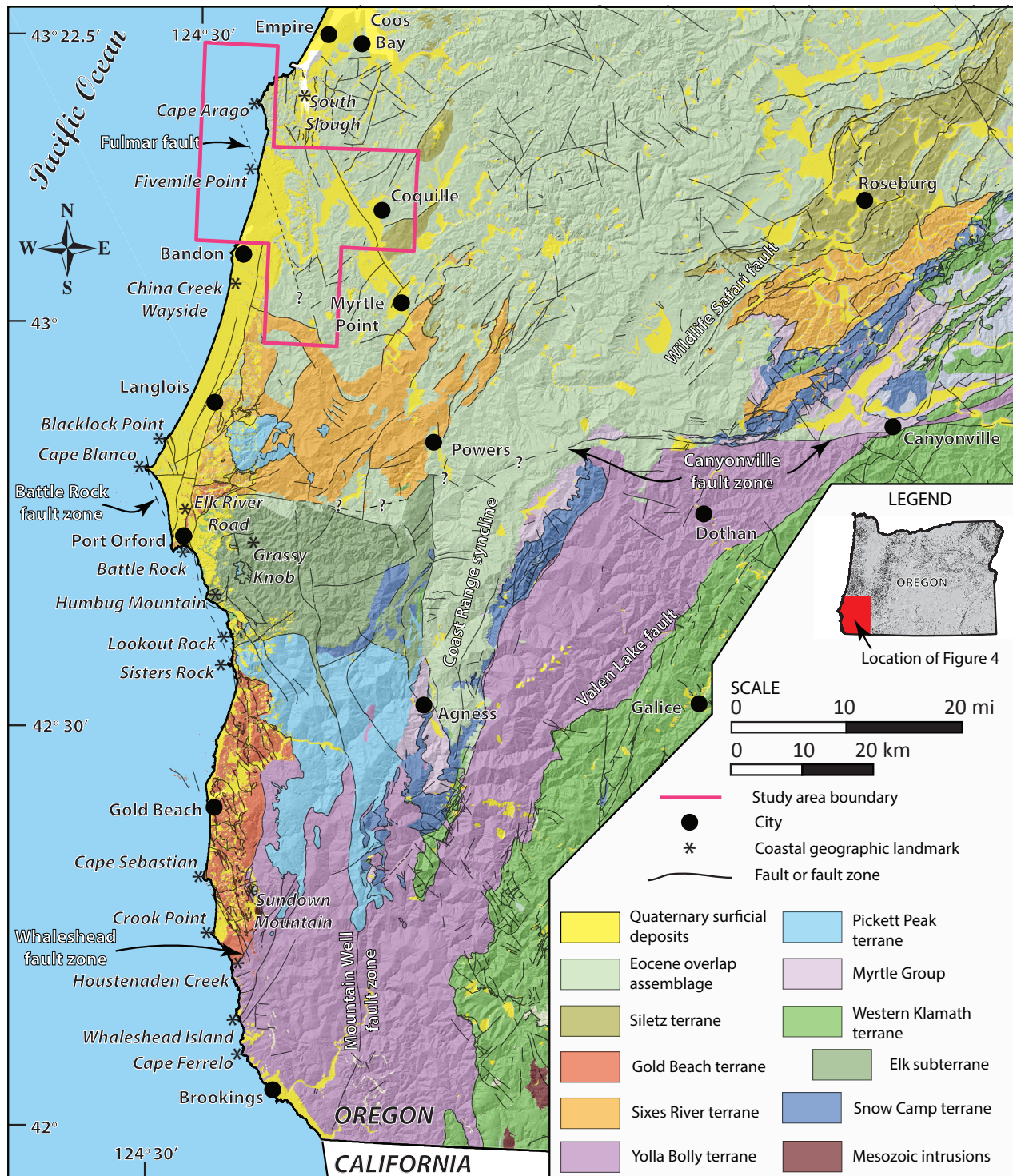


Figure 4. Tectonic sketch map showing tectonostratigraphic terranes of southwestern Oregon. Geology from Ma and others (2009) with terrane boundaries modified from Blake and others (1985). Magenta outline shows the study boundary of the geologic mapping discussed in this report.

Channel Change and Bed-Material Transport in the Umpqua River Basin, Oregon

By J. Rose Wallick, Jim E. O'Connor, Scott Anderson, Mackenzie Keith, Charles Cannon, and John C. Risley

Abstract

The Umpqua River drains 12,103 square kilometers of western Oregon; with headwaters in the Cascade Range, the river flows through portions of the Klamath Mountains and Oregon Coast Range before entering the Pacific Ocean. Above the head of tide, the Umpqua River, along with its major tributaries, the North and South Umpqua Rivers, flows on a mixed bedrock and alluvium bed, alternating between bedrock rapids and intermittent, shallow gravel bars composed of gravel to cobble-sized clasts. These bars have been a source of commercial aggregate since the mid-twentieth century. Below the head of tide, the Umpqua River contains large bars composed of mud and sand.

Motivated by ongoing permitting and aquatic habitat concerns related to in-stream gravel mining on the fluvial reaches, this study evaluated spatial and temporal trends in channel change and bed-material transport for 350 kilometers of river channel along the Umpqua, North Umpqua, and South Umpqua Rivers. The assessment produced (1) detailed mapping of the active channel, using aerial photographs and repeat surveys, and (2) a quantitative estimation of bed-material flux that drew upon detailed measurements of particle size and lithology, equations of transport capacity, and a sediment yield analysis.

Bed-material transport capacity estimates at 45 sites throughout the South Umpqua and main stem Umpqua Rivers for the period 1951–2008 result in wide-ranging transport capacity estimates, reflecting the difficulty of applying equations of bed-material transport to a supply-limited river. Median transport capacity values calculated from surface-based equations of bedload transport for each of the study reaches provide indications of maximum possible transport rates and range from 8,000 to 27,000 metric tons per year (tons/yr) for the South Umpqua River and 20,000 to 82,000 metric tons/yr for the main stem Umpqua River upstream of the head of tide; the North Umpqua River probably contributes little bed material. A plausible range of average annual transport rates for the South and main stem Umpqua Rivers, based on bedload transport capacity estimates for bars with reasonable values for reference shear stress, is between 500 and 20,000 metric tons/yr.

An empirical bed-material yield analysis predicts 20,000–50,000 metric tons/yr on the South Umpqua River and main stem Umpqua River through the Oregon Coast Range, decreasing to approximately 30,000 metric tons/yr at the head of tide. Surveys of individual mining sites in the South Umpqua River indicate minimum local bed-material flux rates that are typically less than 10,000 metric tons/yr but range up to 30,600 metric tons/yr in high-flow years.

On the basis of all of these analyses, actual bedload flux in most years is probably less than 25,000 metric tons/yr in the South Umpqua and main stem Umpqua Rivers, with the North Umpqua River probably contributing negligible amounts. For comparison, the estimated annual volume of commercial gravel extraction from the South Umpqua River between 2001 and 2004 ranged from 610 to 36,570 metric tons, indicating that historical in-stream gravel extraction may have been a substantial fraction of the overall bedload flux.

Introduction

The Umpqua River drains 12,103 km² of western Oregon before entering the Pacific Ocean at Winchester Bay near the town of Reedsport ([fig. 1](#)). For much of its length, the Umpqua River and its two main tributaries, the North Umpqua and South Umpqua Rivers, flow on a bed alternating between bedrock and coarse alluvium, locally flanked by gravel bars and sandy flood-plain deposits ([fig. 2](#)). The lowermost 40 km of the Umpqua River is tidally affected, where the low gradient river flows over a sand and gravel bottom flanked by muddy tidal flats and flood-plain deposits.

For the last several decades, some of these gravel bars and in-stream alluvial deposits, particularly along the South Umpqua River and main stem Umpqua River, have been mined for aggregate. Ongoing permitting actions have instigated questions of possible effects from such mining and other land-use activities on physical channel conditions (for example, Kondolf, 1994, 1997), prompting the U.S. Army Corps of Engineers (USACE), in conjunction with regulatory agencies and stakeholder groups, to request from the U.S. Geological Survey (USGS) an assessment of bed-material transport and changes in channel and gravel-bar conditions for the Umpqua River and alluvial reaches of the North and South Umpqua Rivers. This study incorporates and supersedes a 2009 reconnaissance study (O'Connor and others, 2009).

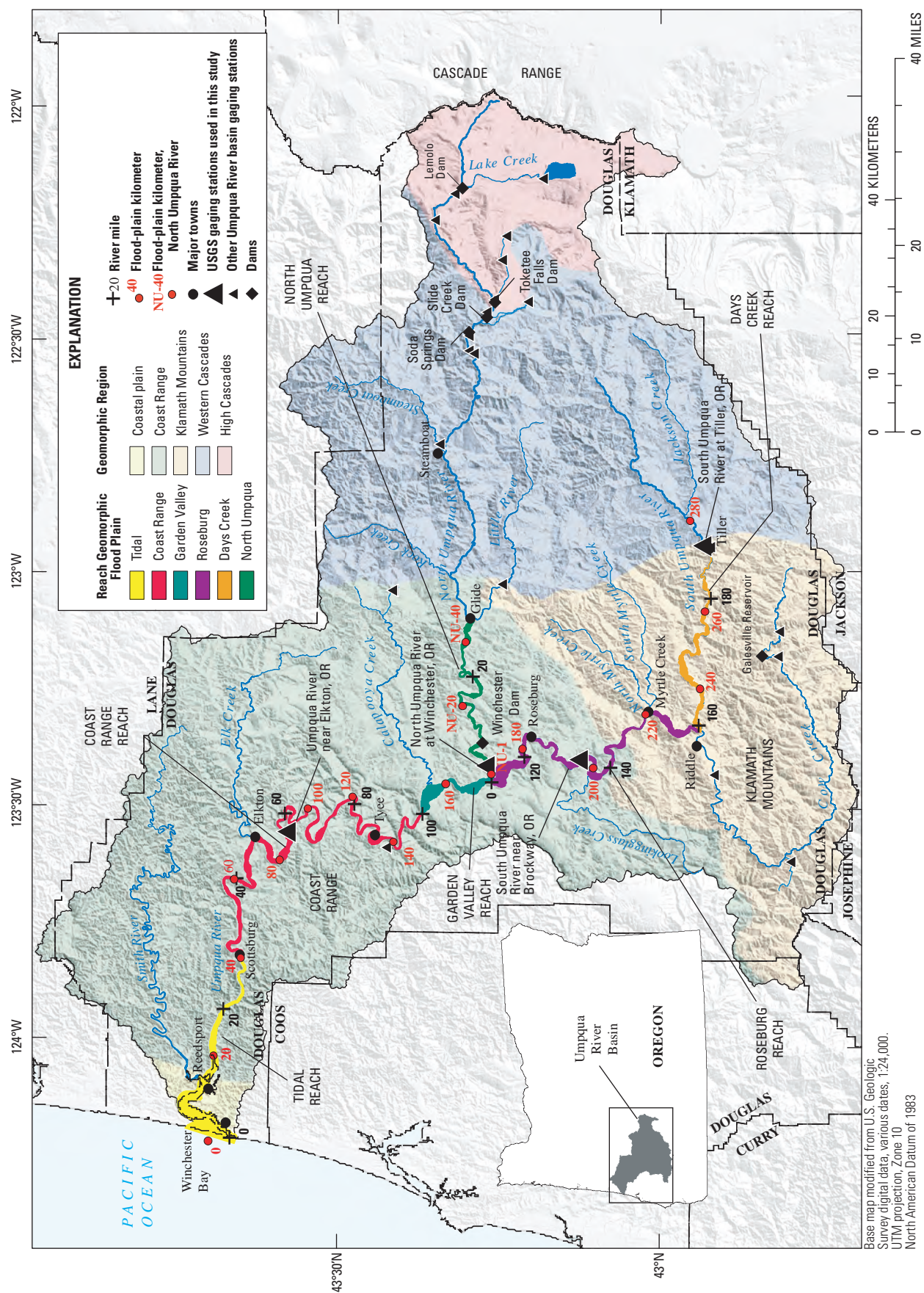


Figure 1. The Umpqua River, Oregon, drainage basin and study area. Reaches analyzed are defined by valley geomorphology and tributary junctions. Colored reach extents indicate the geomorphic flood plain. Topography based on U.S. Geological Survey 10-m digital elevation.

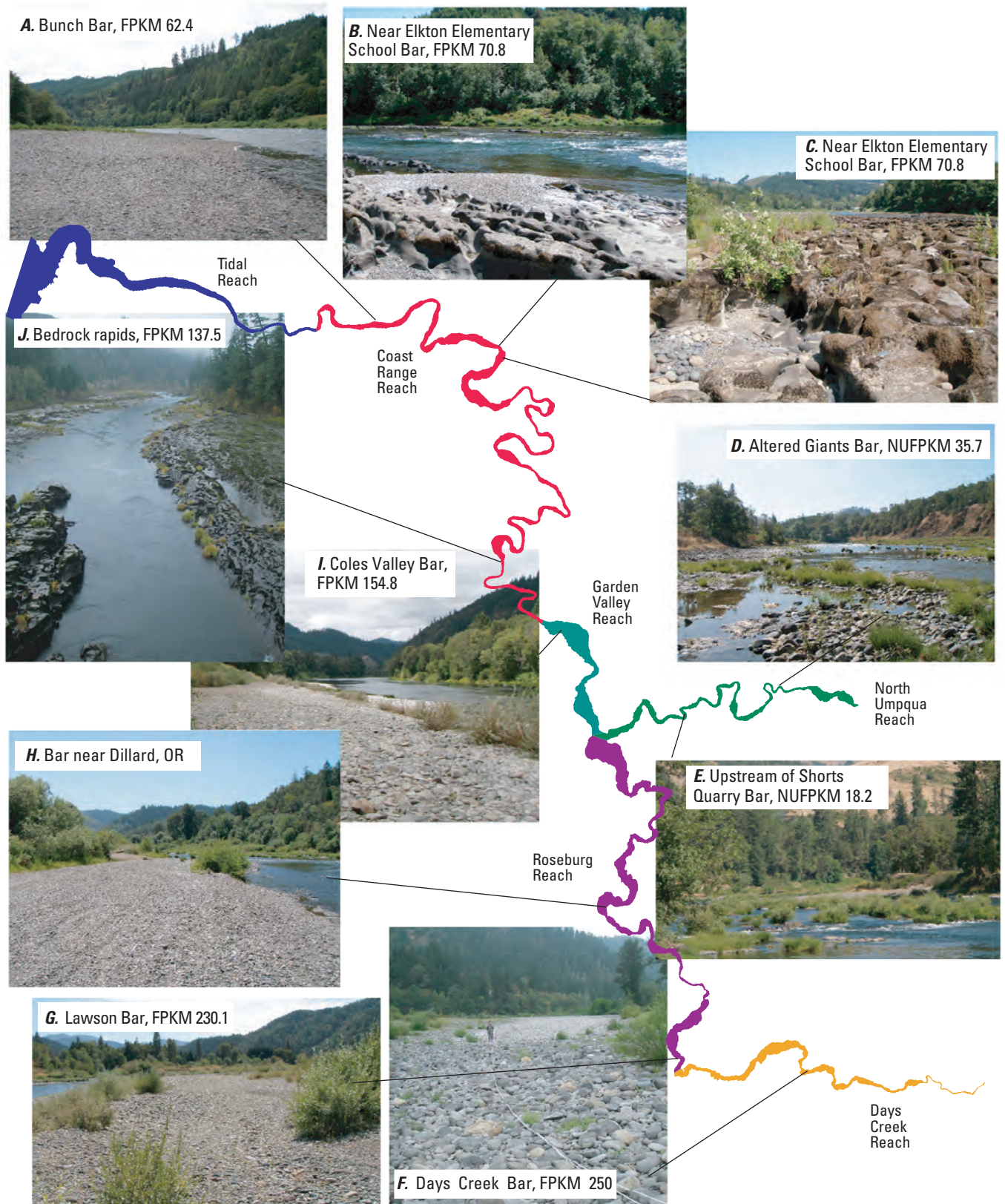


Figure 2. Gravel bars and bedrock outcrops in the Umpqua River, Oregon. Descriptions include flood-plain kilometer (FPKM) and North Umpqua River flood-plain kilometer (NUFPM).

Purpose and Scope

This report summarizes temporal trends of channel and gravel-bar area and provides estimates of sediment flux and sediment yield, with the goal of estimating temporal and spatial trends in bedload transport, deposition, and erosion in the main stem Umpqua River, as well as the semi-alluvial portions of the North Umpqua and South Umpqua Rivers. These analyses were based on mapping of the channel and flood plains from historical and current aerial photographs, sampling of bed-material size distributions, survey records from aggregate mining operations, sediment yield estimates derived from regional analyses, and site-specific sediment transport modeling. The detailed channel maps developed in this study can also be used in future analyses to detect changes in planform and bar morphology that may arise due to changes in sediment balances and transport. The scope of the study follows a process established in the State of Oregon to address permitting issues for in-channel gravel extraction.

Background

The natural resources of the Umpqua River basin are numerous, ranging from highly productive Douglas-fir forests in the upper basin, to ranches along the low-lying valleys, to coastal fisheries at its mouth. The basin also provides diverse habitats for aquatic and riparian species and supports populations of steelhead, coho salmon, and Chinook salmon, as well as Pacific lamprey and cutthroat trout (Geyer, 2003 a–d). Issues of fish habitat, water quality, and changing land-use laws, similar to other basins in the Western United States, have motivated new efforts to manage the Umpqua River and its tributaries for multiple resources.

In Oregon, rivers potentially subject to in-channel gravel extraction undergo a two-phase process of review and assessment by an interagency team co-chaired by the USACE and the Oregon Department of State Lands. The first phase is a preliminary assessment of “vertical stability” primarily based on available information. If Phase I analysis shows no clear evidence of adverse channel or flood-plain conditions, a Phase II analysis may be initiated to provide more information relevant to permitting decisions. For the Umpqua River, the Phase I assessment was completed by the USGS in 2009 (O’Connor and others, 2009). Among the findings from this preliminary assessment of gravel transport and historical changes to channel conditions was that the Umpqua River was in a “long-term (over time scales of thousands of years) state of incision” and that the extensive presence of in-channel bedrock indicated that the main stem Umpqua River was historically, and presently is, sediment supply limited—meaning that the transport capacity of the channel (the amount of sediment the channel could, theoretically, transport given its geomorphic and hydrologic characteristics) probably exceeds the volume of sediment entering the river system.

These findings prompted the interagency team to consider permitting of future in-stream gravel extraction subject to the completion of a more extensive Phase II analysis consisting of data acquisition and analysis aimed at:

1. Assessing planform changes to the Umpqua River, as well as the semi-alluvial portions of the North Umpqua and South Umpqua Rivers;
2. Determining spatial and temporal trends in bed-material flux; and
3. Evaluating linkages between sediment source areas in the upper basin and channel conditions along lower reaches of the main stem Umpqua River.

Locations and Reporting Units

Analyses and results are presented in SI (metric) units, except for bed-material flux values, which are presented in terms of mass in metric tons, which is equivalent to the SI unit megagram. Conversions to English units are provided in the report front matter. To convert between sediment mass and volume, we used an in situ bulk density value of 2.1 metric tons/m³ on the basis of measurements conducted by Milhous (2001) and reported in Bunte and Abt (2001).

Locations along the channel are referenced to river kilometers (RKM) measured along the channel centerline from the mouth of the Umpqua River and continuing upstream along the South Umpqua River, as mapped from orthoimagery acquired in summer 2005 by the National Agriculture Inventory Program (NAIP). These distances do not correspond exactly with river miles (RM) shown on current USGS quadrangle maps. Measured from the same orthoimagery, river kilometers for the North Umpqua River (NURKM) begin at the confluence of the North Umpqua and South Umpqua Rivers, and continue upstream along the centerline of the North Umpqua River.

To avoid ambiguity due to channel shifting, locations and analyses for the study area are referenced to a flood-plain kilometer (FPM) centerline, measured from the river mouth along the centerline of the Holocene flood plain upstream along the main stem Umpqua and South Umpqua Rivers ([fig. 1](#)). This flood-plain reference frame provides a static template from which to consider temporal changes in channel morphology and is not intended for use as a regulatory or flood-hazard tool. In 2005, approximately 179.5 km of river channel lay along 169 km of the main stem Umpqua River flood plain and 123.4 km of river channel were within 106 km of flood plain flanking the South Umpqua River. The North Umpqua flood-plain kilometer (NUFPM) centerline begins at the mouth of the North Umpqua and extends 45 km along the North Umpqua River valley bottom, containing 47 km of river channel in 2005.

Prominent landmarks and locations along the main stem Umpqua River include the mouth of Umpqua River near Winchester Bay FPKM 0 (RKM 0), the head of tide near Scottsburg at FPKM 40 (RKM 44), and the confluence of the North Umpqua and South Umpqua Rivers FPKM 169 (RKM 179.4). Major landmarks on the South Umpqua River include the city of Roseburg at FPKM 182 (RKM 197), and the mouth of Cow Creek at FPKM 230.9 (RKM 256). On the North Umpqua River, Winchester Dam is located at NUFPM 10.2 (NURKM 11.3). Numerous gravel bars are referenced in this report, some of which have place names derived from USGS topographic maps and gravel mining permits, whereas others were assigned informal names during this study using nearby place names.

The Umpqua River

The Umpqua River drains 12,103 km² of western Oregon, heading in the Cascade Range and Klamath Mountains before traversing the Coast Range and entering the Pacific Ocean through Winchester Bay at Reedsport (fig. 1). The Umpqua River begins 179 km from its mouth at the confluence of the

North and South Umpqua Rivers near the city of Roseburg. The main tributaries of the main stem Umpqua River and their drainage areas are the Smith River (961 km²), Elk Creek (756 km²), and the Calapooya Creek (637 km²) (figs. 1 and 3).

The North Umpqua River drains 3,520 km², with headwaters in the High Cascades. Major tributaries and their drainage areas include the Little River (533 km²) and Steamboat Creek (425 km²), both located upstream of the study area. The upper North Umpqua River is noteworthy for its scenery and native fish populations, with approximately 55 km of the channel between Soda Springs Powerhouse and Rock Creek designated as a Wild and Scenic River. The South Umpqua River drains the northern Klamath Mountains and part of the Western Cascades. At its confluence with the North Umpqua River, the South Umpqua River has a drainage area of 4,665 km². The main tributaries in the study area and their drainage areas are Lookingglass Creek (417 km²), Myrtle Creek (308 km²), Cow Creek (1,292 km²), and Jackson Creek (490 km²) (figs. 1 and 3).

The Umpqua River basin contains two federally designated wilderness areas, the Boulder Creek Wilderness in the North Umpqua River subbasin, and the Rogue–Umpqua Divide Wilderness in the South Umpqua River subbasin.

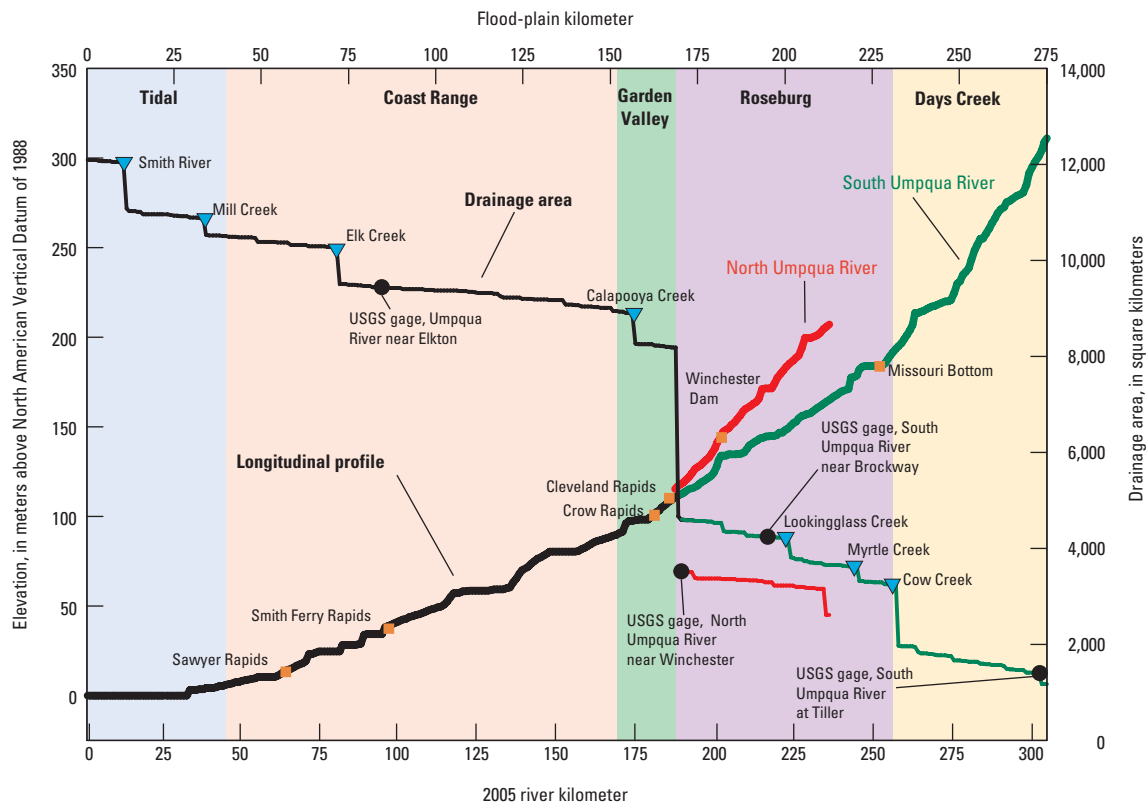


Figure 3. Longitudinal profile and cumulative drainage area of the Umpqua River basin, Oregon.

Geography and Geology

The drainage basin is flanked to the north by the Siuslaw and Willamette River basins, to the east by the Deschutes and Klamath River drainages, and to the south by the Rogue and Coquille River basins. The basin has its headwaters in the Cascade Range, is bounded on the south by the Klamath Mountains, and transects the Coast Range before entering the Pacific Ocean ([fig. 1](#)).

The Umpqua River basin can be divided into five distinctive geomorphic provinces ([fig. 1](#)), each of which has a unique physiography. The North Umpqua River originates in the predominantly low-relief High Cascades province, where highly permeable Pliocene and Quaternary lava flows result in low rates of surface-water runoff and sediment transport (Jefferson and others, 2010).

Downstream of the High Cascades province, the North Umpqua River drains parts of the steeply dissected Western Cascades province, where the South Umpqua River has its headwaters. The weathered Tertiary volcanic rocks of the Western Cascades support higher rates of runoff and erosion than the High Cascades terrain, and mass wasting processes are a dominant mechanism of hillslope sediment production (Stillwater Sciences, 2000).

Downstream of the Western Cascades province, the South Umpqua River enters the Klamath Mountains province near Tiller at FPKM 281. The rugged terrain of the Klamath Mountains is underlain by a Cretaceous and Jurassic accretionary complex composed of weakly to intensely metamorphosed sedimentary, volcanic, and intrusive igneous rocks, primarily of Early Cretaceous and Jurassic age (Ramp, 1972; Wells and others, 2001). The Klamath Mountains are the source of several gravel-rich rivers in southern Oregon and northern California, including the Chetco and Smith Rivers (Wallick and others, 2010; MFG, Inc. and others, 2006).

The South Umpqua River leaves the Klamath Mountains and enters the Paleocene and Eocene marine volcanic sedimentary rocks of the Coast Range province at about FPKM 200. Similarly, the North Umpqua River leaves the Western Cascades at NUFPM 45 and enters the Coast Range province. Both rivers first flow through the predominantly volcanic rocks of the Siletz River Volcanics before entering the soft sandstones and siltstones of the Umpqua Group near their confluence at FPKM 170 (Wells and others, 2001). From there, the Umpqua River meanders northwestward for about 20 km through Coles and Garden Valleys before bisecting the higher portion of the Coast Range within a narrow valley

trending northwest for 145 km. For this stretch, the river follows large meanders primarily incised into soft marine sediment of the Tyee and Elkton Formations (Ramp, 1972). Approximately 16 km from its mouth, the lower Umpqua River exits the Coast Range and flows through a coastal plain to the Pacific Ocean.

The main stem Umpqua River is locally flanked by flood-plain and terrace deposits within its entrenched meandering course through the Coast Range (Personius, 1993; Personius and others, 2003), reflecting episodes of river aggradation in conjunction with overall incision of the river during the Quaternary period. The youngest terrace, forming a surface 2–15 m above river level, is apparently associated with a period of enhanced gravel transport and channel aggradation about 10,000 years before present (Personius, 1993; Personius and others, 2003), although this surface is locally capped by younger deposits and probably was inundated by a large flood in December 1964. This episode of aggradation broadly correlates with aggradation of several Cascade Range rivers draining into the Willamette River valley (O'Connor and others, 2001; Wampler, 2004). Even higher surfaces are locally preserved, including some reaching 200 m above the present river level. One such surface at FPKM 70 is 41 m above present river level and has a thermoluminescence age of 116 ± 20 thousand years ago (ka) (Personius, 1993; Personius and others, 2003), indicating a long-term valley incision rate of 0.3 to 0.4 mm/yr.

The lower Umpqua River valley, particularly along the lowermost 40 km, has been strongly affected by the 130 m of sea-level rise after the culmination of the last maximum glacial period 18,000 years ago. Along the Oregon coast, rising sea levels have flooded river valleys incised during low stands of sea level, creating estuaries now extending inland from the coast. This is the case for the Umpqua River, as well as for the Smith River, which joins the Umpqua River at FPKM 14 and is tidally affected for its lower 40 km (Personius, 1993). With the onset of sea-level rise, and especially during the last 2,000 years of relatively stable sea level, these estuarine reaches have been filling with fluvial sediment (Komar, 1997, p. 30–32), but for rivers such as the Umpqua and Smith Rivers, the low gradient ([fig. 3](#)) and far upstream propagation of tidal influence indicates that the sediment supply has not matched Holocene sea-level rise and that these rivers have not yet attained a graded profile to the coast. Because of the low gradients in the downstream reaches of the Umpqua and Smith Rivers, coarse bed material probably is not transported through these reaches to the Pacific Ocean.

Hydrology

Information on basin hydrology derives from USGS streamflow-measurement records in the basin extending discontinuously back to 1905. Many of these data are available from the USGS (U.S. Geological Survey, 2010b), with some synthesis provided by Jones and Stearns (1930). The mean annual flow of the Umpqua River near Elkton at FPKM 84.7 for 1955–2004 is $210 \text{ m}^3/\text{s}$, which closely corresponds to the combined mean flows for the North Umpqua River at Winchester (NUFPKM 2.5; $106 \text{ m}^3/\text{s}$), and the South Umpqua River near Brockway (FPKM 195.3, $78 \text{ m}^3/\text{s}$) for the same period ([fig. 4](#), [table 1](#)). Despite a contributing area 25 percent smaller than the South Umpqua River, the North Umpqua River supplies more than 50 percent of the water at Elkton (compared to 37 percent provided by the South Umpqua River), primarily because of a greater area of high-elevation terrain subject to orographically enhanced precipitation ([fig. 1](#), [table 1](#)). This high terrain, associated with Quaternary volcanic rocks of the High Cascades province, also explains the much lower intra-annual flow variability of the North Umpqua River, where the mean January flow is only 6.7 times that of August. By contrast, the mean January flow for the South Umpqua River is 57 times greater than the mean August flow. The young volcanic uplands of the North Umpqua River headwaters have poorly integrated surface drainage networks and host large-volume groundwater systems, resulting in attenuated surface runoff and large spring complexes that maintain relatively high and steady summer flows. By contrast, the more dissected and older rocks of the Western Cascades and Klamath Mountains terrains underlying much of the South Umpqua River headwaters generate flows that more quickly respond to episodes of precipitation and drought (Jones and Stearns, 1930).

Peak flows in the Umpqua River basin typically derive from winter frontal systems, with the largest flows resulting from regional rain-on-snow events. The peak of record for the South Umpqua, North Umpqua, and main stem Umpqua Rivers was in late December 1964, when $7,505 \text{ m}^3/\text{s}$ was reported for the main stem near Elkton, and 4,250 and $3,540 \text{ m}^3/\text{s}$ were reported for the North Umpqua River at Winchester and South Umpqua River near Brockway, respectively ([table 1](#)). The December 1964 flood probably was the largest since the rain-on-snow flood of 1861. The 2-year recurrence-interval flow is about $1,256 \text{ m}^3/\text{s}$ for the North Umpqua River near Winchester, $1,292 \text{ m}^3/\text{s}$ for the South Umpqua River at Brockway, and $2,660 \text{ m}^3/\text{s}$ for the main stem Umpqua River at Elkton ([table 1](#)).

At least two smaller episodes of widespread flooding have occurred in recent decades. From November 1996 through January 1997, a series of storms caused extensive regional flooding, resulting in three distinct periods of high flows in the Umpqua River basin ([fig. 4](#)). Most stream gages in the South Umpqua River basin, as well as the Elkton gage on the Umpqua River, had their highest flows during December 4–9, 1996, but the largest flows for the North Umpqua gages were about 2 weeks earlier on November 18, 1996 ([table 1](#); Risley, 2004). Heavy rains in late December 1996 led to a third period of high flows during January 1–2, 1997. These high flows triggered numerous landslides, but the discharges for this flood were lower than for the November and December 1996 floods (Risley, 2004). The peak discharges for the November–December 1996 floods ranged from 5- to 10-year recurrence-interval flows at most sites, except for the Tiller gage on the South Umpqua River, where discharge was approximately similar to the 30-year recurrence interval event ([table 1](#), [fig. 5](#)). A flood peaking on December 31, 2005, and continuing into early January 2006, was similar in magnitude to peak flows from the winter of 1996–97 ([table 1](#)).

Since the early 1950s, flow has been regulated by Pacific Power hydroelectric projects on the North Umpqua River, which include eight developments in the upper basin ([fig. 1](#)). These dams only minimally affect peak flows because they have limited storage, and much of their contributing area lies in the groundwater-dominated High Cascades terrain (Stillwater Sciences, 1998). For example, within the bypass reaches of these hydroelectric dams, the 1.5-year recurrence interval flood has been reduced by 15–30 percent, but larger floods (greater than 5-year recurrence interval) are unchanged (Stillwater Sciences, 1998).

In the South Umpqua River basin, Galesville Reservoir was constructed in the upper Cow Creek basin in 1985 to reduce flooding along the lower reaches of Cow Creek. Although Galesville Reservoir almost certainly has a pronounced effect on peak flows on Cow Creek, peak flows farther downstream on the South Umpqua River near Brockway did not show a marked decline following dam construction ([fig. 5](#)). It is unlikely that either Galesville Reservoir or the North Umpqua hydroelectric dams strongly influence peak flows as far downstream as the USGS gage near Elkton on the Umpqua River because they control only a small portion of the total drainage-area runoff at this gage ([fig. 3](#)).

Description of Study Area

The study area encompasses the downstream semi-alluvial sections of the North Umpqua and South Umpqua Rivers and the entire main stem Umpqua River ([fig. 1](#), [table 3](#)). For both the North and South Umpqua Rivers, the semi-alluvial sections begin where the rivers exit the mountainous headwaters, widen, and flow on a mixed bed of bedrock and alluvium flanked by variable widths of flood plain and terraces. For the North Umpqua River, this transition to a dominantly alluvial character approximately corresponds with the confluence of the Little River at NUFPM 44.8 (flood-plain kilometers for the North Umpqua River are measured with respect to the confluence with the South Umpqua River). Downstream of the Little River confluence, the North Umpqua River generally is 60–85 m wide and flows on a bed of sandstone and basalt, locally mantled by thin accumulations of sand and gravel. The average gradient from the Little River confluence to the confluence with the South Umpqua River is 0.00177 ([table 3](#)). In this reach, the North Umpqua River is flanked by a valley bottom typically less than 0.8 km wide formed of recent flood-plain deposits and small terrace remnants.

For the South Umpqua River, the confluence of Jackson Creek at FPKM 280.9 near Tiller approximately marks the transition from a confined mountain stream to a mixed alluvial and bedrock channel locally flanked by active gravel bars, flood-plain surfaces, and terraces. Between the junction of Jackson and Cow Creeks, the South Umpqua River flows generally westward with an average gradient of 0.00249 ([table 3](#)) and a width typically less than 45 m. In this reach, the valley alternates between confined canyon reaches and sections as wide as 1.6 km. Wider sections contain channel flanking gravel bars, flood plains, tributary fans, and terrace deposits. With the confluence of Cow Creek at FPKM 230.9, the drainage area of the South Umpqua River increases by about one-third and the channel widens to 60–120 m ([fig. 3](#)) as the river flows generally northward on an alternating bed of bedrock and alluvium for 76 km to the junction with the North Umpqua River. Within this reach, the average gradient is 0.001 as the South Umpqua River winds through canyons alternating with valleys as wide as 3.5 km, and is locally flanked by gravel bars, flood plains, and terraces. The channel widens, and the number of gravel bars decreases for the 19 km of the main stem Umpqua River downstream of the confluence of the North Umpqua and South Umpqua Rivers. From FPKM 152 to about FPKM 40, the river flows within deep and narrow

meanders incised through the Coast Range, with narrow flanking flood plains and terraces almost everywhere less than 0.8 km wide. The channel in this reach typically is 85–170 m wide and consists of long pools separated by bedrock rapids; the average gradient between FPKM 152 and the head of tide at FPKM 40 is 0.00073 ([table 3](#)). From FPKM 40 to the mouth, the Umpqua River progressively widens and is flanked by low flood plains, tidal marshes, and sand bars, especially downstream of the mouth of the Smith River at FPKM 14.

The overall physical setting, as well as the distribution of in-stream gravel-mining permits (Jo Ann Miles and Robert Lobdell, Oregon Department of State Lands, written commun., 2008), lends itself to delineation of valley reaches to help organize sediment-related issues, analyses, and findings ([fig. 1](#), [table 3](#)). These reaches are, from downstream to upstream:

1. Tidal reach ([fig. 6](#)), between FPKM 0 and approximately 40, distinguished by tidal influence, low gradients, expansive sediment deposits, and historical sand and gravel removal for navigation and commercial aggregate;
2. Coast Range reach ([fig. 7](#)), between approximately FPKM 40 and 152, characterized by a confined valley with bedrock channel and few gravel deposits;
3. Garden Valley reach ([fig. 8](#)) of broad valleys, between where the Umpqua River enters the Coast Range at FPKM 152 and the confluence of the South Umpqua and North Umpqua Rivers at approximately FPKM 169, a relatively short reach with several historically mined gravel bars;
4. Roseburg reach ([fig. 9](#)) of the South Umpqua River, between the confluence with the North Umpqua River (FPKM 169) and the Cow Creek confluence at FPKM 231, where there are abundant gravel bars and several recently active in-stream gravel mining operations;
5. Days Creek reach of the South Umpqua River ([fig. 10](#)), between the Cow Creek confluence at approximately FPKM 231 and 275, which constitutes the uppermost semi-alluvial reach of the South Umpqua River; and
6. North Umpqua reach of the North Umpqua River ([fig. 11](#)) between NUFPM 0 and the Little River confluence at NUFPM 45, a reach locally flanked by alluvial deposits but with no recent in-stream gravel mining.

Table 3. Geomorphic and channel characteristics for reaches in the Umpqua River basin, Oregon.

[Abbreviations: FPKM, flood-plain kilometer; km², square kilometer; m, meter; m², square meter, m²/m, meter squared per meter; m³/s, cubic meter per second]

Attribute	Reach					
	Tidal	Coast Range	Garden Valley	Roseburg	Days Creek	North Umpqua
Position	FPKM 0–40	FPKM 40–152	FPKM 152–168.5	FPKM 168.5–231	FPKM 231–274.5	FPKM 0–44.5
Reach definition	Tidally affected	Confined valley, bedrock channel	Unconfined below North and South Umpqua River confluence	Cow Creek confluence to North Umpqua River confluence	Downstream of Jackson Creek confluence to Cow Creek confluence	Little River confluence to South Umpqua River confluence
General valley setting	Estuary, confined valley opening to bay within coastal plain	Confined valley with local valley widenings	Unconfined	Alternating confined and unconfined	Alternating confined and unconfined	Alternating confined and unconfined
General channel character	Low gradient, sand and gravel bed	Steep, bedrock rapids separated by flats	Alternating bedrock and gravel	Alternating bedrock and gravel	Alternating bedrock and gravel	Bedrock dominant, pool and drop
Drainage area at downstream end of segment (km ²)	12,102	10,492	8,904	4,666	1,962	3,522
Drainage area at upstream end of segment (km ²)	10,492	8,904	8,188	3,254	1,127	3,151
Average gradient	0.00012	0.00073	0.00098	0.00100	0.00249	0.00177
Unit bar area 2005 (m ² /m) ¹	114.5	5.1	5.0	13.6	17.6	6.7
Total area of gravel bars in 2005 (m ²)	3,837,380	593,360	93,093	1,030,751	835,873	317,358
Total area of bedrock in 2005 (m ²)	1,337	3,122,615	266,223	488,550	146,882	1,213,280
Total area of channel (secondary channel features) in 2005 (m ²)	16,576,148 (346,575)	11,672,878 (170,575)	1,668,568 (1,848)	4,297,485 (73,742)	1,536,393 (37,687)	3,358,262 (86,977)
0.5 annual exceedance probability discharge (m ³ /s) ²	³ 2,660	³ 2,660	³ 2,660	⁴ 1,292	⁵ 481	⁶ 1,256
Figures showing channel morphology	1, 6, 33	1, 2, 7, 16, 22, 23	1, 2, 8	1, 2, 9, 16, 22, 23	1, 2, 10, 16, 22, 23	1, 2, 11, 16, 28

¹2005 mapped bar area divided by reach centerline.

²Following Bulletin 17-B guidelines for gage record through water year 2008.

³U.S. Geological Survey streamflow-gaging station on Umpqua River at Elkton.

⁴U.S. Geological Survey streamflow-gaging station on South Umpqua River near Brockway.

⁵U.S. Geological Survey streamflow-gaging station on South Umpqua River at Tiller.

⁶U.S. Geological Survey streamflow-gaging station on North Umpqua River at Winchester.

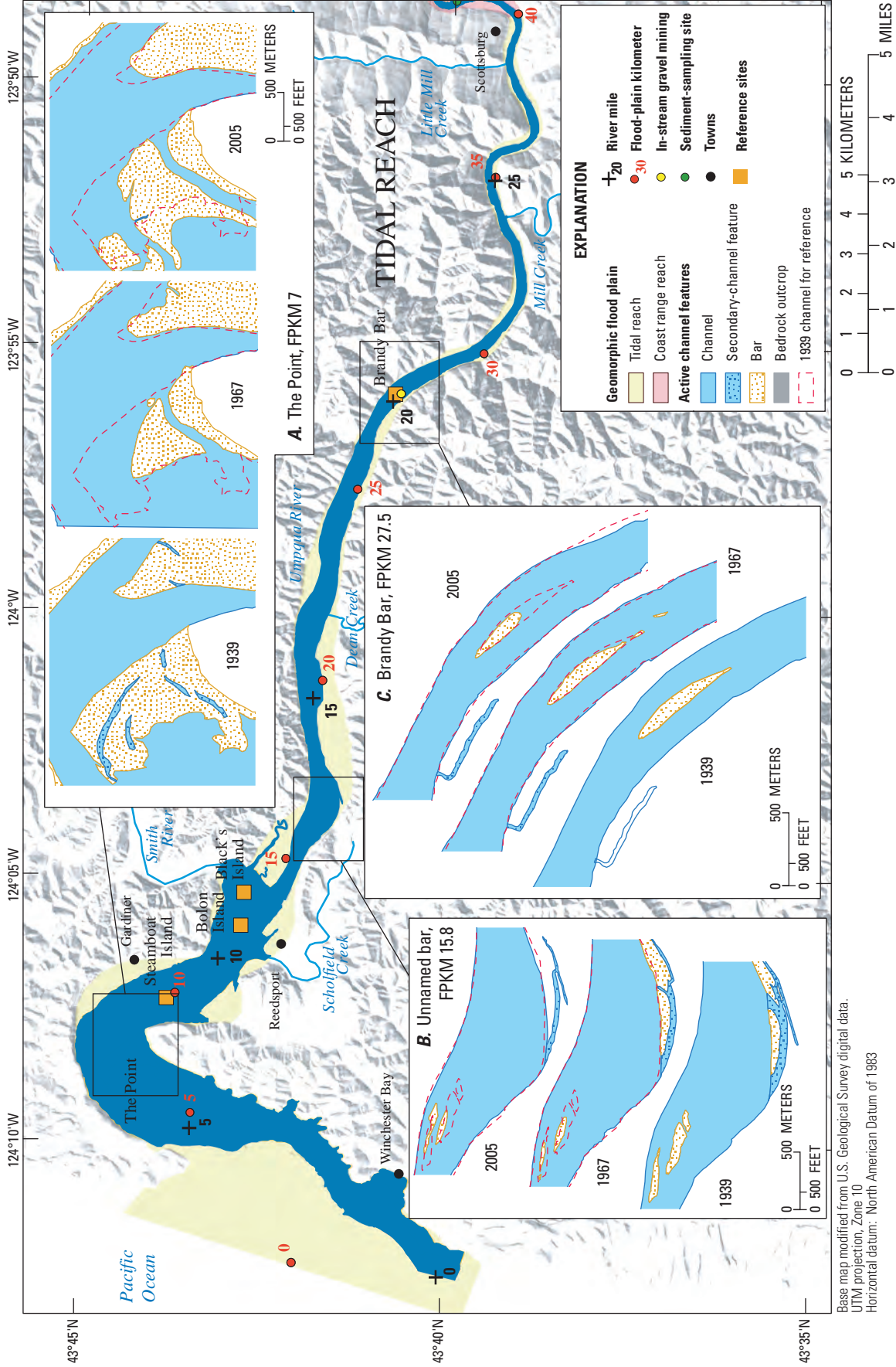


Figure 6. Channel planform in the Tidal reach of the Umpqua River, Oregon. Insets show historical changes to selected bars, as mapped from aerial photographs. Topography based on U.S. Geological Survey 10-meter digital elevation data.

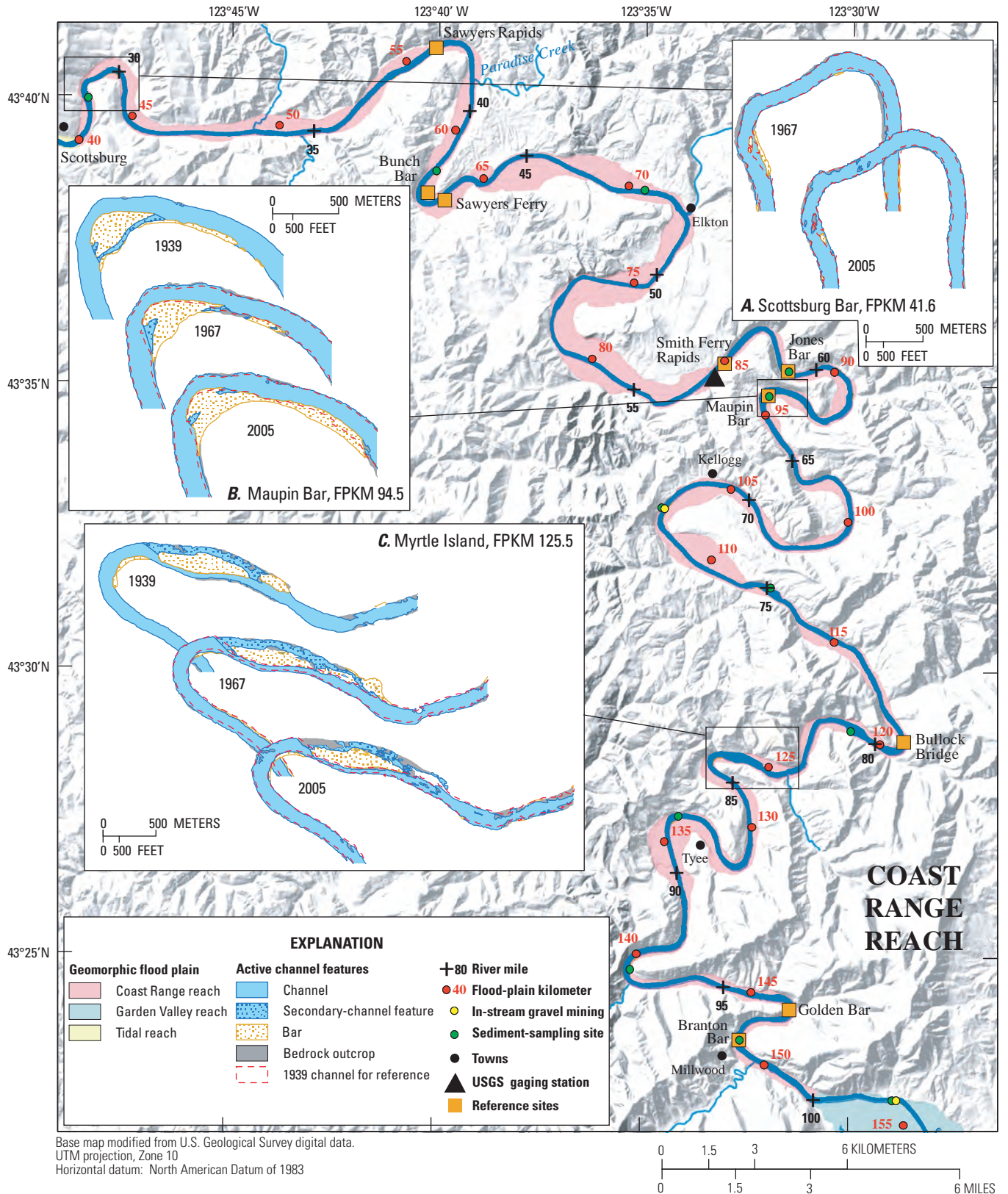


Figure 7. Channel planform in the Coast Range reach of the Umpqua River, Oregon. Insets show historical changes to selected bars, as mapped from aerial photographs. Topography based on U.S. Geological Survey 10-meter digital elevation data.

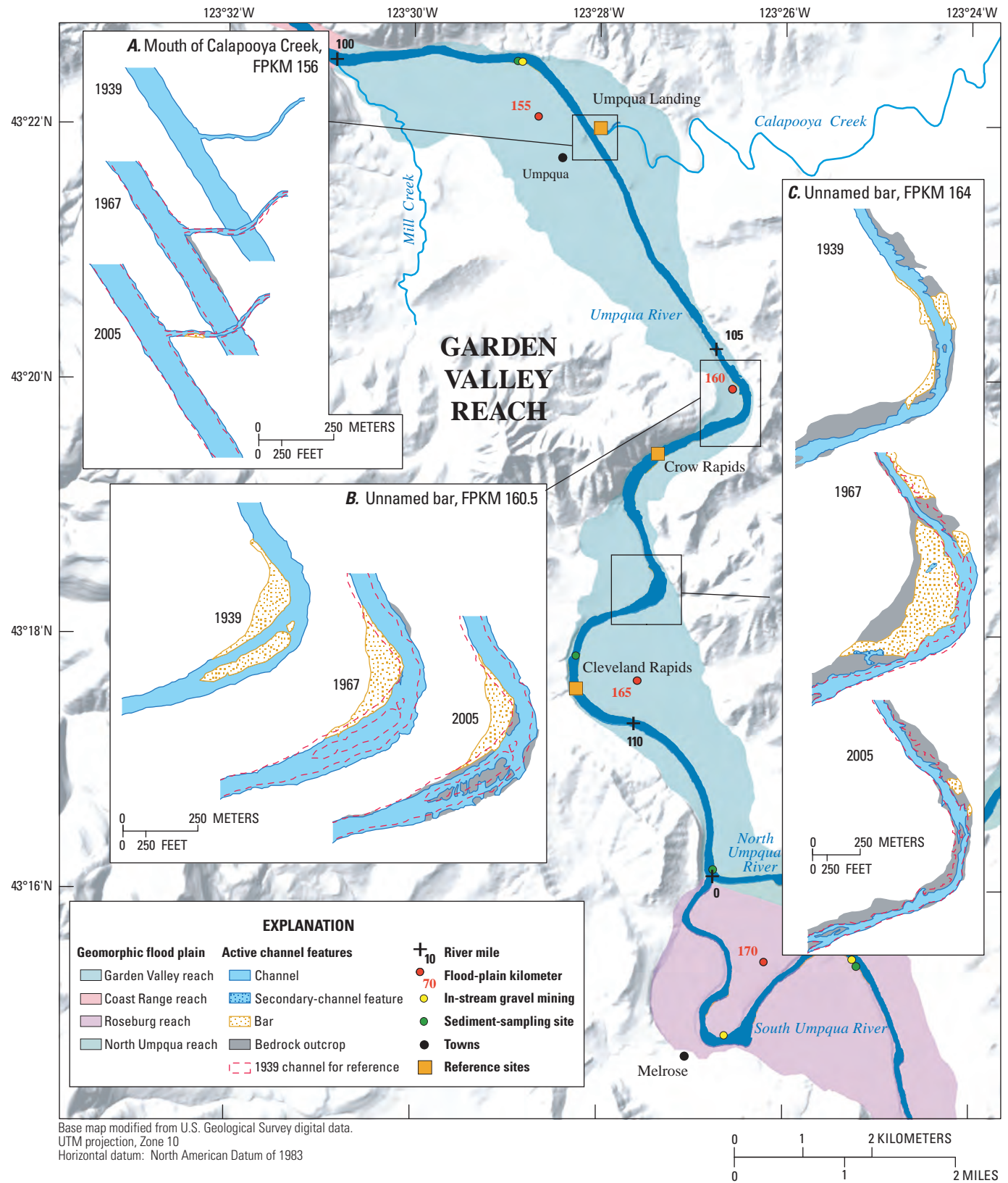


Figure 8. Channel planform of the Garden Valley reach of Umpqua River, Oregon. Insets show historical changes to selected bars, as mapped from aerial photographs. Topography based on U.S. Geological Survey 10-meter digital elevation data.

Historical Descriptions of the Umpqua River

We reviewed several Umpqua River basin historical documents (many also summarized by Beckham [1986], Winterbotham [1994], and Markers [2000]) for observations and accounts pertinent to channel conditions. The most useful of these are reports of early exploration and navigation surveys documenting channel characteristics at first European-American settlement. Accounts of historical land-use activities are also relevant to understanding historical and present channel conditions. Abundant archival photographs, at the Douglas County Historical Society and elsewhere, locally document channel conditions as far back as circa 1900. A primary conclusion from inspection of these historical sources is that gravel was scarce in many reaches of the Umpqua River. This is particularly evident for the Coast Range reach of the main stem Umpqua River. For example, David Douglas, a botanist (and county namesake) accompanying an expedition of the Hudson's Bay Company, describes his October 16, 1826, evening activities at their camp near the present location of Elkton (Douglas, 1914, p. 223; FPKM 72.1; Coast Range reach):

I employed myself chopping wood, kindling the fire, and forming the encampment; and after, in the twilight, bathed in the river: course north-west; bed sandstone; ninety yards broad; not deep, but full of holes and deep chinks worn out by the water.

Similarly John Work, employed by the Hudson's Bay Company, describes following the main stem Umpqua River between Elkton and Scottsburg (FPKM 40) in his journal entry for June 8, 1834 (Scott, 1923): "No stones worth mentioning all the way: the river runs on a bed of soft slaty rock." Two weeks later, on June 17, John Work was camping along the Umpqua River just downstream of the Calapooya Creek confluence (FPKM 156; Garden Valley reach) where he reported:

The Umpqua here is about 150 yards wide & runs over a rocky bottom of soft slaty rock & is not very deep. A horse can ford it at present.

The most extensive early survey was by U.S. Army Engineers lieutenant R.S. Williamson in 1870 while investigating navigation possibilities. His report (U.S. House of Representatives, 1871) described the several bedrock rapids between Scottsburg and Roseburg and provided a general characterization of the river:

The average width of the river, when bankfull, appeared to be about 200 feet; but at its extreme low-water stage the water is divided at many places into half a dozen or more streams, varying in width from two to thirty feet, and separated from each other by walls of rock sometimes five or six feet

in height. In passing through some of these narrow place[s] the velocity of the current was 400 feet per minute. At each of these rapids between the channel and the shore there is a bench of sandstone, generally flat, varying from two to five feet in height above the low-water mark, and averaging about seventy-five feet in width. During ordinary stages of the river this is covered with water. The river contains no sand-bars, its bottom being coarse gravel, on solid bed-rock; consequently any improvements which may be made to the river are likely to be permanent.

A subsequent survey in 1910 encompassing most of the Roseburg, Garden Valley, and Coast Range reaches by the Junior Engineer F.E. Leefe of the U.S. Engineer Office (U.S. House of Representatives, 1911) reiterates Williamson's findings:

In the stretch of river under examination between Roseburg and Scottsburg, a distance of 86 miles, the low water fall is about 465 feet. Throughout this distance the river at low water is a succession of rocky rapids with pools of quiet water between, of varying lengths and depths. The river flows over a rocky sandstone bottom much of the way, with many dangerous reefs and projections. With such a fall, averaging nearly 5½ per mile, the current is strong over the rapids at all stages.

Although sand and gravel accumulations are barely mentioned in many of these accounts of the South Umpqua and main stem Umpqua Rivers, except for noting their scarcity, some historical photographs show bars flanking the channel ([fig. 12](#)). We have found fewer early descriptions of the Days Creek reach of the South Umpqua River at the time of first exploration, but it too was apparently locally flowing on bedrock, at least near its downstream end, because in-channel potholes near the Cow Creek confluence were targets for gold miners in the 1850s (Beckham, 1986, p. 93).

Although no detailed surveys were conducted for the North Umpqua River, reports by the Wilkes Expedition on their 1841 overland trip between the Willamette Valley and San Francisco Bay (including geologist James Dwight Dana) state that the North Umpqua River ran on bedrock where they crossed it near the present location of Winchester (North Umpqua RM 7; Dana, 1849, p. 662). Similarly, Markers (2000, p. 133) noted:

The North Umpqua River has been pronounced, by experts in the driving of streams, to be the best driving stream in Oregon or Washington. It is singularly free from shifting sand bars and gravel shoals....

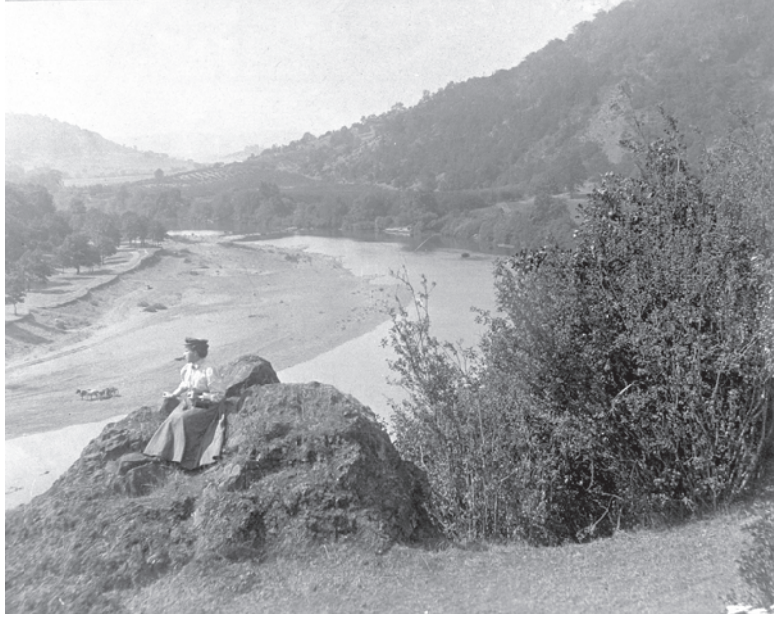


Figure 12. Circa 1890s, of the South Umpqua River upstream of Mount Nebo near Roseburg, Oregon. Photograph courtesy of Douglas County Museum (Photograph N5549a).

The character of the Tidal reach was distinctly different; drifting sand and gravel bars caused persistent navigation problems between the mouth and the head of tide at Scottsburg (FPKM 40), leading to multiple bathymetric surveys beginning in the late 18th century (summarized by Beckham, 1986, p. 149–152). These issues ultimately resulted in construction of the jetties and substantial and ongoing dredging of the lower channel. Shallow gravel bars near Brandy Bar (FPKM 27.5) also caused navigation hazards; this area ultimately became the reach of primary 20th and 21st century sand and gravel mining by Umpqua River Navigation Company and its successors.

Land-Use and Landscape Disturbance in the Umpqua River Basin

Although fur traders and early explorers entered the mouth of the Umpqua River basin in the late 18th century, European-American settlement of the basin did not fully

commence until the mid-19th century following the passage of the Donation Land Act in 1850 and subsequent Federal programs (Beckham, 1986). The earliest immigrants to the basin claimed the fertile bottomlands and broad prairies of the central Umpqua River basin leaving more marginal ground, including rugged forest lands and flood-prone tributary valleys to later arrivals. These early settlement patterns are still evident today, as most of the basin's population lives in the wide valley bottoms in the incorporated areas of Roseburg, Winston, and nearby towns (Geyer, 2003b, 2003c, 2003d). The upper parts of the North Umpqua and South Umpqua River basins primarily are federally held forest lands, but the lower parts of these drainage basins mostly are privately owned, and the basins are managed for forestry and agriculture (Geyer, 2003a, 2003b, 2003c, 2003d). Nearly 70 percent of lands in the main stem Umpqua River basin (downstream of the confluence of North Umpqua and South Umpqua Rivers) are managed primarily for forestry, with the balance being for agriculture, residential, industrial, or other land uses (Oregon State University, 2010).

Descriptions of historical land-use and landscape disturbance that have potentially affected channel and bed-material conditions are summarized by Beckham (1986), although watershed studies and other sources provide supplementary information. In the Umpqua River basin, the disturbances that are most likely to influence channel conditions and bed-material transport include navigational dredging, placer mining, in-stream gravel mining, impoundments for hydropower and flood control, and forestry and other land-use practices (table 4).

Placer Mining

Gold mining in the Umpqua River basin began in 1852 on the South Umpqua River near Riddle and in lower Cow Creek (Beckham, 1986, p. 225–226). The widespread placer mining on the South Umpqua River and its tributaries Olalla Creek (a tributary of Lookingglass Creek), Myrtle, Cow, and Coffee Creeks (Diller, 1914; Ramp, 1972) probably had the most significant effects on in-stream gravel conditions (figs. 9 and 10). All these drainages enter the South Umpqua River within the Roseburg and Days Creek reaches. Placer mining in the late 19th and early 20th centuries involved extensive excavation of alluvial terraces flanking the present watercourses, in places aided by elaborate hydraulic works (fig. 13). Beckham (1986, p. 93) noted the impact of these activities on the stream channels:

Mining generated terrible problems for the Indians. The cascade of debris down the creeks and rivers had calamitous impact on the fish runs: mining destroyed the spawning grounds by washing away the gravels and coating the river bottom with mud.

Such effects, as well as possible large inputs of gravel to South Umpqua tributaries, may still have implications for the present-day sediment conditions in the Umpqua River system.

Umpqua River Gravel Mining

Gravel bars in the Umpqua River basin have provided a local source of aggregate used in local road building and construction projects since the early 1900s. Although records describing mining practices, quantities, and locations prior to 2001 are scarce, anecdotal accounts from landowners and limited information on gravel mining permits (Oregon Department of State Lands, written commun., 2008) indicate that at least 17 sites along the South Umpqua and main stem Umpqua Rivers either had active permits for gravel removal or documented mining in recent decades.

Longtime residents and gravel operators report that the 1970s was a period of particularly high extraction rates, during which time gravel bars were mined with a dragline and scraped of all available sediment until bedrock was reached (Kelly Guido, Umpqua Sand and Gravel, oral commun., 2008). By the mid-1980s, mined volumes had decreased; in recent decades, most bars owned by the main gravel operators have been mined only 2 to 3 times each (Mike Flewling, Knife River Corporation, oral commun., 2008; Joy Smith, Umpqua Sand and Gravel, oral commun., 2008). Gravel mining regulations have changed substantially since the 1970s, and now near-channel gravel typically is harvested by bar skimming, whereby scrapers or other heavy equipment are used to remove only the surface of the bar, typically to an elevation close to the low-flow water level. No permits for in-stream gravel extraction have been issued since 2004, the last year in which mining occurred upstream of the Tidal reach. In the intervening years, two main operators continue to seek approval for future mining at six sites (figs. 1 and 9) on the South Umpqua River:

- Umpqua Sand and Gravel Bar, FPKM 171.4, operated by Umpqua Sand and Gravel
- Shady Bar, FPKM 186.2, operated by Knife River Corporation
- Little Valley Bar, FPKM 189.7, operated by Knife River Corporation
- Weigle Bar, FPKM 211, operated by Knife River Corporation
- Gazley East Bar, FPKM 232, operated by Knife River Corporation
- Days Creek Bar, FPKM 249.9, operated by Knife River Corporation

Extraction volumes for 2001–04 provided by the Umpqua Sand and Gravel and Knife River Corporation show that mining in 2001, 2003, and 2004 removed volumes at individual sites ranging from 610 to 21,500 metric tons (based on volumes provided in bar surveys and a bulk density of 2.1 metric tons/m³). In 2001 and 2003, 9,260 and 610 metric tons of gravel were removed from Umpqua Sand and Gravel Bar, respectively, and in 2004, a combined total of 36,570 metric tons was extracted from Days Creek, Weigle, and Umpqua Sand and Gravel bars. Other sites also may have been mined during this period, but no records were available.

Table 4. Channel trends and anthropogenic impacts for reaches in the Umpqua River basin, Oregon.[Abbreviations: FPKM, flood-plain kilometer; mi², square mile]

Attribute	Reach					
	Tidal	Coast Range	Garden Valley	Roseburg	Days Creek	North Umpqua
Major flow factors	Tidally affected	Minimal regulation	Minimal regulation	Galesville Reservoir, Oct. 7, 1985, regulates 74.3 mi ² of Cow Creek basin (5.9 percent of contributing area at upper end of segment)	None	Pacific Power dams constructed 1952–1955 regulate (slightly) drainage from 430 mi ² (35 percent of the upper end of segment)
Major sedimentation factors	Gradient change promotes deposition of sediment load; Smith River sediment inputs; dredging (100,000–500,000 cubic yards per year)	Sediment input from tributaries; local landuse and forest practices	Local sand and gravel mining; forest practices; Calapooya Creek sediment input	Late 19th century placer mining in reach and tributaries; forest practices; sand and gravel mining; tributary sediment inputs	Forest practices; sand and gravel mining; tributary sediment inputs	Pacific Power dams trap upstream sediment; forest practices
Channel disturbance factors	Historic navigation dredging, sand and gravel mining, rock removal for navigation near Scottsburg; road corridor	Late 19th century navigation improvements; temporary mill dam at Kellogg (removed 1871); road corridor	Late 19th century navigation improvements; sand and gravel mining	Local navigation improvements; transportation infrastructure; log driving; 19th century mill dams; sand and gravel mining; placer mining	Transportation infrastructure; log driving (?); sand and gravel mining; placer mining	Navigation improvement; log driving; Winchester Dam at FPKM 10.2
General channel trends	Some evidence of local incision historically near gravel mining operations (CH2M Hill, 1972)	Channel historically and presently on bedrock; little or no evident change (photos, specific gage analysis for Elkton gage)	Channel historically and presently on bedrock. No obvious change evident from inspection of aerial and oblique photographs, analysis of bar area	Channel historically and presently on bedrock. No obvious change evident from inspection of aerial and oblique photographs, analysis of bar area, and specific gage analysis	Channel locally on bedrock. No evident trends, although limited data for this reach	Channel historically and presently on bedrock. No evident change from specific gage analysis

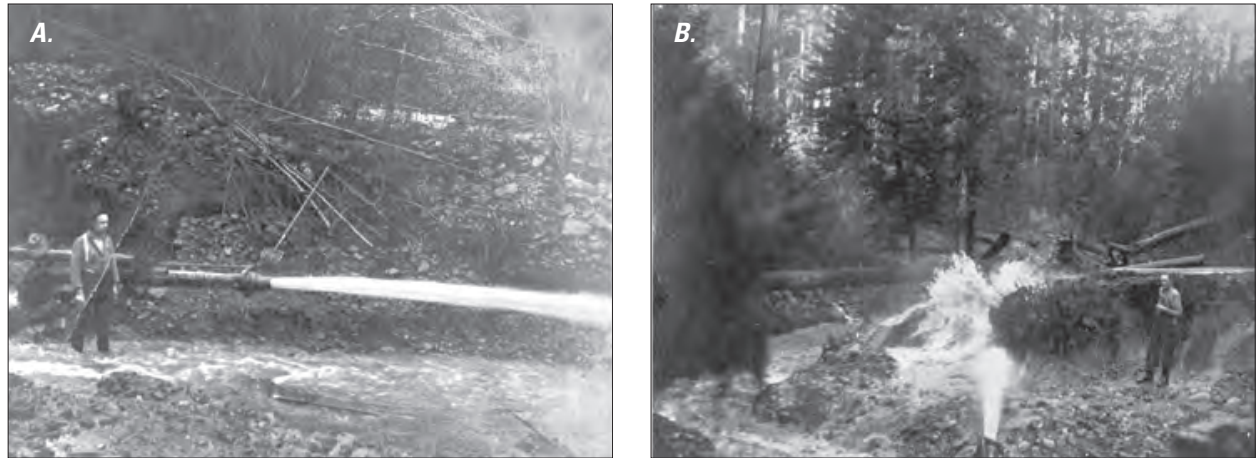


Figure 13. Hydraulic mining in the Olalla District, Lookingglass Creek drainage, Oregon. Photographs courtesy of Douglas County Museum. (Photographs (A) N5155a and (B) N5155b.)

Dams

Mill dams and other small obstructions served various needs of early settlers, and later, larger dams have provided for hydropower and flood control. Of these early dams near Kellogg (FPKM 105.4; Coast Range reach), Roseburg (FPKM 182; Roseburg reach), and Winchester (NUFPKM 10.2; North Umpqua reach), only the Winchester Dam, a 3-m-high concrete structure on the lower North Umpqua River, remains. Anecdotal accounts indicate that some gravel passes over Winchester Dam, although most bed-material sediment is likely trapped in its shallow upstream reservoir, which has aggraded approximately 2 m since dam construction in 1904 (Timothy Brady, City of Roseburg Water Plant Superintendent, oral commun., November 15, 2010).

Pacific Power's North Umpqua Hydroelectric Project was constructed during 1952–55 and now traps bedload from the upstream 32 percent of the North Umpqua River basin. However, a 2002 amendment to the 2001 Federal Energy Regulatory Commission (FERC) re-licensing settlement for PacifiCorp's hydroelectric project in the North Umpqua Basin calls for a gravel augmentation plan to increase the amount of spawning habitat downstream of Soda Springs Dam (fig. 1, PacifiCorp, 2002). The augmentation plan included a one-time experimental pulse of 2,300 m³ of spawning size gravel, equivalent to the long-term average annual bedload input to this reach, or approximately 3,680 metric tons (based on a bulk density of 1.6 metric tons/m³ as provided by Stillwater Sciences, written commun., 2010), which was added to the river in August of 2004 (Stillwater Science, 2006). Additionally, 56 m³ (approximately 90 metric tons) will be distributed seven times during the course of the new FERC license (PacifiCorp, 2002). Sediment studies conducted as part of relicensing these facilities and to monitor the gravel

augmentation are summarized later in the section "[Previous Water and Sediment Studies in the Umpqua River Basin.](#)" Galesville Reservoir on Cow Creek began filling in 1985, and since then has trapped all bed material from the upper 192.4 km² of Cow Creek, encompassing 5.9 percent of the South Umpqua River basin at the Cow Creek confluence.

Forest Management and Fire

Because they potentially influence large portions of the basin, watershed-scale disturbances, including forest fires, development and logging, and related activities can affect channel morphology and bed-material conditions throughout the Umpqua River basin. Timber harvest and associated road building can increase peak flows (Wemple and others, 1996; Jones and Grant, 1996, 2001; Bowling and others, 2000) and the frequency of landslides (Kelsey and others, 1995), resulting in sedimentation along lower reaches of affected basins (Madej, 1995). Douglas County, whose boundaries closely follow that of the Umpqua River basin, was second in the nation in timber harvest from Federal lands between 1949 and 1970 (Beckham, 1986, p. 174).

Peak timber production was during the 1950s–1960s, when annual timber harvest from National Forest Lands in Douglas County ranged from 149.6 to 637.6 million board feet (Beckham, 1986, p. 174). Log production from public lands decreased substantially after 1988 when management emphasis shifted from timber production to habitat protection. For comparison, log production in 1988 was 397 million board feet, but annual average harvest 1991–2000 was 29 million board feet, which diminished to 6.7 million board feet during 2001–03 (as calculated from data provided by U.S. Forest Service, 2006). Although detailed records describing historical logging practices, road building, and associated landscape

changes are lacking for the Umpqua River basin, it is possible that intensive timber harvest peaked in the 1950s–1960s, but remained elevated through the 1980s, likely affecting bed-material influx to the Umpqua River and its major tributaries.

Linking historical patterns of forest fire with changes to channel character is difficult due to sparse records connecting fire extent and severity to subsequent changes in channel condition. Historically, Native Americans used annual, late-summer fires to clear brush and ensure open areas for hunting and berry gathering along valley bottoms (Beckham, 1986). By the early 1900s, however, Federal fire-suppression programs became more aggressive (Beckham, 1986; Geyer, 2003a–d). In recent decades, fires have burned increasingly larger areas of the basin, including fires in 1987 (31 km² burned area), 1996 (73 km²), and 2002 (341.8 km²) (as determined from U.S. Forest Service [2010] mapping data). Most of the fires in 2002, including the Boulder Fire (193 km²), were in the South Umpqua River basin, where 6 percent of the total drainage basin area was burned (as determined by the U.S. Forest Service [2010]). Possible long-term effects of these fires include increased runoff and erosion associated with canopy removal (U.S. Forest Service, 2003).

Navigation Improvements and Commercial Dredging

Historical navigation improvements were focused in the Tidal reach, which has been the only section of river with extensive commercial boat traffic, but upstream reaches also had many rapids modified in the early 1870s in an attempt to promote navigation from the Pacific Ocean to Roseburg (Markers, 2000). Likewise, some bedrock rapids were modified in the late 19th century on the South Umpqua and North Umpqua Rivers to facilitate log drives (Beckham, 1986).

By 1900, the emphasis on improving navigation on the Umpqua River shifted to the river's mouth, and between the 1920s and 1940s, the USACE, together with local entities, constructed major jetties to ensure a stable entrance to the lower river channel (Beckham, 1986). Beginning in 1927, the Corps of Engineers also began deepening the channel between the river's mouth and Reedsport, and constructed a boat turning basin in Winchester Bay in 1945 (Beckham, 1986, p. 153). Navigational dredging by the Corps of Engineers has continued, with annual removal volumes from 1991 to 2008 averaging 157,070 m³ (fig. 14; Judy Linton, U.S. Army Corps of Engineers, written commun., 2008).

Commercial dredging of the Umpqua River estuary for sand and gravel aggregate began in 1918 and has been focused primarily in the area near Brandy Bar, between FPKM 25.9 and 30.6, where Umpqua River Navigation Company and its successor Knife River Corporation operated between 1949 and 2002 (Lidstone and Associates, written commun., 2008). The amount of bed-material sediment removed by commercial dredging during this period ranged from 22,070 to 339,250 m³/yr, averaging 136,380 m³/yr (fig. 14; as determined from records provided by Lidstone and Associates, written commun., 2008; CH2M Hill, 1971).

Previous Water and Sediment Studies in the Umpqua River Basin

Previous reports from hydrology and sediment transport studies for the Umpqua River basin were reviewed for this study. Although many studies are peripherally related (such as turbidity and other water-quality studies), two previous studies are directly relevant to gravel transport and channel morphology in the study area: (1) the basinwide analysis of sediment transport by Curtiss (1975) and (2) the sediment transport analyses by Stillwater Sciences (2000) in support of the FERC relicensing of the Pacific Power hydroelectric facilities on the North Umpqua River.

The Curtiss (1975) report expands on an earlier USGS report by Onions (1969) by providing estimates of annual suspended-sediment discharge for 11 sites in the Umpqua River basin based on as many as 18 years of suspended-sediment measurements between 1956 and 1973. Although there were no measurements of bedload in this study, Curtiss (1975) calculated total sediment loads (bedload plus suspended load) on the basis of measurements at Flynn Creek (a Coast Range stream in the Alsea River basin), where bedload constituted 3 percent of the mean annual suspended-sediment yield. This ratio was applied for the sites in the Umpqua River basin, except for Cow Creek, where field observations implied that bedload composed 5 percent of the total load. Although no known bedload measurements for the Umpqua River system substantiate these values, bedload transport rates typically scale with suspended load, and the analysis by Curtiss (1975) probably provides a reasonable guide to the relative contributions of bed material to the Umpqua River system. For the calculated mean annual total sediment discharge of 1.54×10^6 metric tons/yr of the South Umpqua River at Brockway, the Curtiss (1975) analysis indicates that 0.28×10^6 metric tons/yr enters through Lookingglass Creek, 0.34×10^6 metric tons/yr joins at Cow Creek, and 0.28×10^6 metric tons/yr comes from the upper basin upstream of the Tiller gaging station.

Table 12. Reach-segregated bed-material flux values for the Umpqua and South Umpqua Rivers, as calculated from surveys at mined sites, transport capacity equations, sediment yield analysis, and suspended-sediment measurements.

[Bedload flux: Estimates of bedload flux from suspended-sediment data from Curtiss (1975). Abbreviaton: FPKM, flood-plain kilometer; –, no data]

Reach Name	FPKM	Range of surveyed fill volumes and net deposition rates	Calculated median transport capacity value 1951–2008 (metric tons)				Bed-material flux from sediment yield analysis (metric tons)	Bedload flux from suspended sediment measurements (metric tons)
			Parker-Klingeman-McLean	Parker-Klingeman	Parker	Wilcock-Crowe		
Coast Range reach	40–152	–	56,440	53,740	20,280	24,165	30,500–49,800	¹ 95,200
Garden Valley reach	152–169	–	35,115	34,265	39,625	81,855	43,600–49,700	² 68,060
Roseburg reach	169–231	170–15,920	14,950	9,640	16,270	27,200	41,600–48,000	³ 46,260
Days Creek reach	231–275	80–20,810	4,450	4,400	7,585	12,260	19,200–25,800	⁴ 3,800

¹ From Elkton gaging station.² Sum of Brockway and North Umpqua gaging stations.³ From Brockway gaging station.⁴ From Tiller gaging station.

Summary and Conclusions

This study, done in cooperation with the U.S. Army Corps of Engineers, assessed spatial and temporal trends in channel change and bed-material transport for 350 km of alluvial and semi-alluvial river channel in the Umpqua River basin. Basin network structure and channel geomorphology led to subdivision of the river system into six contiguous analysis reaches. The North Umpqua reach includes 47 km of channel extending upstream of the North Umpqua River confluence with the South Umpqua River. The Days Creek reach encompasses 47 km of the South Umpqua River from the upstream extent of the study area near Tiller, Oregon, to the Cow Creek confluence. The Roseburg reach continues 76 km downstream of Cow Creek to the South Umpqua River confluence with the North Umpqua River. The Garden Valley reach contains the Umpqua River for the 19 km from the confluence of the North Umpqua and South Umpqua Rivers to the entrance of the Coast Range, from where the Coast Range reach of the Umpqua River extends another 116 km downstream to the head of tide near Scottsburg, Oregon. The much lower gradient and partly estuarine Tidal reach encompasses the final 45 km of river channel and through Winchester Bay to the Pacific Ocean at Reedsport. These reaches have distinct physiographic and bed-material transport conditions, as well as distinct histories of instream gravel mining, thereby providing an efficient analysis and discussion framework.

The findings reported here draw largely upon two components: (1) historical analyses, including detailed mapping of the active channel using aerial photographs and repeat surveys, to document spatial and temporal changes in channel morphology and bed-material storage and (2) quantitative investigation of the bed-material flux

through the study reaches. These analyses provide a basis for understanding the recent history of the active channel and also allow for inferences regarding the spatial and temporal variation of production, fluxes, and routing of bed material through the study reaches.

Primary Findings

The overall character of the Umpqua River reflects its geologic history. For the past 10,000 years, the overall trend for fluvial reaches of the Umpqua River has been incision, where transport capacity has exceeded the supply of coarse bed-material sediment, as indicated by abundance of exposed bedrock in and flanking the active channel throughout the study area. This channel characteristic, as well as the sparse gravel cover, was specifically noted by 19th and 20th-century Euro-American explorers. Repeat mapping from multiple aerial-photograph sets spanning 1939–2009 shows that the fluvial reaches of the Umpqua, South Umpqua, and North Umpqua Rivers flow within largely stable, single-thread channels of bedrock or coarse boulder and cobble substrates. Coarse bed-material sediment locally mantles the bedrock, forming shallow bars in and flanking the low-flow channel, whose position and overall size are dictated primarily by valley geometry rather than channel migration processes.

Gravel bars have historically been most abundant on the South Umpqua River within the Roseburg and Days Creek reaches, where there has been as much as 1.3–4 times the area of gravel bars per unit length of stream (approximately 12.7–31.8 m²/m) compared with the Coast Range and Garden Valley reaches (where specific bar area has ranged from 5.0 to 13.7 m²/m). Although bedrock rapids and channel-flanking bedrock shoals are common features throughout the study area, they are most abundant along the Umpqua and

North Umpqua Rivers, where 2005 aerial photographs show 3–5 times more exposed bedrock (by area) than mapped gravel. Most of the gravel in the study area is stored in large bars with areas greater than 20,000 m², many of which apparently become active areas of bed-material transport only during exceptionally large floods, such as the December 1964 flood. Although many numerous smaller gravel patches (less than 2,000 m²) flank the river at the heads of rapids and immediately downstream, these smaller depositional zones account for less than 6 percent of the total mapped gravel in the study area in 2005.

The abundance of gravel bars along the lower South Umpqua River most likely results from Klamath Mountains source areas underlying much of the South Umpqua River basin. The tectonically deformed and metamorphosed Mesozoic rocks of the Klamath Mountains terrain, together with its steep slopes and dense stream network, enhance production and delivery of bed material to the South Umpqua River. High bed-material fluxes from this terrain have been documented for the Chetco River (Wallick and others, 2010) and Smith River (MFG, Inc. and others, 2006) to the south. Additionally, clasts from this terrain are probably more resistant to abrasion than bed material from the High Cascade and Western Cascade terrains, and consequently are a persistent component of Umpqua River bed material as far downstream as the Tidal reach. Cow Creek, a large tributary draining Klamath Mountains terrain, probably is a major supplier of gravel to the South Umpqua River, judging from the extensive gravel deposits near its mouth, the increased abundance of bars downstream of its confluence, and the low armoring ratio of bars within Cow Creek. Historically, several Klamath Mountains tributaries, including Cow Creek, Myrtle Creek, and Lookingglass Creek, were subject to extensive placer mining, which may have further enhanced sediment output from these streams, although historical photographs of the Roseburg reach do not indicate significantly greater gravel volumes during the early 20th century.

Bed-material sediment from Cascade Range streams originates mainly in the Western Cascades, because the much younger lava flows of the High Cascades are highly porous and have little capacity for sediment transport. Although the Western Cascades terrain yields more bed-material sediment than the High Cascades terrain, sediment production from the Western Cascades probably is small compared to that from Klamath Mountains terrain as evidenced by: (1) the North Umpqua reach, which exclusively drains the Cascade Range, had less than one-half of the gravel bars per unit stream length in 1939 than the South Umpqua reaches, and (2) the South Umpqua River upstream of the Days Creek reach drains only the Western Cascades terrain, and unlike the more gravel-rich lower reaches downstream of Klamath Mountains terrain tributaries, the river within the Western Cascades terrain is a narrow bedrock stream with boulder-dominated rapids and few gravel bars.

Farther downstream of its confluence with the South Umpqua River, sedimentary rocks supplied to the main stem Umpqua River by Coast Range tributaries are highly erodible, and although this region produces high suspended-sediment loads (for example, Beschta [1978]), bed-material clasts from these geologic units disintegrate readily. Therefore, although the terrain of Klamath Mountains comprises only 21 percent of the Umpqua River basin, it probably supplies a disproportionately large amount of bed-material sediment to the channel system. Further, the importance of this terrain to total basinwide sediment production is even larger because of the effects of dams on sediment transport in the North Umpqua River.

The primary observation from the repeat channel mapping and surveys is the overall stability of the Umpqua River planform. All fluvial reaches showed little change in sinuosity or channel width throughout the 70-year analysis timeframe, mainly because of lateral and vertical bedrock control. Consistent with this, repeat stage measurements at USGS streamflow-gaging stations show only local areas of slight channel deepening (on the order of 0.1–0.2 m), some of which may be associated with bedrock erosion.

The main temporal trend evident from repeat channel mapping from aerial photographs is a 29-percent decrease in the area of mapped gravel bars between 1939 and 2005. Most of this decrease was between 1967 and 2005, and was partly due to vegetation colonization on formerly active, upper bar surfaces, converting some of these high bar surfaces to floodplain. Also important was erosion of lower elevation bars to bedrock, particularly for the Coast Range and Garden Valley reaches. The decrease in mapped gravel bar area probably resulted from a combination of factors, including decreasing peak flows, gravel extraction, and dam construction. Several unregulated tributary streams, as well as the South Umpqua River gaging station at Brockway, show significant trends of decreasing peak flows since the 1950s, which is probably due mainly to decadal-scale climate cycles. Because three of the five streams that show this trend drain Klamath Mountains terrain, even small decreases in peak flows on these tributaries may have a disproportionate effect on overall gravel transport in the study area. The cumulative effects of instream gravel extraction in recent decades likely also affects bed-material storage in the active channel because mined volumes in some years probably constituted a substantial portion of the overall gravel flux.

For the North Umpqua River, the 59-percent decrease in gravel between 1967 and 2005 is probably due to a combination of trapping of bed material by hydropower dams constructed in 1952–55 and climate-driven decreases in peak flows, as detected for the gaging station at Winchester. For this reach, decreased gravel bar area has led to much more exposure of active channel bedrock.

Although the overall trend was of decreasing bar area, many bars have episodically grown, mainly as a consequence of large floods. This is particularly the case for the major flood of December 1964, which had an annual exceedance probability of about 1 percent. Total bar area throughout the fluvial reaches increased by more than 11 percent between 1939 and 1967, which probably is attributable mainly to the 1964 flood. Evident in the 1967 photographs are (1) removal of vegetation and bed-material deposition on upper bar surfaces, and (2) bed-material deposition extending the margins of low-elevation bars into areas mapped as water in 1939. Later but smaller floods in December 1996 and December 2005 resulted in smaller increases in bar area, but these increases have been offset by erosion and bar diminishment during intervening and subsequent years.

Bed-material flux was estimated for fluvial reaches of the Umpqua and South Umpqua Rivers by two independent approaches, supplemented by bed-material recruitment measurements at six sites of past gravel mining and by earlier measurements of suspended-sediment transport. Bed-material transport capacity estimates at 44 sites throughout the South Umpqua and main stem Umpqua Rivers for the period 1951–2008 result in transport capacity estimates that vary spatially and temporally. The temporal variations relate to flow history, with most transport associated with large peak flows. The diminishment in peak discharges over the last three decades, at least partly to climate cycles, has led to an overall temporal trend of reduced gravel transport.

The even wider spatial variations in calculated bed-material transport rates reflect the more fundamental difficulty of applying equations of bed-material transport capacity to a supply-limited river, where bar textures chiefly reflect local hydraulics rather than reach-scale supply conditions. Nevertheless, the transport capacity values should provide an indication of maximum possible bed-material transport rates; reach-averaged median transport capacity values calculated by the bed-material surface-based equations of Parker (1990a, 1990b) and Wilcock–Crowe (2003) equations for 1951–2008 yields a transport capacity of 7,000–27,000 metric tons/yr for the South Umpqua River and 20,000–81,000 metric tons/yr for the main stem Umpqua River upstream of the head of tide (tables 11 and 12). The values of bed-material transport capacity values for the intermediate mobility sites, generally ranging between 500 and 20,000 metric tons/yr as predicted by the Parker (1990a, 1990b) equation, may be the best estimate for actual bed-material transport rates, although confidence in this assessment would be bolstered substantially by actual transport measurements.

These estimates of bed-material transport capacity are broadly consistent with an empirical bed-material yield analysis developed from regional bed-material transport measurements. The most satisfactory regional relation predicts bed-material yield as a function of source area slope and precipitation (fig. 43). Adopting this relation in conjunction with estimates of in-channel attrition, results in predicted bed-material fluxes of as much as 25,000 metric tons/yr on the

Days Creek reach, increasing to nearly 50,000 metric tons for the Roseburg, Garden Valley, and Coast Range reaches, but then decreasing to approximately 30,000 metric tons/yr at the entrance to the Tidal reach.

Both of these approaches—the transport capacity estimates and the regional bed-material sediment yield analysis—give results consistent with site surveys at individual bars within the Days Creek and Roseburg reaches. These surveys indicate minimum local bed-material flux rates of up to 30,600 metric tons/yr in high-flow years, but more typically less than 10,000 metric tons/yr.

The two approaches adopted by this study give estimates less than those predicted by Curtiss (1975) from suspended-sediment transport measurements made during 1956–1973. By applying an assumed bedload transport ratio to measured suspended-sediment loads, the Curtiss (1975) analysis predicts bedload transport rates of 8,400 metric tons/yr at Tiller, near the upstream end of the Days Creek reach at FPKM 273; 46,000 metric tons/yr at the Brockway streamflow measurement site on the South Umpqua River within the Roseburg reach near FPKM 195.3; and 160,000 metric tons/yr at the Elkton measurement site on the main stem Umpqua River in the Coast Range reach at FPKM 72.1. Although these bed-material transport values for the Days Creek and South Umpqua reaches are slightly higher than those we infer from the sediment yield and capacity analyses, they are within realistic uncertainty bounds. The estimate of 160,000 metric tons/yr of bedload at the Elkton measurement site on the main stem Umpqua River greatly exceeds likely bed-material transport rates for this reach as estimated from the capacity and yield analyses, and is almost certainly high as a result of substantially elevated suspended loads derived from Coast Range sedimentary rocks, which produce little bed material.

In consideration of all these analyses, together with the depositional volumes measured by individual gravel bar surveys, we judge that the actual bedload flux in most years is probably less than 25,000 metric tons/yr in the Days Creek and Roseburg reaches, although Cow Creek probably adds substantial bed material to the South Umpqua River at its confluence. Bed-material transport in the Garden Valley and Coast Range reaches may be similar or slightly less because of bed-material attrition exceeding tributary addition. For comparison, the estimated annual volume of commercial gravel extraction from the South Umpqua River was 9,260 metric tons in 2001, 610 metric tons in 2003, and 36,570 metric tons in 2004, based on data supplied by the two main operators in the South Umpqua River—which indicates that historical instream gravel extraction may have been a substantial fraction of the total bed-material flux in the Umpqua River system.

The Tidal reach has a distinctly different morphologic character and transport regime. The Umpqua River along the Tidal reach contains the largest bars in the study area, particularly at the expansive valley bottom near the confluence of the Smith River. These bars are mainly composed of sand and mud, contrasting with the gravel bars upstream.

Commercial dredging has historically focused on the section between the Smith River confluence and upstream to the head of tide at FPKM 40, where there are few bars and repeat surveys show persistent channel deepening even in areas that had not been mined for several years.

Like other coastal streams in Oregon, the lower Umpqua River has been strongly affected by the 130 m of sea-level rise after the culmination of the last maximum glacial period 18,000 years ago, resulting in long-term aggradation and trapping of bed material and suspended coarse sand transported from upstream. Consequently, it is unlikely that substantial bed material from the upstream fluvial reaches (and the upper Smith River) is transported into the Pacific Ocean. The long Tidal reach (and lack of graded profile to the Pacific Ocean mouth) is evidence that upstream sediment supply has not kept pace with Holocene sea level rise inundating the lower Umpqua River valley.

The sediment yield analysis indicates that about 30,000–40,000 metric tons of bed-material sediment enters the Tidal reach annually, but bed-material accumulation within the lower Tidal reach may be substantially greater, because much of the sand transported in suspension upstream is likely transported as bedload in the Tidal reach due to the lower gradients. Consequently, while annual commercial instream mining averaged 140,000 m³ annually during 1949–2002, this volume is not indicative of bed-material transport rates in the upstream fluvial reaches because much of this material probably entered the Tidal reach as sand transported as suspended load from the upstream reaches.

Implications Regarding Future Trends and Monitoring Strategies

For a mixed bedrock and alluvial river such as the Umpqua River, the physical character of the channel is mainly the result of its geologic history and physiography. Throughout the Holocene, transport capacity has exceeded the supply of bed-material sediment, causing the Umpqua River to incise through Pleistocene valley fill and bedrock, resulting in a modern channel that flows mostly on bedrock. The character of individual bars is highly variable and depends on the history of flow and sediment transport, time lags involved in eroding and redepositing sediment, and other local and drainage-basin-scale disturbances that might affect the channel directly or indirectly.

Although many factors influence the abundance and character of Umpqua River gravel bars, the decreases in bar areas observed on all of the fluvial reaches between 1967 and 2005 will likely continue if future gravel removal exceeds bed-material influx. Continued decreases in bar area may also be accompanied by the coarsening of low-elevation active bars that currently have low armoring ratios. In the absence of future mining, bar building will probably be greatest in the lower Days Creek reach and throughout the Roseburg reach, as this area has historically had the greatest concentration of

gravel bars because of the high influx of bed-material sediment from tributaries draining the Klamath Mountains terrain.

However, even prior to gravel extraction and dam construction, transport capacities throughout the Umpqua River study area were much greater than sediment supply, so bar building may proceed slowly following cessation of gravel extraction, and the rate of bar growth will depend on the timing and magnitude of peak flows and the sediment influx accompanying these floods. Although gravel augmentation on the North Umpqua River began in 2004 (Stillwater Sciences, 2006), this additional gravel is not likely to have a substantial effect on bar area in the lower North Umpqua River and main stem Umpqua River because the total augmentation volume is small relative to the long-term gravel deficit introduced by the hydropower dams (based on data provided by PacifiCorp, 2002 and Stillwater Sciences, 2006).

To better understand variation in bed-material storage under different management scenarios, actual bed-material influx to the Umpqua River study reaches must be accurately quantified. However, it is difficult to characterize bed-material fluxes in gravel-rich settings, and even more so for the supply-limited Umpqua River, where bar characteristics and sediment transport are highly variable. Improving our understanding of bed-material fluxes on the Umpqua River will require a variety of independent methodologies, bolstered by high-resolution datasets. The approaches that will potentially be most useful for future characterization of bed-material storage in the Umpqua River study area include (1) the application of transport capacity equations, similar to the methodology used here, but updated using a detailed hydraulic model and up-to-date bar texture information, and (2) direct measurements of bedload transport, which could be difficult to obtain and interpret, but as part of a sustained monitoring program would significantly aid in characterizing bed-material fluxes across a range of flows.

A detailed hydraulic model, along with several key datasets, would support these approaches and form the basis for a future adaptive management program. The nonlinear response of calculated transport capacities to variation in grain size and slope indicates the need for accurate, detailed data describing Umpqua River bar textures and hydraulics. The hydraulic model encompassing the South Umpqua and Umpqua Rivers above the head of tide could be developed from LIDAR topography, and bathymetric surveys would provide a more accurate method of calculating energy slope under a variety of discharge scenarios. At a minimum, the modeling approach would entail a 1D hydrodynamic model with closely spaced cross sections to characterize the highly variable channel. Ideally, the approach would entail a blend of both 1D and 2D models so that the complex hydraulics at large key bars in sharp bends (such as Maupin Bar and Days Creek Bar) are accurately characterized. Such a modeling framework could be used to more accurately calculate energy slope under a variety of discharge scenarios, enabling better understanding of transport conditions and refining our overall understanding of longitudinal patterns in bed-material transport. A detailed

hydraulic model, if coupled with a spatially discrete sediment transport model, could also be used to simulate morphological changes to the channel bed under different management and flood scenarios.

If repeated at regular intervals or following large floods, the LIDAR and bathymetric surveys underlying the hydraulic model would provide a comprehensive basis for evaluating future changes to channel morphology and bar topography. Such data, combined with detailed measurements of bar thickness, could also be used to calculate volumetric sediment flux and deposition rates throughout the study area (similar to a morphology-based approach applied on alluvial rivers). Because the channel is primarily underlain by bedrock and is in many places shallow, the bathymetric survey could consist of depth soundings along the centerline of deep pools, as the LIDAR acquired at low flows would provide an adequate approximation of bed elevation in rapids. Future monitoring could also incorporate sampling of bar textures at regular intervals (perhaps every 2–5 years, or following a flood of a certain magnitude) in order to improve our transport capacity calculations. Textural information, combined with repeat mapping of vegetation densities from aerial photographs would also aid in evaluating temporal evolution of bars in response to different management scenarios and floods.

Acknowledgments

The framework for this study was established with the guidance of Judy Linton of the Portland District of the U.S. Army Corps of Engineers. Information on past gravel mining, access to measurement sites and detailed topographic surveys of mining sites were provided by Umpqua Sand and Gravel, Knife River Corporation, and IE Engineering. Joy Smith and Kelly Guido of Umpqua Sand and Gravel, and Mike Flewelling of Knife River Corporation were especially responsive to our data requests. Chris Lidstone, Lidstone and Associates, supplied reports and surveys from the historically dredged area of the Umpqua River estuary, and provided thoughtful feedback during both phases of this study. Peter Klingeman, Professor Emeritus, Oregon State University, provided instructive comments and observations concerning sediment transport in the Umpqua River basin and reviewed this manuscript. Janine Castro, U.S. Fish and Wildlife Service lent her expertise to both phases of this study by providing helpful comments regarding our study approach and numerous datasets and documents regarding Umpqua River sediment issues. Chuck Wheeler, NOAA Fisheries provided historical data, helpful comments and a field tour of the Umpqua River Basin. Adam Stonewall, USGS Oregon Water Science Center, assisted with the specific gaging station analysis. Jeff Coe, USGS Landslide Hazards Program, provided LIDAR datasets of the Oregon Coast Range. Chauncey Anderson, USGS Oregon Water Science Center, shared resources, reports, and

photographs of the Umpqua River basin. Mikeal Jones of the U.S. Forest Service provided helpful comments following the preliminary Phase I study of this report. Field assistance was provided by Dan Polette, Norman Buccola, Esther Duggan, Rachel Peavler, and Tara Chestnut, all of the USGS Oregon Water Science Center. Steve Sobieszczyk, USGS Oregon Water Science Center, assisted with the Phase I version of this study and with field measurements. Tana Haluska, USGS Oregon Water Science Center, contributed to GIS analyses and metadata preparation. Bedload transport modeling was facilitated by assistance with the Bedload Assessment for Gravel-bed Streams (BAGS) software by John Pitlick, Yantao Cui, and Peter Wilcock.

References Cited

- Aalto, R., Dunne, T., and Guyot, J.L., 2006, Geomorphic controls on Andean denudation rates: *The Journal of Geology*, v. 114, p. 85–99.
- Ambers, R.K., 2001, Using the sediment record in a western Oregon flood-control reservoir to assess the influence of storm history and logging on sediment yield: *Journal of Hydrology*, v. 244, p. 181–200.
- Andrews, D.J., and Buckman, R.C., 1987, Fitting degradation of shoreline scarps by a nonlinear diffusion model: *Journal of Geophysical Research*, v. 92, p. 12857–12867.
- Atwood, Kay, 2008, *Chaining Oregon, Surveying the public lands of the Pacific Northwest, 1851–1855*: Granville, Ohio, The McDonald and Woodward Publishing Company, 267 p.
- Bakke, P.D., Basdekas, P.O., Dawdy, D.R., and Klingeman, P.C., 1999, Calibrated Parker–Klingeman model for gravel transport: *Journal of Hydraulic Engineering*, v. 125, p. 657–660.
- Beckham, S.D., 1986, *Land of the Umpqua, a history of Douglas County, Oregon*: Roseburg, Ore., Douglas County Commissioners, 285 p.
- Benda, Lee, and Dunne, Thomas, 1997, Stochastic forcing of sediment supply to channel networks from landsliding and debris flow: *Water Resources Research*, v. 33, no. 12, p. 2849–2863.
- Beschta, R.L., 1978, Long-term patterns of sediment production following road construction and logging in the Oregon Coast Range: *Water Resources Research*, v. 14, p. 1011–1016.
- Bowling, L.C., Storck, Pascal, and Lettenmaier, D.P., 2000, Hydrologic effects of logging in western Washington, United States: *Water Resources Research*, v. 36, no. 11, p. 3223–3240.